



UNIVERSITY OF  
BIRMINGHAM

# ION-MOLECULE REACTION MASS SPECTROMETRY AND VACUUM- ULTRAVIOLET NEGATIVE PHOTOION SPECTROSCOPY

by

Matthew James Simpson

A thesis submitted to  
The University of Birmingham  
for the degree of  
DOCTOR OF PHILOSOPHY

School of Chemistry  
University of Birmingham  
August 2010

UNIVERSITY OF  
BIRMINGHAM

**University of Birmingham Research Archive**

**e-theses repository**

This unpublished thesis/dissertation is copyright of the author and/or third parties. The intellectual property rights of the author or third parties in respect of this work are as defined by The Copyright Designs and Patents Act 1988 or as modified by any successor legislation.

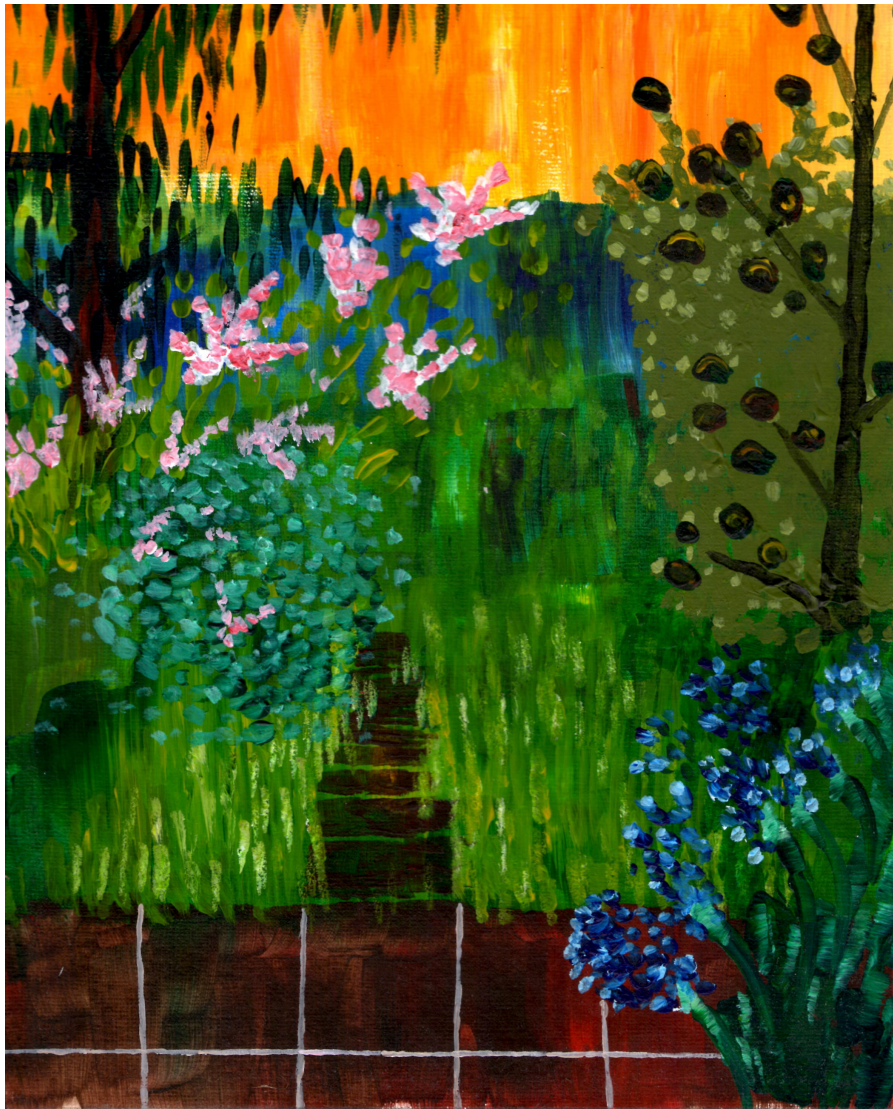
Any use made of information contained in this thesis/dissertation must be in accordance with that legislation and must be properly acknowledged. Further distribution or reproduction in any format is prohibited without the permission of the copyright holder.

# Abstract

Two separate experimental techniques have been used to investigate the fundamental properties of small polyatomic molecules in the gas phase.

Selected ion flow tube mass spectrometry has been used to study the reactions of cations and anions with ethene, monofluoroethene, 1,1-difluoroethene, trifluoroethene and tetrafluoroethene. Calculated collisional reaction rate coefficients are compared to those measured by the experiment. The product ions from these reactions have been detected and their branching ratios measured. Many of these results have been explained using arrow-pushing mechanisms.

Using tunable vacuum-ultraviolet radiation from a synchrotron, negative ions have been detected following photoexcitation of 24 gaseous molecules. The majority of the molecules studied are halogen-substituted methanes. Product anions resulting from unimolecular ion-pair dissociation reactions were detected, and their ion yields recorded in the range 8-35 eV. Absolute cross sections for ion-pair formation and resulting quantum yields are calculated. This vast collection of data is summarised and ion-pair formation from polyatomic molecules is reviewed.



*The Garden at 21 King Edward*

Thank you Sahangir Ali, Liam Cox, Ken Dunn, Nelly Harvey, David Holland, Adam Hunniford, Colin Latimer, Chris Mayhew, Victor Mikhailov, Mike Parkes, Nicola Rogers, David Shaw and Richard Tuckett.

# Publications

N. J. Rogers, M. J. Simpson, R. P. Tuckett, K. F. Dunn, and C. J. Latimer, *Physical Chemistry Chemical Physics* **12**, 10971 (2010).

M. J. Simpson and R. P. Tuckett, *Journal of Physical Chemistry A* **114**, 8043 (2010).

N. J. Rogers, M. J. Simpson, R. P. Tuckett, K. F. Dunn, and C. J. Latimer, *Molecular Physics* **108**, 895 (2010).

M. J. Simpson, R. P. Tuckett, K. F. Dunn, C. A. Hunniford, and C. J. Latimer, *Journal of Chemical Physics* **130**, 194302 (2009).

M. A. Parkes, S. Ali, M. J. Simpson, R. P. Tuckett, and A. E. R. Malins, *Molecular Physics* **106**, 1739 (2008).

V. A. Mikhailov, M. A. Parkes, M. J. Simpson, R. P. Tuckett, and C. A. Mayhew, *Journal of Physical Chemistry A* **112**, 9012 (2008).

M. J. Simpson, R. P. Tuckett, K. F. Dunn, C. A. Hunniford, C. J. Latimer, and S. W. J. Scully, *Journal of Chemical Physics* **128**, 124315 (2008).

# Contents

---

## Chapter 1: Introduction and background information

---

<b>1.A.</b> Ion-molecule reactions	3
1.A.1. Cation-molecule reactions	3
1.A.2. Anion-molecule reactions	4
1.A.3. Collisional rate coefficients	5
<b>1.B.</b> Ion-pair formation	8
1.B.1. Rydberg states	11
<b>1.C.</b> Thermochemistry	13
1.C.1. Thermochemistry applied to ion-molecule reactions	14
1.C.2. Thermochemistry applied to ion-pair formation	14
1.C.3. Energy and enthalpy	16

---

## Chapter 2: The experiments

---

<b>2.A.</b> Ion-molecule reactions	18
2.A.1. The selected ion flow tube	18
2.A.2. Determining the reaction rate coefficient	23
2.A.3. Determining the product branching ratios	26
<b>2.B.</b> Negative photoion spectroscopy	27
2.B.1. The synchrotron radiation source	27
2.B.2. The experimental endstation	30
2.B.3. Determining absolute ion-pair cross sections	32
2.B.4. Determining absolute ion-pair cross sections	33
2.B.5. Considerations when detecting ions with the QMS	34

---

## Chapter 3: The reactions of $CF_n^+$ ( $n = 1-3$ ) with $C_2H_4$ , $C_2H_3F$ , $CH_2CF_2$ and $C_2HF_3$

---

<b>3.A.</b> Background information	35
<b>3.B.</b> The reactions of $CF^+$	37
<b>3.C.</b> The reactions of $CF_2^+$	41
<b>3.D.</b> The reactions of $CF_3^+$	43
<b>3.E.</b> Conclusions	48

---

## Chapter 4: The reactions of $C_2F_4^+$ with $C_2H_4$ , $C_2H_3F$ , $CH_2CF_2$ and $C_2HF_3$

---

<b>4.A.</b> Background information	50
<b>4.B.</b> Results and discussion	51
<b>4.C.</b> Conclusions	63

---

## Chapter 5: The reactions of $OH^-$ , $O^-$ , $CF_3^-$ , $F^-$ , and $O_2^-$ with $C_2H_4$ , $C_2H_3F$ , $CH_2CF_2$ , $C_2HF_3$ and $C_2F_4$

---

<b>5.A.</b> Background information	64
<b>5.B.</b> Results	66
<b>5.C.</b> The reactions of $OH^-$	73
<b>5.D.</b> The reactions of $O^-$	79
<b>5.E.</b> The reactions of $CF_3^-$	83
<b>5.F.</b> The reactions of $F^-$	85
<b>5.G.</b> The reactions of $O_2^-$	87
<b>5.H.</b> Conclusions	91

<b>Chapter 6:</b> <i>Vacuum ultraviolet negative photoion spectroscopy of SF<sub>5</sub>CF<sub>3</sub>, SF<sub>6</sub> and CF<sub>4</sub></i>		<b>Chapter 9:</b> <i>Vacuum ultraviolet negative photoion spectroscopy of small polyatomic molecules</i>	
<b>6.A.</b> Background information	94	<b>9.A.</b> Summary of results	154
<b>6.B.</b> Sulphur hexafluoride (SF <sub>6</sub> )	97	<b>9.B.</b> Ion-pair appearance energies and thermochemical thresholds	158
<b>6.C.</b> Tetrafluoromethane (CF <sub>4</sub> )	101	<b>9.C.</b> Ion-pair formation below the ionisation energy	160
<b>6.D.</b> Trifluomethyl sulphur pentafluoride (SF <sub>5</sub> CF <sub>3</sub> )	106	<b>9.D.</b> Quantum yields	161
<b>6.E.</b> Conclusions	113	<b>9.E.</b> Competing ion-pair reactions	164
<b>Chapter 7:</b> <i>Vacuum ultraviolet negative photoion spectroscopy of CF<sub>3</sub>Cl, CF<sub>3</sub>Br and CF<sub>3</sub>I</i>		<b>9.F.</b> Electron attachment	167
<b>7.A.</b> Background information	115	<b>9.G.</b> Concluding remarks	169
<b>7.B.</b> The anions observed from CF <sub>3</sub> Cl, CF <sub>3</sub> Br, and CF <sub>3</sub> I	117	<b>Notes:</b> two blank pages	171
<b>7.C.</b> F <sup>-</sup> from CF <sub>3</sub> Cl, CF <sub>3</sub> Br, and CF <sub>3</sub> I	117	<b>References</b>	173
<b>7.D.</b> Cl <sup>-</sup> from CF <sub>3</sub> Cl	125	<b>Appendices</b>	
<b>7.E.</b> Br <sup>-</sup> from CF <sub>3</sub> Br and I <sup>-</sup> from CF <sub>3</sub> I	127	Appendix I	181
<b>7.F.</b> F <sub>2</sub> <sup>-</sup> and FX <sup>-</sup> (X = Cl, Br) from CF <sub>3</sub> Cl, CF <sub>3</sub> Br and CF <sub>3</sub> I	130	Appendix II	187
<b>7.G.</b> CF <sub>n</sub> <sup>-</sup> (n = 1-3) from CF <sub>3</sub> Cl, CF <sub>3</sub> Br and CF <sub>3</sub> I	132	Appendix III	189
<b>7.H.</b> Bond dissociation energies	136	Appendix IV	193
<b>7.I.</b> Conclusions	139	Appendix V	206
<b>Chapter 8:</b> <i>Vacuum ultraviolet negative photoion spectroscopy of SF<sub>5</sub>Cl</i>			
<b>8.A.</b> Background information	141		
<b>8.B.</b> F <sup>-</sup> from SF <sub>5</sub> Cl	144		
<b>8.C.</b> Cl <sup>-</sup> from SF <sub>5</sub> Cl	148		
<b>8.D.</b> SF <sub>5</sub> <sup>-</sup> from SF <sub>5</sub> Cl	150		
<b>8.E.</b> Conclusions	151		

# Chapter 1:

## *Introduction and background information*

### *1.A. Ion-molecule reactions*

The first part of this thesis reports and discusses the results collected from an experiment designed to investigate the gas-phase reactions of ions with neutral molecules. A variety of cations and anions have been reacted with ethene and some fluorine-substituted ethenes. The experiment is described in Chapter 2 and the results are discussed in Chapters 3 to 5. Additional data is presented in Appendix III.

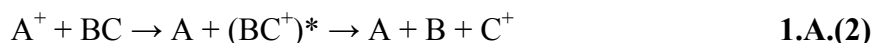
#### *1.A.1. Cation-molecule reactions*

Charge transfer is important in the reaction between a cation and a neutral molecule. If the energy gained by the cation recombining with an electron [its *Recombination Energy* (*RE*)] exceeds the energy required to remove an electron from the neutral molecule [its *Ionisation Energy* (*IE*)], then charge transfer may occur:





The *RE* of the cation  $A^+$  is the same as the *IE* of neutral  $A$ , and takes a positive value. If the  $RE(A^+) \gg IE(BC)$ , several eV for example, the resulting excess energy may fragment the newly formed cation:



Dissociative and non-dissociative charge transfer has been observed from a variety of different cation-molecule reactions. Results have shown that in most cases, if charge transfer is energetically allowed, it will occur and is usually the dominant reaction channel.<sup>1-12</sup> The same experiments have shown that some cations and molecules do not react when the energetics do not allow for charge transfer. In these instances for a reaction to happen, the two species must engage ‘intimately’, and steric effects become important in addition to energetics. The term *intimate* is used to describe a reaction where the two species interact at close proximity, and bonds are formed and/or broken.

#### 1.A.2. Anion-molecule reactions

Consider the generic anion-molecule reaction below:



For an electron to transfer from  $A^-$  to  $BC$ , the *Electron Affinity* (*EA*) of  $BC$  must be greater than the *EA* of  $A$ . This is not the case for many anion-molecule reactions because usually the  $EA(A) > EA(BC)$ . Indeed when charge transfer *has* been observed, the *EA* of the neutral reactant molecule is large; dissociative and non-dissociative charge transfer has been identified in some reactions of  $O_2^-$ ,  $O^-$ ,  $CF_3^-$ ,  $OH^-$  and  $F^-$  with  $SF_6$  ( $EA = 1.1$  eV),  $SeF_6$  ( $EA =$

2.9 eV), and  $\text{TeF}_6$  ( $EA = 3.3$  eV).<sup>13</sup> To put these values into context, the  $EA$  values of  $\text{O}_2$ ,  $\text{O}$ ,  $\text{CF}_3$ ,  $\text{OH}$  and  $\text{F}$  are 0.45, 1.46, 1.82, 1.83, and 3.40 eV, respectively.<sup>14</sup>

Such charge transfer is not common, anions are more likely to react intimately with molecules. Anion-molecule reactions have been shown to commonly occur by abstraction (*e.g.*  $\text{H}^+$  abstraction), or addition-elimination/substitution (*e.g.*  $\text{F}^-$  elimination) mechanisms.<sup>15-</sup>

17

### 1.A.3. Collisional rate coefficients

In bimolecular reactions a *collisional* rate, also known as a *capture* rate, represents an upper limit which assumes every collision leads to a reaction. The efficiency of a reaction can be determined by comparing the maximum rate with that measured by experiment. The ratio of an experimentally measured rate coefficient,  $k_{\text{exp}}$ , to a calculated collisional value,  $k_{\text{c}}$ , represents the reaction efficiency. Bimolecular collisional rate coefficients for ion-molecule reactions are typically in the order of  $10^{-9} \text{ cm}^3 \text{ molecule}^{-1} \text{ s}^{-1}$ .

The values for  $k_{\text{c}}$  given in this work use the model formulated by Chesnavich *et al.*,<sup>18</sup> and further modified by Su and Chesnavich.<sup>19-21</sup> It assumes the potential energy interaction between the reactant ion and molecule takes the form:

$$V(r, \theta) = -\frac{\alpha' q^2}{8\pi\epsilon_0 r^4} - \frac{q\mu_D}{4\pi\epsilon_0 r^2} \cos \theta \quad \mathbf{1.A.(5)}$$

where  $V$  is the potential energy of interaction in J,  $\alpha'$  is the polarisability volume of the neutral molecule in  $\text{m}^3$ ,  $q$  is the charge on the ion in C,  $\epsilon_0$  is the permittivity of free space ( $8.854 \times 10^{-12} \text{ C}^2 \text{ m}^{-1} \text{ J}^{-1}$ ),  $r$  is the distance between the centres of mass of the ion and neutral molecule

in m,  $\mu_D$  is the dipole moment of the neutral molecule in C m, and  $\theta$  is the angle between the direction of the dipole with respect to  $r$ . The resulting expression for the collisional rate constant is:

$$k_c = k_L K_c \quad \mathbf{1.A.(6)}$$

where  $k_c$  and  $k_L$  are defined here in units of  $\text{m}^3 \text{ molecule}^{-1} \text{ s}^{-1}$ , and  $K_c$  is dimensionless.  $k_L$  is the *Langevin* rate coefficient, named after the scientist who first modelled the dynamics of ion-molecule interactions,<sup>22</sup> and formulated by Gioumousis and Stevenson:<sup>23</sup>

$$k_L = \left( \frac{\pi \alpha' q^2}{\epsilon_0 \mu} \right)^{\frac{1}{2}} \quad \mathbf{1.A.(7)}$$

where  $\mu$  is the reduced mass of the colliding species in kg. The other term in equation 1.A.(6),  $K_c$ , is defined as follows:<sup>21</sup>

$$K_c = \begin{cases} \frac{(x + 0.5090)^2}{10.526} + 0.9754; & x \leq 2 \\ 0.4767x + 0.6200; & 2 \leq x \leq 3 \\ 0.5781x + 0.3165; & 3 \leq x \leq 35 \\ 0.6201x - 1.153; & 35 \leq x \leq 60 \\ 0.6347x - 2.029; & x \geq 60 \end{cases} \quad \mathbf{1.A.(8)}$$

$$x = \left( \frac{\mu_D^2}{8\pi\epsilon_0\alpha'k_BT} \right)^{\frac{1}{2}} \quad \mathbf{1.A.(9)}$$

where  $k_B$  is the Boltzmann constant in  $\text{J K}^{-1}$ , and  $T$  is the temperature in K.

It should be acknowledged that equations 1.A.(5) to 1.A.(9) are expressed in *International Standard* (SI) units, and so may differ to those in older scientific literature where *centimetre-gram-second* (cgs) units are commonly used. The first difference to note is that a ‘polarisability’ in cgs units of  $\text{cm}^3$  is often expressed as  $\alpha$ , whereas in SI units the equivalent quantity is referred to as the polarisability *volume* in  $\text{m}^3$  with the symbol  $\alpha'$ . In SI units the *polarisability*,  $\alpha$ , has units of  $\text{C}^2 \text{ m}^2 \text{ J}^{-1}$  and is related to the *polarisability volume* by the following expression:

$$\alpha' = \frac{\alpha}{4\pi\epsilon_0} \quad \text{1.A.(10)}$$

The second difference to note is how the unit of ‘charge’ is expressed. Charge in cgs units ( $\text{cm}^{3/2} \text{ g}^{1/2} \text{ s}^{-1}$ ) can be converted to SI units (C or A s) by using the relationship below:

$$\text{charge (cgs)} = \text{charge (SI)} \times \left( \frac{1}{4\pi\epsilon_0} \right)^{\frac{1}{2}} \quad \text{1.A.(11)}$$

This is relevant in the equations above to the terms  $q$  and  $\mu_D$  which have SI units of C and C m, respectively.

In order to calculate  $k_c$  for a reaction, the polarisability volume and dipole moment (if applicable) of the neutral molecule are required. The values used in this thesis, and their sources, are given in Table 1.A.(I). While dipole moments of molecules are not difficult to find in scientific literature, molecular polarisabilities often are. However, a very successful method to calculate polarisability volumes has been developed by Miller:<sup>24</sup>

$$\alpha'(ahc) = \left( \frac{4}{N} \right) \left[ \sum_A \tau_A(ahc) \right]^2 \quad \text{1.A.(12)}$$

where  $N$  is the total number of electrons in the molecule and  $\tau_A$  is an atomic hybrid component (ahc) for each atom  $A$  in a given state of hybridisation.

<b>Table 1.A.(I).</b> Polarisability volumes and dipole moments for ethene and the fluorinated ethenes.					
molecule	$\text{C}_2\text{H}_4$	$\text{C}_2\text{H}_3\text{F}$	$\text{CH}_2\text{CF}_2$	$\text{C}_2\text{HF}_3$	$\text{C}_2\text{F}_4$
$\alpha' / \text{\AA}^3$ <sup>a</sup>	4.25 <sup>c</sup>	3.99 <sup>d</sup>	5.01 <sup>c</sup>	4.16 <sup>d</sup>	4.35 <sup>d</sup>
$\mu_D / \text{D}$ <sup>b</sup>	-	1.47 <sup>c</sup>	1.39 <sup>c</sup>	1.32 <sup>c</sup>	-

<sup>a</sup> The polarisability volume,  $\alpha'$ . For simplicity, units of  $\alpha'$  are often given in  $\text{\AA}^3$  where  $1 \text{\AA}^3 = 10^{-24} \text{cm}^3 = 10^{-30} \text{m}^3$ .

<sup>b</sup> The dipole moment,  $\mu_D$ . Values of  $\mu_D$  are commonly expressed in units of debyes (D), where  $1 \text{D} = 3.336 \times 10^{-30} \text{C m}$  (SI units).

<sup>c</sup> Value taken from the CRC handbook of Chemistry and Physics.<sup>25</sup>

<sup>d</sup> Value calculated using the method developed by Miller.<sup>24</sup>

### 1.B. Ion-pair formation

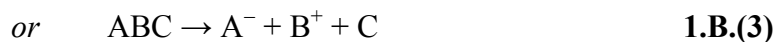
The second part of this thesis reports and discusses the results collected from an experiment designed to investigate the formation of ion pairs following the vacuum ultraviolet photoexcitation of a gas-phase molecule. The experiment is described in Chapter 2 and the results are discussed in Chapters 6 to 9.

The production of a cation-anion pair of fragments, following the unimolecular dissociation of a molecule, is called ion-pair formation. This is generically described for a diatomic molecule in reaction 1.B.(1).



For polyatomic molecules, the ion-pair process may also produce neutral fragments, as shown in reaction 1.B.(3), for example:





Typically, these unimolecular reactions are endothermic by between 8 and 25 eV. Therefore, energy in the vacuum ultraviolet (VUV) region of the electromagnetic spectrum must be absorbed by the molecule; Figure 1.B.(i) shows this region of the electromagnetic spectrum.

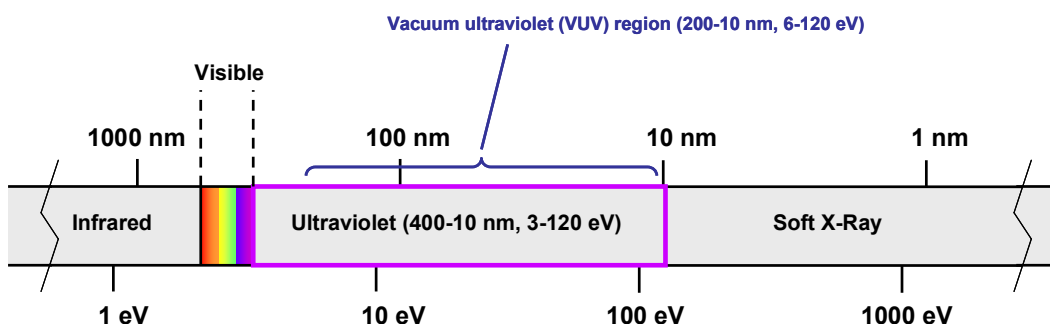


**Figure 1.B.(i).** Part of the electromagnetic spectrum, showing the vacuum ultraviolet region.

Lawley and Donovan suggest a model for the potential energy function of an ion-pair state. It incorporates an exponential repulsion term with a long-range Coulombic interaction:<sup>26</sup>

$$V(r) = A \exp(-\alpha r) - \frac{e^2}{4\pi\epsilon_0 r} + E_{\text{ip}} \quad \mathbf{1.B.(4)}$$

where  $V$  is potential energy,  $r$  is a bond distance along the reaction coordinate,  $A$  and  $\alpha$  are constants,  $e$  is the elementary charge ( $1.602\,18 \times 10^{-19}$  C), and  $\epsilon_0$  is the permittivity of free space ( $8.854\,19 \times 10^{-12}$  C<sup>2</sup> m<sup>-1</sup> J<sup>-1</sup>).  $E_{\text{ip}}$  is the energy required to place  $V(r)$  onto an absolute scale. For reaction 1.B.(1), for example,  $E_{\text{ip}} = D(\text{AB}) + IE(\text{B}) - EA(\text{A})$  where  $D$ ,  $IE$  and  $EA$  represent the bond dissociation energy, ionisation energy and electron affinity values,

respectively [the thermochemistry of ion-pair formation is discussed in more detail in Section 1.C.2]. This model assumes pure ionic behaviour and the equilibrium bond distance,  $r_e$ , is large.

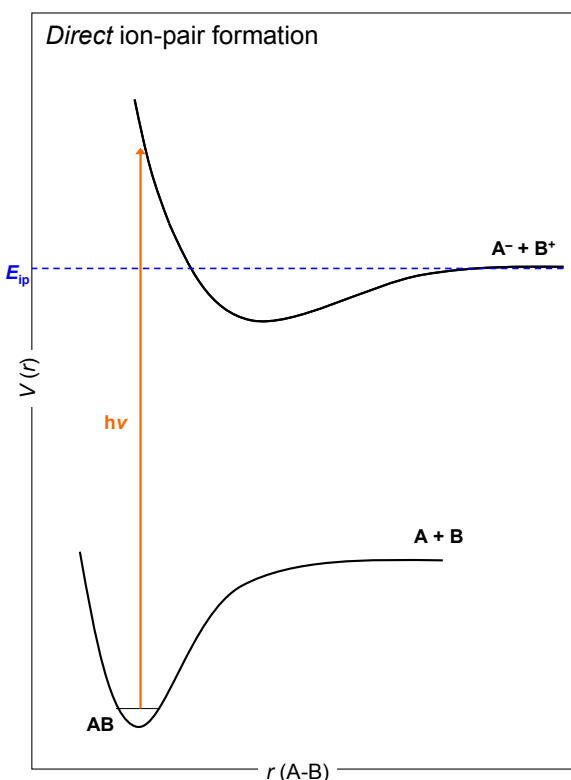


**Figure 1.B.(ii).** Potential energy ( $V$ ) as a function of bond distance ( $r$ ) showing the direct ion-pair formation process for the generic example  $AB \rightarrow A^- + B^+$ .  $E_{ip}$  represents the asymptotic ion-pair dissociation energy.

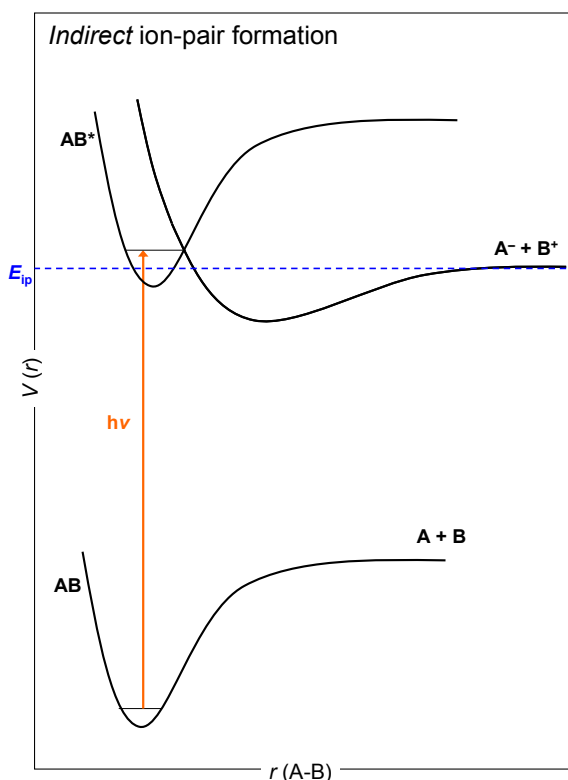


**Figure 1.B.(iii).** Potential energy ( $V$ ) as a function of bond distance ( $r$ ) showing the indirect ion-pair formation process, by the predissociation of a neutral excited state ( $AB^*$ ) for the generic example  $AB \rightarrow A^- + B^+$ .  $E_{ip}$  represents the asymptotic ion-pair dissociation energy.

Ion pairs may be formed by *direct* excitation to the ion-pair state [Figure 1.B.(ii)] or by *indirect* formation *via* predissociation of an initially-excited neutral state [Figure 1.B.(iii)]. Direct ion-pair formation involves excitation to the repulsive inner-wall of the potential energy surface above the asymptotic dissociation energy. Consequently, the transition has

very small Franck-Condon overlap and cannot probe vibrational states. By contrast, for the indirect process the restricting factor is not Franck-Condon overlap, but rather the degree of coupling between the initially-excited state and the ion-pair state. In addition, vibrational levels within the neutral excited state can be probed. Nevertheless, regardless of which process leads to the formation of ion pairs, competing exit channels resulting in neutral dissociation, ionisation or fluorescence are more probable. Quantum yields for ion-pair formation from polyatomic molecules are typically 0.1 % or less.<sup>27</sup>

### 1.B.1. Rydberg states

Rydberg states are commonly identified as the initially-excited intermediate involved in the indirect ion-pair formation process [*i.e.* AB\* in Figure 1.B.(iii)].<sup>28,29</sup> A molecular Rydberg state is a high-lying *neutral* state where an electron is excited such that it observes the molecule as a distant positively-charged core.<sup>30</sup> The *Rydberg electron* resides in a large *Rydberg orbital*, an atomic-like orbital which is very large compared to the size of the molecule. Series of Rydberg states converge to ionisation limits and generally obey the Rydberg formula:<sup>29,31</sup>

$$E_n = IE - \left[ \frac{R_\infty}{(n - \delta)^2} \right] \quad \mathbf{1.B.(5)}$$

where  $E_n$  is the energy of the  $n$ th Rydberg state,  $IE$  is the ionisation energy to which the Rydberg series converges,  $R_\infty$  is the Rydberg constant ( $109\,737\text{ cm}^{-1}$  or  $13.606\text{ eV}$ , the  $IE$  of atomic hydrogen),  $n$  is the principal quantum number of the Rydberg orbital, and  $\delta$  is the quantum defect. The fragment of equation 1.B.(5) in square brackets is often defined in the literature as the *term value*.



The value of  $\delta$  depends on the angular momentum quantum number,  $l$ , of the Rydberg orbital. For example, following equation 1.B.(5), the value of  $\delta$  will be the same for each member of an  $ns$  (or  $np$  or  $nd$ ... *etc.*) Rydberg series. Typical values of  $\delta$  for period 1 and 2 elements are: for  $ns$  series, 0.9-1.2; for  $np$  series, 0.3-0.6; for  $nd$  series,  $< 0.1$ .<sup>31</sup> In addition,  $\delta$  values increase with increasing period number within the periodic table of elements. For example, an  $np$  Rydberg orbital in Cl will have a larger quantum defect than an  $np$  Rydberg orbital in F. Thus,  $\delta$  represents an arbitrary number, the magnitude of which reflects the degree of orbital-core penetration, including the shielding effects of ‘core’ electrons on the Rydberg electron. The Rydberg formula originated from the analysis of the spectrum of atomic hydrogen – a single-electron system with no requirement to define  $\delta$  [for atomic H, in equation 1.B.(5),  $\delta = 0$ ]. The quantum defect is introduced for many-electron systems to account for electron-electron interactions. Thus, the smaller the value of  $\delta$ , the more the system behaves like a hydrogen atom.

Peaks in an ion-pair spectrum (providing a value for  $E_n$ ) may be assigned to a Rydberg orbital using the Rydberg formula if the value for the  $IE$  is known. In practice, it is common that several assignments exist for the same value of  $E_n$  because of many available combinations for  $IE$ ,  $n$  and  $\delta$ . Assignments presented in Chapters 6 to 9 are therefore given with an appropriate degree of uncertainty. A difficulty in assigning *molecular* Rydberg orbitals is that only quantum defect values for atomic systems are well known. In this work the tabulations by Theodosiou *et al.*<sup>32</sup> were used as a guide to identify appropriate quantum defect values. More confident assignments require  $E_n$  to be known more accurately (*i.e.* from higher-resolution spectra), or several peaks to be fitted to the same Rydberg series (more common from total photoabsorption spectroscopy or atomic spectra).

### 1.C. Thermochemistry

The standard enthalpy of a reaction ( $\Delta_r H^\circ$ ) can be calculated if the standard enthalpies of formation ( $\Delta_f H^\circ$ ) for each individual reactant and product species are known. The two experiments discussed in this thesis are performed at 298 K, and thus the following relationship is used:

$$\Delta_r H_{298}^\circ = \sum \Delta_f H_{298}^\circ(\text{products}) - \sum \Delta_f H_{298}^\circ(\text{reactants}) \quad \text{1.C.(1)}$$

Values for  $\Delta_r H_{298}^\circ$  are presented in the text. The  $\Delta_f H_{298}^\circ$  values used to calculate these enthalpies of reaction, and their sources, are tabulated in Appendix I. Enthalpy values are commonly expressed in units of  $\text{kJ mol}^{-1}$ .

In reality it is the change in standard *Gibbs energy* of reaction ( $\Delta_r G^\circ$ ), and not *enthalpy*, which determines the thermodynamic feasibility of a reaction. The relationship between  $\Delta_r G^\circ$  and  $\Delta_r H^\circ$  is given below:

$$\Delta_r G^\circ = \Delta_r H^\circ - T\Delta_r S^\circ \quad \text{1.C.(2)}$$

where  $T$  is temperature in K and  $\Delta_r S^\circ$  is the standard entropy of reaction (note that usually  $\Delta_r S^\circ$  is expressed in  $\text{J K}^{-1} \text{mol}^{-1}$ ). Thus, the effects of entropy are ignored when using enthalpies calculated for ion-molecule reactions or ion-pair dissociation reactions in this thesis (see Sections 1.C.1 and 1.C.2 below). In equation 1.C.(2) the  $T\Delta_r S^\circ$  term is usually small compared to the magnitude of  $\Delta_r G^\circ$  or  $\Delta_r H^\circ$ , so the use of  $\Delta_r H^\circ$  is justified – provided this is acknowledged, particularly when considering small positive values for  $\Delta_r H^\circ$ . In addition, the magnitude of  $T\Delta_r S^\circ$  may often lie within the uncertainty of a calculated change in enthalpy for the reaction.

*1.C.1. Thermochemistry applied to ion-molecule reactions*

When performing ion-molecule reaction experiments, the reactant species are known and the product ion can be detected. However, using the SIFT apparatus (described in Chapter 2) there is no means by which any neutral product species can unambiguously be identified. Some insight into the neutral products can be gained by calculating reaction enthalpies for the different possible outcomes – only exothermic reaction channels need to be considered. For example, in the reaction of the cation  $A^+$  with molecule BCD, the product  $AB^+$  is detected, and so there are two possible outcomes:



If reaction 1.C.(3) is exothermic and reaction 1.C.(4) is endothermic, then by the process of elimination the neutral product CD can be assigned to this reaction. In practice it is not often this clear cut, however, knowing such thermochemical information about a reaction is useful and can uncover interesting information. For example, experimentally two species may not react, even though theoretically exothermic product channels are available. Therefore, if only indirectly, energetics can provide information about the dynamics of a reaction.

*1.C.2. Thermochemistry applied to ion-pair formation*

For the generic reaction  $AB \rightarrow A^- + B^+$ , the asymptotic ion-pair formation energy,  $E_{ip}$ , may be expressed using either of the following two equations:

$$E_{ip} = D(A-B) + IE(B) - EA(A) \quad \mathbf{1.C.(5)}$$

$$E_{ip} = IE(AB) + D(A-B^+) - EA(A) \quad 1.C.(6)$$

where  $D$  is a bond dissociation energy,  $IE$  an ionisation energy and  $EA$  an electron affinity. One advantage of equation 1.C.(6) is to identify that ion-pair formation often occurs energetically before the onset to ionisation:  $E_{ip} < IE$  when  $EA(A) > D(A-B^+)$ . This is usually the case when  $A$  is a halogen atom because its  $EA$  is large. Below the  $IE$  any ion formed must arise as a result of an ion-pair reaction, and positive or negative species can be detected by experiment with relative ease. Above the  $IE$ , however, cations and free electrons are produced which provide additional experimental challenges.

In practice  $E_{ip}$  is not known and it is more convenient to use the experimental appearance energy,  $AE$ , instead. The  $AE$  is the lowest energy at which ion-pair formation is detected, *i.e.* when a signal is first observed above the background noise (see Chapter 2 for experimental details). This can be considered as the value for  $h\nu$  as shown earlier in Figures 1.B.(ii) and 1.B.(iii). Equations 1.C.(5) and 1.C.(6) may now be re-written as inequalities:

$$AE \geq D(A-B) + IE(B) - EA(A) \quad 1.C.(7)$$

$$AE \geq IE(AB) + D(A-B^+) - EA(A) \quad 1.C.(8)$$

These inequalities can then be used to calculate upper limits to bond dissociation energy or ionisation energy values, or indeed lower limits to electron affinities.<sup>28</sup>

In the experiments discussed in this work the negative ion formed is detected and identified by its mass (see Chapter 2). However, the positive ion and any neutral fragments also produced by the ion-pair reaction are not known. The enthalpy change for a unimolecular ion-pair reaction may be calculated using equation 1.C.(1) and compared with

onsets to features in a spectrum. Previous experimental results show that the  $AE$  determined by experiment commonly occurs at, or just after the calculated threshold (*i.e.* the calculated value for  $E_{ip}$ ).<sup>28</sup> Assigning a reaction to the  $AE$  is straightforward because usually only one ion-pair dissociation is energetically possible; for the lowest-energy ion-pair process only one bond is broken and no neutral fragments are produced. Assigning a reaction to higher-energy features in a spectrum is more difficult because of the many different energetically-accessible ion-pair dissociation channels.

### 1.C.3. Energy and enthalpy

In this work the ‘calculated  $E_{ip}$ ’ values are determined from equation 1.C.(1) and are in fact, *enthalpy* changes. Before proceeding, *energy* and *enthalpy* must be distinguished. Consider a molecule of an ideal gas reacting with a photon to produce a positive-negative pair of ions. The enthalpy change,  $\Delta H$ , does not allow for the fact that some internal energy is transferred to the surroundings as an increase in volume and/or pressure; the number of gaseous species increases due to the unimolecular dissociation reaction [(the number of product species minus the number of reactant species)  $> 0$ ], and the products are produced with translational momentum. The enthalpy change of a perfect gas is defined by:

$$\Delta H = \Delta U + RT\Delta n \quad \text{1.C.(9)}$$

where  $U$  is the internal energy,  $R$  the gas constant and  $T$  absolute temperature. Energy and enthalpy are only equivalent quantities when  $T = 0$  or  $\Delta n = 0$ . Corrections to  $AE_T$  values, so that they may be compared to those for  $\Delta H_T$ , have been outlined by Traeger and McLoughlin.<sup>33</sup> At 298 K, however, such corrections are relatively small (typically  $< 0.1$  eV), falling within the combination of uncertainty in calculated  $\Delta_r H^\circ$  and experimental energy

values determined in this work. The thermal correction is therefore ignored here: experimental *energy* values are compared like-for-like with calculated *enthalpy* changes. All measurements were made at 298 K. Note that this paragraph applies equally to ion-molecule reactions (*e.g.* the recombination energy of an ion compared to a reaction enthalpy change).

# Chapter 2:

## *The experiments*

### **2.A. Ion-molecule reactions**

#### *2.A.1. The selected ion flow tube*

The Selected Ion Flow Tube (SIFT) is an experimental apparatus used to study gas-phase ion-molecule reactions. An experimental rate coefficient can be measured and the ionic product species for the reaction can be identified. The relative branching ratios (BRs) for the detected products can also be determined. The SIFT technique has been described in detail in several review papers.<sup>34-36</sup> A description of the experiment, and how rate coefficients and BRs are determined, is also presented here.

The SIFT is vacuum sealed, and consists of three distinct sections. First is the ion source, where cations and/or anions are produced from a neutral precursor molecule by electron impact ionisation. Second is the flow tube, where helium buffer gas carries the ions downstream to a point where the neutral reactant is injected, and the reaction may occur. Third is the detection region, where the product ions are mass filtered and detected. Figure 2.A.(i) presents a basic schematic of the SIFT, showing how these three sections relate to one another.

The ion source consists of a small closed chamber containing a tungsten filament and a series of electrostatic lenses. A simple cartoon of the ion source, showing the example of selecting  $\text{C}_2\text{F}_4^+$  ions from  $\text{C}_3\text{F}_8$  source gas, is presented in Figure 2.A.(ii).

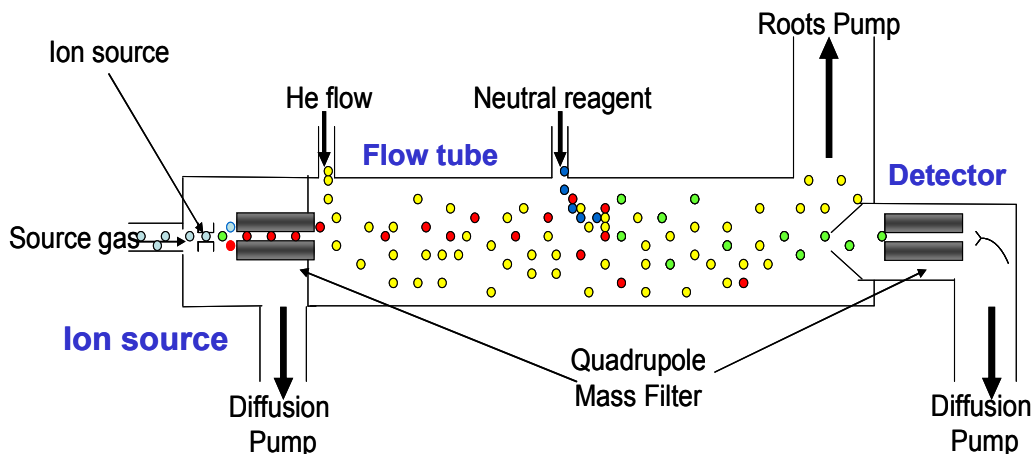


**Figure 2.A.(i).** A basic schematic of the Selected Ion Flow Tube apparatus. The red circles represent the ions generated in the ion source, the yellow circles represent the helium buffer gas, the blue circles represent the neutral reactant gas, and the green circles represent the product species.

When no gas is flowing a diffusion pump, backed by a common rotary pump, achieves a vacuum pressure of *ca.*  $10^{-6}$  mbar. During operation, a neutral source gas is introduced into the chamber such that a relatively high pressure is maintained, *ca.*  $10^{-4}$  mbar. Molecules from the source gas are ionised by 70 eV electrons; the filament emits electrons which are subsequently accelerated by an applied potential difference. This process may produce many different cation and anion species. For example,  $\text{C}_2\text{F}_6$  may be used to produce the ions  $\text{F}^+$ ,  $\text{CF}^+$ ,  $\text{CF}_2^+$ ,  $\text{CF}_3^+$ ,  $\text{F}^-$  and  $\text{CF}_3^-$ . The reactant ions used in this work and their corresponding source gases are listed in Table 2.A.(I). For the ions to enter the flow tube they must first pass through the electrostatic lenses and then through a quadrupole mass filter. The quadrupole



can be set to a desired mass-to-charge ratio ( $m/z$ ) value, with 1 atomic mass unit (a.m.u) resolution, such that only the desired reactant ion is selected.

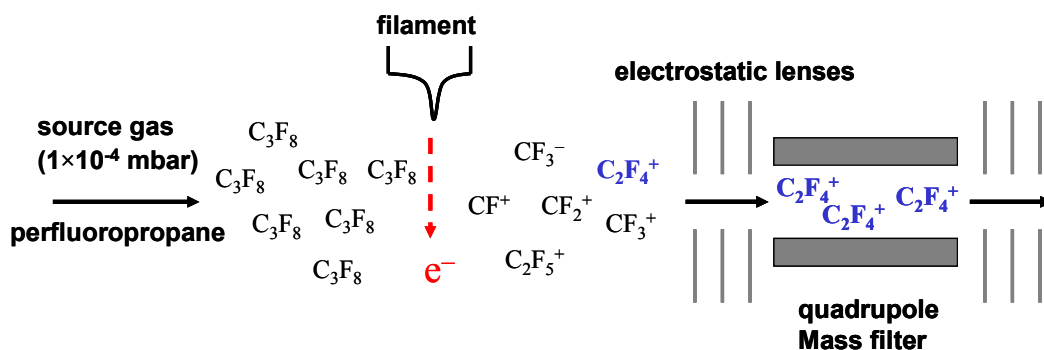


**Figure 2.A.(ii).** A simple cartoon of the ion source in the Selected Ion Flow Tube, showing the example of selecting  $C_2F_4^+$  ions using perfluoropropane source gas.

The ion signal is then maximised by monitoring the signal at the detection region (discussed below) by tuning the electrostatic lenses. The lens settings in the ion source are significantly different for positive or negative ions. For example, if the signal is maximised to transmit  $CF_3^+$  ions (detection region set to positive mode) then  $CF_3^-$  anions produced will be repelled by the lens system, and not reach the mass filter. In addition, altering the pressure in the ion source can have an effect on the resultant ion signal.

The selected ions enter the flow tube along with helium (99.997% purity) buffer gas. The helium gas is passed through liquid nitrogen to increase its purity, and injected into the flow tube in a way which is designed to minimise back streaming of helium into the ion source.<sup>34</sup> The flow tube is 1 m in length and 8 cm in diameter. During operation it is filled with 0.5 Torr of buffer gas, which is drawn downstream at a velocity of *ca.*  $100 \text{ m s}^{-1}$  by an Edwards EH 2600 roots pump, backed by an Edwards E1M176 rotary pump. The conditions inside the

flow tube are thermal, and the measurements in this work are all reported at 298 K. Any excited ions produced in the ion source are expected to be collisionally cooled by the buffer gas.

**Table 2.A.(I).** Source gases used to produce reactant cations and anions in the ion source.

<b>Ion</b>	<b>Source gas</b>	<b>Process</b>
$\text{CF}^+$	$\text{CF}_4 / \text{C}_2\text{F}_6 / \text{C}_3\text{F}_8$	single electron impact
$\text{CF}_2^+$	$\text{CF}_4 / \text{C}_2\text{F}_6 / \text{C}_3\text{F}_8$	single electron impact
$\text{CF}_3^+$	$\text{CF}_4 / \text{C}_2\text{F}_6 / \text{C}_3\text{F}_8$	single electron impact
$\text{C}_2\text{F}_4^+$	$\text{C}_3\text{F}_8$	single electron impact
$\text{O}_2^-$	$\text{N}_2 + \text{O}_2$ mixture	collisionally stabilised electron attachment
$\text{O}^-$	$\text{N}_2\text{O}$	dissociative electron attachment
$\text{OH}^-$	$\text{N}_2\text{O} + \text{CH}_4$ mixture	dissociative electron attachment forming $\text{O}^-$ , followed by H abstraction from $\text{CH}_4$
$\text{F}^-$	$\text{C}_2\text{F}_6$	dissociative electron attachment
$\text{CF}_3^-$	$\text{C}_2\text{F}_6$	dissociative electron attachment

At a known distance along the flow tube the neutral reactant gas is introduced. A simple cartoon of the flow tube is shown in Figure 2.A.(iii), using the example of  $\text{C}_2\text{F}_4^+$  ions reacting with  $\text{C}_2\text{H}_3\text{F}$ . All species, including helium, reactants and products, will then continue down the flow tube towards the detection region of the apparatus.

A simple cartoon of the detection region of the SIFT apparatus is shown in Figure 2.A.(iv). At the end of the flow tube is a cone shaped end plate, with a 1 mm diameter hole at the centre. It is this orifice which samples the gas from the flow tube, and is the only connection to the detection region. The main bulk gas flow is drawn away by the roots pump as shown in Figures 2.A.(iii) and in 2.A.(iv). The detection region is differentially pumped by a diffusion pump backed by a common rotary pump; the base pressure in this region is *ca.*  $10^{-6}$  mbar (compared to 0.7 mbar in the flow tube) and during operation the small amount of sampled gas through the end plate raises the pressure to *ca.*  $10^{-5}$  mbar. The end plate not only

samples the gas, but also acts as a Faraday plate. It has a floating voltage applied (being electrically isolated from the rest of the system), and the current produced is proportional to the number of ions hitting it.

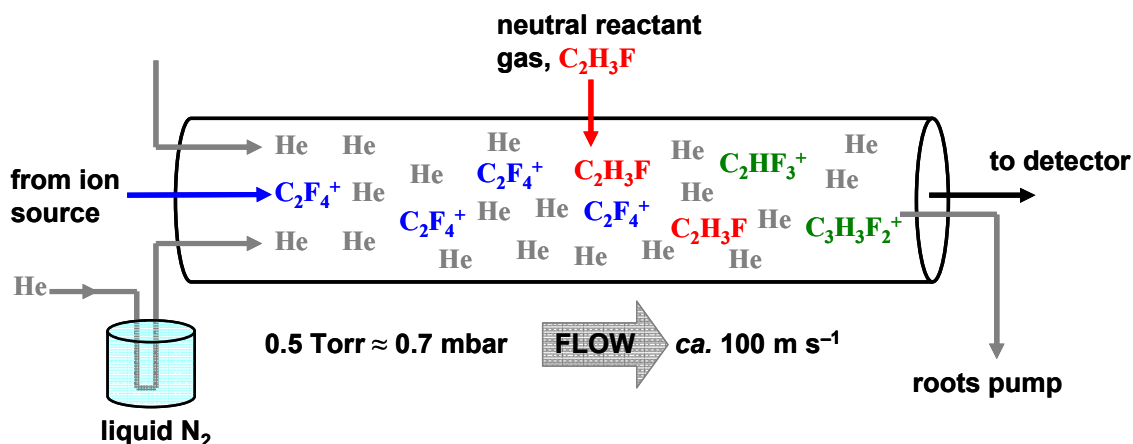


**Figure 2.A.(iii).** A simple cartoon showing the flow tube part of the Selected Ion Flow Tube apparatus. The example of the reaction between  $\text{C}_2\text{F}_4^+$  with  $\text{C}_2\text{H}_3\text{F}$  is used. The helium buffer gas is shown in grey, the reactant ion in blue, the reactant neutral in red, and the product ions in green.

Measurement of the current is therefore useful to tune the ion signal from the ion source, as discussed above. In addition, when reacting anions in the SIFT, a drop in the ion current can indicate a reaction is ejecting electrons; an electron is much lighter than an atomic or molecular anion, and so hits the wall of the flow tube rather than reaching the Faraday plate, which results in the total ion current decreasing. Ions are drawn into the quadrupole mass filter by electrostatic lenses, and then towards a channeltron electron multiplier which records the resultant ion signal. The ion signal is recorded as a function of  $m/z$ , and a mass spectrum is obtained.

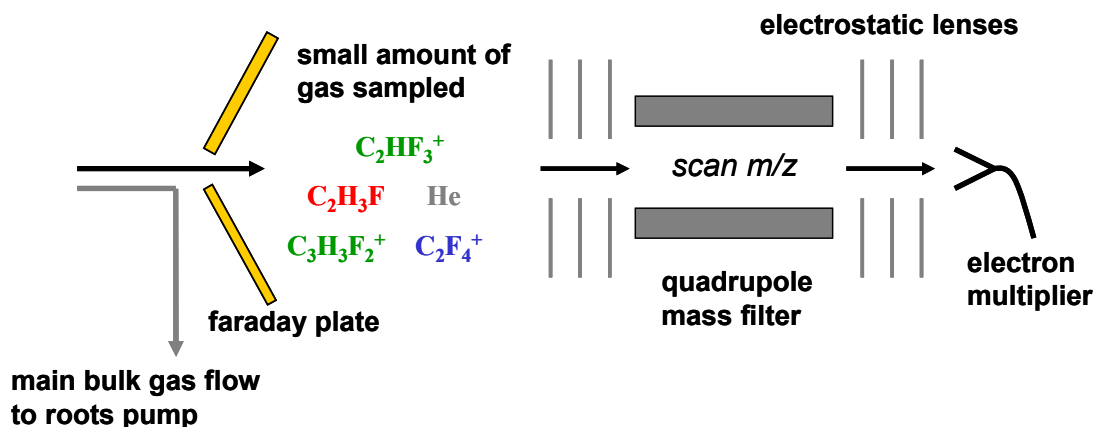


**Figure 2.A.(iv).** A simple cartoon showing the detection region of the Selected Ion Flow Tube apparatus showing the example of reacting  $\text{C}_2\text{F}_4^+$  with  $\text{C}_2\text{H}_3\text{F}$ .

### 2.A.2. Determining the reaction rate coefficient

In the reactions performed in the SIFT the concentration of the reactant neutral molecule is much greater than the concentration of the reactant ion. This allows pseudo first-order kinetics to be applied, and if we consider the generic ion-molecule reaction as being  $\text{A}^+ + \text{B}$ , then the integrated rate equation can be given as:

$$\frac{\ln[\text{A}^+]_{\text{rel}}}{[\text{B}]} = -_2kt \quad \text{2.A.(1)}$$

where  $[\text{A}^+]_{\text{rel}}$  is the relative ion concentration (this is simply the ion count recorded by the mass spectrometer),  $[\text{B}]$  is the neutral reactant concentration [the absolute concentration of B (in molecules  $\text{cm}^{-3}$ ) is measured during the experiment as described in Appendix II],  $_2k$  is the bimolecular rate coefficient, and  $t$  is the reaction time. Equation 2.A.(1) shows that the

gradient of a linear plot of  $\ln[A^+]_{rel}$  vs.  $[B]$  will be equal to  $-_2kt$ . An example of such a plot, for the reaction between  $CF_3^+$  and  $C_2H_3F$ , is shown in Figure 2.A.(v).

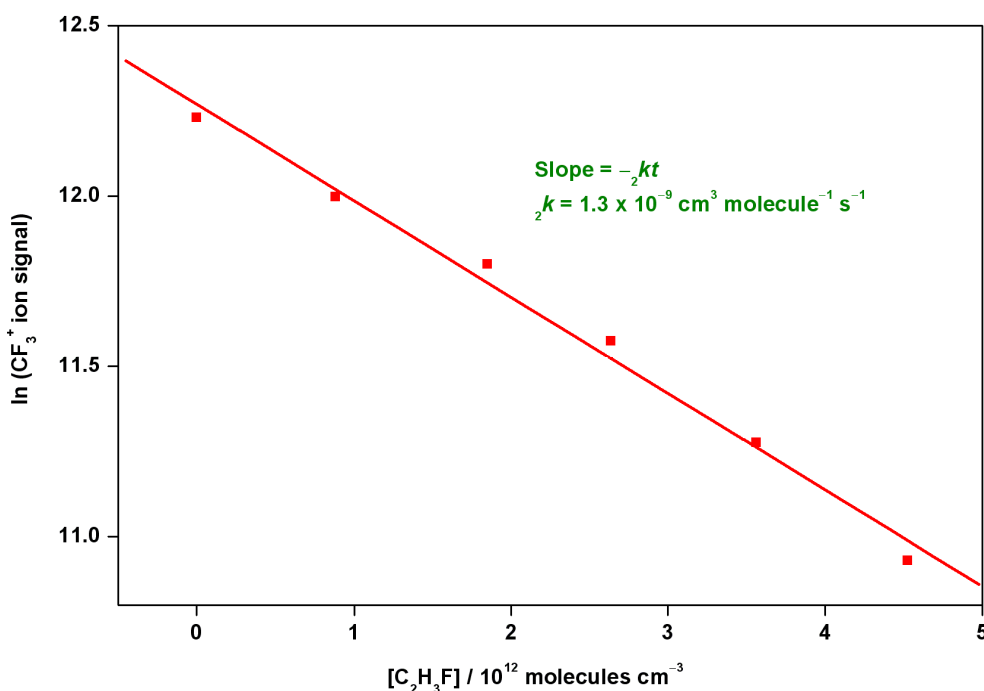


**Figure 2.A.(v).** A rate coefficient plot for the reaction between  $CF_3^+$  and  $C_2H_3F$ . Computer software fits the data points to a straight line. The reaction time in s,  $t$ , is also calculated by the data analysis software, and a value for the bimolecular rate coefficient,  $_2k$ , is given in units of  $\text{cm}^3 \text{ molecule}^{-1} \text{ s}^{-1}$ .

The reaction time cannot be measured independently, but can be calculated by dividing the reaction length,  $z$ , by the ion flow velocity,  $v_i$ . The reaction length is a known value defined by the point along the flow tube where the neutral reactant enters, and Smith and Adams have given a detailed account of how  $v_i$  can be measured.<sup>34</sup> An experimental value for  $_2k$  (in  $\text{cm}^3 \text{ molecule}^{-1} \text{ s}^{-1}$ ) can therefore be calculated. Such measurements are repeated several times until a consistent result is achieved, and the estimated uncertainty in the value obtained is *ca.*  $\pm 20\%$ . Experimentally-measured bimolecular rate coefficients are referred to as  $k_{\text{exp}}$ .

In some reactions performed in the SIFT, an association product is observed. These reactions are pressure dependent due to the involvement of a third body,  $M$ , and so the rate equation includes a third-order rate coefficient,  ${}_3k$ :



$$rate = {}_3k [M][A^+][B] \quad \mathbf{2.A.(3)}$$

where the square brackets represent concentrations of the respective species in molecule  $\text{cm}^{-3}$ ,  ${}_3k$  has units of  $\text{cm}^6 \text{ molecule}^{-2} \text{ s}^{-1}$ , and the *rate* has units of  $\text{molecule cm}^{-3} \text{ s}^{-1}$ . In the SIFT  $M$  is most likely to be helium, and in equation 2.A.(3)  $[M]$  can be considered constant. A bimolecular rate coefficient is still measured for association reactions as described above, and shown in Figure 2.A.(v), but in these cases it is a *pseudo* second-order rate coefficient,  ${}_2k'$ . This value can be related to  ${}_3k$  if the concentration of  $M$  is known:

$${}_2k' = {}_3k [M] \quad \mathbf{2.A.(4)}$$

In association reactions discussed in this report the value for  ${}_2k'$  is quoted because it can then be compared with other bimolecular rate coefficients. However, the rate coefficient of an association reaction is only valid at a given pressure of  $M$ , and so where  ${}_2k'$  is quoted the pressure of helium recorded at the time is also given. Knowing the pressure of  $M$  allows  $[M]$  to be calculated in much the same way as  $[B]$  is calculated, as described in Appendix II.

### 2.A.3. Determining the product branching ratios

Product branching ratios (BRs) are recorded in much the same way as the rate coefficient is measured, however, rather than the reactant ion signal, it is the *product* ion signals which are recorded as a function of neutral reactant concentration.

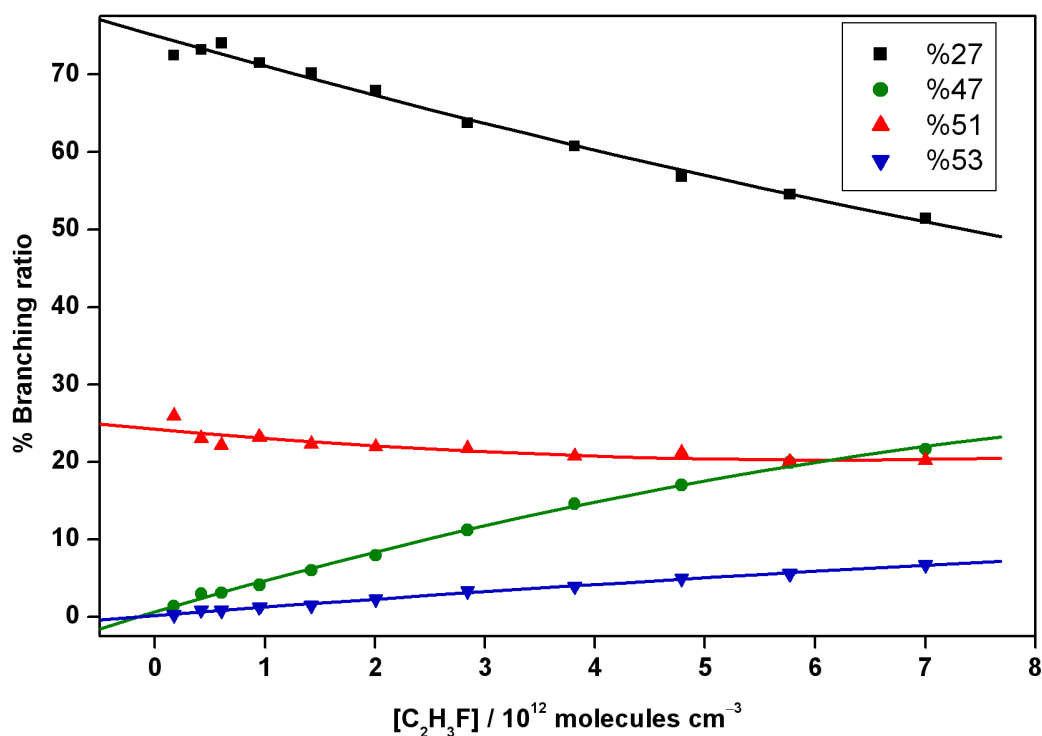


**Figure 2.A.(vi).** A branching ratio (BR) plot for the products detected from the reaction between  $\text{CF}_3^+$  and  $\text{C}_2\text{H}_3\text{F}$ . The products are indicated by their  $m/z$  values shown in the top right corner of the graph. At zero  $\text{C}_2\text{H}_3\text{F}$  concentration the BRs are 75 % and 25 % for the primary products  $\text{C}_2\text{H}_3^+$  ( $m/z$  27 in black) and  $\text{CHF}_2^+$  ( $m/z$  51 in red), respectively. The plots corresponding to  $m/z$  47 (green) and  $m/z$  53 (blue) show a BR of 0 %, indicating they are secondary products.

The individual product ion counts are converted into a percentage of the total product ion counts, and plotted using data analysis software. A line through the data points is added using a polynomial fit, and the % BR values are taken by extrapolating to zero neutral reactant

concentration, which aims to eliminate any contributions from secondary reactions. An example of such a plot is provided in Figure 2.A.(vi) for the reaction between  $\text{CF}_3^+$  and  $\text{C}_2\text{H}_3\text{F}$ . The mass spectrum recorded for this reaction showed product peaks at  $m/z$  27 ( $\text{C}_2\text{H}_3^+$ ), 47 ( $\text{C}_2\text{H}_4\text{F}^+$ ), 51 ( $\text{CHF}_2^+$ ) and 53 ( $\text{CH}_2\text{F}_2\cdot\text{H}^+$ ). For the products at  $m/z$  47 and 53 a BR of 0 % is determined, indicating these are secondary products. The primary products for this reaction are  $m/z$  27 ( $\text{C}_2\text{H}_3^+$ ) and  $m/z$  51 ( $\text{CHF}_2^+$ ) with BRs of 75 % and 25 %, respectively.

The reported BR values have a  $\pm 20$  % uncertainty. This error is an estimate based on the variation in experimentally detected relative ion signals and the polynomial data fitting; it is noteworthy that  $\pm 20$  % is a modest estimate for the example data provided in Figure 2.A.(vi).

## **2.B. Negative photoion spectroscopy**

### *2.B.1. The synchrotron radiation source*

Energy must be absorbed by a molecule in order for ion-pair dissociation to occur. *Synchrotron radiation* is ideal for such experiments because it provides a bright, monochromated and tunable energy source across the entire electromagnetic spectrum.<sup>37</sup> Synchrotron radiation sources accelerate electrons at relativistic velocities in a circular orbit using magnets; this takes place in a *storage ring*, tens of metres in diameter. The accelerating charges emit collimated light tangentially to the orbital path. Collected from the storage ring at a *beamline*, the light is optically focused into a monochromator prior to entering the experimental endstation. The experiments described in Chapters 6-8 utilised vacuum ultraviolet (VUV) radiation from beamline 3.1 at the UK Daresbury Synchrotron Radiation Source (SRS).



The Wadsworth monochromator, focal length 1 m, installed on beamline 3.1 is designed to provide the user with a high flux beam, albeit at the expense of wavelength resolution; it does not have an entrance slit limiting the amount of light hitting the *diffraction grating*, as is common in many other designs.<sup>38</sup> A diffraction grating consists of a large number of equally spaced parallel grooves cut into a reflective surface.

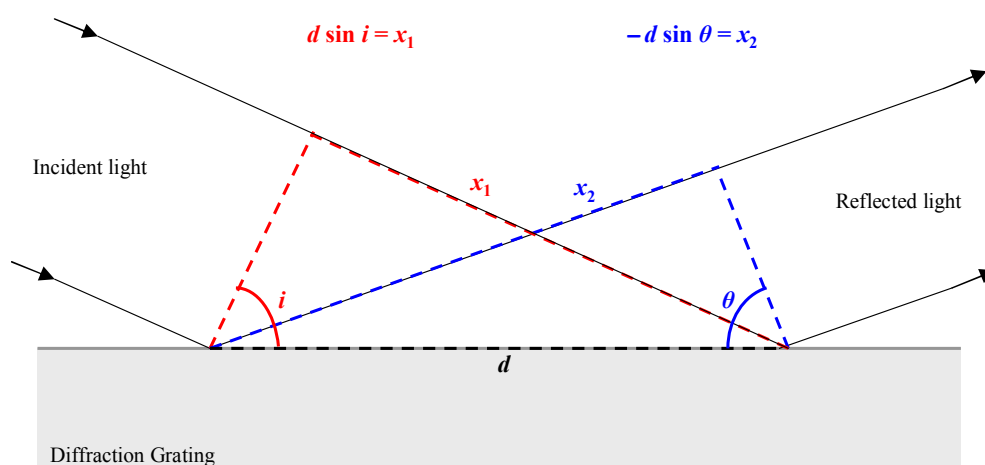


**Figure 2.B.(i).** A simple diagram to show how a diffraction grating works. Distances  $x_1$  and  $x_2$  represent the side of a right angle triangle ‘opposite’ to the angles  $i$  and  $\theta$ , respectively. Distance  $d$  represents the spacing between grooves on the surface of the grating.

The angle of the grating relative to the incident light determines which wavelengths will interfere constructively when reflected from the surface. It can be observed from Figure 2.B.(i), that for constructive interference of light to occur, the difference between distances  $x_1$  and  $x_2$  when divisible by an integer must equal the wavelength,  $\lambda$ ; note that angles  $i$  and  $\theta$  are both measured relative to the same normal reference, one angle taking a positive value, the other a negative value. Distance  $d$  represents the spacing between grooves on the surface of the grating. The relationship between the relative position of the grating (with respect to angles  $i$  and  $\theta$ ),  $d$  and  $\lambda$  can be written as follows:

$$m\lambda = d (\sin i + \sin \theta) \quad \mathbf{2.B.(1)}$$

where  $m$  represents an integer value. When angles  $i$  and  $\theta$  are equal and opposite, all wavelengths of light are constructively reflected and  $m$  takes the value of zero: hence the term *zero-order* radiation. During scanning experiments, however, *first-order* radiation is used ( $m = 1$ ). Higher orders of radiation become a problem when the desired energy of radiation is relatively low, *i.e.* between 8 and 16 eV. For example, a first-order spectrum at 10 eV may contain unwanted contributions from second-order radiation at 20 eV. In such cases, a lithium fluoride window may be placed in the path of the beam; LiF absorbs all radiation above 11.7 eV, thus eliminating contributions from higher-orders.

Two different diffraction gratings are installed within the beamline 3.1 monochromator. The medium energy grating (MEG) is efficient in the range 8 to 18 eV and the high energy grating (HEG) from 12 to 35 eV. The beam of light reflected from the diffraction grating is directed through a manually controlled slit, known as the *exit slit*, before passing into the experimental endstation. A reduced slit width provides a higher resolution of light for the experiment, but the total flux is reduced; likewise a larger slit provides higher flux for the experiment, but at the expense of resolution.

A few experiments discussed in Chapter 9 used the 5 m focal length McPherson monochromator installed on beamline 3.2 at the SRS. This monochromator provides superior resolution for a given exit slit width compared to 3.1 due to the longer focal length, but the principles of operation are exactly the same as described above.

### 2.B.2. The experimental endstation

A simple diagram showing the main components and setup of the experimental endstation is presented in Figure 2.B.(ii), and should be referred to when reading the description below.

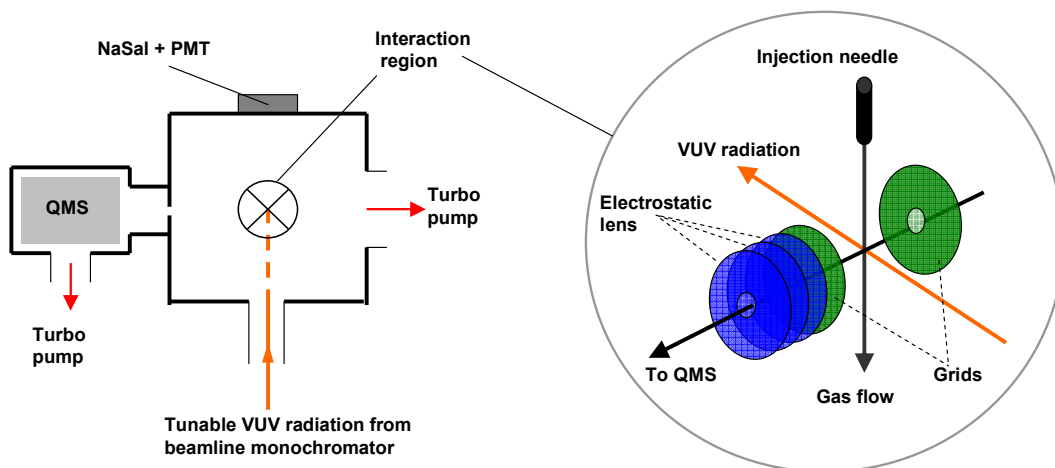


**Figure 2.B.(ii).** A simple diagram of the experimental endstation used for detecting negative photoions.

A 2 mm diameter, 300 mm long capillary light guide connecting the experimental apparatus to the beamline directs the monochromatised light to the interaction region. The gas under study is injected *via* a needle generating an effusive directed jet (with no internal cooling) which bisects orthogonally the incident photon beam. The crossing point, which dictates the centre of the interaction region, is positioned in the middle of two grids on the third orthogonal axis. A potential difference across the grids sweeps negative ions along this axis towards a 3-element electrostatic lens for focusing, and into a Hiden Analytical HAL IV triple quadrupole mass spectrometer (QMS) for mass selection. Detection is achieved by a channeltron electron multiplier. Sensitivity is considerably enhanced by differential pumping which reduces the number of free electrons and secondary collisions in the QMS. Spectra in

which the monochromator is scanned are flux normalised using a sodium salicylate (NaSal) window and visible photomultiplier tube (PMT) combination, which has a constant response over the energy range of the experiments. The apparatus and QMS, connected *via* a 1 mm diameter aperture, are pumped separately by turbo pumps which are backed by a common rotary pump, and the base pressure of the apparatus is approximately  $10^{-7}$  mbar. With sample gas running, the typical pressure in the chamber is raised to  $10^{-5}$  mbar. The pressure inside the chamber is measured using an ionisation gauge, the sensitivity of which to the sample gas under study is calibrated in a separate experiment relative to  $N_2$  gas using a capacitance manometer.<sup>39</sup>

Mass spectra are recorded to observe all anions produced from photoabsorption of the sample gas by exposure to white light (*i.e.* zero-order radiation). The mass-to-charge ratio ( $m/z$ ) of each peak in the mass spectrum is then fixed and the signal recorded as a function of photon energy, typically over the range 8 to 35 eV. In addition, for each anion, its signal is recorded at a fixed photon energy (usually the energy of a peak observed in the spectrum) as a function of sample gas pressure over the typical range  $(0.5 - 5.0) \times 10^{-5}$  mbar. Anions which show a non-linear dependence with pressure cannot be assigned as ion pair products, and their signal is most likely influenced by secondary processes. Anions which show a linear dependence of signal with pressure can be attributed to ion-pair formation; being a unimolecular process, the rate of formation of ion pairs is expected to obey first-order kinetics. Full details of the pressure dependencies are given in Chapters 6-9.

### 2.B.3. Determining absolute ion-pair cross sections

Anion spectra resulting from ion-pair formation are presented as cross sections,  $\sigma$ , in absolute units of  $\text{cm}^2$ . The value of  $\sigma$  at a given photon energy  $h\nu$  is calculated as follows:

$$\sigma(h\nu) = k \left( \frac{SM}{f r p} \right) \quad \text{2.B.(2)}$$

where  $S$  is the detected signal in counts  $\text{s}^{-1}$ ,  $M$  is the relative mass sensitivity of the QMS,  $f$  is the relative photon flux (effectively a measure of the grating efficiency),  $r$  is the storage ring current,  $p$  is the sample gas pressure corrected for ionisation gauge sensitivity and  $k$  is a normalisation constant. Normalisation to  $f$ ,  $r$  and  $p$  is straight forward, but this is not the case for  $M$ . An extensive set of experiments was performed to determine  $M$  as a function of  $m/z$ , described below in Section 2.B.4.

The corrected signal (to  $M$ ,  $f$ ,  $r$  and  $p$ ) for  $\text{F}^-$  from  $\text{SF}_6$  is normalised to the known cross section at 14.3 eV of  $(7 \pm 2) \times 10^{-21} \text{ cm}^2$ .<sup>40</sup> Likewise, the corrected signal for  $\text{F}^-$  from  $\text{CF}_4$  is normalised to its value at 13.9 eV of  $(1.25 \pm 0.25) \times 10^{-21} \text{ cm}^2$ .<sup>41</sup> [It is noted that these known cross section values are not strictly absolute, but are obtained from calibrated measurements of  $\text{O}^-$  yields from  $\text{O}_2$ .]<sup>42</sup> Thus, normalisation factors  $k(\text{SF}_6)$  and  $k(\text{CF}_4)$  are determined. An average of these two  $k$  values is then used in equation 2.B.(2) to determine cross section values for anions from other gases. In theory, these two values should be the same. In practice, they vary by a factor ranging from 1.2 to 1.7. These measurements were made at every visit to the SRS, and the appropriate average value of  $k$  was used.

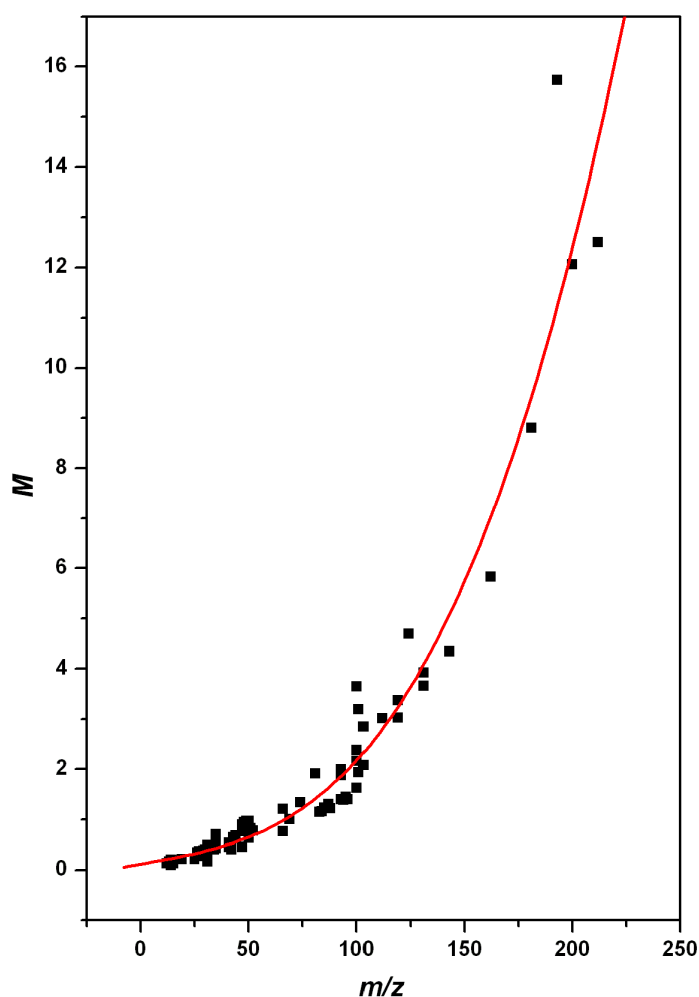


**Figure 2.B.(iii).** Graph to determine the relative mass sensitivity,  $M$ , of the Hidden Analytical HAL IV quadrupole mass spectrometer (QMS) as a function of  $m/z$ . Sample gases include  $\text{CF}_4$ ,  $\text{SF}_6$ ,  $\text{SF}_5\text{CF}_3$ ,  $\text{CH}_3\text{F}$ ,  $\text{CH}_3\text{Cl}$ ,  $\text{CH}_3\text{Br}$ ,  $\text{CH}_2\text{Cl}_2$ ,  $\text{CF}_2\text{Cl}_2$ ,  $\text{CFCl}_3$ ,  $\text{C}_2\text{H}_4$ ,  $\text{C}_2\text{H}_6$ ,  $\text{C}_3\text{H}_8$ ,  $\text{C}_2\text{F}_4$ ,  $\text{C}_2\text{F}_6$ ,  $\text{C}_3\text{F}_8$ , 2- $\text{C}_4\text{F}_8$ ,  $c$ - $\text{C}_4\text{F}_8$ ,  $c$ - $\text{C}_5\text{F}_8$ . The mass spectrum of each sample was measured with 70 eV electron impact ionisation, and compared with the NIST spectrum.<sup>43</sup> At each  $m/z$  value, the % yield from NIST is divided by the % yield from the QMS spectrum, and the data are normalised to unity at  $m/z$  69 (*i.e.*  $\text{CF}_3^+$ ). The squares show data points, the solid line shows the best fit to a third-order polynomial.

#### 2.B.4. Determining quantum yields

The ion-pair cross section from a molecule, calculated as described above in Section 2.B.3, can be divided by the *total* photoabsorption cross section for that molecule (absolute

values are taken from the literature, where available, and are referenced where appropriate in Chapters 6-9) to provide an ion-pair formation quantum yield,  $\Phi$ . Thus, the value for  $\Phi$  represents the probability that the absorption of a photon will lead to ion-pair formation. Individual values for  $\Phi$  are quoted with the photon energy at which the ion-pair and total photoabsorption cross section values are taken.

#### 2.B.5. Considerations when detecting ions with the QMS

All quadrupole mass spectrometers exhibit an element of mass discrimination, with a tendency to transmit heavier ions less efficiently.<sup>44</sup> To correct for this effect the mass factor,  $M$ , has been determined by comparing the cation mass spectra of many polyatomic molecules in the QMS, following 70 eV electron impact ionisation, to ‘true’ mass spectra published in the electronic NIST database.<sup>43</sup> The values for  $M$  used in equation 2.B.(2) are taken from the plot shown in Figure 2.B.(iii). It can be seen that as  $m/z$  increases, the detection efficiency of the QMS decreases and a higher  $M$  value is required to correct this effect.

The zero-blast effect arises because *all* ions entering the QMS may be transmitted when the applied potentials are set to detect  $m/z$  values close to zero.<sup>44</sup> This becomes important when studying hydrogen-containing molecules; the tail of the zero-blast peak in the mass spectrum overlaps with  $m/z$  1. Therefore,  $\text{H}^-$  spectra can only be trusted where there is no resemblance to other anion spectra recorded from the same molecule. Examples where this has caused problems include  $\text{H}^-$  detected from  $\text{CH}_3\text{X}$  molecules ( $\text{X} = \text{F}, \text{Cl}, \text{Br}$ ), which mimic the  $\text{X}^-$  spectra.<sup>45</sup> By contrast,  $\text{H}^-$  detected from  $\text{CH}_4$  is an example where this is not an issue because the  $\text{H}^-$  signal is dominant.<sup>46</sup>

# Chapter 3:

## *The reactions of $CF_n^+$ ( $n = 1-3$ ) with $C_2H_4$ , $C_2H_3F$ , $CH_2CF_2$ and $C_2HF_3$*

This chapter reports a fundamental study which investigates on two fronts the effects of fluorination on the reactivity of small molecules. First, how increasing fluorine substitution in neutral ethene affects its reactivity, and second how using different fluorocarbon cation species in the reactions changes the outcome. These data were collected by myself, Dr Michael Parkes, Dr Victor Mikhailov and Dr Chris Mayhew in the Department of Physics and Astronomy at The University of Birmingham between Spring 2007 and Autumn 2009.

### **3.A. Background information**

A consequence of the 1987 Montreal Protocol, and the many amendments made to it since, has been the significant reduction over the last two decades in the use and production of many ozone-depleting substances. These substances include chlorofluorocarbons (CFCs) and halons, commonly used in applications such as fire protection, refrigeration and aerosols. Many hydrofluorocarbons (HFCs) are considered to be *less* environmentally unfriendly alternatives to CFCs. This is because HFCs are greenhouse gases, whereas CFCs and halons are both greenhouse and ozone-depleting gases. It is therefore important to study these HFCs in order to learn more about their fundamental properties.



The main aim of this study is to investigate the effects on reactivity as the degree of fluorine substitution in ethene increases. This extends other earlier studies by the *Molecular Physics* group at Birmingham, for which the reactions of a series of cations with a number of *chloroethenes*, including the three isomers of dichloroethene, were investigated.<sup>12,47</sup> This present study focuses on the reactions of ethene ( $\text{C}_2\text{H}_4$ ), monofluoroethene ( $\text{C}_2\text{H}_3\text{F}$ ), 1,1-difluoroethene ( $\text{CH}_2\text{CF}_2$ ), and trifluoroethene ( $\text{C}_2\text{HF}_3$ ) with the cations  $\text{CF}^+$ ,  $\text{CF}_2^+$ , and  $\text{CF}_3^+$  using a Selected Ion Flow Tube (SIFT). Unfortunately, owing to expense and availability, the two 1,2-difluoroethene isomers have not been investigated.

The results presented here are compared with previous work, where available, on the reactions of the  $\text{CF}_n^+$  ( $n = 1-3$ ) ions with tetrafluoroethene ( $\text{C}_2\text{F}_4$ ) and the chlorinated ethenes. The aim of these comparisons is to give a more complete account on the effects of fluorination, and to aid the explanation of any trends observed. This is the first SIFT study on the reactions of  $\text{CF}^+$ ,  $\text{CF}_2^+$ , and  $\text{CF}_3^+$  with  $\text{C}_2\text{H}_3\text{F}$ ,  $\text{CH}_2\text{CF}_2$ , and  $\text{C}_2\text{HF}_3$ . The reactions of  $\text{CF}_n^+$  with  $\text{C}_2\text{F}_4$  have been investigated by several groups.<sup>48-50</sup> Of these investigations, the work by Morris *et al.*,<sup>50</sup> who also use a SIFT apparatus, is particularly relevant when making comparisons. Some of the reactions presented have also been studied previously by different techniques. The reaction of  $\text{CF}_3^+$  with  $\text{C}_2\text{H}_4$  has been investigated by SIFT Mass Spectrometry<sup>51</sup> and using an ion beam apparatus.<sup>52</sup> The reactions of  $\text{CF}^+$  with  $\text{C}_2\text{HF}_3$ ,<sup>49</sup> and  $\text{CF}^+$  and  $\text{CF}_3^+$  with  $\text{CH}_2\text{CF}_2$ <sup>53</sup> have also been observed previously using ion cyclotron resonance mass spectrometry (ICR-MS).

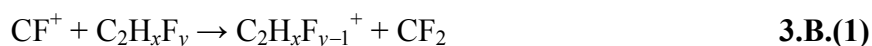
The adiabatic ionisation energies (*IE*) for  $\text{C}_2\text{H}_4$ ,  $\text{C}_2\text{H}_3\text{F}$ ,  $\text{CH}_2\text{CF}_2$  and  $\text{C}_2\text{HF}_3$  are 10.51, 10.36, 10.29 and 10.14 eV, respectively.<sup>54,55</sup> Comparisons of these values with the recombination energy (*RE*) of the reagent ion (equal in magnitude to the adiabatic *IE* of the

corresponding neutral) determines if charge transfer is energetically possible; the  $RE$  values are 9.11,<sup>56</sup> 11.44<sup>57</sup> and 9.04 eV<sup>58</sup> for  $\text{CF}^+$ ,  $\text{CF}_2^+$ , and  $\text{CF}_3^+$ , respectively, and so charge transfer is only exothermic for the reactions with  $\text{CF}_2^+$ .

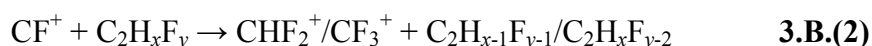
### 3.B. The reactions of $\text{CF}^+$

A summary of the results for the reactions of  $\text{CF}^+$  with  $\text{C}_2\text{H}_4$ ,  $\text{C}_2\text{H}_3\text{F}$ ,  $\text{CH}_2\text{CF}_2$ , and  $\text{C}_2\text{HF}_3$  is presented in Table 3.B.(I). The experimental results identify the product cations, their branching ratios (BRs) and the bimolecular reaction rate coefficient,  $k_{\text{exp}}$ . In addition, neutral products are proposed, the corresponding reaction enthalpies calculated and collisional rate coefficients,  $k_c$ , are also included.

First, the reactions of the *fluorinated* ethenes will be considered. The summary of results in Table 3.B.(I) reveals that only two different types of reaction mechanism are occurring involving  $\text{CF}^+$ . One is  $\text{F}^-$  transfer from the neutral species:



As the degree of fluorination increases, reaction 3.B.(1) becomes *less* favourable. For  $\text{C}_2\text{H}_3\text{F}$  this reaction represents the major product channel (88 %). However, for  $\text{CH}_2\text{CF}_2$  the BR falls to just 7 %, and for  $\text{C}_2\text{HF}_3$  this reaction is not observed at all, presumably because it is endothermic. The second type of reaction involves either HF or  $\text{F}_2$  abstraction:



For  $\text{C}_2\text{H}_3\text{F}$  reaction 3.B.(2) represents the minor product channel (12 %), although it is more exothermic than the  $\text{F}^-$  abstraction channel. However, it has often been noted that energetics

alone do not necessarily dictate the reaction pathway. Now, as the degree of fluorination increases the BR associated with reaction 3.B.(2) increases; the BR for  $\text{CH}_2\text{CF}_2$  is  $(88 + 5) \%$ , and for  $\text{C}_2\text{HF}_3$ , 100 %.

$\text{F}^-$  abstraction [as in reaction 3.B.(1)] suggests that the  $\text{CF}^+$  cation attacks the electron rich fluorine in  $\text{C}_2\text{H}_x\text{F}_y$  rather than the carbon-carbon double bond. Thus, it is the decrease in dipole moment as fluorination increases [Table 1.A.(I)] which is responsible for the trend noted; the larger the dipole moment, the more concentrated the electron density is on an individual fluorine atom, and so it becomes more nucleophilic.

**Table 3.B.(I).** A summary of results for the gas-phase reactions of  $\text{CF}^+$  with ethene and the fluorinated ethenes.

Reaction <sup>a</sup>		$\Delta_r H_{298}^\circ$ <sup>b</sup> / kJ mol <sup>-1</sup>	Product Branching Ratio	Rate Coefficient <sup>c</sup> / 10 <sup>-9</sup> cm <sup>3</sup> molecule <sup>-1</sup> s <sup>-1</sup>
$\text{CF}^+ + \text{C}_2\text{H}_4$	$\rightarrow \text{CH}_2\text{F}^+ + \text{C}_2\text{H}_2$	-141	80 %	1.1 [1.3] 85 %
	$\rightarrow \text{C}_3\text{H}_3^+ + \text{HF}$	-295	20 %	
$\text{CF}^+ + \text{C}_2\text{H}_3\text{F}$	$\rightarrow \text{C}_2\text{H}_3^+ + \text{CF}_2$	-81	88 %	2.1 [2.0] 100 %
	$\rightarrow \text{CHF}_2^+ + \text{C}_2\text{H}_2$	-172	12 %	
$\text{CF}^+ + \text{CH}_2\text{CF}_2$	$\rightarrow \text{CF}_3^+ + \text{C}_2\text{H}_2$	-170	88 %	1.4 [1.9] 74 %
	$\rightarrow \text{C}_2\text{H}_2\text{F}^+ + \text{CF}_2$	-35	7 %	
	$\rightarrow \text{CHF}_2^+ + \text{C}_2\text{HF}$	-86	5 %	
$\text{CF}^+ + \text{C}_2\text{HF}_3$	$\rightarrow \text{CF}_3^+ + \text{C}_2\text{HF}$	-145	100 %	1.0 [1.7] 59 %

<sup>a</sup> Note that the neutral products in these reactions are not detected in the experiment, but are proposed as the most likely candidate species.

<sup>b</sup> The reaction enthalpy calculated from 298 K enthalpies of formation.

<sup>c</sup> The experimentally determined rate coefficient,  $k_{\text{exp}}$ . In square brackets are the collisional values,  $k_{\text{c}}$ , and the rate efficiency is given as the percentage of  $k_{\text{exp}}$  with respect to  $k_{\text{c}}$ .

For reaction 3.B.(2), there is no obvious mechanism to explain the observed products, but a tight transition state is expected to be formed. It is also unclear if this mechanism involves breaking the carbon-carbon double bond or not. The reaction of  $\text{CF}^+$  with  $\text{CH}_2\text{CF}_2$  produces

two different outcomes resulting from reaction 3.B.(2);  $\text{CF}_3^+ + \text{C}_2\text{H}_2$  and  $\text{CHF}_2^+ + \text{C}_2\text{HF}$ , the former being significantly more favourable. It is also worth noting that  $\text{H}_2$  abstraction is not observed in either the reaction with  $\text{C}_2\text{H}_3\text{F}$  or  $\text{CH}_2\text{CF}_2$ . For  $\text{CH}_2\text{CF}_2$ ,  $\text{H}_2$  abstraction is *endothermic* by  $56 \text{ kJ mol}^{-1}$ , but  $\text{H}_2$  abstraction from  $\text{C}_2\text{H}_3\text{F}$  is *exothermic* by  $64 \text{ kJ mol}^{-1}$ . Although the competition between reactions 3.B.(1) and 3.B.(2) is not considered to be energetically driven, when considering reaction 3.B.(2) alone,  $\text{F}_2$  abstraction is more exothermic than  $\text{HF}$  abstraction, which is more exothermic than  $\text{H}_2$  abstraction – and this is reflected in the results. It is also considered, however, that there will be a preference for  $\text{CF}^+$  to attack one side of the fluorinated ethene in preference to another; again it is the dipole moment of these molecules which is likely to dictate the products, and  $\text{CF}^+$  will attack the side of the molecule with more fluorine substituents.

The reaction of  $\text{CF}^+$  with  $\text{C}_2\text{F}_4$  has been reported by Morris *et al.*,<sup>50</sup> and this reaction fits in with the trends observed from the present study;  $\text{F}_2$  abstraction described by reaction 3.B.(2) is observed as the major product ( $\text{CF}^+ + \text{C}_2\text{F}_4 \rightarrow \text{CF}_3^+ + \text{C}_2\text{F}_2$ ) and reaction 3.B.(1) is not observed at all. However, the reaction with  $\text{C}_2\text{F}_4$  also produces the minor products  $\text{C}_3\text{F}_5^+$  and  $\text{C}_2\text{F}_4^+$  by association and charge transfer reactions, respectively.<sup>50</sup> The adiabatic *IE* of  $\text{C}_2\text{F}_4$  is  $10.12 \text{ eV}$ ,<sup>59</sup> and so charge transfer is endothermic; its observation is attributed to the reaction with excited-state  $\text{CF}^+$  (produced from electron impact ionisation of  $\text{CF}_3\text{Br}$ ). It is noted that in the present experiment  $\text{CF}^+$  ions are produced by electron impact ionisation from  $\text{C}_3\text{F}_8$ . Charge transfer products from the reaction of  $\text{CF}^+$  with  $\text{C}_2\text{H}_3\text{F}$ ,  $\text{CH}_2\text{CF}_2$  and  $\text{C}_2\text{HF}_3$  have not been observed.

The results from the reaction with  $\text{C}_2\text{H}_4$  [Table 3.B.(I)] also fit into the general trend.  $\text{C}_2\text{H}_4$  has no fluorine substituent nor dipole moment and reaction 3.B.(1) is not observed. The

analogous outcome of reaction 3.B.(2), producing  $\text{CH}_2\text{F}^+ + \text{C}_2\text{H}_2$ , is the dominant channel. It is, however, interesting that HF elimination *is* observed in this reaction, but not in those of the fluorinated ethenes.

In summary, it is proposed that the reactions between  $\text{CF}^+$  and  $\text{C}_2\text{H}_3\text{F}$ ,  $\text{CH}_2\text{CF}_2$  and  $\text{C}_2\text{HF}_3$  are largely dictated by the dipole moments of these neutral species. The outcome of competition between reactions 3.B.(1) and 3.B.(2) is down to the *magnitude* of the dipole moment; the larger the value the more preference there is for reaction 3.B.(1) to dominate. The outcome of reaction 3.B.(2), *i.e.*  $\text{F}_2$  vs HF abstraction, is favoured towards  $\text{F}_2$  abstraction because  $\text{CF}^+$  attacks the molecule preferentially where more fluorine substituents are present. For  $\text{C}_2\text{H}_4$  and  $\text{C}_2\text{F}_4$  there is no dipole moment and the outcome is the equivalent to reaction 3.B.(2);  $\text{H}_2$  and  $\text{F}_2$  abstraction, respectively.

The reactions of  $\text{CF}^+$  with the chlorinated ethenes have also been performed by Mayhew *et al.* using the SIFT apparatus,<sup>12,47</sup> and some similarities can be drawn when comparing the two studies. Comparisons show that the reactions of  $\text{CF}^+$  with  $\text{C}_2\text{H}_3\text{Cl}$ ,  $\text{CH}_2\text{CCl}_2$ ,  $\text{C}_2\text{HCl}_3$  and  $\text{C}_2\text{Cl}_4$  all follow the same general trend as discussed above for the fluorinated ethene study. That is, the equivalent of reactions 3.B.(1) and 3.B.(2) can be used to describe all of the observed products, with the dominance of reaction 3.B.(1), *i.e.*  $\text{Cl}^-$  transfer, decreasing with decreasing dipole moment. The results from the chlorinated ethenes reveal information about reaction 3.B.(2) which is not possible from this fluorinated ethene study. For example, the reaction of  $\text{CF}^+$  with  $\text{C}_2\text{HCl}_3$  produces 23 %  $\text{CHCl}_2^+ + \text{C}_2\text{FCl}$ , and it is interesting that the neutral substituted ethyne product contains the fluorine atom. In the analogous reaction with  $\text{C}_2\text{HF}_3$  it could easily be assumed that the atoms in the neutral ethyne product,  $\text{C}_2\text{HF}$ , all originate from the  $\text{C}_2\text{HF}_3$  reactant, and that  $\text{CF}^+$  simply strips two fluorine atoms from it. The

chlorinated ethene study shows that this may not be the case and a more complicated mechanism needs to be considered. The study of the three isomers of dichloroethene also reveals additional information.<sup>47</sup> Most significantly, the reaction of *cis*-1,2-dichloroethene shows no products from the equivalent of reaction 3.B.(1) whereas in the reactions of  $\text{C}_2\text{H}_3\text{Cl}$  and  $\text{CH}_2\text{CCl}_2$  reaction 3.B.(1) dominates. This is interesting because of these three chlorinated ethenes it is the *cis*-1,2 isomer which has the largest dipole moment. In fact, of the complete series of chlorinated ethenes reacting with  $\text{CF}^+$ , only  $\text{C}_2\text{H}_3\text{Cl}$  and  $\text{CH}_2\text{CCl}_2$  show products from reaction 3.B.(1) – all others show products from reaction 3.B.(2) only. It could be significant that these two species are the only ones where the chlorine substituents are only on one of the carbon atoms. If this is indeed important in determining if reaction 3.B.(1) or 3.B.(2) dominates, it is not easy to explain why from  $\text{CH}_2\text{CF}_2$  it is reaction 3.B.(2) which is dominant (88 %  $\text{CF}_3^+ + \text{C}_2\text{H}_2$ ), but from  $\text{CH}_2\text{CCl}_2$  reaction 3.B.(1) dominates (69 %  $\text{C}_2\text{H}_2\text{Cl}^+ + \text{CFCl}$ ).

Clearly similar mechanisms are involved in the reactions of  $\text{CF}^+$  with both the fluorinated and chlorinated series of ethenes. It is, however, difficult to explain the relative trends observed in *both* sets of results with the same arguments. Some similarities in the results suggest there should be a common explanation, but the difference in the chemistry of fluorine and chlorine could easily explain otherwise.

### 3.C. The reactions of $\text{CF}_2^+$

A summary of the results for the reactions of  $\text{CF}_2^+$  with  $\text{C}_2\text{H}_4$ ,  $\text{C}_2\text{H}_3\text{F}$ ,  $\text{CH}_2\text{CF}_2$  and  $\text{C}_2\text{HF}_3$  are presented in Table 3.C.(I). The equality between experimental and collisional rate coefficients indicates all reactions occur with 100 % efficiency. Non-dissociative charge

transfer is the only channel observed for the reaction of  $\text{CF}_2^+$  with  $\text{CH}_2\text{CF}_2$  and  $\text{C}_2\text{HF}_3$ . The reaction of  $\text{CF}_2^+$  with  $\text{C}_2\text{H}_3\text{F}$ , however, yields two different ionic products, although the major product still arises from non-dissociative charge transfer. The minor product is  $\text{C}_2\text{H}_3^+$ , which can only arise from an intimate chemical reaction involving  $\text{F}^-$  abstraction:



It is noted that dissociative charge transfer,  $\text{CF}_2^+ + \text{C}_2\text{H}_3\text{F} \rightarrow (\text{C}_2\text{H}_3\text{F}^+)^* + \text{CF}_2 \rightarrow \text{C}_2\text{H}_3^+ + \text{F} + \text{CF}_2$ , is endothermic by  $206 \text{ kJ mol}^{-1}$ .

**Table 3.C.(I).** A summary of results for the gas-phase reactions of  $\text{CF}_2^+$  with ethene and the fluorinated ethenes.

Reaction <sup>a</sup>		$\Delta_r H_{298}^\circ$ <sup>b</sup> / $\text{kJ mol}^{-1}$	Product Branching Ratio	Rate Coefficient <sup>c</sup> / $10^{-9} \text{ cm}^3 \text{ molecule}^{-1} \text{ s}^{-1}$
$\text{CF}_2^+ + \text{C}_2\text{H}_4$	$\rightarrow \text{C}_3\text{H}_3\text{F}_2^+ + \text{H}$	?	55 %	1.1 [1.1] 100 %
	$\rightarrow \text{C}_2\text{H}_4^+ + \text{CF}_2$	− 109	45 %	
$\text{CF}_2^+ + \text{C}_2\text{H}_3\text{F}$	$\rightarrow \text{C}_2\text{H}_3\text{F}^+ + \text{CF}_2$	−124	88 %	1.8 [1.8] 100 %
	$\rightarrow \text{C}_2\text{H}_3^+ + \text{CF}_3$	−161	12 %	
$\text{CF}_2^+ + \text{CH}_2\text{CF}_2$	$\rightarrow \text{CH}_2\text{CF}_2^+ + \text{CF}_2$	−131	100 %	1.6 [1.6] 100 %
$\text{CF}_2^+ + \text{C}_2\text{HF}_3$	$\rightarrow \text{C}_2\text{HF}_3^+ + \text{CF}_2$	−146	100 %	1.5 [1.5] 100 %

<sup>a</sup> Note that the neutral products in these reactions are not detected in the experiment, but are proposed as the most likely candidate species.

<sup>b</sup> The reaction enthalpy calculated from 298 K enthalpies of formation.

<sup>c</sup> The experimentally determined rate coefficient,  $k_{\text{exp}}$ . In square brackets are the collisional values,  $k_{\text{c}}$ , and the rate efficiency is given as the percentage of  $k_{\text{exp}}$  with respect to  $k_{\text{c}}$ .

The results from the reaction with  $\text{C}_2\text{H}_4$  are anomalous with respect to the other reactions; charge transfer is observed, but it is not the major channel. In addition, the product  $\text{C}_3\text{H}_3\text{F}_2^+$  (H elimination) is surprising. On the other hand, this product has also been observed in the reactions of ethene with  $\text{CF}_3^+$  and  $\text{C}_2\text{F}_4^+$ , and from the reaction of  $\text{C}_2\text{F}_4^+$  with  $\text{C}_2\text{H}_3\text{F}$  [see

Tables 3.D.(I) and 4.B.(I)]. The exact structure of this species is unknown, but its frequent observation suggests it is a relatively stable species. Unfortunately its  $\Delta_f H^\circ$  value is unknown, so  $\Delta_r H^\circ$  values for the reactions where it is produced cannot be calculated.

The adiabatic  $IE$  of  $\text{C}_2\text{F}_4$  is 10.12 eV<sup>59</sup> and so charge transfer in its reaction with  $\text{CF}_2^+$  is exothermic. The reaction of  $\text{CF}_2^+$  with  $\text{C}_2\text{F}_4$  has been reported by Morris *et al.*,<sup>50</sup> and unsurprisingly, this reaction proceeds exclusively by charge transfer at the collisional rate.

### 3.D. The reactions of $\text{CF}_3^+$

A summary of the results for the reactions of  $\text{CF}_3^+$  with  $\text{C}_2\text{H}_4$ ,  $\text{C}_2\text{H}_3\text{F}$ ,  $\text{CH}_2\text{CF}_2$ , and  $\text{C}_2\text{HF}_3$  are presented in Table 3.D.(I). Where an association reaction is observed the He buffer gas pressure is quoted due to its involvement in collisionally stabilising the energised intermediate formed. The data in Table 3.D.(I) highlights some trends in the reactions of the *fluorinated* ethenes with  $\text{CF}_3^+$ .  $\text{F}^-$  abstraction from the neutral appears *less* favourable as the degree of fluorine substitution increases; in the reaction with  $\text{C}_2\text{H}_3\text{F}$  the BR is 75 %,  $\text{CH}_2\text{CF}_2$  only 50 % and for  $\text{C}_2\text{HF}_3$  this reaction is not observed. Recall the discussion in Section 3.B where the same trend is apparent in the analogous reaction with  $\text{CF}^+$ , and the larger the dipole moment of the fluorinated ethene, the more likely  $\text{F}^-$  abstraction is to occur. Three points need to be made regarding  $\text{F}^-$  transfer to  $\text{CF}_3^+$ , in comparison with the  $\text{CF}^+$  reactions: first, only the reaction of  $\text{CF}_3^+$  with  $\text{C}_2\text{H}_3\text{F}$  can be *directly* compared with  $\text{CF}^+$  because the same two product cations are observed with similar BRs; second, as the BR for  $\text{F}^-$  abstraction decreases there is no common mechanism in all three reactions taking its place, *i.e.* there is no significant competition to the  $\text{F}^-$  abstraction reaction; third, although the value for  $\Delta_f H^\circ_{298}$



( $\text{C}_2\text{HF}_2^+$ ) is not known,  $\text{F}^-$  abstraction in the reaction with  $\text{C}_2\text{HF}_3$  is expected to be endothermic.

**Table 3.D.(I).** A summary of results for the gas-phase reactions of  $\text{CF}_3^+$  with ethene and the fluorinated ethenes.

Reaction <sup>a</sup>		$\Delta_r H_{298}^\circ$ <sup>b</sup> / kJ mol <sup>-1</sup>	Product Branching Ratio	Rate Coefficient <sup>c</sup> / 10 <sup>-9</sup> cm <sup>3</sup> molecule <sup>-1</sup> s <sup>-1</sup>
$\text{CF}_3^+ + \text{C}_2\text{H}_4$	$\rightarrow \text{C}_3\text{H}_3\text{F}_2^+ + \text{HF}$	?	60 %	0.7 [1.1] 64 %
	$\rightarrow \text{C}_2\text{H}_3^+ + \text{CHF}_3$	- 43	40 %	
$\text{CF}_3^+ + \text{C}_2\text{H}_3\text{F}$	$\rightarrow \text{C}_2\text{H}_3^+ + \text{CF}_4$	- 88	75 %	1.3 [1.6] 81 %
	$\rightarrow \text{CHF}_2^+ + \text{CH}_2\text{CF}_2$ <sup>d</sup>	- 1	25 %	
$\text{CF}_3^+ + \text{CH}_2\text{CF}_2$	$\rightarrow \text{C}_2\text{H}_2\text{F}^+ + \text{CF}_4$	- 43	50 %	0.7 [1.5] 47 % $p(\text{He}) = 0.5$ Torr
	$\rightarrow \text{C}_3\text{H}_2\text{F}_5^+$ (adduct)	?	44 %	
	$\rightarrow \text{C}_3\text{HF}_4^+ + \text{HF}$	?	6 %	
$\text{CF}_3^+ + \text{C}_2\text{HF}_3$	$\rightarrow \text{C}_3\text{HF}_6^+$ (adduct)	?	100 %	0.2 [1.3] 15 % $p(\text{He}) = 0.5$ Torr

<sup>a</sup> Note that the neutral products in these reactions are not detected in the experiment, but are proposed as the most likely candidate species.

<sup>b</sup> The reaction enthalpy calculated from 298 K enthalpies of formation. Absence of a value indicates the  $\Delta_r H^\circ$  for the product cation is not known.

<sup>c</sup> The experimentally determined rate coefficient,  $k_{\text{exp}}$ . In square brackets are the collisional values,  $k_c$ , and the rate efficiency is given as the percentage of  $k_{\text{exp}}$  with respect to  $k_c$ .

<sup>d</sup> The (Z) and (E) - 1,2 isomers give endothermic reaction enthalpies, and so it is proposed 1,1-difluorethene is the neutral product species formed.

Note the trend in the reaction enthalpies in Table 3.D.(I), and that the reaction  $\text{CF}_3^+ + \text{C}_2\text{F}_4 \rightarrow \text{C}_2\text{F}_3^+ + \text{CF}_4$  is endothermic by 111 kJ mol<sup>-1</sup>. Considering these points, the energetics *are* likely to be important in interpreting the results from the reactions of  $\text{CF}_3^+$  with the fluorinated ethenes. Key supporting evidence is that adduct formation is observed, and the BR increases with *increasing* fluorine substitution; no adduct is formed in the reaction with  $\text{C}_2\text{H}_3\text{F}$ , the BR for adduct formation is 44 % with  $\text{CH}_2\text{CF}_2$ , and with  $\text{C}_2\text{HF}_3$  the BR is 100 %. As  $\text{F}^-$  abstraction becomes energetically less favourable, the results suggest that the lifetime

of the reaction complex increases and it is more likely to be collisionally stabilised and hence observed.

There are also other interesting reactions occurring which do not lead to  $\text{F}^-$  abstraction or association; for example, the observation of  $\text{CHF}_2^+$  as the minor product (25 %) from the reaction with  $\text{C}_2\text{H}_3\text{F}$ :

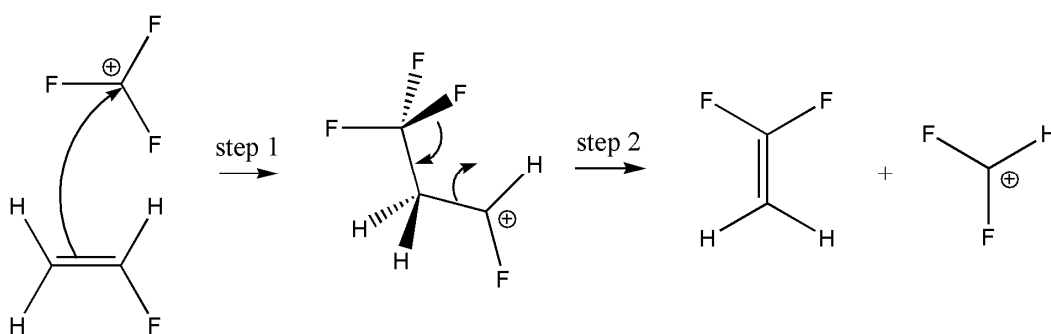


**Figure 3.D.(i).** A proposed mechanism for the reaction  $\text{CF}_3^+ + \text{C}_2\text{H}_3\text{F} \rightarrow \text{CHF}_2^+ + \text{CH}_2\text{CF}_2$ .

The proposed neutral product species is 1,1-difluoroethene because this is the only exothermic outcome, based on thermochemical calculations. (The *cis* and *trans* isomers for 1,2-difluoroethene give reaction enthalpies endothermic by 47 and 51  $\text{kJ mol}^{-1}$ , respectively.) Another interesting reaction which does not fit the general trend is that of  $\text{CF}_3^+$  with  $\text{CH}_2\text{CF}_2$ :



The BR for this reaction, elimination of HF, is only 6 %. Reactions 3.D.(1) and 3.D.(2) represent thermodynamically favourable exit channels from the adduct complex which is formed. It is expected that the adduct species in this series of reactions is covalently bonded,

rather than involving intramolecular forces, because reactions 3.D.(1) and 3.D.(2) are expected to result from a covalently-bonded complex [proposed mechanisms for these reactions are presented in Figures 3.D.(i) and 3.D.(ii), respectively], and previous work has shown that  $\text{CF}_3^+$  reacts with neutral  $\text{C}_2\text{F}_4$  to produce  $\text{C}_3\text{F}_7^+$ .<sup>50</sup>

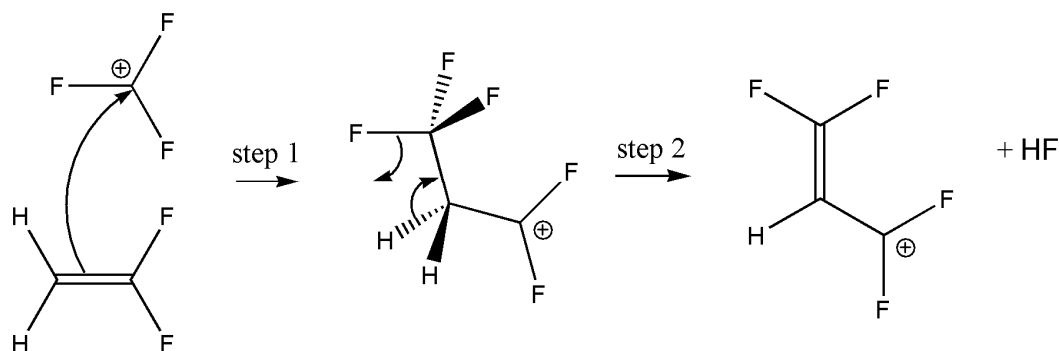


**Figure 3.D.(ii).** A proposed mechanism for the reaction  $\text{CF}_3^+ + \text{CH}_2\text{CF}_2 \rightarrow \text{C}_3\text{HF}_4^+ + \text{HF}$ .

In the reaction of  $\text{CF}_3^+$  with  $\text{C}_2\text{H}_4$ ,  $\text{H}^-$  abstraction is observed, which is not observed in the reactions with the fluorinated ethenes because it cannot compete with  $\text{F}^-$  abstraction. Recall the comparisons made above between  $\text{F}^-$  abstraction in the reactions of both  $\text{CF}^+$  and  $\text{CF}_3^+$  with the fluorinated ethenes, and it should be noted that the same comment cannot be made regarding  $\text{H}^-$  abstraction in ethene because this outcome in the reaction with  $\text{CF}^+$  is endothermic by  $36 \text{ kJ mol}^{-1}$ . The other product from the reaction of  $\text{CF}_3^+$  with  $\text{C}_2\text{H}_4$  is  $\text{C}_3\text{H}_3\text{F}_2^+$ , a product of HF elimination with a BR of 60 %. HF elimination is also observed from the reaction with  $\text{CH}_2\text{CF}_2$ , but as the *minor* product, further demonstrating the dominance of the  $\text{F}^-$  abstraction channel in the fluorinated ethenes and the comparatively less dominant  $\text{H}^-$  abstraction reaction from  $\text{C}_2\text{H}_4$ . Another SIFT study has also reacted  $\text{CF}_3^+$  with ethene, and the results are in excellent agreement with this work;<sup>51</sup> the dominant product is

$\text{C}_3\text{H}_3\text{F}_2^+$ , the minor product is  $\text{C}_2\text{H}_3^+$ , and the 300 K rate coefficient is  $0.98 \times 10^{-9} \text{ cm}^3 \text{ molecule}^{-1} \text{ s}^{-1}$ .

The previous work on ion-molecule reactions with the chlorinated ethenes report their gas-phase reactions with  $\text{CF}_3^+$ .<sup>12,47</sup> Similarities are noted in the reaction with  $\text{C}_2\text{H}_3\text{Cl}$  and  $\text{CH}_2\text{CCl}_2$ , particularly the former.  $\text{CF}_3^+$  reacting with  $\text{C}_2\text{H}_3\text{Cl}$  produces  $\text{C}_2\text{H}_3^+ + \text{CF}_3\text{Cl}$  (65 %), and  $\text{CHFCl}^+ + \text{C}_2\text{H}_2\text{F}_2$  (35 %). Note the similarities here with the reaction of  $\text{C}_2\text{H}_3\text{F}$  in Table 3.D.(I). It is inferred that in *both* reactions, the  $\text{C}_2\text{H}_2\text{F}_2$  neutral product is the 1,1-difluoroethene isomer, because the *cis*-1,2 and *trans*-1,2 isomers give endothermic reaction enthalpies. The similarities in the reaction of  $\text{CH}_2\text{CF}_2$  and  $\text{CH}_2\text{CCl}_2$  are less striking;  $\text{CF}_3^+ + \text{CH}_2\text{CCl}_2$  exclusively produces  $\text{C}_2\text{H}_2\text{Cl}^+ + \text{CF}_3\text{Cl}$  *via*  $\text{Cl}^-$  abstraction, whereas the analogous  $\text{F}^-$  abstraction reaction with  $\text{CH}_2\text{CF}_2$  forms only 50 % of the observed products [Table 3.D.(I)]. Also note that  $\text{Cl}^-$  abstraction *is* observed in the reactions of  $\text{C}_2\text{HCl}_3$  and  $\text{C}_2\text{Cl}_4$ , but the analogous  $\text{F}^-$  abstraction reaction is *not* observed from  $\text{C}_2\text{HF}_3$  (this work) or  $\text{C}_2\text{F}_4$ .<sup>50</sup> Recall from the discussion above that the latter two reactions are expected to be endothermic, whereas the former two reactions are clearly exothermic. In fact all other reactions observed in the chlorinated ethene series, which are not equivalently observed in the fluorinated ethene series, are simply because of the new atom involved – chlorine. For example,  $\text{CF}_3^+ + \text{C}_2\text{HCl}_3$  produces 24 %  $\text{CFCl}_2^+ + \text{C}_2\text{HClF}_2$ , whereas this reaction for  $\text{C}_2\text{HF}_3$  would have a thermoneutral outcome, *i.e.* it will revert back to the reactants. So, although on the surface the differences in the reactions of  $\text{CF}_3^+$  with the fluorinated and chlorinated series of ethenes appear significant, they are actually explained by two simple statements: first,  $\text{Cl}^-$  abstraction is energetically more favourable than the equivalent  $\text{F}^-$  abstraction reactions; second, reactions with the chlorinated ethenes involve the atoms C, H, F *and* Cl, allowing for a larger

number of viable (both dynamically and energetically) exit channels to be available to the reaction complex.

### 3.E. Conclusions

The gas-phase reactions of  $\text{CF}^+$ ,  $\text{CF}_2^+$  and  $\text{CF}_3^+$  with  $\text{C}_2\text{H}_4$ ,  $\text{C}_2\text{H}_3\text{F}$ ,  $\text{CH}_2\text{CF}_2$  and  $\text{C}_2\text{HF}_3$  have been studied using a Selected Ion Flow Tube. For energetic reasons, the reactions with  $\text{CF}_2^+$  can proceed by non-dissociative charge transfer, whereas those with  $\text{CF}^+$  and  $\text{CF}_3^+$  only produce products from a reaction complex where bonds break and new ones form. The discussion has focused on the reactions of  $\text{CF}^+$  and  $\text{CF}_3^+$  with ethene and the three fluorinated ethenes, and some similarities are noted between these and a previous study on the chlorinated ethenes.<sup>12,47</sup>

The dipole moment of the fluorinated ethene is significant because it is a measure of how nucleophilic a fluorine atom in the molecule is. This has been highlighted when analysing the results for the  $\text{CF}^+$  and  $\text{CF}_3^+$  reactions. The dynamics involved for an  $\text{F}^-$  abstraction reaction are favoured when the dipole moment is large. The branching into this channel decreases as the dipole moment of the fluorinated ethene decreases. It is unclear if this trend is due to dynamics alone, or if energetics play a part. It is noted that as branching into  $\text{F}^-$  abstraction decreases, so does the exothermicity of the reaction – in both  $\text{CF}^+$  and  $\text{CF}_3^+$  reactions with  $\text{C}_2\text{HF}_3$ , this channel is expected to be endothermic. However, the reaction of  $\text{CF}^+$  with  $\text{C}_2\text{H}_3\text{F}$  provides an example where dynamics are more important than energetics;  $\text{F}^-$  abstraction is competing with  $\text{HF}$  abstraction, and the former mechanism dominates despite the latter being significantly more exothermic, and it is  $\text{C}_2\text{H}_3\text{F}$  which has the largest dipole moment of the

three fluoroethenes studied here. It is also unclear if dynamics or energetics are responsible for the apparent preference for  $\text{F}_2$  abstraction over  $\text{HF}$  abstraction in the reactions with  $\text{CF}^+$ .

The comparisons of the fluorinated ethene reactions with those of ethene show how the reaction mechanisms, and hence the products and their branching ratios, often differ due to the significance of the dipole moment. It has been observed that adding one or two fluorine substituents can increase the reactivity of ethene, but adding three or four fluorine atoms can then have the opposite effect, resulting in stabilising the molecule and/or the reaction complex.

# Chapter 4:

## *The reactions of $C_2F_4^+$ with $C_2H_4$ , $C_2H_3F$ , $CH_2CF_2$ and $C_2HF_3$*

This chapter continues the investigation on the effects of fluorination in ethene, but the reactant ion is now a fluorinated ethene itself, the tetrafluoroethene cation,  $C_2F_4^+$ . In the original study of the reactions with  $CF^+$ ,  $CF_2^+$  and  $CF_3^+$  (see Chapter 3) a new source gas was used, perfluoropropane ( $C_3F_8$ ). This gas was used simply out of curiosity to see if it yielded the ions in question more efficiently than the usual choice of source gases – either tetrafluoromethane ( $CF_4$ ) or hexafluoroethane ( $C_2F_6$ ). It was then discovered, albeit unintentionally, that  $C_3F_8$  can be used to produce  $C_2F_4^+$  ions and the decision was made to include this reactant in the fluorinated ethene investigation. These data were collected by myself and Dr Chris Mayhew using the SIFT apparatus in the University of Birmingham Department of Physics and Astronomy in the spring and summer of 2009.

### **4.A. Background information**

A general introduction into the fluorinated ethene series of molecules including the motivations for undertaking these studies has been given in Chapter 3, and the same comments are not repeated here. Ion Cyclotron Resonance Mass Spectrometry (ICR-MS) has been used previously to observe ion-molecule reactions of  $C_2F_4^+$  with ethene,<sup>60,61</sup> and all

possible neutral fluorinated ethene molecules.<sup>49,62</sup> This is thought to be the first study of this set of reactions using the SIFT technique. The reaction between  $\text{C}_2\text{F}_4^+$  and  $\text{C}_2\text{F}_4$ , which is not investigated here, has been studied by Morris *et al.* also using a SIFT apparatus,<sup>50</sup> and provides a useful comparison when looking at trends in how the results change with increasing fluorine substitution.

#### 4.B. Results and discussion

The results for the reactions of  $\text{C}_2\text{F}_4^+$  with ethene ( $\text{C}_2\text{H}_4$ ), monofluoroethene ( $\text{C}_2\text{H}_3\text{F}$ ), 1,1-difluoroethene ( $\text{CH}_2\text{CF}_2$ ), and trifluoroethene ( $\text{C}_2\text{HF}_3$ ) are presented in Table 4.B.(I). The experimental results identify the product cations, their branching ratios (BRs) and the bimolecular reaction rate coefficient,  $k_{\text{exp}}$ . Where an association reaction is observed the helium buffer gas pressure is given due to its involvement in collisionally stabilising the energised intermediate formed. In addition, neutral reaction products are proposed, the corresponding reaction enthalpies calculated, and collisional rate coefficients,  $k_{\text{c}}$ , are also included. The adiabatic ionisation energies for ethene and the fluoroethenes are 10.51, 10.36, 10.29, and 10.14 eV for  $\text{C}_2\text{H}_4$ ,  $\text{C}_2\text{H}_3\text{F}$ ,  $\text{CH}_2\text{CF}_2$  and  $\text{C}_2\text{HF}_3$ , respectively.<sup>54,55</sup> The recombination energy for  $\text{C}_2\text{F}_4^+$ , defined as the adiabatic ionisation energy for neutral  $\text{C}_2\text{F}_4$ , is 10.12 eV.<sup>59</sup> Charge transfer in this set of reactions is therefore endothermic, and indeed as is seen from the results in Table 4.B.(I), interesting intimate chemical reactions are occurring.

All of the reactions with  $\text{C}_2\text{F}_4^+$  are relatively slow:  $k_{\text{exp}} < k_{\text{c}}$ . Many of the ionic products detected are relatively large species containing three or four carbon atoms. This complicates the data analysis for two reasons: first, it is difficult to assign a mechanism to these reactions, or to suggest confidently a particular isomeric structure for these product ions; second, many



$\Delta_f H^\circ_{298}$  values are not known which prevents  $\Delta_r H^\circ_{298}$  being calculated in these instances. As a result, the structures and/or mechanisms assigned to some of the reactions in the discussion below are made tentatively.

**Table 4.B.(I).** A summary of results for the gas-phase reactions of  $C_2F_4^+$  with ethene and the fluorinated ethenes.

Reaction <sup>a</sup>		$\Delta_r H^\circ_{298}{}^b / \text{kJ mol}^{-1}$	Product Branching Ratio	Rate Coefficient <sup>c</sup> / $10^{-9} \text{ cm}^3 \text{ molecule}^{-1} \text{ s}^{-1}$
$C_2F_4^+ + C_2H_4$	$\rightarrow C_2H_2F_2^+ + C_2H_2F_2^d$	$-65^e$	95 %	0.7 [1.0] 70 %
	$\rightarrow C_3H_3F_2^+ + CHF_2$	?	5 %	
$C_2F_4^+ + C_2H_3F$	$\rightarrow C_2HF_3^+ + CH_2CF_2^f$	$-35$	45 %	0.6 [1.5] 40 % $p(\text{He}) = 0.5 \text{ Torr}$
	$\rightarrow C_3H_3F_2^+ + CF_3$	?	40 %	
	$\rightarrow C_3H_2F_3^+ + CHF_2$	?	10 %	
	$\rightarrow CH_2CF_2^+ + C_2HF_3$	$-20$	3 %	
	$\rightarrow C_4H_3F_5^+ \text{ (adduct)}$	?	2 %	
$C_2F_4^+ + CH_2CF_2$	$\rightarrow C_4H_2F_6^+ \text{ (adduct)}$	?	60 %	0.7 [1.4] 50 % $p(\text{He}) = 0.5 \text{ Torr}$
	$\rightarrow C_3H_2F_3^+ + CF_3$	?	30 %	
	$\rightarrow C_3HF_4^+ + CHF_2$	?	10 %	
$C_2F_4^+ + C_2HF_3$	$\rightarrow C_2HF_3^+ + C_2F_4$	$+2$	72 %	0.2 [1.2] 17 %
	$\rightarrow C_3HF_4^+ + CF_3$	?	28 %	

<sup>a</sup> Note that the neutral products in these reactions are not detected in the experiment, but are proposed as the most likely candidate species.

<sup>b</sup> The reaction enthalpy calculated from 298 K enthalpies of formation. Absence of a value indicates the  $\Delta_f H^\circ$  for the product cation is not known.

<sup>c</sup> The experimentally determined rate coefficient,  $k_{\text{exp}}$ . In square brackets are the collisional values,  $k_c$  (see section 2), and the rate efficiency is given as the percentage of  $k_{\text{exp}}$  with respect to  $k_c$ .

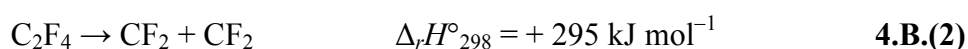
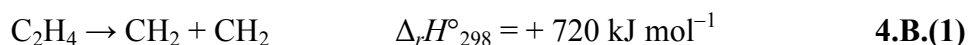
<sup>d</sup> The isomeric forms of these two product species are not known, however, it is proposed that both the cation and neutral are the 1,1- isomers of difluoroethene.

<sup>e</sup> The calculated  $\Delta_r H^\circ$  value if the two product species are *both* the 1,1- isomers.

<sup>f</sup> The (Z) and (E) – 1,2 isomers give endothermic reaction enthalpies, and so we propose 1,1-difluoroethene is the neutral product species formed.

First the structure of the reagent ion,  $C_2F_4^+$ , is discussed. It is perhaps inaccurate to assume this species will have a generic double bond as in neutral  $C_2H_4$ , for example, and given the importance of double bonds in the reactive behaviour of a species this point will be addressed. Figure 4.B.(i) shows various ways which  $C_2F_4^+$  can be pictorially represented,

showing differing degrees of double-bonding character. Species 1 and 2 are preferred because both give an indication of the effects perfluorination and ionisation will have on the double bond. Certainly, species 3 is misleading. Perfluorination of ethene significantly weakens the double bond; a calculation of  $\Delta_r H^\circ_{298}$  for reactions 4.B.(1) and 4.B.(2) clearly shows this:



The ionised species will be even further destabilised with respect to the C-C bond. It has been observed both from this work, and by Su and Kevan,<sup>63</sup> that  $\text{C}_2\text{F}_4^+$  is metastable and will produce  $\text{CF}_3^+$  by collision induced dissociation. This of course involves some rearrangement, and breaking of the carbon-carbon bond. Of the three species in Figure 4.B.(i), species 1 will be used to represent  $\text{C}_2\text{F}_4^+$  when using arrow-pushing mechanisms to explain some of the observed reactions.

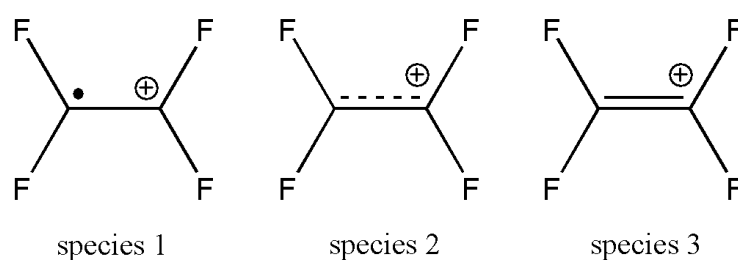


**Figure 4.B.(i).** Three examples of how the tetrafluoroethene cation,  $\text{C}_2\text{F}_4^+$ , can be pictorially represented for the use in reaction mechanisms.

All of the reaction products shown in Table 4.B.(I) can be divided into three different categories: the first is the observation of the adduct species; the second is the observation of a fluorinated ethene cation which is *different* to the neutral ethene-type reactant; the third is the observation of a cation containing three carbon atoms, with the corresponding neutral species as either  $CHF_2$  or  $CF_3$ . The third category is generically shown below:

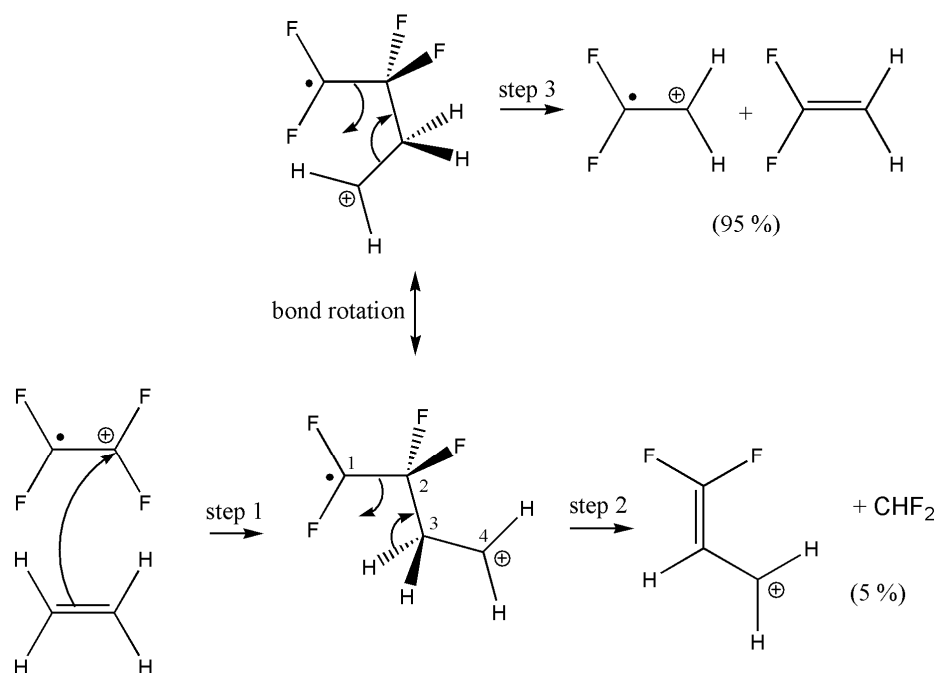
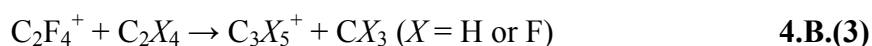


**Figure 4.B.(ii).** The proposed mechanism for the reaction between the tetrafluoroethene cation ( $C_2F_4^+$ ), and ethene ( $C_2H_4$ ).

In fact, all product species from any of the three categories described above may be explained by one common reaction mechanism. This involves a branched, 4-carbon chain adduct being formed, which may subsequently fragment to either eliminate  $CX_3$ , as in reaction 4.B.(3), or

produce two fluorinated ethenes with one retaining the positive charge. Figure 4.B.(ii) shows this mechanism for the reaction between  $C_2F_4^+$  and  $C_2H_4$ . It shows how both observed product channels can be produced from the same 4-carbon chain intermediate formed by step 1 [see Table 4.B.(I)]. Note that this mechanism suggests the observed product channel  $C_2H_2F_2^+ + C_2H_2F_2$  produces both species as the 1,1-difluoroethene isomers, and thermochemistry also suggests this is the most exothermic outcome. There is also a preference for step 3 to follow step 1, rather than step 2, and the reasons for this are not entirely clear from analysing this mechanism alone. It does, however, follow the same trend as is seen in the reactions of  $C_2F_4^+$  with the fluorinated ethenes (see Table 4.B.(I), and discussion below). The reaction channel eliminating  $CHF_2$  is always a minor one, and the product channels analogous to that in step 3, where possible, are all significant ones. It is suggested that step 2 in Figure 4.B.(ii) is unfavourable and relatively slow which allows for bond rotation to occur in the intermediate species, thus allowing step 3 to dominate. It would perhaps shed some light on this argument if the heat of formation of  $C_3H_3F_2^+$  was known;  $\Delta_f H^\circ$  for producing this product could then be calculated and compared to that for producing  $C_2H_2F_2^+$ .

Figure 4.B.(iii) shows the proposed mechanism for the reaction between  $C_2F_4^+$  and  $C_2H_3F$ . Note how all products from this reaction shown in Table 4.B.(I) are produced by the mechanism in Figure 4.B.(iii). Steps 1a and 1b show that there are two isomerically different intermediate adduct species which can be formed, depending on which carbon in  $C_2H_3F$  forms the bond with a carbon in  $C_2F_4^+$ . Step 1a followed by 2a will always produce  $C_3H_2F_3^+$  and  $CHF_2$ ; both substituents on carbon 3 in the intermediate adduct are hydrogens. If one considers step 1b followed by 2b, however, carbon 3 now has a hydrogen *and* a fluorine substituent, so a product mixture of  $C_3H_2F_3^+$  (+  $CHF_2$ ) *and*  $C_3H_3F_2^+$  (+  $CF_3$ ) would be

expected (note, Figure 4.B.(iii) only shows the latter outcome). It is clear from the product branching ratios that there is a preference to eliminate  $CF_3$  over  $CHF_2$ .

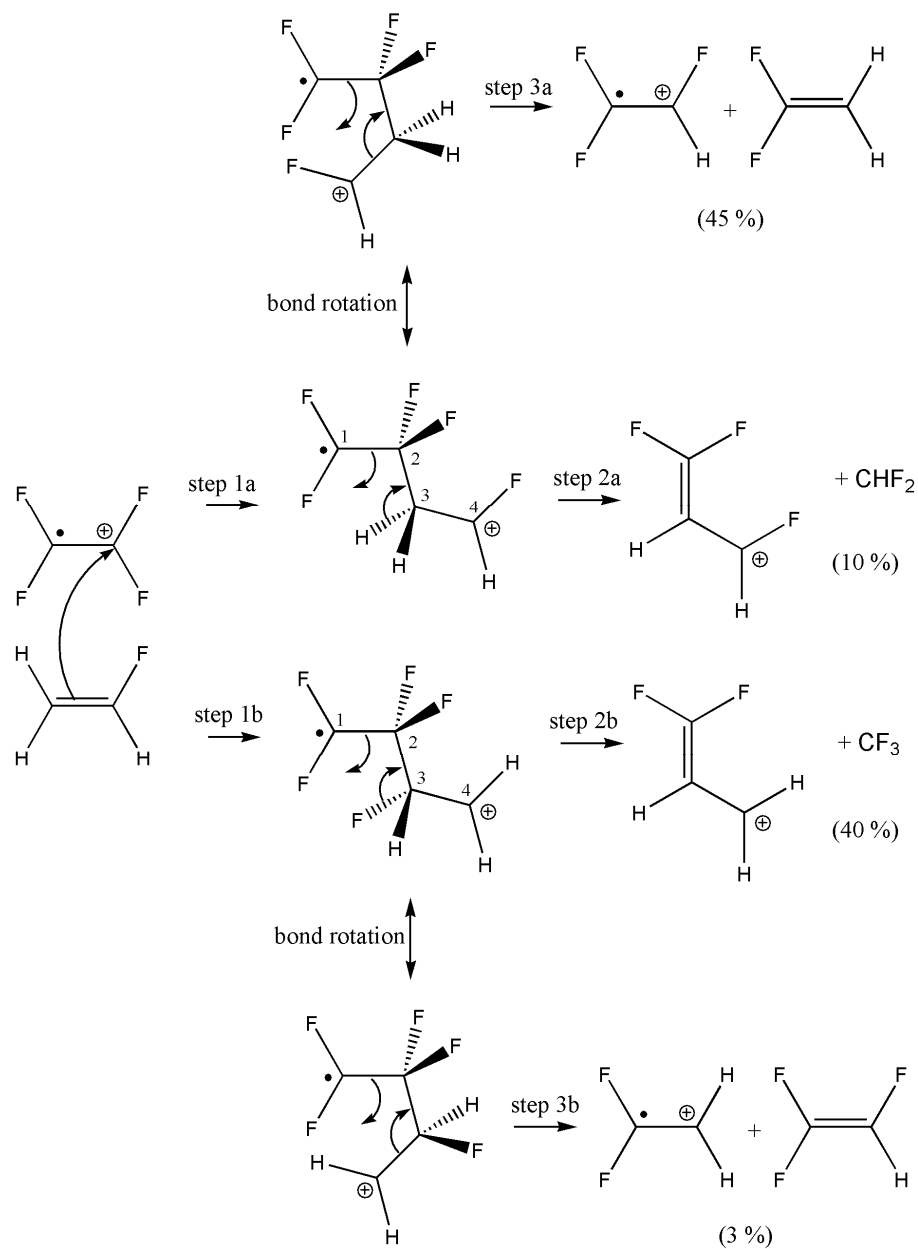


**Figure 4.B.(iii).** The proposed mechanism for the reaction between the tetrafluoroethene cation ( $C_2F_4^+$ ) and monofluoroethene ( $C_2H_3F$ ).

Indeed fluorine is a larger and more polarisable substituent than hydrogen, and the C-F bond distance will be greater. Perhaps this may qualitatively explain how step 2b will preferably eliminate  $CF_3$  rather than  $CHF_2$ , and also how step 2b may occur more readily than step 2a.

The other products shown in Figure 4.B.(iii) are  $C_2HF_3^+$  and  $CH_2CF_2^+$ , resulting from steps 3a and 3b, respectively. Again, it is clear which of these products is preferred;  $C_2HF_3^+$  is the major product of the reaction (BR = 45 %), whereas  $CH_2CF_2^+$  is only a minor product (BR = 3 %). A bond rotation is required for either step 3a or 3b to occur, which is sterically unfavourable, and so the more favourable step 2b is, the less likely step 3b will be. Likewise, the same comment is made with respect to steps 2a and 3a. This then explains why, following step 1a, formation of  $C_2HF_3^+$  by step 3a is the dominant outcome, whereas following step 1b, elimination of  $CF_3$  by step 2b is the dominant outcome. A previous ICR-MS study of the reaction  $(C_2H_3F + C_2F_4)^+$  revealed the products  $C_2HF_3^+$  (62 %),  $C_3H_3F_2^+$  (32 %), and  $C_3H_2F_3^+$  (7 %),<sup>62</sup> which is in agreement with the dominant products observed in this SIFT study [Table 4.B.(I)]. If *only* the mechanism in Figure 4.B.(iii) is considered, then the adduct species, observed as the minor product with BR = 2 %, is the detection of either intermediate species produced by steps 1a or 1b. Given the number of hydrogen and fluorine atoms in the two reactants, it should also be considered that the observed adduct may be a hydrogen-bonded species.

Figure 4.B.(iv) shows how the same mechanism can be used to explain the products observed from the reaction of  $C_2F_4^+$  with  $CH_2CF_2$ . In particular, how elimination of  $CF_3$  and  $CHF_2$  *are* observed, yet fluorinated ethene cation products (from steps 3a or 3b) are *not* observed; in Figure 4.B.(iv), step 3a will revert back to the reactants and step 3b is endothermic. Again, a preference to eliminate  $CF_3$  over  $CHF_2$  is observed.

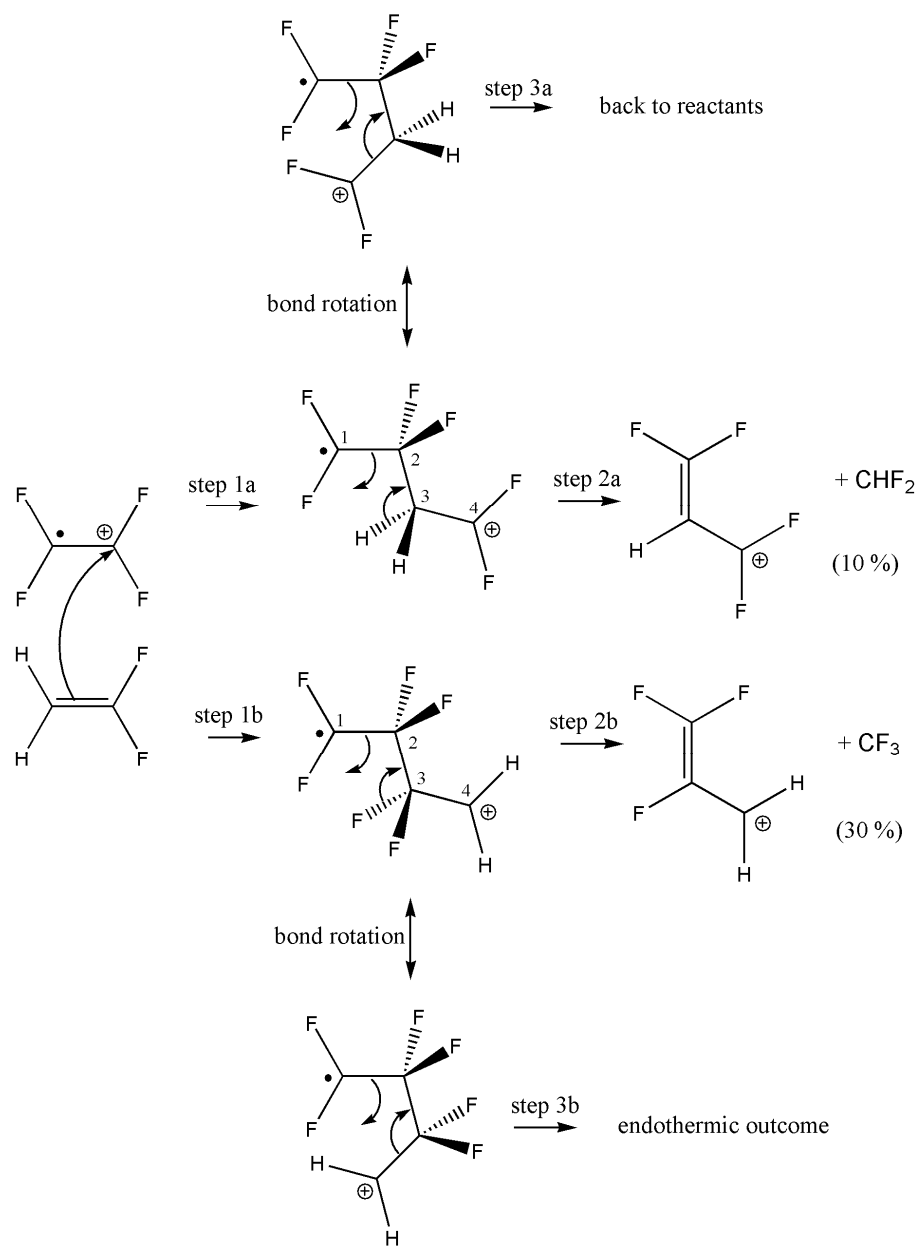


**Figure 4.B.(iv).** The proposed mechanism for the reaction between the tetrafluoroethene cation ( $C_2F_4^+$ ) and 1,1-difluoroethene ( $CH_2CF_2$ ).

The major difference in the reaction of  $C_2F_4^+$  with  $CH_2CF_2$  compared to that with  $C_2H_4$ ,  $C_2H_3F$  or  $C_2HF_3$  is the large BR recorded for the adduct species (60 % compared to 0 %, 2 %, and 0 %, respectively). There is no obvious explanation. It is also worth noting that in the

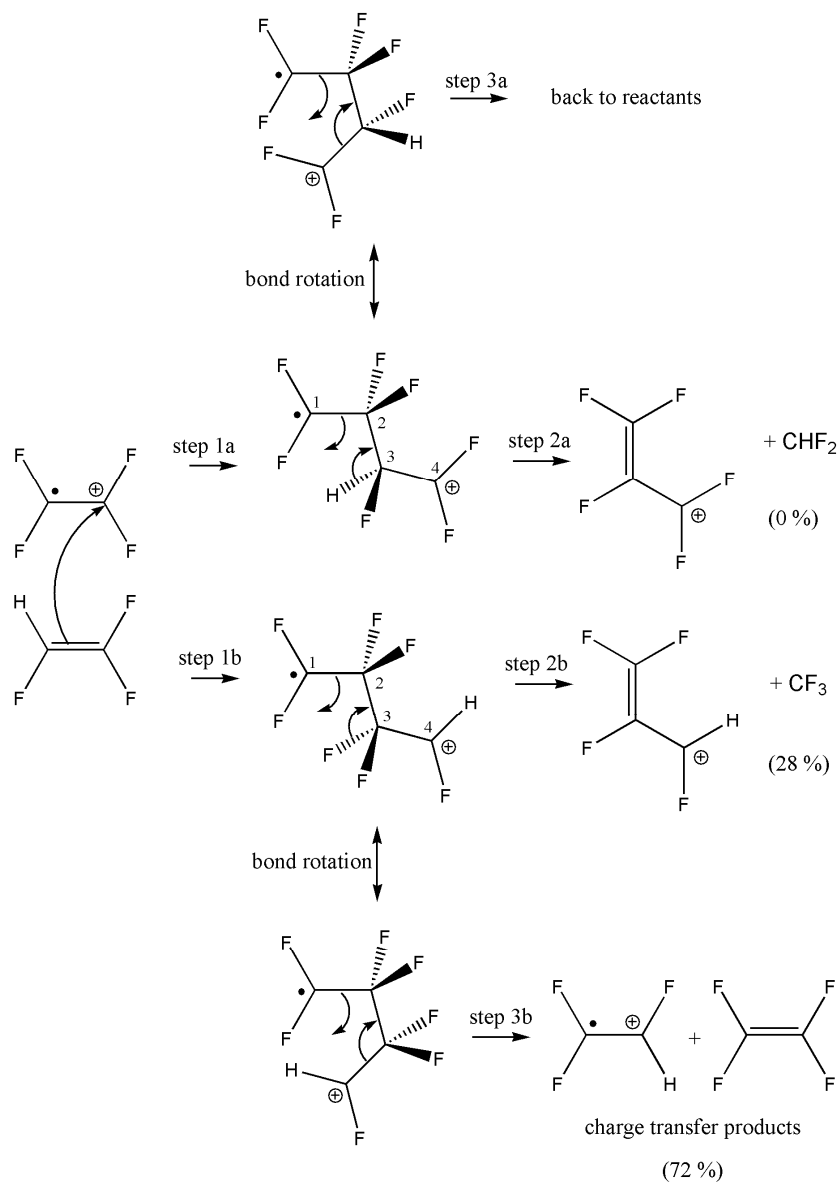
reaction of  $C_2F_4^+$  with  $C_2F_4$ , no adduct species is observed, and the only product is  $C_3F_5^+$  (+  $CF_3$ ).<sup>50</sup> In addition, the ICR-MS study by Anicich and Bowers showed the *only* product in the reaction  $(CH_2CF_2 + C_2F_4)^+$  was  $C_3H_2F_3^+$  (+  $CF_3$ ).<sup>62</sup>

Figure 4.B.(v) shows the same mechanism when applied to the reaction of  $C_2F_4^+$  with  $C_2HF_3$ . Consistent with the results discussed above, the preference for the intermediate species to eliminate  $CF_3$  rather than  $CHF_2$  is observed, but now  $CHF_2$  elimination is not observed at all. In the reaction  $(C_2HF_3 + C_2F_4)^+$ , Anicich and Bowers observed 92 %  $C_3HF_4^+$  (+  $CF_3$ ) and 8 %  $C_3F_5^+$  (+  $CHF_2$ ).<sup>62</sup> In Figure 4.B.(v), step 2a shows how  $CHF_2$  elimination is possible, but this step could also lead to  $CF_3$  elimination given that carbon 3 in the intermediate species has both hydrogen and fluorine substituents. It is therefore proposed that the channel leading to 28 %  $CF_3$  elimination is a contribution from steps 2a and 2b.

$C_2HF_3^+$  is detected with a BR of 72 % [Table 4.B.(I)]. Figure 4.B.(v) shows how this can arise from step 3b, however, a charge transfer mechanism could also be the origin of this species. Certainly in ion-molecule reactions when charge transfer is observed, it is commonly the dominant product channel. As discussed above, however, this reaction is endothermic, albeit by only + 2 kJ mol<sup>-1</sup>. Therefore, the observation of  $C_2HF_3^+$  is perhaps unsurprising, and could result from vibrationally-excited  $C_2F_4^+$  present in the flow tube, or by considering thermal energy in overcoming the reaction endothermicity. Also, when the magnitude of the endothermicity is so small, errors in the thermochemical values used to calculate this enthalpy could mean that the reaction is actually exothermic. The *IE* of  $C_2F_4$  is 10.12 eV,<sup>59</sup> that of  $C_2HF_3$  is 10.14 eV,<sup>55</sup> but experimental errors are not quoted for these values. A ‘charge transfer’ reaction does not imply the two species react intimately, but rather an electron from



the neutral molecule ‘hops’ over a given distance to combine with the cation. These reactions are usually fast and occur at the collisional rate.



**Figure 4.B.(v).** The proposed mechanism for the reaction between the tetrafluoroethene cation ( $C_2F_4^+$ ) and trifluoroethene ( $C_2HF_3$ ).

The intimate chemical reaction shown by step 3b in Figure 4.B.(v), in which the two species come into contact and form/break bonds, does also explain the observation of  $C_2HF_3^+$  from the reaction of  $C_2HF_3$  with  $C_2F_4^+$ . Evidence in support of this mechanism can be found in the values for  $k_{\text{exp}}$  and  $k_c$  for this reaction [Table 4.B.(I)]; if 72 % of products formed were from a fast charge transfer reaction, it is unlikely that the rate efficiency would be as low as 17 %. In addition, this efficiency in the reaction of  $C_2F_4^+$  with  $C_2HF_3$  is lower than that for  $C_2F_4^+$  with  $C_2H_4$  (70 %),  $C_2H_3F$  (40 %) or with  $CH_2CF_2$  (50 %). None of the products from the latter three reactions are expected to arise from ‘fast’ processes, and so it becomes difficult to explain the relatively low rate efficiency when  $C_2F_4^+$  reacts with  $C_2HF_3$  if 72 % of products occur by charge transfer. On the other hand, the slight endothermicity of this reaction might explain why a charge transfer reaction might not occur at a collisional rate. Another reason to consider the reaction shown in Figure 4.B.(v) is that all other products observed in the four reactions with  $C_2F_4^+$  can be explained if a similar reaction mechanism is considered (see discussion above).

In Figures 4.B.(ii) to 4.B.(v), steps 3, 3a, and 3b show the proposed mechanism to explain the formation of two substituted ethene products different to the reacting species. In similar ion-molecule reactions of substituted ethene species it has been suggested that a cycloadduct intermediate is formed, rather than a 4-carbon chain, which then dissociates to form products.<sup>60,62</sup> The cycloaddition reaction is shown in Figure 4.B.(vi) for the example of  $C_2H_3F$  reacting with  $C_2F_4^+$ . Note that in these earlier studies a 4-carbon chain intermediate is still suggested to explain the  $C_3X_5^+$  products ( $X = H$  or  $F$ ), shown in Figures 4.B.(ii) to 4.B.(v) by steps 2, 2a, and 2b. The 4-carbon chain intermediate is considered a preferable mechanism to the cycloaddition intermediate for the following reasons. Firstly because the cycloaddition reaction requires  $C_2F_4^+$  to be represented as species 3, when in fact species 1 is much more

realistic [see discussion above and Figure 4.B.(i)]. If species 1 was used to represent  $C_2F_4^+$  in Figure 4.B.(vi), it becomes more difficult to rationalise the formation of a cycloadduct in step 1. Secondly, the relative BRs in the observed products (excluding the adduct) are better explained by one mechanism, rather than by two different mechanisms; for example in Figure 4.B.(iii) step 3a is more likely to occur than step 3b because step 2b is considered a more favourable outcome than step 2a (see discussion above).

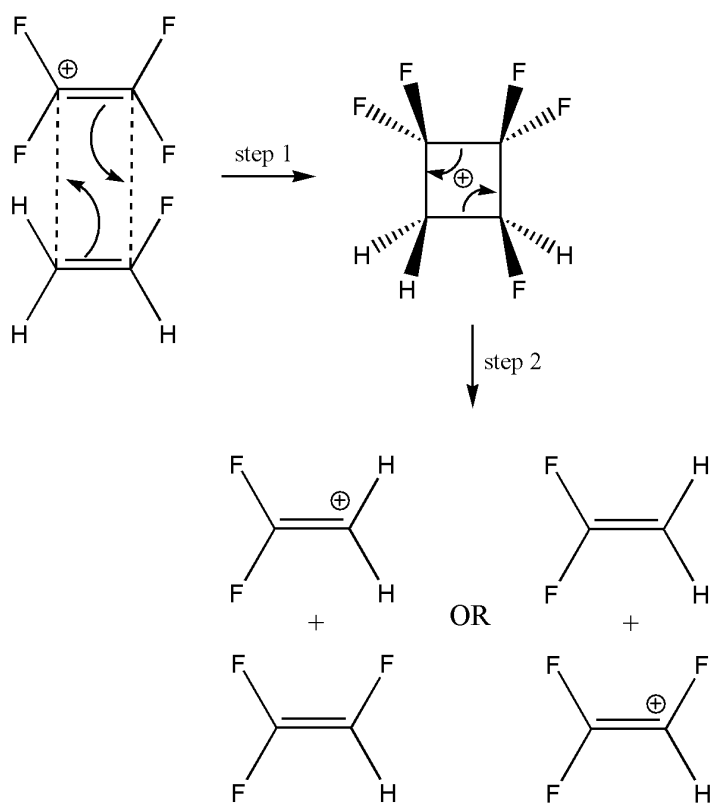
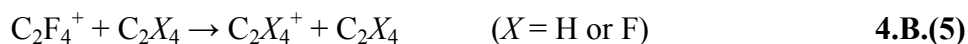
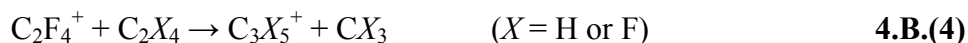


**Figure 4.B.(vi).** An example of the reaction between  $C_2F_4^+$  and  $C_2H_3F$  showing the production of two fluorinated ethene products which are different to the reactant species, using a cycloaddition mechanism.

### 4.C. Conclusions

The reactions between  $\text{C}_2\text{F}_4^+$  and  $\text{C}_2\text{H}_4$ ,  $\text{C}_2\text{H}_3\text{F}$ ,  $\text{CH}_2\text{CF}_2$ , and  $\text{C}_2\text{HF}_3$  have been performed using a Selected Ion Flow Tube. Some interesting intimate chemical reactions have been observed, and the product channels have been explained using arrow-pushing mechanisms. The same generic mechanism can be used to explain all products observed from each of the reactions studied.

The proposed mechanisms suggest that there are two major reaction pathways competing which both arise from the same 4-carbon branched intermediate species. In one instance,  $\text{CF}_3$  or  $\text{CHF}_2$  is eliminated from the intermediate [generically described by reaction 4.B.(4)], and in the other case the intermediate dissociates to yield two fluorinated ethene products [generically described by reaction 4.B.(5)].



In reaction 4.B.(4), a clear preference for  $\text{CF}_3$  elimination *vs.*  $\text{CHF}_2$  elimination is observed. Other trends in the results are less clear-cut but arguments, albeit suggested tentatively, are proposed in an attempt to explain them. This work shows how common organic chemistry-type arrow pushing mechanisms can help to explain seemingly complex gas-phase reactions.

# Chapter 5:

## *The reactions of $\text{OH}^-$ , $\text{O}^-$ , $\text{CF}_3^-$ , $\text{F}^-$ , and $\text{O}_2^-$ with $\text{C}_2\text{H}_4$ , $\text{C}_2\text{H}_3\text{F}$ , $\text{CH}_2\text{CF}_2$ , $\text{C}_2\text{HF}_3$ and $\text{C}_2\text{F}_4$*

This chapter takes a new approach in the investigation of fluorination in ethene by looking at some *anion*-molecule reactions. The data presented were collected by Drs Richard Kennedy and Chris Mayhew many years ago. The raw data was given to me for a project which I started in the fourth year of my undergraduate MSci degree, and continued over the first few years of my Ph.D. The discussion and interpretation of the results presented here is almost entirely my own work, but I would like to thank Dr Liam Cox for many helpful discussions about organic chemistry reaction mechanisms, Dr Michael Parkes and Professor Richard Tuckett for continued guidance during these early stages of my research.

### **5.A. Background information**

The reactions of ethene ( $\text{C}_2\text{H}_4$ ), monofluoroethene ( $\text{C}_2\text{H}_3\text{F}$ ), 1,1-difluoroethene ( $\text{CH}_2\text{CF}_2$ ), trifluoroethene ( $\text{C}_2\text{HF}_3$ ) and tetrafluoroethene ( $\text{C}_2\text{F}_4$ ) with some cations have been discussed in Chapters 3 and 4. The electron density around the fluorine atom(s), and the dipole moment are important factors in understanding how the molecule interacts with the cation. It is now

*anions* which are being reacted with this same group of substituted ethene molecules, and so it is the *acidity* of the molecule and the *electropositivity* of the carbon atoms which becomes important. It has been discussed by Sullivan and Beauchamp that single fluorine substitution in both ethane<sup>64</sup> and ethene<sup>65</sup> increases the acidity of the molecule by approximately  $100 \text{ kJ mol}^{-1}$ , and that additional fluorine substitution will increase the acidity further, but to a much lesser extent.

Some of the reactions presented here have been studied previously by other groups. The gas-phase reaction of  $\text{O}^-$  with  $\text{C}_2\text{H}_4$  has been studied by Drift Tube mass spectrometry,<sup>66,67</sup> and using a SIFT.<sup>68</sup> Ion Cyclotron Resonance Mass Spectrometry (ICR-MS) has been used to study the reaction of  $\text{O}^-$  with  $\text{C}_2\text{H}_4$ ,  $\text{C}_2\text{H}_3\text{F}$  and  $\text{CH}_2\text{CF}_2$ ,<sup>69</sup> and a Flowing Afterglow apparatus used to study  $\text{O}^-$  and  $\text{OH}^-$  reactions with  $\text{C}_2\text{H}_4$ .<sup>70</sup> Some anions reacting with  $\text{C}_2\text{F}_4$  have also been investigated by SIFT mass spectrometry;  $\text{O}^-$  and  $\text{O}_2^-$  by Morris,<sup>71</sup> and  $\text{F}^-$  and  $\text{CF}_3^-$  by Su *et al.*<sup>72</sup>

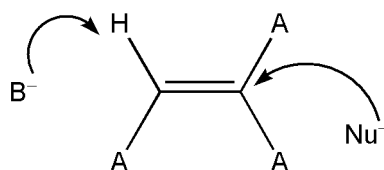


**Figure 5.A.(i).** A pictorial representation of the differences in the initial reaction step depending if the anion acts as a base ( $\text{B}^-$ ) or as a nucleophile ( $\text{Nu}^-$ ). A represents either H or F.

The data presented here forms the continuation of a study into the gas-phase reactions of anions with halogen substituted ethenes by the *Molecular Physics* group in Birmingham, and

the reactions of  $\text{OH}^-$ ,  $\text{O}^-$ ,  $\text{CF}_3^-$ ,  $\text{F}^-$  and  $\text{O}_2^-$  with the *chlorinated* ethenes have already been investigated.<sup>15</sup>

The discussion below often refers to the reactant anion species either acting as a *base*, or as a *nucleophile*. Figure 5.A.(i) clarifies what is meant by these two terms, and the intended differentiation between them: when the anion acts as a base it will attack a hydrogen atom, and when acting as a nucleophile it will attack a carbon atom.

### 5.B. Results

In this section the results are presented and some general comments are made. In particular, comparisons are made to previous studies, and some ambiguous details regarding some of the observed anion species are discussed.

The results for the reactions of  $\text{OH}^-$ ,  $\text{O}^-$ ,  $\text{CF}_3^-$ ,  $\text{F}^-$  and  $\text{O}_2^-$  with ethene ( $\text{C}_2\text{H}_4$ ), monofluoroethene ( $\text{C}_2\text{H}_3\text{F}$ ), 1,1-difluoroethene ( $\text{CH}_2\text{CF}_2$ ), trifluoroethene ( $\text{C}_2\text{HF}_3$ ) and tetrafluoroethene ( $\text{C}_2\text{F}_4$ ) are presented in Table 5.B.(I). These include the product anions, their branching ratios (BRs) and the bimolecular reaction rate coefficient,  $k_{\text{exp}}$ . Collisional rate coefficients,  $k_{\text{c}}$ , are also included. Where an association reaction is observed the helium buffer gas pressure is given due to its involvement in collisionally stabilising the energised intermediate formed.

The reactions of  $\text{C}_2\text{H}_4$  provide a useful comparison to those of the fluorinated ethenes. As seen from Table 5.B.(I) only  $\text{O}^-$  and  $\text{F}^-$  react with  $\text{C}_2\text{H}_4$ , and the experimental rate coefficients are significantly below the corresponding collisional values. For the reaction with  $\text{F}^-$  an association product is observed, but the depletion in  $\text{F}^-$  signal was too small to determine the

value for  $k_{\text{exp}}$ , and the value of  $1.0 \times 10^{-13} \text{ cm}^3 \text{ molecule}^{-1} \text{ s}^{-1}$  represents the lowest value which can be measured by the Birmingham SIFT apparatus.

**Table 5.B.(I).** A summary of results for the gas-phase reactions of some anions with ethene and the fluorinated ethenes. All reaction rate coefficients,  $k$ , are given in units of  $\text{cm}^3 \text{ molecule}^{-1} \text{ s}^{-1}$  and branching ratios are expressed as percentages.

	<b>C<sub>2</sub>H<sub>4</sub></b>	<b>C<sub>2</sub>H<sub>3</sub>F</b>	<b>CH<sub>2</sub>CF<sub>2</sub></b>	<b>C<sub>2</sub>HF<sub>3</sub></b>	<b>C<sub>2</sub>F<sub>4</sub></b>
<b>OH<sup>-</sup></b>	No reaction	$k_{\text{exp}} = 3.1 \times 10^{-9}$ $k_c = 2.5 \times 10^{-9}$ H <sub>2</sub> O.F <sup>-</sup> (53 %) C <sub>2</sub> H <sub>2</sub> F <sup>-</sup> (40 %) F <sup>-</sup> (5 %) C <sub>2</sub> H <sub>3</sub> O <sup>-</sup> (2 %)	$k_{\text{exp}} = 1.8 \times 10^{-9}$ $k_c = 2.4 \times 10^{-9}$ C <sub>2</sub> HF <sub>2</sub> <sup>-</sup> (97 %) H <sub>2</sub> O.F <sup>-</sup> (3 %)	$k_{\text{exp}} = 2.8 \times 10^{-9}$ $k_c = 2.2 \times 10^{-9}$ C <sub>2</sub> F <sub>3</sub> <sup>-</sup> (100 %)	$k_{\text{exp}} = 1.2 \times 10^{-9}$ $k_c = 1.3 \times 10^{-9}$ CF <sub>3</sub> <sup>-</sup> (48 %) FCO <sup>-</sup> (18 %) C <sub>2</sub> F <sub>3</sub> O <sup>-</sup> (15 %) F <sup>-</sup> (10 %) HF <sub>2</sub> <sup>-</sup> (9 %)
<b>O<sup>-</sup></b>	$k_{\text{exp}} = 6.3 \times 10^{-10}$ $k_c = 1.5 \times 10^{-9}$ C <sub>2</sub> H <sub>2</sub> <sup>-</sup> (71 %) e <sup>-</sup> (26 %) <sup>a</sup> C <sub>2</sub> H <sub>3</sub> O <sup>-</sup> (3 %)	$k_{\text{exp}} = 3.9 \times 10^{-9}$ $k_c = 2.5 \times 10^{-9}$ e <sup>-</sup> (72 %) <sup>a</sup> C <sub>2</sub> HF <sup>-</sup> (24 %) C <sub>2</sub> H <sub>2</sub> O <sup>-</sup> (4 %)	$k_{\text{exp}} = 2.0 \times 10^{-9}$ $k_c = 2.4 \times 10^{-9}$ e <sup>-</sup> (80 %) <sup>a</sup> C <sub>2</sub> F <sub>2</sub> <sup>-</sup> (20 %)	$k_{\text{exp}} = 2.2 \times 10^{-9}$ $k_c = 2.2 \times 10^{-9}$ e <sup>-</sup> (65 %) <sup>a</sup> C <sub>2</sub> F <sub>3</sub> <sup>-</sup> (35 %)	$k_{\text{exp}} = 1.0 \times 10^{-9}$ $k_c = 1.3 \times 10^{-9}$ F <sup>-</sup> (68 %) e <sup>-</sup> (18 %) <sup>a</sup> C <sub>2</sub> F <sub>3</sub> O <sup>-</sup> (6 %) CF <sub>3</sub> <sup>-</sup> (4 %) FCO <sup>-</sup> (4 %)
<b>CF<sub>3</sub><sup>-</sup></b>	No reaction	No reaction	No reaction	$k_{\text{exp}} = 8.5 \times 10^{-10}$ $k_c = 1.3 \times 10^{-9}$ C <sub>2</sub> F <sub>3</sub> <sup>-</sup> (100 %)	$k_{\text{exp}} = 2.6 \times 10^{-10}$ $k_c = 7.6 \times 10^{-10}$ F <sup>-</sup> (100 %)
<b>F<sup>-</sup></b>	$k_{\text{exp}} < 1.0 \times 10^{-13}$ $k_c = 1.4 \times 10^{-9}$ $p(\text{He}) = 0.6 \text{ Torr}$ C <sub>2</sub> H <sub>4</sub> F <sup>-</sup> (100 %)	$k_{\text{exp}} = 5.6 \times 10^{-12}$ $k_c = 2.4 \times 10^{-9}$ $p(\text{He}) = 0.6 \text{ Torr}$ C <sub>2</sub> H <sub>3</sub> F <sub>2</sub> <sup>-</sup> (100 %)	$k_{\text{exp}} = 1.1 \times 10^{-11}$ $k_c = 2.3 \times 10^{-9}$ $p(\text{He}) = 0.5 \text{ Torr}$ C <sub>2</sub> H <sub>2</sub> F <sub>3</sub> <sup>-</sup> (100 %)	$k_{\text{exp}} = 2.3 \times 10^{-10}$ $k_c = 2.1 \times 10^{-9}$ $p(\text{He}) = 0.6 \text{ Torr}$ C <sub>2</sub> HF <sub>4</sub> <sup>-</sup> (95 %) C <sub>2</sub> F <sub>3</sub> <sup>-</sup> (5 %)	$k_{\text{exp}} = 3.0 \times 10^{-10}$ $k_c = 1.2 \times 10^{-9}$ $p(\text{He}) = 0.5 \text{ Torr}$ C <sub>2</sub> F <sub>5</sub> <sup>-</sup> (100 %)
<b>O<sub>2</sub><sup>-</sup></b>	No reaction	$k_{\text{exp}} = 1.1 \times 10^{-12}$ $k_c = 2.0 \times 10^{-9}$ $p(\text{He}) = 0.65 \text{ Torr}$ C <sub>2</sub> H <sub>3</sub> FO <sub>2</sub> <sup>-</sup> (100 %)	$k_{\text{exp}} = 2.0 \times 10^{-11}$ $k_c = 1.9 \times 10^{-9}$ e <sup>-</sup> (100 %) <sup>a</sup>	$k_{\text{exp}} = 4.8 \times 10^{-10}$ $k_c = 1.7 \times 10^{-9}$ F <sup>-</sup> (100 %)	$k_{\text{exp}} = 1.0 \times 10^{-9}$ $k_c = 1.0 \times 10^{-9}$ F <sup>-</sup> (46 %) e <sup>-</sup> (35 %) <sup>a</sup> F <sub>2</sub> <sup>-</sup> (8 %) C <sub>2</sub> F <sub>4</sub> O <sup>-</sup> (8 %) FCO <sup>-</sup> (3 %)

<sup>a</sup> The production of electrons, e<sup>-</sup>, from a reaction is monitored in the experiment by observing a drop in the current across the Faraday plate (see Chapter 2 for experimental details).

The fluorinated ethenes show a much higher level of reactivity, highlighting the effect electronegative fluorine atoms have on the molecule; a fluorine substituent on ethene will



generate electropositivity in carbon (making it more susceptible to nucleophilic attack), and increase the acidity of the molecule (increasing susceptibility to attack from a base).

Several other groups have studied the gas-phase reaction of O<sup>-</sup> with C<sub>2</sub>H<sub>4</sub>. In agreement with this study, using a SIFT Viggiano and Paulson observe three anion products: e<sup>-</sup>, C<sub>2</sub>H<sub>2</sub><sup>-</sup>, and a minor product, C<sub>2</sub>H<sub>3</sub>O<sup>-</sup>.<sup>68</sup> The major difference between these studies is the difference in BRs for the two major products: C<sub>2</sub>H<sub>2</sub><sup>-</sup> and electrons. This work suggests C<sub>2</sub>H<sub>2</sub><sup>-</sup> is the dominant product (BR = 71 %), whereas Viggiano and Paulson record it as e<sup>-</sup> detachment (BR = 68 %). Using drift tube apparatus, Parkes<sup>66</sup> and Lindinger *et al.*<sup>67</sup> not only observe C<sub>2</sub>H<sub>2</sub><sup>-</sup> and C<sub>2</sub>H<sub>3</sub>O<sup>-</sup>, but also OH<sup>-</sup> and C<sub>2</sub>HO<sup>-</sup> which are not seen in either SIFT study. Lindinger *et al.* did not monitor electrons in their study, however, Parkes also reports electron detachment as the major channel. In a Flowing Afterglow experiment, O<sup>-</sup> was found to react with C<sub>2</sub>H<sub>4</sub> by electron detachment only.<sup>70</sup> Using ICR-MS, C<sub>2</sub>H<sub>2</sub><sup>-</sup> was the only observed reaction, although electron detachment was not monitored.<sup>69</sup> Given the differences in techniques used to study the reaction of O<sup>-</sup> with C<sub>2</sub>H<sub>4</sub>, it is difficult to compare and explain all these results, but it is clear that when electron detachment was monitored it was found to be the dominant reaction in all experiments except this SIFT study.

The reaction of OH<sup>-</sup> with C<sub>2</sub>H<sub>4</sub> has also been studied previously, and in agreement with the results of this study, these species were found not to react.<sup>70</sup> This is not surprising, as the expected H<sup>+</sup> abstraction reaction forming water is endothermic by 71 kJ mol<sup>-1</sup>.

The reactions of C<sub>2</sub>H<sub>3</sub>F and CH<sub>2</sub>CF<sub>2</sub> show few trends when comparing the data of each individual neutral as the reactant anion changes. For C<sub>2</sub>H<sub>3</sub>F only association is observed in the reactions with F<sup>-</sup> and O<sub>2</sub><sup>-</sup>, whereas the reactions with OH<sup>-</sup> and O<sup>-</sup> afford a wider range of

product anions. Similarly for CH<sub>2</sub>CF<sub>2</sub>, an equally diverse range of products are detected; exclusive electron detachment results from the reaction with O<sub>2</sub><sup>-</sup>, with F<sup>-</sup> only association is observed, but the reactions with OH<sup>-</sup> and O<sup>-</sup> produce products such as C<sub>2</sub>HF<sub>2</sub><sup>-</sup> and C<sub>2</sub>F<sub>2</sub><sup>-</sup>, respectively. These basic observations from Table 5.B.(I) show that the reactant anion probably holds the key to interpreting the outcome from these reactions, and when looking at *all* of the results shown, trends are more obviously identified when comparing results from all the reactions with one single anion [*i.e.* looking from left to right in Table 5.B.(I)]. In Sections 5.C to 5.G the discussion focuses on this, looking at how the reaction of one anion with the series of ethenes changes as the degree of fluorination increases.

The exception to the comment made above is perhaps in the reactions with C<sub>2</sub>HF<sub>3</sub>. Its reactions with OH<sup>-</sup>, O<sup>-</sup>, CF<sub>3</sub><sup>-</sup> and F<sup>-</sup> all yield a common product: C<sub>2</sub>F<sub>3</sub><sup>-</sup>. Certainly C<sub>2</sub>HF<sub>3</sub> is expected to be the most acidic of the neutral reactants, which favours proton abstraction reactions being dominant:



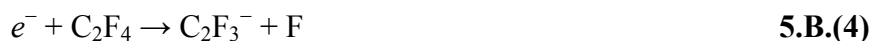
where B<sup>-</sup> represents the reactant anion acting as a base. It is also noted that C<sub>2</sub>F<sub>3</sub><sup>-</sup> is a relatively stable anion and the negative charge is delocalised by the electronegative fluorine atoms. Simmonett *et al.* performed theoretical calculations for the fluorinated vinyl anion series, attributing the greater relative stability of C<sub>2</sub>F<sub>3</sub><sup>-</sup> to inductive and negative hyperconjugative effects.<sup>73</sup> The thermochemical tabulations of Lias *et al.*<sup>74</sup> contain three quite different values for the enthalpy of formation of C<sub>2</sub>F<sub>3</sub><sup>-</sup>:  $-391 \pm 19$ ,<sup>75</sup>  $-637 \pm 58$ ,<sup>76</sup> and  $-420 \pm 42$  kJ mol<sup>-1</sup>.<sup>77</sup> The first value comes from an experiment in which C<sub>2</sub>F<sub>3</sub><sup>-</sup> was observed as a product of dissociative electron attachment to C<sub>3</sub>F<sub>8</sub>:



The value extracted from this work by Lias *et al.* comes from the estimated  $\Delta_r H^\circ$  for reaction 5.B.(2), and assumes the structure of C<sub>2</sub>F<sub>3</sub><sup>-</sup> to be CF<sub>2</sub>=CF<sup>-</sup>. The second value comes from the threshold for formation of C<sub>2</sub>F<sub>3</sub><sup>-</sup> from CF<sub>3</sub>CHO:



Note the isomeric form of C<sub>2</sub>F<sub>3</sub><sup>-</sup> in reaction 5.B.(3) has all fluorines bonded to *one* of the carbon atoms. The third and preferred value, of -420 kJ mol<sup>-1</sup>, was derived from the observed threshold for reaction 5.B.(4):



Clearly there is uncertainty in all of the values discussed above, but when calculating initial enthalpy changes for reactions 5.B.(5) to 5.B.(9), the value of -420 ± 42 kJ mol<sup>-1</sup> is used.

The only reaction of C<sub>2</sub>HF<sub>3</sub> which does not yield C<sub>2</sub>F<sub>3</sub><sup>-</sup> as a product is that with O<sub>2</sub><sup>-</sup>. The thermochemistry for the expected H<sup>+</sup> abstraction resulting in C<sub>2</sub>F<sub>3</sub><sup>-</sup> is endothermic:



This can then be compared to the thermochemistry for the other anion reactions with C<sub>2</sub>HF<sub>3</sub>, where C<sub>2</sub>F<sub>3</sub><sup>-</sup> is a common product:



<sup>‡</sup> The enthalpy changes for reactions 5.B.(5) to 5.B.(9) are considered incorrect, because of uncertainty in the value of  $\Delta_r H^\circ$  (C<sub>2</sub>F<sub>3</sub><sup>-</sup>) used, -420 kJ mol<sup>-1</sup>. A new value, -504 kJ mol<sup>-1</sup>, is evaluated from recent theoretical calculations, and from the presented experimental observations shown by reactions 5.B.(5) to 5.B.(9). The updated reaction enthalpies are +38, -113, -76, -69, and -36 kJ mol<sup>-1</sup>, respectively. See text for a more detailed discussion.



The calculated enthalpies are positive for reactions 5.B.(7) to 5.B.(9), yet the product C<sub>2</sub>F<sub>3</sub><sup>-</sup> is observed. It is very likely that uncertainty in the value for Δ<sub>r</sub>H° (C<sub>2</sub>F<sub>3</sub><sup>-</sup>), as discussed above, when used to calculate the Δ<sub>r</sub>H° values is responsible for this inconsistency. If it is assumed that reaction 5.B.(5) is endothermic because the C<sub>2</sub>F<sub>3</sub><sup>-</sup> product is not observed, then the true value for Δ<sub>r</sub>H° (C<sub>2</sub>F<sub>3</sub><sup>-</sup>) should lie between -468 and -543 kJ mol<sup>-1</sup> (the actual value used is -420 ± 42 kJ mol<sup>-1</sup>). Reactions 5.B.(6) to 5.B.(9) then all become exothermic – a much better reflection of the results.

Since the tabulations of Lias *et al.*,<sup>74</sup> theoretical calculations on the electron affinity (*EA*) and Δ<sub>r</sub>H° of C<sub>2</sub>F<sub>3</sub> have been performed. Thus, a new value for Δ<sub>r</sub>H° (C<sub>2</sub>F<sub>3</sub><sup>-</sup>) can be determined. The calculations by Bauschlicher and Ricca give a value for Δ<sub>r</sub>H° (C<sub>2</sub>F<sub>3</sub>) = -224 kJ mol<sup>-1</sup>,<sup>78</sup> and data collected for the *EA* (C<sub>2</sub>F<sub>3</sub>) is summarised in a recent review article.<sup>14</sup> The values for the *EA* range from 2.06 to 2.90 eV. As discussed above, it is expected that Δ<sub>r</sub>H° (C<sub>2</sub>F<sub>3</sub><sup>-</sup>) takes the values between -468 and -543 kJ mol<sup>-1</sup>, which corresponds to the *EA* being between 2.53 and 3.31 eV, respectively. This clearly suggests the *EA* (C<sub>2</sub>F<sub>3</sub>) is towards the higher end of the values given. Therefore, for the purposes of this thesis, a value for the *EA* of 2.90 eV (280 kJ mol<sup>-1</sup>) and the Δ<sub>r</sub>H° of -224 kJ mol<sup>-1</sup> for C<sub>2</sub>F<sub>3</sub> are used to give Δ<sub>r</sub>H°<sub>298</sub> (C<sub>2</sub>F<sub>3</sub><sup>-</sup>) = -504 kJ mol<sup>-1</sup>, with an estimated ± 20 kJ mol<sup>-1</sup> uncertainty. Using this new value,

<sup>‡</sup> The enthalpy changes for reactions 5.B.(5) to 5.B.(9) are considered incorrect, because of uncertainty in the value of Δ<sub>r</sub>H° (C<sub>2</sub>F<sub>3</sub><sup>-</sup>) used, -420 kJ mol<sup>-1</sup>. A new value, -504 kJ mol<sup>-1</sup>, is evaluated from recent theoretical calculations, and from the presented experimental observations shown by reactions 5.B.(5) to 5.B.(9). The updated reaction enthalpies are +38, -113, -76, -69, and -36 kJ mol<sup>-1</sup>, respectively. See text for a more detailed discussion.

the updated enthalpy changes for reactions 5.B.(5) to 5.B.(9) are +38, -113, -76, -69, and -36 kJ mol<sup>-1</sup>, respectively.

Absence of hydrogens in C<sub>2</sub>F<sub>4</sub> eliminates any possibility of the reactant anions acting as bases in their reactions. Attack of an anionic species on electron-rich fluorine is unlikely, and it is therefore expected to see anions only acting as nucleophiles in their reactions with C<sub>2</sub>F<sub>4</sub>.

The reactions of OH<sup>-</sup>, O<sup>-</sup> and O<sub>2</sub><sup>-</sup> with C<sub>2</sub>F<sub>4</sub> proceed at, or close to the collisional rate. Inspection of Table 5.B.(I) shows the diversity of anion products observed from these reactions. Morris also studied the reactions of O<sup>-</sup> and O<sub>2</sub><sup>-</sup> with C<sub>2</sub>F<sub>4</sub>.<sup>71</sup> An equally broad range of anion products was observed, and Morris rationalised this by comparing the weak double bond in C<sub>2</sub>F<sub>4</sub> with the strong C=O bonds which can form, concluding that specific mechanisms to account for all the products are difficult to propose.

F<sup>-</sup> reacts with C<sub>2</sub>F<sub>4</sub> to produce C<sub>2</sub>F<sub>5</sub><sup>-</sup> by association, and this same result was observed by Su *et al.*<sup>72</sup>



This association reaction fits into the trend of the other reactions with F<sup>-</sup>, and it is discussed in detail in Section 5.F.

F<sup>-</sup> anions were detected as the major product species (> 95 %) from the reaction of CF<sub>3</sub><sup>-</sup> with C<sub>2</sub>F<sub>4</sub>. The only thermochemically viable reaction is the addition of CF<sub>3</sub><sup>-</sup>, followed by the elimination of F<sup>-</sup> to produce hexafluoropropene:



In addition to F<sup>-</sup> ions, C<sub>2</sub>F<sub>5</sub><sup>-</sup> was also observed but as a minor product (< 5 %). The BR studies for this reaction, however, showed that C<sub>2</sub>F<sub>5</sub><sup>-</sup> is a *secondary* product. It must be that F<sup>-</sup> anions produced from reaction 5.B.(11) react with C<sub>2</sub>F<sub>4</sub> by association, which has already been shown to occur independently. Su *et al.* report C<sub>2</sub>F<sub>5</sub><sup>-</sup> is the *only* product from the reaction of CF<sub>3</sub><sup>-</sup> with C<sub>2</sub>F<sub>4</sub> suggesting it is produced by F<sup>-</sup> transfer:



It is more likely that they are observing C<sub>2</sub>F<sub>5</sub><sup>-</sup> from the secondary reaction as discussed above, and *not* that shown in reaction 5.B.(12) which is endothermic.

### 5.C. The reactions of OH<sup>-</sup>

Inspection of Table 5.B.(I) shows that the large majority of the observed anionic products from the reactions of OH<sup>-</sup> can be explained with the anion acting as a base. However, the minor products F<sup>-</sup> and C<sub>2</sub>H<sub>3</sub>O<sup>-</sup> from the reaction with C<sub>2</sub>H<sub>3</sub>F result from OH<sup>-</sup> acting as a nucleophile. The proposed addition-elimination mechanisms for producing these two anions are shown in Figure 5.C.(i). A stepwise addition-elimination mechanism is suggested rather than a concerted S<sub>N</sub>2 (bimolecular nucleophilic substitution) mechanism because the former allows for the carbanion intermediate to eliminate F<sup>-</sup> *or* HF (*i.e.* step 2a *vs.* step 2b). The only expected anionic product from an S<sub>N</sub>2 reaction would be F<sup>-</sup>. The elimination of F<sup>-</sup> following step 2a forms neutral C<sub>2</sub>H<sub>4</sub>O, presumably the isomeric form CH<sub>2</sub>=CHOH. The change in enthalpy for this reaction is -91 kJ mol<sup>-1</sup>. Step 3a, however, shows how CH<sub>2</sub>=CHOH could rearrange to form CH<sub>3</sub>CHO, a possibility given that Δ<sub>f</sub>H<sup>o</sup><sub>298</sub> (CH<sub>2</sub>=CHOH) = -125, and Δ<sub>f</sub>H<sup>o</sup><sub>298</sub> (CH<sub>3</sub>CHO) = -166 kJ mol<sup>-1</sup>. The competing mechanism, elimination of HF

following step 2b, suggests the isomeric form of the observed  $\text{C}_2\text{H}_3\text{O}^-$  anion is in fact  $\text{CH}_2=\text{CHO}^-$ , and the enthalpy change for this reaction is  $-155 \text{ kJ mol}^{-1}$ . This anion has two resonance forms, which are also shown in Figure 5.C.(i), where the negative charge is delocalised across the oxygen and carbon atoms – the likely reason for the relative stability of this species, and hence its observation as a product.

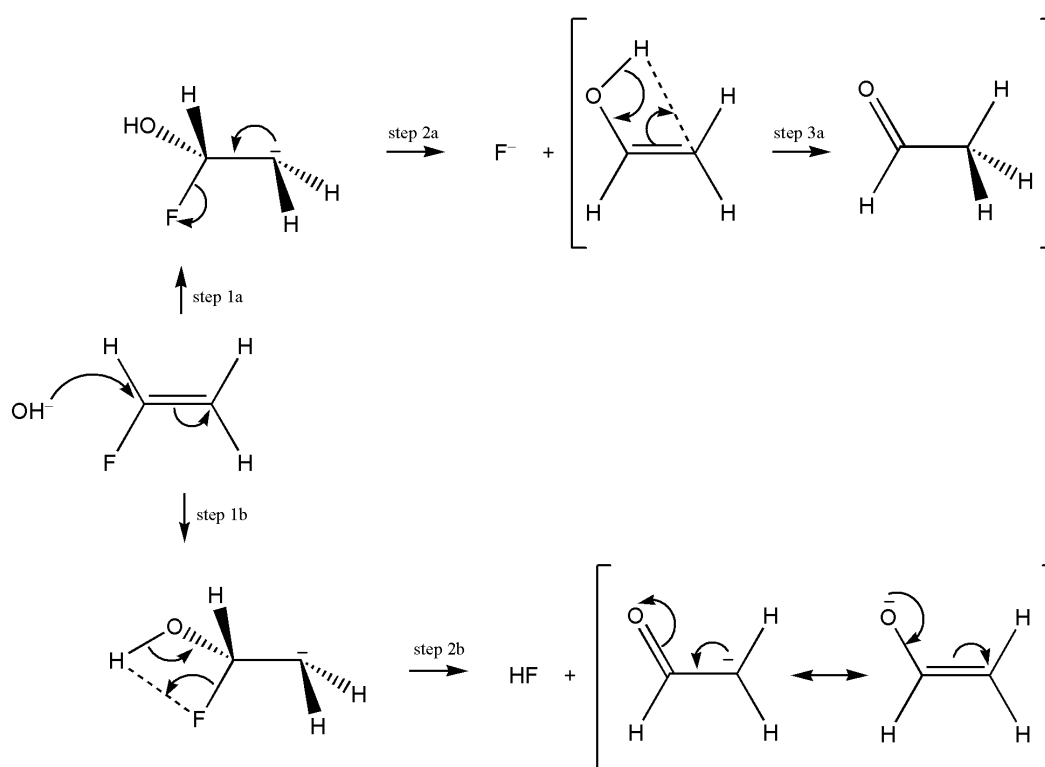
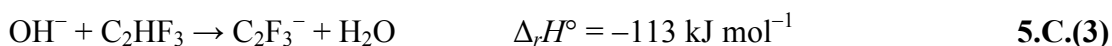
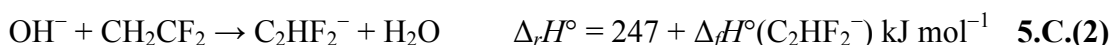
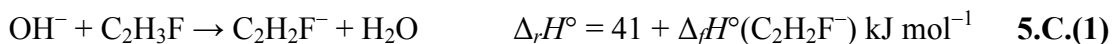


**Figure 5.C.(i).** Addition-elimination mechanisms showing the formation of  $\text{F}^-$  and  $\text{C}_2\text{H}_3\text{O}^-$  in the reaction of  $\text{OH}^-$  with  $\text{C}_2\text{H}_3\text{F}$ . The dotted lines represent bonds between atoms which are formed following the next reaction step.

In the reactions with  $\text{C}_2\text{H}_3\text{F}$ ,  $\text{CH}_2\text{CF}_2$  and  $\text{C}_2\text{HF}_3$ , it is  $\text{OH}^-$  acting as a base which accounts for the majority of the products detected. The products  $\text{C}_2\text{H}_2\text{F}^-$ ,  $\text{C}_2\text{HF}_2^-$  and  $\text{C}_2\text{F}_3^-$  are produced from  $\text{H}^+$  abstraction reactions:



Unfortunately no values for  $\Delta_f H^\circ$  (C<sub>2</sub>H<sub>2</sub>F<sup>-</sup> or C<sub>2</sub>HF<sub>2</sub><sup>-</sup>) have been found in the literature or thermochemical databases. Reactions 5.C.(1) and 5.C.(2) are expected to be exothermic, and so upper limits to these  $\Delta_f H^\circ$  values can be calculated:  $\Delta_f H^\circ_{298}(\text{C}_2\text{H}_2\text{F}^-) \leq -41 \text{ kJ mol}^{-1}$ , and  $\Delta_f H^\circ_{298}(\text{C}_2\text{HF}_2^-) \leq -247 \text{ kJ mol}^{-1}$ . There has been much discussion surrounding the structure of these two anionic species because of the potential for hydrogen-bonding to occur.<sup>73,79-82</sup>

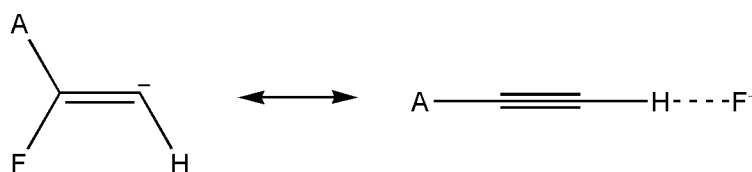


**Figure 5.C.(ii).** The two different structures suggested for C<sub>2</sub>H<sub>2</sub>F<sup>-</sup> (when A = H) and C<sub>2</sub>HF<sub>2</sub><sup>-</sup> (when A = F). Here, the dotted line represents hydrogen-bonding.

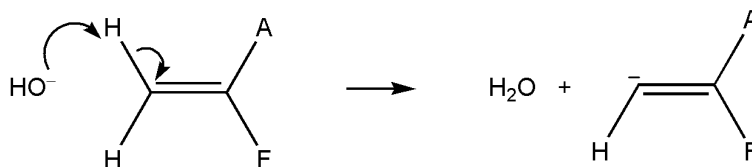
The two different suggested structures are shown in Figure 5.C.(ii). The general conclusion is that the hydrogen-bonded structure for C<sub>2</sub>H<sub>2</sub>F<sup>-</sup> is in the region of 50 kJ mol<sup>-1</sup> *lower* in energy than the vinyl anion,<sup>73,79</sup> but for C<sub>2</sub>HF<sub>2</sub><sup>-</sup> the difference in energies of the two structures is negligible.<sup>73</sup>

In the reactions of OH<sup>-</sup> with C<sub>2</sub>H<sub>3</sub>F and CH<sub>2</sub>CF<sub>2</sub>, the structures of the anion products C<sub>2</sub>H<sub>2</sub>F<sup>-</sup> and C<sub>2</sub>HF<sub>2</sub><sup>-</sup>, respectively, are not known. The mechanism for H<sup>+</sup> abstraction is



straightforward, as shown by mechanism 1 in Figure 5.C.(iii), and suggests it is the vinyl anion structure which is being observed.

Mechanism 1



Mechanism 2

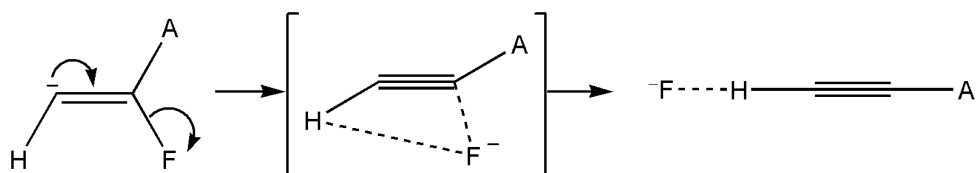


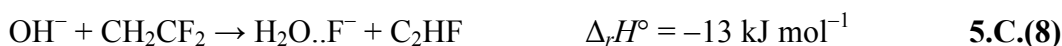
**Figure 5.C.(iii).** Mechanism 1 showing H<sup>+</sup> abstraction by OH<sup>-</sup> forming water and the corresponding vinyl anion. Mechanism 2 shows the rearrangement of the vinyl anion to form a hydrogen-bonded ethyne structure *via* the elimination of F<sup>-</sup>. In both mechanisms A = H showing the reaction with C<sub>2</sub>H<sub>3</sub>F, and A = F showing the reaction with CH<sub>2</sub>CF<sub>2</sub>.

On the other hand, mechanism 2 in Figure 5.C.(iii) shows a possible way for rearrangement to occur where the hydrogen-bonded species is formed – essentially the elimination of F<sup>-</sup>. The elimination of F<sup>-</sup>, and it forming the hydrogen bond, are shown to occur in a concerted fashion because reactions 5.C.(4) and 5.C.(5) are endothermic.



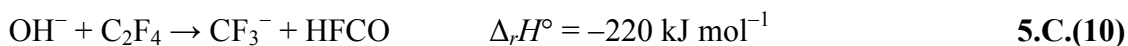
Thus, the energy gained on forming the hydrogen bond is required to drive the elimination of F<sup>-</sup>. Indeed the endothermicity of the elimination reactions above supports the suggestion made earlier that F<sup>-</sup> from the reaction with C<sub>2</sub>H<sub>3</sub>F is produced by an addition-elimination mechanism [Figure 5.C.(i)], with OH<sup>-</sup> acting as a nucleophile.

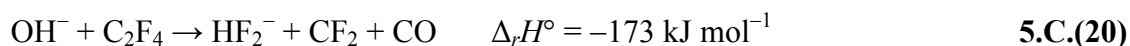
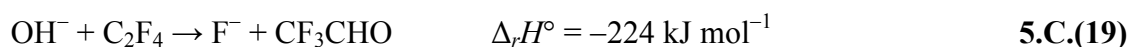
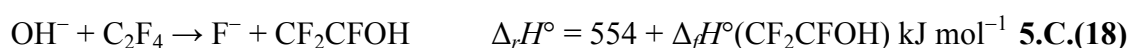
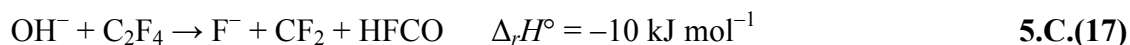
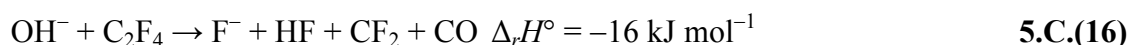
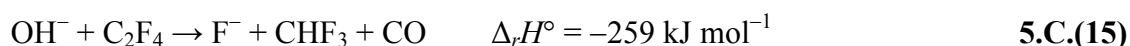
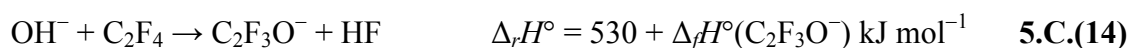
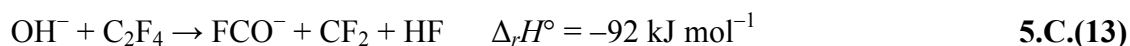
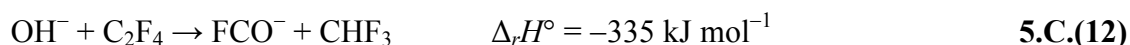
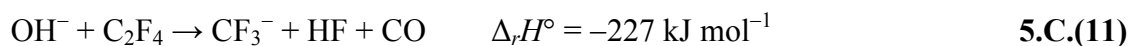
The formation of H<sub>2</sub>O..F<sup>-</sup> (H<sub>2</sub>O and F<sup>-</sup> hydrogen-bonded to one another) is the abstraction by OH<sup>-</sup> of HF:



The thermochemistry of reactions 5.C.(7) to 5.C.(9) reflect the products which are observed; the production of H<sub>2</sub>O..F<sup>-</sup> in reactions with C<sub>2</sub>H<sub>3</sub>F (53 %) and CH<sub>2</sub>CF<sub>2</sub> (3 %), but not with C<sub>2</sub>HF<sub>3</sub>. Energetics alone are unlikely to explain why the BR is much larger in the reaction of C<sub>2</sub>H<sub>3</sub>F than in that of CH<sub>2</sub>CF<sub>2</sub>; for HF to be abstracted from CH<sub>2</sub>CF<sub>2</sub> the hydrogen and fluorine must come from different ends of the double bond, which is not the case for C<sub>2</sub>H<sub>3</sub>F.

The reaction of OH<sup>-</sup> with C<sub>2</sub>F<sub>4</sub> is more complicated. It seems fair to assume OH<sup>-</sup> will be drawn towards the electropositive carbon atoms in C<sub>2</sub>F<sub>4</sub>, and acts as a nucleophile. The range of products observed show that the resulting reaction complex will readily rearrange, break bonds, and form new ones. Some exothermic reactions are listed below which show how the stable neutral products which can be formed are the likely driving force in this reaction:





The formation of F<sup>-</sup> and C<sub>2</sub>F<sub>3</sub>O<sup>-</sup> from C<sub>2</sub>F<sub>4</sub> are analogous to the products F<sup>-</sup> and C<sub>2</sub>H<sub>3</sub>O<sup>-</sup> from C<sub>2</sub>H<sub>3</sub>F, and so the suggested mechanism in Figure 5.C.(i) is also considered to describe reactions 5.C.(14) and 5.C.(18). Reactions 5.C.(18) and 5.C.(19) show different isomeric forms of the neutral product C<sub>2</sub>HF<sub>3</sub>O. The product CF<sub>2</sub>CFOH would be the expected species following a substitution reaction, whereas the product CF<sub>3</sub>CHO would require additional rearrangement. Unfortunately, Δ<sub>f</sub>H<sup>°</sup> (CF<sub>2</sub>CFOH) is not known.

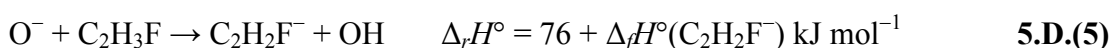
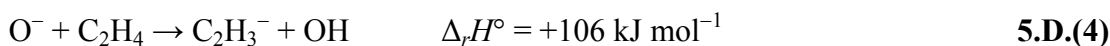
**5.D. The reactions of O<sup>-</sup>**

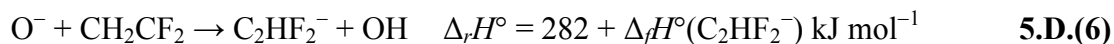
The first observation noted from this set of reactions is the production of the anion product following H<sub>2</sub><sup>+</sup> abstraction by O<sup>-</sup> to form water:



The isomeric forms of the anion products are H<sub>2</sub>C=C<sup>-</sup>, HFC=C<sup>-</sup> and F<sub>2</sub>C=C<sup>-</sup> for reactions 5.D.(1) to 5.D.(3), respectively. Note that there is some uncertainty in the  $\Delta_r H^\circ$  values for these species (see Appendix I). It is therefore assumed that the reaction mechanism leads to both hydrogen atoms being abstracted from the same carbon atom, and certainly this *must* be the case for C<sub>2</sub>F<sub>2</sub><sup>-</sup> production with CH<sub>2</sub>CF<sub>2</sub>.

These reaction products have been observed previously by Dawson and Jennings when performing reactions of O<sup>-</sup> with a variety of molecules using ICR-MS, and the same conclusion regarding the structure of the product anion was reached.<sup>69</sup> It seems very likely that H<sub>2</sub><sup>+</sup> abstraction is energetically more favourable than H<sup>+</sup> abstraction in the reactions of O<sup>-</sup> with C<sub>2</sub>H<sub>3</sub>F and CH<sub>2</sub>CF<sub>2</sub>; it is certainly the case for C<sub>2</sub>H<sub>4</sub>. In the case of C<sub>2</sub>HF<sub>3</sub>, H<sub>2</sub><sup>+</sup> abstraction is no longer possible and H<sup>+</sup> abstraction is observed instead. Consider the reactions below:





The values for  $\Delta_f H^\circ(\text{C}_2\text{H}_2\text{F}^-)$  and  $\Delta_f H^\circ(\text{C}_2\text{HF}_2^-)$  have been discussed in Section 5.C [see reactions 5.C.(1) to 5.C.(3)], and upper-limit values of  $\leq -41 \text{ kJ mol}^{-1}$ , and  $\leq -247 \text{ kJ mol}^{-1}$ , respectively, were evaluated. Also recall the discussion in Section 5.B about H<sup>+</sup> abstraction reactions with C<sub>2</sub>HF<sub>3</sub>. It is difficult to predict if reactions 5.D.(5) and 5.D.(6) are exothermic or not, and given that Dawson and Jennings observed these two reactions,<sup>69</sup> albeit as minor product channels, it is unclear why they are not observed in the present SIFT study.

It is very interesting that electron ejection is observed in the reactions of O<sup>-</sup> with ethene and the fluorinated ethenes. The fact that O<sup>-</sup> is a radical anion with an odd number of electrons is the likely cause. This represents the major product channel in the reactions of C<sub>2</sub>H<sub>3</sub>F (72 %), CH<sub>2</sub>CF<sub>2</sub> (80 %), and C<sub>2</sub>HF<sub>3</sub> (65 %), but the BRs are less in the case of C<sub>2</sub>H<sub>4</sub> (26 %) and C<sub>2</sub>F<sub>4</sub> (18 %). The reason for these differences in BRs is unclear, but it may be no coincidence that C<sub>2</sub>H<sub>4</sub> and C<sub>2</sub>F<sub>4</sub> are the only two of the five molecules with no dipole moment. Understanding the mechanism for the electron ejection reaction is not easy, and it is not even obvious if it is initiated by O<sup>-</sup> acting as a base or as a nucleophile.

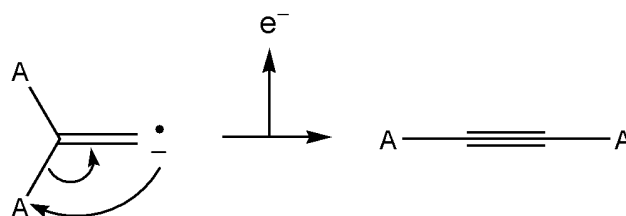


**Figure 5.D.(i).** A possible mechanism to account for electron ejection in the reactions of O<sup>-</sup> with C<sub>2</sub>H<sub>4</sub>, C<sub>2</sub>H<sub>3</sub>F and CH<sub>2</sub>CF<sub>2</sub>. The radical carbene structure results from the abstraction of H<sub>2</sub><sup>+</sup> by O<sup>-</sup>. A represents either H or F.

One possibility arises from the radical anion species produced following H<sub>2</sub><sup>+</sup> abstraction, shown in Figure 5.D.(i), where a rearrangement to generate a carbon-carbon triple bond will result in electron ejection. This seems reasonable given that neutral carbenes, *e.g.* CF<sub>2</sub>=C, are known to convert into the corresponding ethyne, *e.g.* CFCF, by a Fritsch-Buttenberg-Wiechell rearrangement.<sup>83,84</sup> The mechanism in Figure 5.D.(i) can only be applied to the reactions of C<sub>2</sub>H<sub>4</sub>, C<sub>2</sub>H<sub>3</sub>F and CH<sub>2</sub>CF<sub>2</sub>, because the radical carbene is produced following H<sub>2</sub><sup>+</sup> abstraction. It seems reasonable to assume a similar mechanism is responsible for electron ejection from *all* of the neutral ethenes, C<sub>2</sub>HF<sub>3</sub> and C<sub>2</sub>F<sub>4</sub> included, and so this possibility is not convincing.

Another possibility is if O<sup>-</sup> acts as a nucleophile, forming an intermediate complex with the neutral ethene and ejecting an electron to form an oxirane species [Figure 5.D.(ii)].

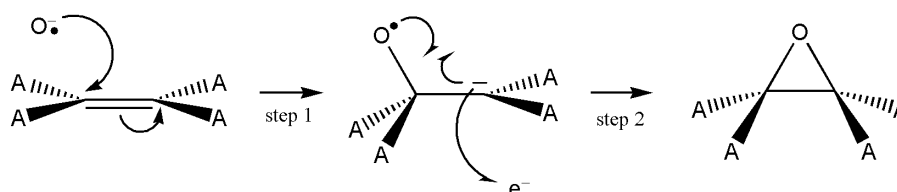


**Figure 5.D.(ii).** A possible mechanism to explain electron ejection observed from the reactions of O<sup>-</sup> with ethene and the fluorinated ethenes. It shows the formation of a neutral oxirane species following step 2. A represents either H or F.

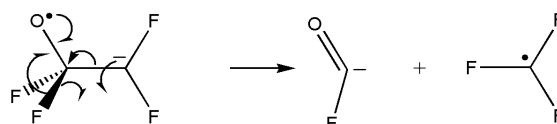
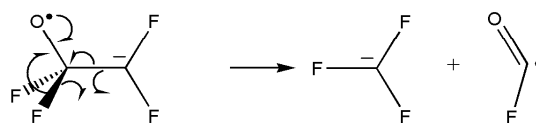
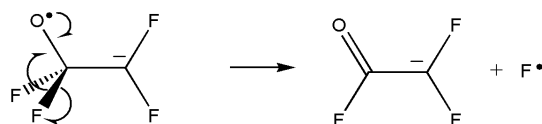
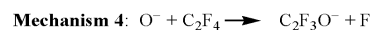
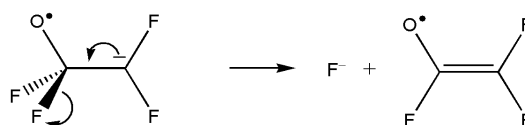
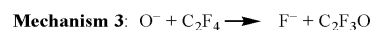
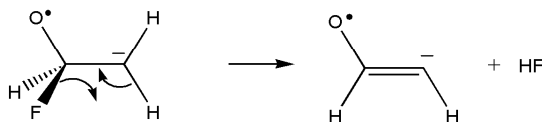
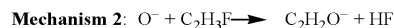
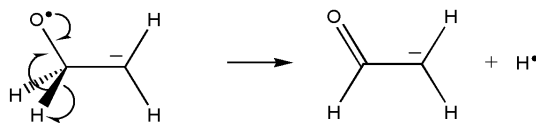
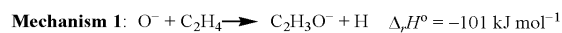
Heats of formation for the *fluorinated* oxirane species are not available, but the reaction in Figure 5.D.(ii) is exothermic when all A substituents are hydrogen (*i.e.* for ethene):



This mechanism for nucleophilic attack seems reasonable, and certainly other anion products observed in the reactions with O<sup>-</sup> surely arise from the same initial step. These include

$\text{C}_2\text{H}_3\text{O}^-$  from  $\text{C}_2\text{H}_4$ ,  $\text{C}_2\text{H}_2\text{O}^-$  from  $\text{C}_2\text{H}_3\text{F}$ , and all of the products in the reaction with  $\text{C}_2\text{F}_4$ . Suggested arrow-pushing mechanisms for the formation of these anions are shown in Figure 5.D.(iii). All of these mechanisms follow the same initial step: the nucleophilic addition of  $\text{O}^-$  to the neutral ethene. Figure 5.D.(iii) only presents the subsequent step, which shows how the resulting carbanion intermediate may rearrange and/or dissociate to generate the observed products.

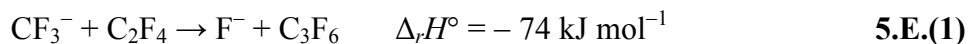
**Figure 5.D.(iii).** Reaction mechanisms showing how the carbanion intermediate formed following the nucleophilic addition of  $\text{O}^-$  may rearrange and/or dissociate to yield some of the observed anion products in the reactions of ethene and the fluorinated ethenes. Reaction enthalpies are included where  $\Delta_r H^\circ$  values are available for all reactants and products.



### 5.E. The reactions of $\text{CF}_3^-$

Only  $\text{C}_2\text{HF}_3$  and  $\text{C}_2\text{F}_4$  react with  $\text{CF}_3^-$ , and in each of these reactions only one anion product is detected [Table 5.B.(I)].  $\text{C}_2\text{F}_3^-$  produced in the reaction with  $\text{C}_2\text{HF}_3$  arises following  $\text{H}^\bullet$  abstraction, as discussed in Section 5.B and shown in reaction 5.B.(8).  $\text{F}^-$  is produced in the reaction with  $\text{C}_2\text{F}_4$  by addition-elimination (or substitution):



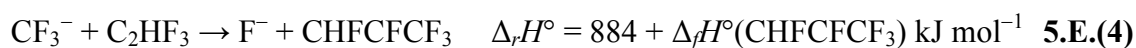
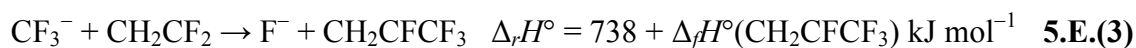


These are the two most likely reactions for CF<sub>3</sub><sup>-</sup> acting as a base or as a nucleophile, respectively, and it is no coincidence that C<sub>2</sub>HF<sub>3</sub> is the most acidic of the neutral ethenes, and C<sub>2</sub>F<sub>4</sub> is the most susceptible to attack from a nucleophile.

The likely reason for the overall low reactivity of CF<sub>3</sub><sup>-</sup> is its relative stability, having a large negative enthalpy of formation (– 641 kJ mol<sup>-1</sup>), but reaction dynamics must also play a part because, for example, the addition-elimination reaction with C<sub>2</sub>H<sub>3</sub>F is not observed despite it being an exothermic channel:



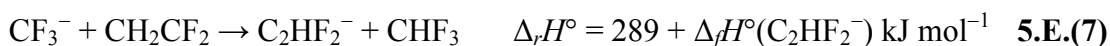
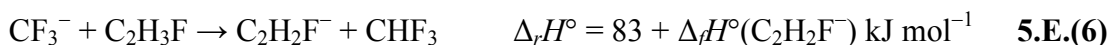
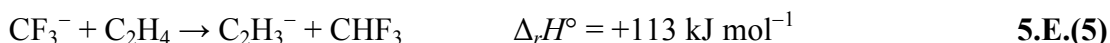
The analogous reactions with CH<sub>2</sub>CF<sub>2</sub> and C<sub>2</sub>HF<sub>3</sub> are also expected to be exothermic, but Δ<sub>r</sub>H<sup>°</sup> values for the neutral product species CH<sub>2</sub>CFCF<sub>3</sub> and CHF<sub>2</sub>CFCF<sub>3</sub>, respectively, are not known:



These reactions occur by CF<sub>3</sub><sup>-</sup> acting as a nucleophile and attacking the electron deficient carbon atoms. The size of CF<sub>3</sub><sup>-</sup> may hinder this type of reaction and only with C<sub>2</sub>F<sub>4</sub> when the electrophilicity of the carbon is relatively large, will a reaction occur. Evidence for this suggestion can be found in the efficiency of the CF<sub>3</sub><sup>-</sup> + C<sub>2</sub>F<sub>4</sub> reaction, which is only 34 %.

The hindering effect that the size of CF<sub>3</sub><sup>-</sup> has on its reactivity is still apparently present, but to a lesser degree, when it attacks a hydrogen substituent (acting as a base); the rate

efficiency of the CF<sub>3</sub><sup>-</sup> + C<sub>2</sub>HF<sub>3</sub> reaction is 65 %. Note that the rates show no evidence of inefficiency in H<sup>+</sup> abstraction reactions of the other anions with C<sub>2</sub>HF<sub>3</sub> [see Table 5.B.(I)] . Nevertheless, the reason for the absence of H<sup>+</sup> abstraction in the reactions of CF<sub>3</sub><sup>-</sup> with C<sub>2</sub>H<sub>4</sub>, C<sub>2</sub>H<sub>3</sub>F, and CH<sub>2</sub>CF<sub>2</sub> is most likely an energetic one:



The values for  $\Delta_f H^\circ(\text{C}_2\text{H}_2\text{F}^-)$  and  $\Delta_f H^\circ(\text{C}_2\text{HF}_2^-)$  have been discussed in Section 5.C, and upper-limit values of  $\leq -41 \text{ kJ mol}^{-1}$  and  $\leq -247 \text{ kJ mol}^{-1}$ , respectively, have been evaluated. Reactions 5.E.(6) and 5.E.(7) are likely therefore to be endothermic.

### 5.F. The reactions of F<sup>-</sup>

F<sup>-</sup> reacts with ethene and the fluorinated ethenes by association, and the experimental rate coefficient increases as the fluorination on ethene increases [see Table 5.B.(I)]. This demonstrates the preference F<sup>-</sup> has to act as a nucleophile rather than a base, and it is only in the reaction with C<sub>2</sub>HF<sub>3</sub> – the most acidic of the neutral ethenes – where H<sup>+</sup> abstraction is observed, albeit only with a BR of 5 % (also see reaction 5.B.(9) and the discussion in Section 5.B).

The expected reaction following nucleophilic attack on carbon is addition-elimination (or substitution), but in this instance the nucleophile and leaving group are both the same: F<sup>-</sup>. Thus, the relative stability of the adduct carbanion must be considered to explain the

observations in this set of reactions. Consider the resonance scheme illustrated in Figure 5.F.(i). It shows how the geometry of a carbanion is dependent on orbital interactions between the carbon atoms and a substituent X. This is essentially describing *anionic hyperconjugation*.<sup>79</sup> Geometry 1 is considered to have large hyperconjugative effects because the  $\text{X}^-$  lone-pair orbital is in the same plane as the adjacent carbon  $\pi$  orbital. In geometry 2 these effects are less because the negative charge is on the  $\beta$  carbon with respect to the X substituent, and the carbon lone-pair orbital is slightly out-of-plane with the X  $p$ -orbitals. The effects of anionic hyperconjugation are significant when X is an electronegative species.

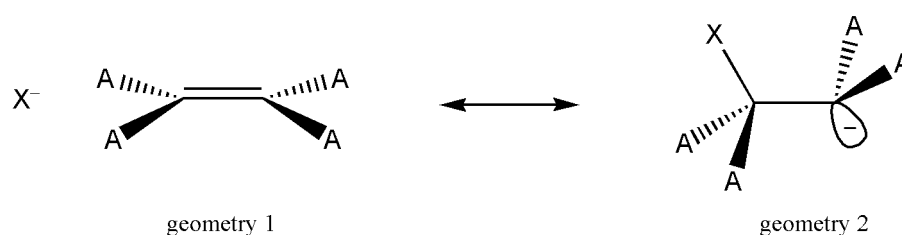


**Figure 5.F.(i).** Resonance effects reflecting the degree of anionic hyperconjugation, essentially the delocalisation of negative charge, in the adduct between  $\text{X}^-$  and either ethene or a fluorinated ethene, where A represents H or F.

In this set of reactions X is fluorine and each A substituent is either hydrogen or fluorine. In the reaction of  $\text{F}^-$  with  $\text{C}_2\text{H}_4$ , all A substituents in Figure 5.F.(i) are hydrogen atoms, and the negative charge in the adduct can only be delocalised by anionic hyperconjugation, so the configuration of this species is expected to be more like geometry 1 than geometry 2. In the other extreme, in the reaction of  $\text{F}^-$  with  $\text{C}_2\text{F}_4$ , all A substituents are fluorines. The resulting adduct may delocalise the negative charge across the whole molecule through the  $\sigma$  network, and so geometry 2 is expected to be more stable than geometry 1. The general trend

therefore, is that the greater the degree of fluorine substitution in ethene, the better representative geometry 2 is for the structure of its adduct with  $\text{F}^-$ . Indeed the strength of the bond formed between X (reactant  $\text{F}^-$ ) and the ethene will be stronger in geometry 2 than geometry 1. This point has also been made by Sullivan and Beauchamp,<sup>64</sup> after calculating binding energies of  $\text{F}^-$  to the fluorinated ethenes. The value increased with increasing fluorine substitution. This trend also matches that observed in the rate coefficients for the reactions of  $\text{F}^-$  with ethene and the fluorinated ethenes [see Table 5.B.(I)].

From another point of view, the scheme in Figure 5.F.(i) can be considered as an equilibrium between reactants (geometry 1) and the formation of the adduct (geometry 2). When more A substituents are fluorines, the adduct is more stable with respect to eliminating  $\text{F}^-$  and regenerating the reactants. Thus, the rate of forming the adduct increases as the degree of fluorine substitution increases.

### 5.G. The reactions of $\text{O}_2^-$

The superoxide anion,  $\text{O}_2^-$ , has been described as an excellent gas-phase nucleophile.<sup>85</sup> Indeed the results in Table 5.B.(I) show product anions which must arise following initial nucleophilic attack, and  $\text{O}_2^-$  is the only reactant ion which does not react with  $\text{C}_2\text{HF}_3$  by proton abstraction.

The reactivity of  $\text{O}_2^-$  towards the fluorinated ethenes increases as the degree of fluorine substitution increases; there is no reaction with  $\text{C}_2\text{H}_4$ , association with  $\text{C}_2\text{H}_3\text{F}$ , electron and  $\text{F}^-$  ejection is observed with  $\text{CH}_2\text{CF}_2$  and  $\text{C}_2\text{HF}_3$ , respectively, and a diverse range of products

are detected with  $\text{C}_2\text{F}_4$ . In addition, the rate coefficient increases as fluorine substitution in ethene increases.

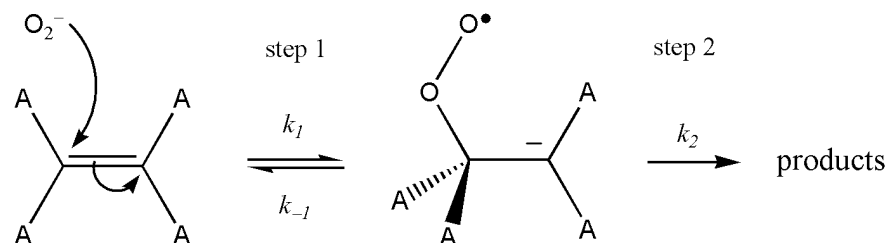
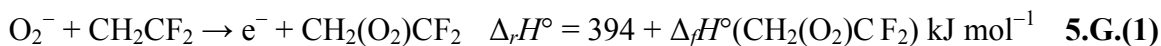


**Figure 5.G.(i).** A generic schematic showing the addition of  $\text{O}_2^-$  to the fluorinated ethenes by nucleophilic attack. A represents either hydrogen or fluorine.

Given that  $\text{C}_2\text{H}_4$  does not react with  $\text{O}_2^-$ , fluorines are important in stabilising the adduct species which is formed after initial nucleophilic addition. More substituted fluorine atoms allow a better delocalisation of the negative charge, leading to a more stable adduct (with respect to the *reactants*). Recall a similar discussion in Section 5.F on the trend in  $k_{\text{exp}}$  values in the reactions of  $\text{F}^-$ . Consider Figure 5.G.(i), where the rate determining step is represented by the ratio of  $k_1 / k_{-1}$ . This ratio is expected to increase when more A substituents are fluorines. If the second step, represented by  $k_2$ , is expected to be fast in comparison, the observed trend in the reaction rate coefficients,  $k_{\text{exp}}$ , is explained.

It is interesting that  $\text{O}_2^-$  with  $\text{CH}_2\text{CF}_2$  reacts exclusively by electron ejection. Reactions 5.G.(1) and 5.G.(2) show the two most likely outcomes for this reaction: formation of a dioxetane, or dissociation into two aldehydes, respectively:





Arrow-pushing mechanisms can explain reactions 5.G.(1) and 5.G.(2), which are shown in Figure 5.G.(ii). The former is explained by step 2 only, and the latter by steps 2 and 3 taking place.

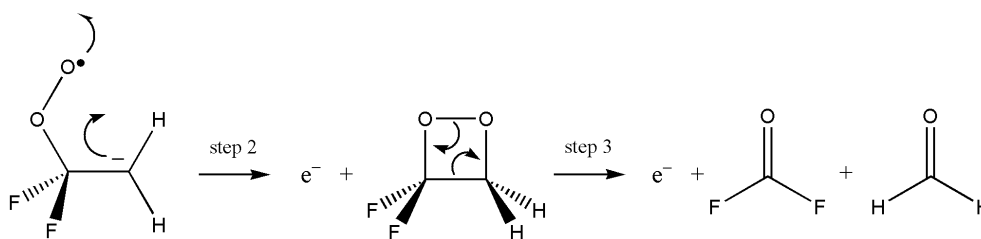
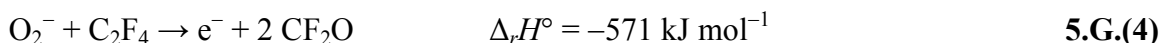
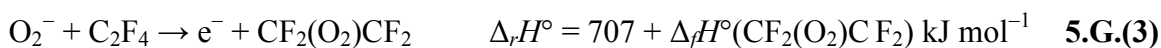
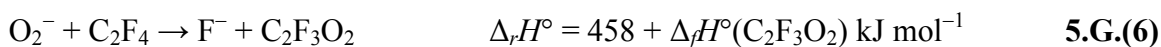
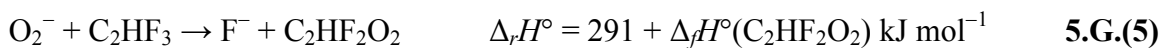


**Figure 5.G.(ii).** A possible mechanism for electron ejection following the nucleophilic addition of O<sub>2</sub><sup>-</sup> to CH<sub>2</sub>CF<sub>2</sub>.

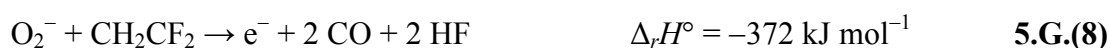
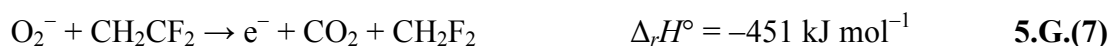
The same mechanism can also be applied to the reaction with C<sub>2</sub>F<sub>4</sub>, where electron ejection is also observed with a BR of 35 %:

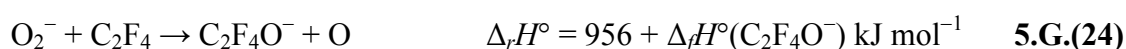


The reactions of O<sub>2</sub><sup>-</sup> with C<sub>2</sub>HF<sub>3</sub> and C<sub>2</sub>F<sub>4</sub> to produce F<sup>-</sup> are likely to follow the same reaction mechanism of nucleophilic substitution:



It is unclear how stable the neutral products are in reactions 5.G.(3), 5.G.(5), and 5.G.(6). It is entirely possible that these products may rearrange and/or fragment, and there are other reasonable exothermic outcomes (see below). Indeed many potential oxygen-containing product species are not well documented in the literature, and some desired  $\Delta_r H^\circ$  values are therefore unavailable (*e.g.* C<sub>2</sub>F<sub>4</sub>O<sup>-</sup>, C<sub>2</sub>F<sub>3</sub>O<sub>2</sub>, CHF<sub>2</sub>O). In addition there are different isomeric forms of many of these species, further preventing any conclusive product assignments. The product assignments discussed so far [reactions 5.G.(1) to 5.G.(6)] are based on reasonable or likely reaction mechanisms, but many more exothermic possibilities exist. These are presented below in reactions 5.G.(7) to 5.G.(21). Possibilities are also given for the anions F<sub>2</sub><sup>-</sup>, C<sub>2</sub>F<sub>4</sub>O<sup>-</sup>, and FCO<sup>-</sup> observed in the reaction of O<sub>2</sub><sup>-</sup> with C<sub>2</sub>F<sub>4</sub> which have not yet been discussed [reactions 5.G.(22) to 5.G.(26)].





### 5.H. Conclusions

The gas-phase reactions of the anions OH<sup>-</sup>, O<sup>-</sup>, CF<sub>3</sub><sup>-</sup>, F<sup>-</sup> and O<sub>2</sub><sup>-</sup> with the neutral ethenes C<sub>2</sub>H<sub>4</sub>, C<sub>2</sub>H<sub>3</sub>F, CH<sub>2</sub>CF<sub>2</sub>, C<sub>2</sub>HF<sub>3</sub> and C<sub>2</sub>F<sub>4</sub> have been investigated using the SIFT technique. The results are shown in Table 5.B.(I). Arrow-pushing reaction mechanisms have been used to help explain the reaction products observed, and to attempt to assign neutral products. This type of analysis, however, has its limitations and many reactions have been observed where significant rearrangement and/or fragmentation of the reaction complex must occur. Using



enthalpies of formation for the reactant and product species to calculate reaction enthalpy changes, a thorough account of the thermochemistry in this set of reactions is presented.

The reaction products are dictated by a combination of the properties of the reactant anion and the reactant neutral. For example, the reactions of  $\text{C}_2\text{F}_4$  show a wide variety of products, many of which result from significant rearrangement and fragmentation of the reaction complex. However, this is not a property of  $\text{C}_2\text{F}_4$  alone and it is only in the reactions with oxygen-containing anions where this is particularly evident. Another example is in the reactions with  $\text{C}_2\text{HF}_3$  which show a preference for  $\text{H}^+$  abstraction. This preference is also limited by the properties of the reactant anion,  $\text{O}_2^-$  for example, which is not basic enough to abstract a proton – even from  $\text{C}_2\text{HF}_3$ . The investigation into these reactions with  $\text{C}_2\text{HF}_3$  has lead to the evaluation of a new value for  $\Delta_f H^\circ (\text{C}_2\text{F}_3^-)$ ,  $-504 \pm 20 \text{ kJ mol}^{-1}$ .

Electron ejection is observed in several reactions with the anions  $\text{O}^-$  and  $\text{O}_2^-$ , and attempts have been made to uncover the reaction mechanisms involved. It is most likely the radical properties of these two anions which are responsible for these interesting reactions.

A general trend can be uncovered when considering the proton affinity ( $PA$ ) values of the reactant anions. The  $PA$ s for  $\text{OH}^-$ ,  $\text{O}^-$ ,  $\text{CF}_3^-$ ,  $\text{F}^-$  and  $\text{O}_2^-$  are listed in Table 5.H.(I). Generally speaking, the type of reaction observed correlates to the relative  $PA$ s of the reactant anion. The anion is more likely to act as a base (*i.e.* attack a hydrogen atom) the higher its proton affinity value. The majority of reactions with  $\text{OH}^-$  are thought to be initiated in this way ( $\text{H}^+$  and  $\text{HF}$  abstraction reactions). With the exception of electron ejection, for which the mechanism is unknown,  $\text{H}_2^+$  abstraction is a significant outcome in the reactions with  $\text{O}^-$ . By contrast, almost all of the reactions involving  $\text{F}^-$  or  $\text{O}_2^-$ , with a lower  $PA$ , are initiated by the anion acting as a nucleophile.

**Table 5.H.(I).** Proton affinities of the reactant anions.

Anion	$PA^a / \text{kJ mol}^{-1}$
$\text{OH}^-$	1634
$\text{O}^-$	1599
$\text{CF}_3^-$	1592
$\text{F}^-$	1560
$\text{O}_2^-$	1486

<sup>a</sup> The proton affinity ( $PA$ ), defined as the enthalpy change for the reaction  $\text{BH} \rightarrow \text{B}^- + \text{H}^+$ , where  $\text{B}^-$  is the anion in question. Therefore, the more positive the value, the higher the affinity  $\text{B}^-$  has for a proton. Values were calculated using enthalpies of formation listed in Appendix I.

The rate coefficients for the reactions with  $\text{F}^-$  and  $\text{O}_2^-$  increase as the degree of fluorination in ethene increases. This trend has been rationalised by resonance and inductive effects influencing the initially formed adduct anion, following nucleophilic addition of the anion to the ethene molecule. There is no obvious trend for the reactions of  $\text{OH}^-$ ,  $\text{O}^-$  and  $\text{CF}_3^-$ .

# Chapter 6:

## *Vacuum ultraviolet negative photoion spectroscopy of $\text{SF}_5\text{CF}_3$ , $\text{SF}_6$ and $\text{CF}_4$*

This chapter focuses on the original data collected for trifluoromethyl sulphur pentafluoride ( $\text{SF}_5\text{CF}_3$ ), however, the discussion extends to include the data also collected for the related molecules sulphur hexafluoride ( $\text{SF}_6$ ) and tetrafluoromethane ( $\text{CF}_4$ ). These results were collected in September 2006 at the Daresbury synchrotron radiation source, on beamline 3.1. Although the majority of the data collection and analysis was performed by myself, it would not have been possible without the help from Richard Tuckett, Colin Latimer, Ken Dunn, Adam Hunniford, Michael Parkes, and David Shaw. This work was published in the *Journal of Chemical Physics* in 2008.<sup>86</sup> The ion-pair cross section values reported in this chapter use the *correct* value for  $M$  (see Section 2.B.3), and they update the data given in this original publication.

### **6.A. Background information**

The presence of the super greenhouse gas trifluoromethyl sulphur pentafluoride,  $\text{SF}_5\text{CF}_3$ , in the atmosphere was first reported in 2000 by Sturges *et al.*<sup>87</sup> Although the known atmospheric concentrations of  $\text{SF}_5\text{CF}_3$  are very low, its lifetime is in the region of 1000 years,<sup>88</sup> and it is thought to have a Global Warming Potential 18,000 times greater than  $\text{CO}_2$ ,

absorbing strongly in the infrared between 750 and 1250 cm<sup>-1</sup>.<sup>89</sup> Of anthropogenic origin, SF<sub>5</sub>CF<sub>3</sub> has been linked to SF<sub>6</sub> production and the manufacture of fluorochemicals,<sup>87</sup> but in truth the main source of this potent greenhouse gas has not yet unambiguously been identified. Since its discovery, SF<sub>5</sub>CF<sub>3</sub> has been the focus of numerous studies aimed to understand better its spectroscopic properties and reactivity. Laboratory experiments have confirmed the original estimates on the severity of SF<sub>5</sub>CF<sub>3</sub> as a greenhouse gas,<sup>89-92</sup> yet more work is required to gather a more comprehensive understanding of its sources and sinks. The original suggestion that SF<sub>5</sub> and CF<sub>3</sub> radicals combine to produce SF<sub>5</sub>CF<sub>3</sub> in high voltage equipment<sup>87</sup> has since been disputed;<sup>93</sup> reactions mimicking these conditions showed no evidence of SF<sub>5</sub>CF<sub>3</sub> production, although small amounts were detected when SF<sub>6</sub> reacted with some hydrofluorocarbons in a spark discharge.<sup>93</sup> Low energy electron attachment to SF<sub>5</sub>CF<sub>3</sub> is dissociative<sup>94-98</sup> and may provide a mechanism for atmospheric removal, but stratospheric UV photolysis is unlikely to contribute due to the absence of photoabsorption by SF<sub>5</sub>CF<sub>3</sub> below 8 eV<sup>90</sup> and the high value of the SF<sub>5</sub>–CF<sub>3</sub> bond dissociation energy (4.06 ± 0.45 eV at 0 K).<sup>99,100</sup> Following a new measurement of the ionisation energy of the CF<sub>3</sub> radical,<sup>58</sup> this bond strength has since been refined to 3.86 ± 0.45 eV.<sup>101</sup>

The surprisingly high value of the S–C bond has spurred investigations into the sink routes for SF<sub>5</sub>CF<sub>3</sub> that might occur at higher altitudes in the mesosphere or ionosphere: ion-molecule reactions, electron attachment, and vacuum ultraviolet (VUV) photodissociation. Ion-molecule reaction studies have shown that both cations<sup>5,6</sup> and anions<sup>17</sup> react rapidly with SF<sub>5</sub>CF<sub>3</sub> and may therefore remove it from the upper atmosphere. However, the concentration of atmospherically-relevant ions (*e.g.* O<sup>+</sup>, O<sub>2</sub><sup>+</sup>, N<sup>+</sup>, N<sub>2</sub><sup>+</sup>) is so low that the pseudo-first-order rate constant for ion-molecule reactions,  $\sum k_{ion}[\text{ion}]$ , is too small for this channel to contribute

to any significant extent.<sup>101</sup> Low-energy electron attachment to SF<sub>5</sub>CF<sub>3</sub> is relatively fast,  $8.0 \times 10^{-8} \text{ cm}^3 \text{ molecule}^{-1} \text{ s}^{-1}$  at 298 K,<sup>97</sup> and the absorption cross section at the Lyman- $\alpha$  wavelength (121.6 nm) is surprisingly high, *ca.*  $10^{-17} \text{ cm}^2$ .<sup>88,102</sup> By comparison with equivalent data for SF<sub>6</sub>, it was shown that the electron attachment process is responsible for ~99 % of the removal of SF<sub>5</sub>CF<sub>3</sub> in the mesosphere, VUV photodissociation ~1 %.<sup>88</sup> However, the long lifetime of SF<sub>5</sub>CF<sub>3</sub> in the earth's atmosphere, ~1000 years, is not determined by these *microscopic* chemical processes that occur in the mesosphere, but by the much slower *macroscopic* meteorology that transports the pollutant from the earth's surface up into the mesosphere.<sup>88</sup> Advances made in the last six years to understand the chemical physics properties and environmental impact of SF<sub>5</sub>CF<sub>3</sub> since its discovery in 2000 have been reviewed.<sup>101</sup>

One of the possible products following VUV photoexcitation of SF<sub>5</sub>CF<sub>3</sub> at 121.6 nm is ion-pair formation, *e.g.* CF<sub>3</sub><sup>+</sup> + SF<sub>5</sub><sup>-</sup>. This chapter describes an experiment to detect anions following VUV excitation as a means to study the dynamics of electronically excited states of SF<sub>5</sub>CF<sub>3</sub>. Absolute cross sections for anion production and, using photoabsorption data,<sup>102</sup> quantum yields have been evaluated for all the anion products observed. In addition to SF<sub>5</sub>CF<sub>3</sub>, the closely-related molecules SF<sub>6</sub> and CF<sub>4</sub> have also been investigated. The photoion-pair formation of SF<sub>6</sub> into SF<sub>5</sub><sup>+</sup> + F<sup>-</sup> and CF<sub>4</sub> into CF<sub>3</sub><sup>+</sup> + F<sup>-</sup> has been studied previously by Mitsuke *et al.*<sup>40,41</sup> and Scully *et al.*<sup>103</sup> The results presented here have seen a much larger number of anions than observed by these groups, and the data of Mitsuke *et al.* has allowed the SF<sub>5</sub>CF<sub>3</sub> data to be put on an *absolute* scale [as outlined in Section 2.B.3].

### 6.B. Sulphur hexafluoride (SF<sub>6</sub>)

The white light negative ion mass spectrum for SF<sub>6</sub> shows eight peaks corresponding to the anions F<sup>−</sup> (100%), F<sub>2</sub><sup>−</sup> (1%), SF<sup>−</sup> (<1%), SF<sub>2</sub><sup>−</sup> (<1%), SF<sub>3</sub><sup>−</sup> (<1%), SF<sub>4</sub><sup>−</sup> (<1%), SF<sub>5</sub><sup>−</sup> (2%), and SF<sub>6</sub><sup>−</sup> (67%). The relative signal strengths are shown in parentheses.

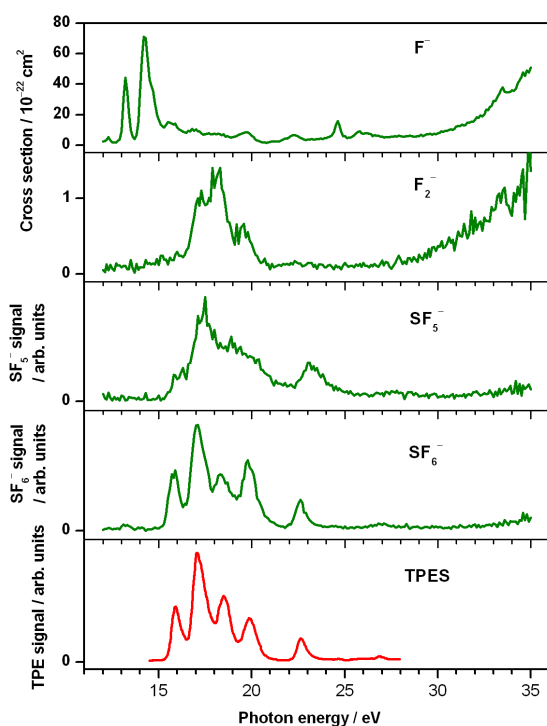


**Figure 6.B.(i).** Cross sections for anion production following photoexcitation of SF<sub>6</sub>. Note that the SF<sub>5</sub><sup>−</sup> and SF<sub>6</sub><sup>−</sup> spectra are not on an absolute scale. Ion yields were recorded as a function of photon energy between 12 and 35 eV with a step size of 0.1 eV and a wavelength resolution of 6 Å. This resolution is equivalent to 0.07 eV at 12 eV, 0.6 eV at 35 eV. The ion yields are compared with the threshold photoelectron spectrum of SF<sub>6</sub>.<sup>104</sup>

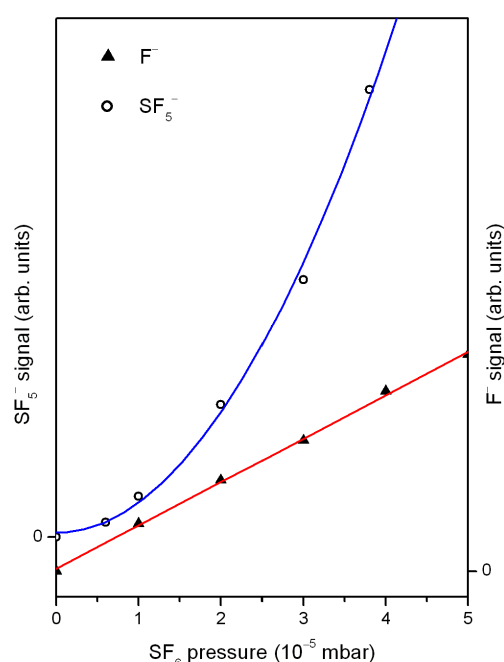
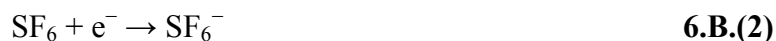


**Figure 6.B.(ii).** Pressure dependence of F<sup>−</sup> and SF<sub>5</sub><sup>−</sup> anion signals from SF<sub>6</sub>. A linear pressure dependence indicates the anion arises from unimolecular ion-pair dissociation. A non-linear pressure dependence suggests a secondary process is involved in the anion formation.

All anion signals from SF<sub>6</sub> recorded as a function of photon energy are presented in Figure 6.B.(i), whilst Table 6.B.(I) shows appearance energy (*AE*) values of the anions, their cross

sections and quantum yields. For comparative purposes, Figure 6.B.(i) includes the threshold photoelectron spectrum (TPES) of SF<sub>6</sub>.<sup>104</sup> Poor signal strengths prevented ion yields for SF<sub>6</sub><sup>−</sup>, SF<sub>2</sub><sup>−</sup>, SF<sub>3</sub><sup>−</sup>, and SF<sub>4</sub><sup>−</sup> from being recorded. The F<sup>−</sup> and F<sub>2</sub><sup>−</sup> signals increase linearly with pressure, those of SF<sub>5</sub><sup>−</sup> and SF<sub>6</sub><sup>−</sup> non-linearly with the rate of change increasing as pressure increases. Figure 6.B.(ii) shows the plot of anion signal vs SF<sub>6</sub> pressure with the example of F<sup>−</sup> compared with SF<sub>5</sub><sup>−</sup>. The linear dependence of the F<sup>−</sup> and F<sub>2</sub><sup>−</sup> anion signals suggest they result from unimolecular ion-pair dissociation, whereas the SF<sub>5</sub><sup>−</sup> and SF<sub>6</sub><sup>−</sup> signals are formed by a secondary process.

Previous ion pair experiments have also observed SF<sub>5</sub><sup>−</sup> and SF<sub>6</sub><sup>−</sup> from SF<sub>6</sub>, their formation being attributed to electron attachment processes:<sup>40,103</sup>



There can be little argument that reaction 6.B.(2) must be responsible for the appearance of SF<sub>6</sub><sup>−</sup>, and certainly SF<sub>6</sub> is a well-known electron scavenger, the rate coefficient at 300 K being  $(2.38 \pm 0.15) \times 10^{-7} \text{ cm}^3 \text{ s}^{-1}$ ,<sup>97</sup> which attaches zero-energy electrons with a very large cross section.<sup>105</sup> Furthermore, Figure 6.B.(i) highlights the striking similarities between the SF<sub>6</sub><sup>−</sup> spectrum and the SF<sub>6</sub> TPES. The only significant difference between the two is the peak at 19.9 eV, which appears stronger in the SF<sub>6</sub><sup>−</sup> spectrum. The same comparison has been discussed by Yenchu *et al.*<sup>106</sup> who compared their TPES of SF<sub>6</sub> with the ion yield of SF<sub>6</sub><sup>−</sup> produced from SF<sub>6</sub> reported by Mitsuke *et al.*;<sup>40</sup> the same discrepancy in relative signal

strengths between the bands at 19.9 eV was observed. It is noted that the cross section for non-dissociative electron attachment to SF<sub>6</sub> peaks at very low energy characteristic of *s*-wave capture,<sup>105</sup> but SF<sub>6</sub><sup>−</sup> anions observed from reaction 6.B.(2) will arise from *all* electrons integrated under the cross section *vs.* electron energy distribution. By contrast, the TPES arises only from low-energy electrons detected within the bandpass of the threshold analyser, *ca.* 4 meV.<sup>104</sup> In practice, the experimentally-observed resolution will depend upon a convolution of the electron energy distribution and the resolution of the photon source. In both experiments the monochromator resolution, *ca.* 0.4 nm or 130 meV at 19.9 eV, will probably dominate. Notwithstanding this point, there is no reason why the intensities of the TPES and SF<sub>6</sub><sup>−</sup> spectra in Figure 6.B.(i) should be *exactly* the same, and this may explain the small differences that have been observed both by us and by Yenchu *et al.*<sup>106</sup> We also note that this difference may not be a particular property of SF<sub>6</sub>, because a similar inconsistency in intensities in the threshold photoelectron and parent anion yields has been observed with another polyatomic molecule which attaches electrons very rapidly, *cyclic*-C<sub>5</sub>F<sub>8</sub>.<sup>107</sup> There are two observations from this work which provide evidence for SF<sub>5</sub><sup>−</sup> arising predominantly from reaction 6.B.(3). First, the SF<sub>5</sub><sup>−</sup> signal increases non-linearly when recorded as a function of pressure, consistent with the two-step mechanism represented by reactions 6.B.(1) and 6.B.(3); an anion signal arising from ion-pair formation, SF<sub>6</sub> + *hν* → F<sup>+</sup> + SF<sub>5</sub><sup>−</sup>, would increase linearly with pressure. This is illustrated in Figure 6.B.(2) which shows clearly the contrast between the signal for the ion-pair product, F<sup>−</sup>, and that for SF<sub>5</sub><sup>−</sup>. Second, the SF<sub>5</sub><sup>−</sup> ion yield shows many similarities to the TPES of SF<sub>6</sub> whereas that of F<sup>−</sup> does not. However, these arguments do not exclude the possibility that a small amount of SF<sub>5</sub><sup>−</sup> is produced *via* the ion-pair reaction above.



The following ion-pair reactions are suggested as mechanisms for F<sup>−</sup> and F<sub>2</sub><sup>−</sup> formation:



The calculated enthalpy changes for reaction 6.B.(4) are 10.4, 14.9, 15.5, 19.7 and 23.7 eV for  $x = 5$  to 1, respectively. For reaction 6.B.(5) they are 13.6, 14.1, 18.4 and 22.4 eV for  $x = 4$  to 1, respectively. F<sup>−</sup> produced from reaction 6.B.(4) has been observed before in the photon energy range 11–31 eV and a detailed analysis performed.<sup>40</sup> Below 14.9 eV the associated cation can only be SF<sub>5</sub><sup>+</sup>, and the present work, Figure 6.B.(i), is in very good agreement with this earlier study. Scully *et al.* have observed the ion-pair products F<sup>−</sup> and F<sub>2</sub><sup>−</sup> from SF<sub>6</sub> in the photon energy range 20 to 205 eV.<sup>103</sup> Both fragment ions show broad bands centred at 35.5 eV. Although not photoexciting SF<sub>6</sub> above 35 eV, this study clearly shows the onsets to these features.

The F<sub>2</sub><sup>−</sup> spectrum in Figure 6.B.(i) shows features in the photon energy range 16 to 21 eV which have not been observed before. Below 18.4 eV it is not possible to say whether the associated cation is SF<sub>4</sub><sup>+</sup> or SF<sub>3</sub><sup>+</sup>. The low F<sub>2</sub><sup>−</sup> cross section is reflected in its low signal strength, resulting in a poor signal-to-noise ratio. Three peaks are identified centered at 17.2, 18.2, and 19.7 eV. They most likely reflect the presence of Rydberg states which couple effectively to the ion-pair state, the peak energies therefore representing Rydberg transitions. Mitsuke *et al.* found that the most prominent features in the F<sup>−</sup> ion yield at 13.2 and 14.3 eV were due to Rydberg transitions.<sup>40</sup> The peaks in the F<sub>2</sub><sup>−</sup> ion yield at 17.2, 18.2, and 19.7 eV approximately match with peaks in the TPES of SF<sub>6</sub> at 17.1, 18.5, and 19.9 eV, respectively. A similar observation is made in the F<sub>2</sub><sup>−</sup> ion yield from SF<sub>5</sub>CF<sub>3</sub> (Section 6.D).

**Table 6.B.(I).** Appearance energies, cross sections, and quantum yields for anions observed from photoexcitation of SF<sub>6</sub>, CF<sub>4</sub>, and SF<sub>5</sub>CF<sub>3</sub>.

Molecule [ <i>IE</i> <sup>a</sup> / eV]	Anion	<i>AE</i> <sup>b</sup> / eV	Cross section <sup>c</sup> / cm <sup>2</sup>	Energy <sup>d</sup> / eV	Quantum Yield <sup>e</sup>
SF <sub>6</sub> [15.1]	F <sup>-</sup>	12.7	$7.1 \times 10^{-21}$	14.2	$2.4 \times 10^{-4}$
	F <sub>2</sub> <sup>-</sup>	16.3	$1.4 \times 10^{-22}$	18.3	$1.9 \times 10^{-6}$
	SF <sub>5</sub> <sup>-</sup>	15.1	— <sup>f</sup>	17.5	— <sup>g</sup>
	SF <sub>6</sub> <sup>-</sup>	15.1	— <sup>f</sup>	17.1	— <sup>g</sup>
CF <sub>4</sub> [15.4]	F <sup>-</sup>	13.0	$1.4 \times 10^{-21}$	14.0	$2.8 \times 10^{-5}$
	F <sub>2</sub> <sup>-</sup>	20.1	$4.0 \times 10^{-23}$	21.6	$5.6 \times 10^{-7}$
SF <sub>5</sub> CF <sub>3</sub> [12.9]	F <sup>-</sup>	11.05	$3.4 \times 10^{-20}$	16.9	$3.4 \times 10^{-4}$
	F <sub>2</sub> <sup>-</sup>	16.1	$1.2 \times 10^{-21}$	17.9	$1.1 \times 10^{-5}$
	SF <sup>-</sup>	24.0	$2.8 \times 10^{-22}$	28.8	$2.4 \times 10^{-6}$
	SF <sub>2</sub> <sup>-</sup>	20.2	$3.9 \times 10^{-22}$	24.2	$2.5 \times 10^{-6}$
	SF <sub>3</sub> <sup>-</sup>	15.4	$1.0 \times 10^{-20}$	17.6	$1.0 \times 10^{-4}$
	SF <sub>4</sub> <sup>-</sup>	13.0	$1.3 \times 10^{-20}$	14.1	$1.7 \times 10^{-4}$
	SF <sub>5</sub> <sup>-</sup>	13.0	— <sup>f</sup>	17.0	— <sup>g</sup>

<sup>a</sup> Adiabatic ionisation energy. Values are taken from the observed onset of ionisation for SF<sub>6</sub>,<sup>106</sup> CF<sub>4</sub>,<sup>104</sup> and SF<sub>5</sub>CF<sub>3</sub>.<sup>99</sup>

<sup>b</sup> Observed appearance energy (*AE*) from this work. The error is estimated to be  $\pm 0.2$  eV (except for F<sup>-</sup> from SF<sub>5</sub>CF<sub>3</sub> for which the error is  $\pm 0.05$  eV), based on the resolution and step size used when recording ion yields.

<sup>c</sup> Cross section for anion production following photoexcitation of the parent molecule.

<sup>d</sup> Energy of strongest peak. It is at this energy, where appropriate, where cross section and quantum yield measurements are taken.

<sup>e</sup> Quantum yields for anion production, obtained by dividing cross sections for anions (column 4) by total photoabsorption cross sections. The latter values are given for SF<sub>6</sub>,<sup>108</sup> CF<sub>4</sub>,<sup>88</sup> and SF<sub>5</sub>CF<sub>3</sub>.<sup>102</sup>

<sup>f</sup> Normalisation of the signal strength to determine an effective cross section is not possible because of the non-linear dependence of signal with pressure.

<sup>g</sup> Quantum yield cannot be determined because the cross section is not defined.

### 6.C. Tetrafluoromethane (CF<sub>4</sub>)

The white light negative ion mass spectrum for CF<sub>4</sub> shows three peaks corresponding to the anions F<sup>-</sup> (100%), CF<sup>-</sup> (1%) and F<sub>2</sub><sup>-</sup> (3%). The F<sup>-</sup> and F<sub>2</sub><sup>-</sup> signals were recorded as a function of photon energy and are shown in Figure 6.C.(1), along with the TPES of CF<sub>4</sub> which is included for comparative purposes.<sup>104</sup> The corresponding data is shown in Table

6.B.(I). The ion yield of CF<sup>−</sup> was not obtained due to the poor signal strength. CF<sub>4</sub> has *T<sub>d</sub>* symmetry, and the outer-valence electronic configuration is ...(*4a*<sub>1</sub>)<sup>2</sup> (*3t*<sub>2</sub>)<sup>6</sup> (*1e*)<sup>4</sup> (*4t*<sub>2</sub>)<sup>6</sup> (*1t*<sub>1</sub>)<sup>6</sup>.

The F<sup>−</sup> and F<sub>2</sub><sup>−</sup> signals both increase linearly with pressure and the following ion-pair reactions are suggested as mechanisms for their formation:



The calculated enthalpy changes for reaction 6.C.(1) are 11.3, 17.7 and 20.7 eV for *x* = 3 to 1, respectively; for 6.C.(2) they are 16.3 and 19.3 eV for *x* = 2 and 1, respectively. The F<sup>−</sup> ion yield recorded here is in good agreement with a previous study in the photon energy range 12 to 31 eV reported by Mitsuke *et al.*<sup>41</sup> The F<sup>−</sup> and F<sub>2</sub><sup>−</sup> yields are also in good agreement with those reported by Scully<sup>109</sup> at higher resolution in the photon range 20 to 35 eV [Figure 6.C.(i)], but *absolute* cross sections were not determined in this earlier work.

It is immediately obvious from Figure 6.C.(i) that the F<sup>−</sup> and F<sub>2</sub><sup>−</sup> yields share a similar feature between 20 and 23 eV. Mitsuke *et al.* assigned this feature in the F<sup>−</sup> yield to three Rydberg transitions (*3t*<sub>2</sub> → *np* where *n* = 4, 5 and 6 at energies 20.96, 21.16 and 21.45 eV, respectively) converging on the third excited valence state of CF<sub>4</sub><sup>+</sup> (*Ĉ* <sup>2</sup>*T*<sub>2</sub>).<sup>41</sup> The Rydberg states excited at these energies would then couple to an ion-pair state which dissociates to F<sup>−</sup>, the corresponding cation, and any neutral fragments. The presence of Rydberg states in this energy region has also been observed in a high resolution threshold photoelectron study of CF<sub>4</sub> by Yenchu *et al.*<sup>110</sup> Autoionising structure is observed from 20.3 to 21.6 eV, preceding the onset of the *Ĉ* <sup>2</sup>*T*<sub>2</sub> state of CF<sub>4</sub><sup>+</sup>. This can be observed in the TPES in Figure 6.C.(i) as a slight rise above the baseline in the same energy range. It is therefore proposed that Rydberg

states converging to CF<sub>4</sub><sup>+</sup>  $\tilde{C}^2T_2$  couple to ion-pair states which dissociate to both F<sup>−</sup> and F<sub>2</sub><sup>−</sup>. At 21.8 eV the F<sup>−</sup> cross section is *ca.* 16 times larger than that for F<sub>2</sub><sup>−</sup>. This may reflect the degree of coupling between states and/or the steric disadvantage on forming an extra bond to produce F<sub>2</sub><sup>−</sup>.

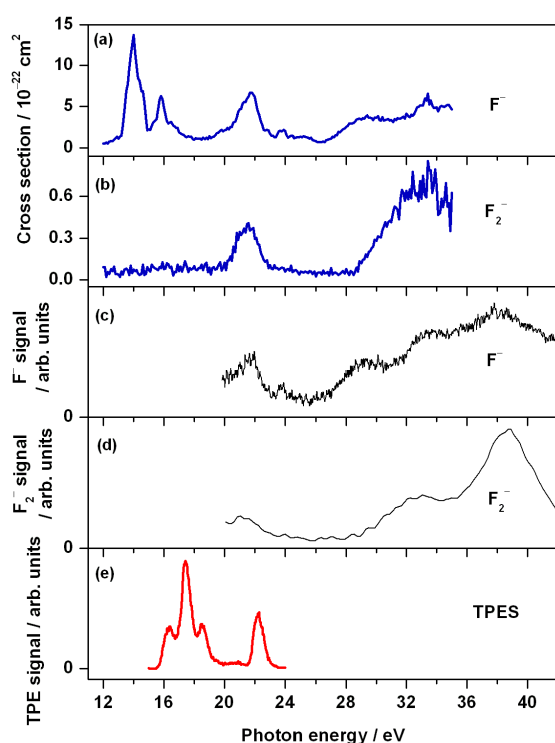


**Figure 6.C.(i).** Cross sections for anion production following photoexcitation of CF<sub>4</sub>. (a) and (b) F<sup>−</sup> and F<sub>2</sub><sup>−</sup> ion yields recorded as a function of photon energy between 12 and 35 eV with a step size of 0.1 eV and a wavelength resolution of 6 Å (this work). This resolution is equivalent to 0.07 eV at 12 eV, 0.6 eV at 35 eV. The cross sections are on an absolute scale. (c) and (d) F<sup>−</sup> and F<sub>2</sub><sup>−</sup> ion yields from Scully<sup>109</sup> recorded over a narrower energy range at a higher resolution of 0.5 and 2.0 Å, respectively. The cross sections are now on a relative scale. (e) Threshold photoelectron spectrum of CF<sub>4</sub> for comparison.<sup>104</sup>

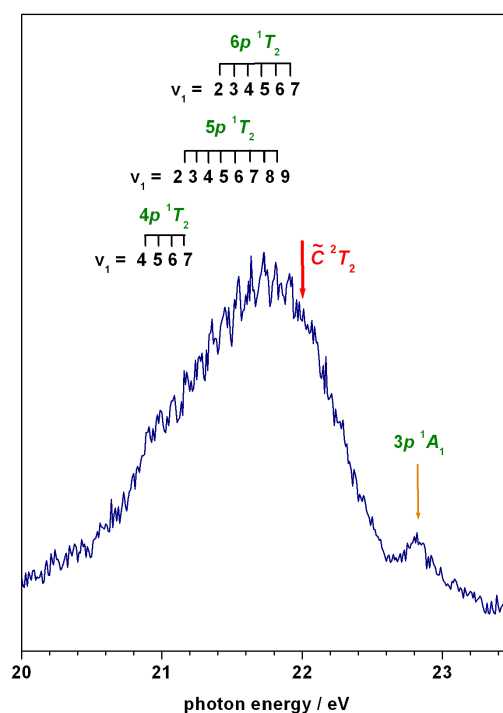


**Figure 6.C.(ii).** F<sup>−</sup> anion signal from CF<sub>4</sub> in the photon energy range 20 to 23.5 eV with a step size of 0.01 eV and a wavelength resolution of 2 Å. This resolution is equivalent to 0.1 eV at 22 eV. Vibrational progressions of the  $\nu_1$  totally symmetric stretching mode in CF<sub>4</sub><sup>+</sup>  $np$  Rydberg states converging on the CF<sub>4</sub><sup>+</sup> ( $\tilde{C}^2T_2$ ) state are shown by black ticks.<sup>41</sup> The vertical ionisation energy for CF<sub>4</sub><sup>+</sup> ( $\tilde{C}^2T_2$ ) is 22.04 eV,<sup>111</sup> shown here by a red arrow. A new feature is observed at 22.82 eV which is assigned to a Rydberg state converging to CF<sub>4</sub><sup>+</sup> ( $\tilde{D}^2A_1$ ), shown by the orange arrow.

The feature between 20 and 23.5 eV in the F<sup>−</sup> ion yield has been recorded with better resolution, and is shown in Figure 6.C.(ii). It shows the CF<sub>4</sub><sup>+</sup>  $4p$ ,  $5p$ , and  $6p$  overlapping

Rydberg states converging on the CF<sub>4</sub><sup>+</sup> ( $\tilde{C}^2T_2$ ) state. Fine structure is also observed in the spectrum which shows the  $\nu_1$  totally symmetric stretching mode in CF<sub>4</sub><sup>\*</sup>.

**Table 6.C.(I).** Peak positions and energy spacings, in eV, for the vibrational states observed in the F<sup>−</sup> ion yield from CF<sub>4</sub> in the photon energy range 20.9 to 22.1 eV.

$3t_2 \rightarrow 4p^1T_2$				$3t_2 \rightarrow 5p^1T_2$				$3t_2 \rightarrow 6p^1T_2$			
$\Delta E^a$	$E^b$	$E^c$	$\Delta E^d$	$\Delta E^a$	$E^b$	$E^c$	$\Delta E^d$	$\Delta E^a$	$E^b$	$E^c$	$\Delta E^d$
$(\nu_1, 0, 0, 0)^e$				$(\nu_1, 0, 0, 0)^e$				$(\nu_1, 0, 0, 0)^e$			
	$\nu_1 =$				$\nu_1 =$				$\nu_1 =$		
	20.90	4	20.87		21.18	2	21.16		21.45	2	21.45
0.09			0.09	0.09			0.07				
	20.99	5	20.96		21.27	3	21.23				
0.09			0.11	0.09			0.11				
	21.08	6	21.07		21.36	4	21.34				
0.1			0.09	0.09	21.38		0.11				
	21.18	7	21.16		21.45	5	21.45		21.45	2	21.45
				0.10	21.48		0.09	0.10	21.48		0.09
					21.53				21.53		
				0.09	21.55	6	21.54		21.55	3	21.54
				0.09			0.10	0.09			0.10
				0.09	21.64	7	21.64		21.64	4	21.64
				0.07			0.09	0.09			0.07
				0.08	21.73	8	21.71		21.73	5	21.71
					21.75		0.11	0.08	21.75		0.11
					21.81	9	21.82		21.81	6	21.82
					21.85			0.10	21.85		0.09
									21.91	7	21.91
											0.09
										8	22.00
											0.08
										9	22.08

<sup>a</sup> Energy spacing between vibrational states, in eV, taken from this work.

<sup>b</sup> Energy of peak maximum, in eV, taken from this work. Values in italics show energy positions of weak shoulder features.

<sup>c</sup> Energy of peak maximum, in eV, taken from the work by Mitsuke *et al.*<sup>41</sup>

<sup>d</sup> Energy spacing between vibrational states, in eV, taken from the work of Mitsuke *et al.*<sup>41</sup>

<sup>e</sup> Assignments for the vibrational quantum number in the  $\nu_1$  mode of CF<sub>4</sub><sup>\*</sup>. These assignments are taken from the ion-pair study of Mitsuke *et al.*<sup>41</sup> and the photoabsorption study of Lee *et al.*<sup>112</sup>

These progressions have been observed before in the ion-pair study by Mitsuke *et al.*, and Table 6.C.(I) compares the two sets of data, listing energy positions, the resulting energy spacings, and the vibrational quantum number assignments. The assignments for these Rydberg transitions and for the vibrational progressions are taken directly from the work of Mitsuke *et al.*,<sup>41</sup> who performed a quantum defect analysis, such that the resulting quantum defect is almost exactly the same for all three vibronic assignments, a value close to 0.60. This analysis also agrees with the photoabsorption study of Lee *et al.*<sup>112</sup> Photoelectron spectroscopy shows a vibrational progression in the band representing the  $\tilde{C}^2T_2$  state of CF<sub>4</sub><sup>+</sup> with a spacing of about 90 meV, assigned to the  $\nu_1$  mode.<sup>110,111</sup> The vibrational spacing of the progressions observed in the *np* Rydberg states in the F<sup>−</sup> ion yield converging to this same ionic state are also about 90 meV, as expected.

Figure 6.C.(ii) shows an additional feature at 22.82 eV which has not been seen in the previous study. It is assigned here as the  $4a_1 \rightarrow 3p$  valence-Rydberg transition. This assignment uses the vertical ionisation energy of 25.11 eV for the fourth excited state of CF<sub>4</sub><sup>+</sup>  $\tilde{D}^2A_1$ ,<sup>111</sup> and the peak position of the observed feature as 22.82 eV. The resulting term value of 2.29 leads to a quantum defect value of 0.56. This assignment is consistent with the observation of features in the F<sup>−</sup> ion yield at 24.0 and 24.45 eV, which Mitsuke *et al.* assign as  $4a_1 \rightarrow 4p$  and  $4a_1 \rightarrow 5p$  Rydberg transitions, respectively,<sup>41</sup> the next two members of this *p* Rydberg series.

The highest outer-valence electronic state of CF<sub>4</sub><sup>+</sup> is the  $\tilde{D}^2A_1$  state at 25.1 eV, whereas the next discrete state in the photoelectron spectrum corresponding to ionisation of the  $2t_2$  inner-valence electron is the  $\tilde{E}^2T_2$  state at 40.3 eV.<sup>104,111</sup> Both the F<sup>−</sup> and F<sub>2</sub><sup>−</sup> yields increase

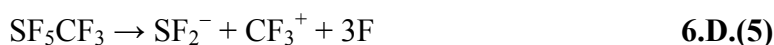
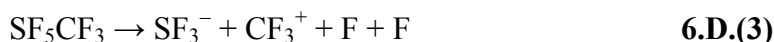
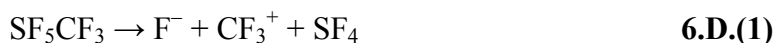
above 25 eV, and the spectral features at higher energies are more clearly observed in the work of Scully<sup>109</sup> which extends up to 110 eV.

#### 6.D. Trifluomethyl sulphur pentafluoride (SF<sub>5</sub>CF<sub>3</sub>)

The white light negative ion mass spectrum for SF<sub>5</sub>CF<sub>3</sub> shows eight peaks corresponding to the anions F<sup>−</sup> (100%), CF<sup>−</sup> (1%), F<sub>2</sub><sup>−</sup> (2%), SF<sup>−</sup> (1%), SF<sub>2</sub><sup>−</sup> (1%), SF<sub>3</sub><sup>−</sup> (1%), SF<sub>4</sub><sup>−</sup> (2%) and SF<sub>5</sub><sup>−</sup> (14%). With the exception of SF<sub>5</sub><sup>−</sup>, all of the anion signals increase linearly with pressure. SF<sub>5</sub><sup>−</sup> formed following photoexcitation of SF<sub>5</sub>CF<sub>3</sub> shows a similar pressure behaviour to SF<sub>5</sub><sup>−</sup> formation from SF<sub>6</sub>, which is discussed in more detail in Section 6.B.

Ion yields for the anions resulting from ion-pair formation are presented in Figure 6.D.(i), the data in Table 6.B.(I). The quantum yields are all in the range 10<sup>−6</sup> to 10<sup>−4</sup>, consistent with those expected for a large polyatomic molecule.<sup>27,28</sup> The ion yield of F<sup>−</sup> below 12 eV was recorded with a LiF window in place to display the threshold region more clearly, and an appearance energy (*AE*) value of 11.05 ± 0.05 eV is determined.

The following reactions are suggested as the main sources of formation of the anions:

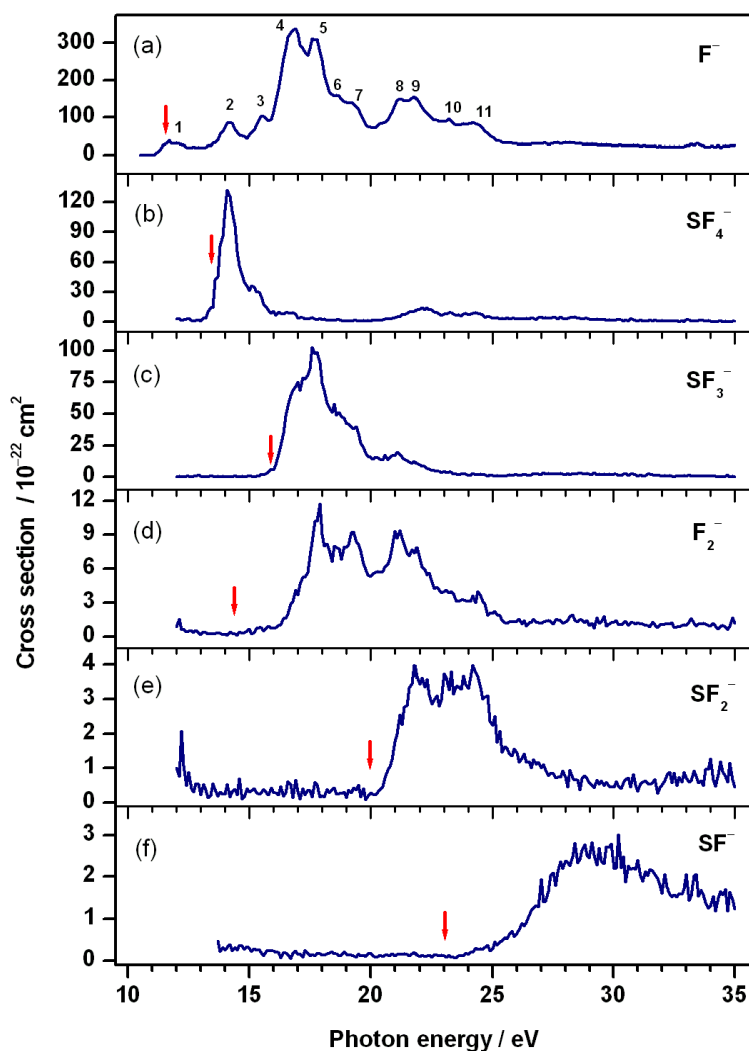




6.D.(6)

In all cases the cation formed is CF<sub>3</sub><sup>+</sup>, the associated anion therefore resulting from the SF<sub>5</sub> part of SF<sub>5</sub>CF<sub>3</sub>. This is reflected in the results; five different anions containing sulphur are detected compared to one containing carbon, CF<sup>−</sup>, which was only just detected above the sensitivity limit of the apparatus.

**Figure 6.D.(i).** Cross sections for anion production following photoexcitation of SF<sub>5</sub>CF<sub>3</sub>. Ion yields were recorded as a function of photon energy between 10.5 and 35.0 eV with a step size of 0.1 eV and a wavelength resolution of 6 Å. This resolution is equivalent to 0.05 eV at 10.5 eV and 0.6 eV at 35 eV. Solid red arrows in spectra (a) through to (f) show enthalpy values of the thermochemical thresholds calculated for reactions 6.D.(1) to 6.D.(6), respectively.





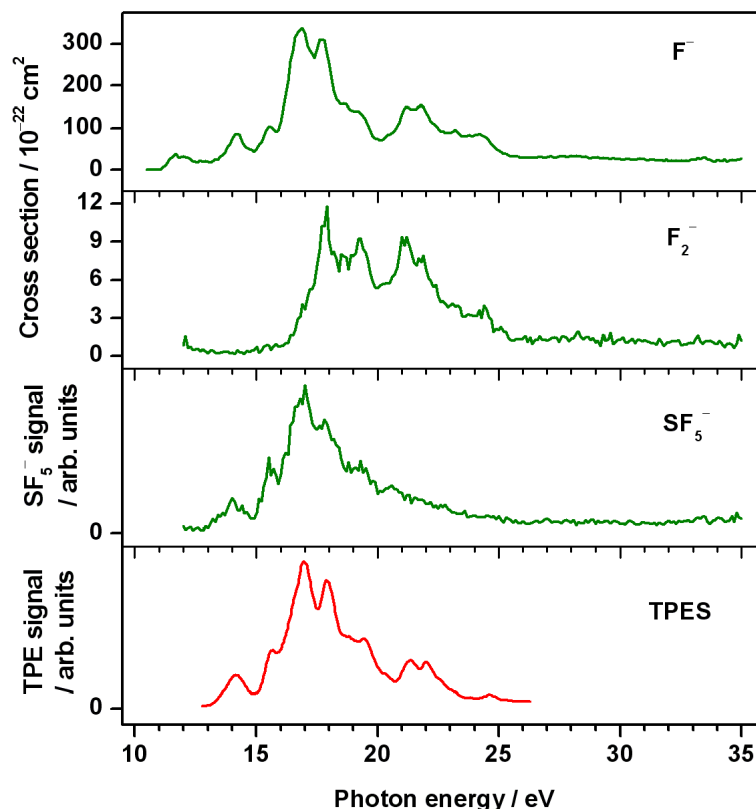
The S–C bond is most likely to be the weakest in the molecule, the 0 K dissociation energy measured as  $3.86 \pm 0.45$  eV.<sup>101</sup> In addition, Xu *et al.* have calculated bond dissociation energies in SF<sub>5</sub>CF<sub>3</sub>, resulting in  $D(\text{SF}_5\text{CF}_2\text{--F}) > D(\text{F--SF}_4\text{CF}_3) > D(\text{SF}_5\text{--CF}_3)$ .<sup>113</sup> One cannot say conclusively that reactions 6.D.(1) to 6.D.(6) are responsible for *all* of the detected anion signals, across the complete energy range studied. Certainly, more channels become energetically accessible at higher energies. It is, however, interesting that the thermochemical thresholds for reactions 6.D.(1) to 6.D.(6) approximately reflect the observed *AE* values [Table 6.B.(I)]. The only apparent exception is reaction 6.D.(4), F<sub>2</sub><sup>−</sup> production, where steric constraints on forming a new bond could be responsible. This trend can be visualised in Figure 6.D.(i) by vertical arrows representing the enthalpies of the calculated thermochemical thresholds. These values for  $\Delta_r H^\circ_{298}$  are 11.5, 13.4, 16.0, 14.3, 20.0 and 23.0 eV for reactions 6.D.(1) to 6.D.(6), respectively. No errors are given but there is significant uncertainty in some of the  $\Delta_r H^\circ_{298}$  values used, which probably explains why the calculated *AE* is sometimes greater than the experimental value [*e.g.* F<sup>−</sup> and SF<sub>4</sub><sup>−</sup> in Figure 6.D.(i)].

The formation of F<sup>−</sup> and F<sub>2</sub><sup>−</sup> over the complete energy range 11–35 eV are unlikely to result exclusively from reactions 6.D.(1) and 6.D.(4) respectively, whereas the channels available to form the sulphur-containing anions are fewer. Indeed, the ion yields for F<sup>−</sup> and F<sub>2</sub><sup>−</sup> do show structure over a much wider energy range than those of SF<sub>*x*</sub><sup>−</sup> (*x* = 1–4).

The ion yields for F<sup>−</sup>, F<sub>2</sub><sup>−</sup> and SF<sub>5</sub><sup>−</sup> are presented in Figure 6.D.(ii) and compared to the TPES of SF<sub>5</sub>CF<sub>3</sub>.<sup>99</sup> SF<sub>5</sub><sup>−</sup> is the only anion detected which is *not* associated with ion-pair formation. Three comparisons can be made between the behaviour of SF<sub>5</sub><sup>−</sup> formed from SF<sub>5</sub>CF<sub>3</sub> and SF<sub>5</sub><sup>−</sup> formed from SF<sub>6</sub> (also see Section 6.B). First, the SF<sub>5</sub><sup>−</sup> signal increases non-linearly with pressure, with the rate of change of signal increasing as the pressure increases.

Second, electron attachment to SF<sub>5</sub>CF<sub>3</sub> is dissociative forming SF<sub>5</sub><sup>−</sup> (and CF<sub>3</sub>) as the only significant channel.<sup>94-98</sup> Third, the ion yield of SF<sub>5</sub><sup>−</sup> shows many similarities to the TPES of SF<sub>5</sub>CF<sub>3</sub>.

**Figure 6.D.(ii).** Cross sections for anion production following photoexcitation of SF<sub>5</sub>CF<sub>3</sub>. Note that the SF<sub>5</sub><sup>−</sup> spectrum is not on an absolute scale. Ion yields were recorded as a function of photon energy between 10.5 and 35.0 eV with a step size of 0.1 eV and a wavelength resolution of 6 Å. This resolution is equivalent to 0.05 eV at 10.5 eV, 0.6 eV at 35 eV. The ion yields are compared with the threshold photoelectron spectrum (shown in red) of SF<sub>5</sub>CF<sub>3</sub>.<sup>99</sup>



It is therefore proposed that the dominant mechanism for the production of SF<sub>5</sub><sup>−</sup> from SF<sub>5</sub>CF<sub>3</sub> is dissociative electron attachment following photoionisation as the source of low-energy electrons:



As shown in Figure 6.D.(ii), the F<sup>-</sup> and F<sub>2</sub><sup>-</sup> ion yields also show similarities to the TPES of SF<sub>5</sub>CF<sub>3</sub>. Due to its higher signal-to-noise ratio, it is in the F<sup>-</sup> spectrum where these similarities are most obvious. In the photon energy range 13–23 eV the agreement between peak positions is good and the relative signal strengths show only small differences. The resemblance of the F<sup>-</sup> ion yield to the TPES could be explained by a process involving electron attachment being significant in F<sup>-</sup> formation. This has been the case in the discussion above, explaining the formation of SF<sub>5</sub><sup>-</sup> from both SF<sub>6</sub> and SF<sub>5</sub>CF<sub>3</sub>. However, the F<sup>-</sup> signal rises *linearly* with increasing gas pressure. This suggests strongly that a primary process, *i.e.* ion-pair formation to F<sup>-</sup> + SF<sub>4</sub>CF<sub>3</sub><sup>+</sup> (or F<sup>-</sup> + CF<sub>3</sub><sup>+</sup> + SF<sub>4</sub>), is dominant.

For the purposes of this discussion the features in the F<sup>-</sup> ion yield are labelled 1 to 11 in Figure 6.D.(i). The experimental *AE* (F<sup>-</sup>) is 11.05 eV, and this anion gives rise to peak 1 centred at 11.7 eV. This peak occurs below the onset of ionisation for SF<sub>5</sub>CF<sub>3</sub>, reported as 12.9 eV,<sup>99</sup> so the presence of photoelectrons from reaction 6.D.(7) is not relevant. The energy of peak 1 is close to peaks observed in the SF<sub>5</sub>CF<sub>3</sub> photoabsorption<sup>102</sup> and total fluorescence yield<sup>114</sup> spectra at 11.4 eV. These two studies give different assignments to this transition. Holland *et al.*<sup>102</sup> assign it to a blend of several valence-valence transitions, whilst Ruiz *et al.*<sup>114</sup> assign it to a valence-Rydberg transition from the 29a' highest-occupied molecular orbital of SF<sub>5</sub>CF<sub>3</sub> to a 4s Rydberg orbital. The contribution of fluorescence at this energy was reported to originate from the CF<sub>3</sub> fragment, following dissociation of SF<sub>5</sub>CF<sub>3</sub><sup>\*</sup> and production of an excited electronic state of the CF<sub>3</sub> radical. In addition, this was the most intense band observed within the photon energy range studied of 10–28 eV.<sup>114</sup> It must represent a transition to the same intermediate state which predissociates into states yielding both CF<sub>3</sub><sup>\*</sup> and F<sup>-</sup> anions. The ion-pair quantum yield at the maximum of the peak in the F<sup>-</sup>

ion yield at 11.7 eV is  $\Phi = 1.5 \times 10^{-4}$ . This small value, coupled with the fact that fluorescence from SF<sub>5</sub>CF<sub>3</sub><sup>\*</sup> is unlikely to have a large quantum yield, suggests strongly that predissociation into neutral fragments is the favoured process at this energy. A similar conclusion was reached by Shaw *et al.* in a comparable study of the dissociation dynamics of Rydberg states of some substituted methane molecules.<sup>115</sup> The agreement of peak positions in SF<sub>5</sub>CF<sub>3</sub> between the photoabsorption spectrum,<sup>102</sup> the total fluorescence yield,<sup>114</sup> and the F<sup>−</sup> ion yield extends up to 17 eV, but above this energy similarities between the spectra are less clear.

**Table 6.D.(I).** F<sup>−</sup> ion-pair quantum yields ( $\Phi_{F^-}$ ) at energies below and above the onsets of ionisation for SF<sub>6</sub>, CF<sub>4</sub> and SF<sub>5</sub>CF<sub>3</sub>. Cross sections from this work are normalised to photoabsorption cross sections for SF<sub>6</sub>,<sup>108</sup> CF<sub>4</sub>,<sup>88</sup> and SF<sub>5</sub>CF<sub>3</sub><sup>102</sup> to give values for  $\Phi_{F^-}$ .

Molecule	$\Phi_{F^-}$ below onset of ionisation	$\Phi_{F^-}$ above onset of ionisation
SF <sub>6</sub>	$2.4 \times 10^{-4}$ at 14.2 eV	$1.5 \times 10^{-5}$ at 24.6 eV
CF <sub>4</sub>	$2.8 \times 10^{-5}$ at 14.0 eV	$9.3 \times 10^{-6}$ at 21.8 eV
SF <sub>5</sub> CF <sub>3</sub>	$1.5 \times 10^{-4}$ at 11.7 eV	$3.4 \times 10^{-4}$ at 16.9 eV

It is interesting that the F<sup>−</sup> ion-pair quantum yield does not decrease above the onset of ionisation of SF<sub>5</sub>CF<sub>3</sub>, 12.9 eV. Features 1 and 4 at 11.7 and 16.9 eV, for example, have  $\Phi = 1.5 \times 10^{-4}$  and  $3.4 \times 10^{-4}$ , respectively [Table 6.D.(I)]. As a result of significant photoabsorption leading to ionisation, one would expect the ion-pair quantum yield to decrease, as observed for both SF<sub>6</sub> and CF<sub>4</sub> [Table 6.D.(I)]. However, above the ionisation energy of SF<sub>5</sub>CF<sub>3</sub> the F<sup>−</sup> ion yield increases, approximately matching the shape of the TPES. In fact features 2–11 of Figure 6.D.(i) occur at, or just below, vertical ionisation energies in the TPES of SF<sub>5</sub>CF<sub>3</sub>.<sup>102</sup> Only feature 1 does not follow this trend. It seems unlikely that valence states of SF<sub>5</sub>CF<sub>3</sub> which predissociate into ion pairs coincidentally lie very close to the ionisation thresholds, certainly across this large energy range. It is much more likely that

Rydberg states play an important role. Certainly the F<sup>−</sup> ion yield would be explained if coupling to ion-pair states was more significant from Rydberg states close to the ionisation thresholds than from those lower in energy. Contributions to the F<sup>−</sup> ion yield from low-lying Rydberg states would then be the dominant cause of peak 1. F<sup>−</sup> ions produced *via* high-lying Rydberg states would be dominant at higher energy, and hence responsible for features 2–11 in the ion yield. If this is true, it negates the generally accepted rule that it is low-*n*, and not high-*n*, Rydberg states which interact most strongly with ion-pair states. However, most of the ion-pair experiments on polyatomics to date have studied halogenated molecules where the lowest ion-pair threshold lies *below* the first ionisation energy,<sup>28</sup> so by definition it is the low-*n* states which have been the most widely studied. The difficulties in assigning peaks in the total fluorescence yield spectrum of SF<sub>5</sub>CF<sub>3</sub> have already been noted by Ruiz *et al.*,<sup>114</sup> and at our modest resolution there are several valence-Rydberg transitions which could be assigned to peaks 2–11 in Figure 6.D.(i). A much higher-resolution spectrum would be needed for such a large molecule in order to give definitive assignments.

An alternative mechanism to reaction 6.D.(1) for production of F<sup>−</sup> might be *via* dissociative electron attachment to SF<sub>5</sub>CF<sub>3</sub>,



This is rejected because it is well known that the only product of low-energy electron attachment to SF<sub>5</sub>CF<sub>3</sub> is SF<sub>5</sub><sup>−</sup> [reaction 6.D.(8)],<sup>94–98</sup> and note the huge signal of the F<sup>−</sup> ion yield to the relatively weak signal of SF<sub>5</sub><sup>−</sup> [Figure 6.D.(ii)].

This analysis also extends to the ion yields for SF<sub>4</sub><sup>−</sup>, SF<sub>3</sub><sup>−</sup>, F<sub>2</sub><sup>−</sup>, SF<sub>2</sub><sup>−</sup>, and SF<sup>−</sup>; the peak positions and the extent of structure observed for these anions can be explained in the same

way as the F<sup>-</sup> ion yield. The SF<sub>4</sub><sup>-</sup>, SF<sub>3</sub><sup>-</sup>, and SF<sub>2</sub><sup>-</sup> ion yields show less structure than is seen from F<sup>-</sup>. In the energy regions where peaks are observed, their energies agree with those in the F<sup>-</sup> ion yield, and hence with vertical ionisation energies. It is suggested here that the number of available ion-pair states reflects the structure seen in the ion yields. SF<sub>4</sub><sup>-</sup>, for example, is likely to arise from reaction 6.D.(2) only. It is certainly the most sterically viable channel. Coupling of high-lying Rydberg states to this ion-pair state will give rise to the peaks in the SF<sub>4</sub><sup>-</sup> yield at 14 and 15 eV [Figure 6.D.(i)]. Lack of structure above 16 eV represents the point where this ion-pair state no longer couples significantly to Rydberg states. SF<sub>3</sub><sup>-</sup> and SF<sub>2</sub><sup>-</sup> also arise through coupling of high-lying Rydberg states to an appropriate ion-pair state, and only over a limited energy range above the onset. In contrast, many more dissociation channels will be available to yield the anions F<sup>-</sup> and F<sub>2</sub><sup>-</sup>. As a result, structure in both ion yields extends extensively from onset up to 25 eV. Finally, it is noted that shape resonances have been observed in the yields of many anions in both SF<sub>6</sub> and CF<sub>4</sub> above 25 eV.<sup>103,109</sup> There is no obvious evidence for such peaks in our ion yields from SF<sub>5</sub>CF<sub>3</sub>, but it would be surprising if they were not present.

## 6.E. Conclusions

The peaks in the F<sup>-</sup> yields from both SF<sub>6</sub> and CF<sub>4</sub> have been assigned to Rydberg transitions,<sup>40,41</sup> and the assignments are not repeated here. However, there is some disagreement whether the transitions observed in the VUV absorption spectrum of SF<sub>5</sub>CF<sub>3</sub>,<sup>92,102</sup> and indeed the CF<sub>3</sub><sup>\*</sup> fluorescence excitation spectrum,<sup>114</sup> are due to intravalence or Rydberg transitions. Peaks in the absorption and electron energy loss spectra of SF<sub>5</sub>CF<sub>3</sub> are assigned by Limao-Vieira *et al.*<sup>92</sup> to valence-Rydberg transitions, and quantum defects

determined. Ruiz *et al.*<sup>114</sup> also assign peaks in the absorption spectrum that led to CF<sub>3</sub><sup>\*</sup> fluorescence to valence-Rydberg transitions. Holland *et al.*,<sup>102</sup> however, assign the main peaks in the absorption spectrum to valence-valence transitions. The spectra presented here observe a different exit channel, *i.e.* photodissociation of excited states of SF<sub>5</sub>CF<sub>3</sub> to production of *anions*. However, the primary excitation process in all these experiments is the same, and their assignment to Rydberg transitions is favoured, for two reasons. First, all previous work on ion-pair production from polyatomic molecules has preferred the process of Rydberg state photoexcitation, followed by predissociation into an ion-pair state.<sup>28</sup> Second, apart from the low-energy peak in the F<sup>-</sup> yield at 11.7 eV below the ionisation energy of SF<sub>5</sub>CF<sub>3</sub>, all the F<sup>-</sup> peaks have energies very close to peaks in the TPES of this molecule. Since it is Rydberg states that have energies converging on ground and excited electronic states of SF<sub>5</sub>CF<sub>3</sub><sup>+</sup>, it seems very likely that these F<sup>-</sup> peaks correspond to photoexcitation of Rydberg states.

A summary of the numerical information obtained from the ion yields from SF<sub>6</sub>, CF<sub>4</sub> and SF<sub>5</sub>CF<sub>3</sub> is given in Table 6.B.(I), listing *AEs* of anions, cross sections and quantum yields. The anions observed from SF<sub>5</sub>CF<sub>3</sub> were all seen in either the SF<sub>6</sub> or CF<sub>4</sub> study. The signal strengths from the SF<sub>x</sub><sup>-</sup> anions, however, are stronger from SF<sub>5</sub>CF<sub>3</sub> than from SF<sub>6</sub>, allowing their ion yields to be recorded. Unsurprisingly, F<sup>-</sup> and F<sub>2</sub><sup>-</sup> are observed from all three molecules. The most prominent features in the F<sup>-</sup> ion yields from SF<sub>6</sub> and CF<sub>4</sub> occur below the onset of ionisation. This is not the case for F<sup>-</sup> from SF<sub>5</sub>CF<sub>3</sub>. This observation is clearly demonstrated in Table 6.D.(I) when comparing the ion-pair quantum yields of F<sup>-</sup> above and below the onset of ionisation for these three molecules.

# Chapter 7:

## *Vacuum ultraviolet negative photoion spectroscopy of $\text{CF}_3\text{Cl}$ , $\text{CF}_3\text{Br}$ and $\text{CF}_3\text{I}$*

This chapter presents and analyses the data collected for trifluorochloromethane ( $\text{CF}_3\text{Cl}$ ), trifluorobromomethane ( $\text{CF}_3\text{Br}$ ) and trifluoroiodomethane ( $\text{CF}_3\text{I}$ ). This series of molecules will be referred to as the  $\text{CF}_3\text{X}$  series, where  $\text{X} = \text{Cl}$ ,  $\text{Br}$  or  $\text{I}$ , and the main aim of this study is to compare the data and see the effects and resulting trends of changing substituent  $\text{X}$ . These results were collected in September 2006 at the Daresbury synchrotron radiation source, on beamline 3.1. Many thanks go to Professors Richard Tuckett and Colin Latimer, Drs Ken Dunn, Adam Hunniford, and David Shaw for their individual contributions in the data collection. I also thank Richard Tuckett and Michael Parkes for their part in analysing the data. This work was published in the *Journal of Chemical Physics* in 2009.<sup>116</sup>

### **7.A. Background information**

$\text{CF}_3\text{Cl}$ ,  $\text{CF}_3\text{Br}$  and  $\text{CF}_3\text{I}$  are all greenhouse gases and potential ozone depleters. The use of these molecules in industrial applications has inevitably led to their release into the atmosphere. For example,  $\text{CF}_3\text{Cl}$  (CFC-13) was used as a refrigerant and  $\text{CF}_3\text{Br}$  (halon 1301) as a fire suppressor, but both are now banned in accordance with the Montreal Protocol.<sup>117</sup>  $\text{CF}_3\text{I}$  is considered less environmentally unfriendly than  $\text{CF}_3\text{Cl}$  or  $\text{CF}_3\text{Br}$  and it is expected to



have a relatively low atmospheric lifetime.<sup>118</sup> This increases the potential for CF<sub>3</sub>I applications, for example, as a plasma etching gas<sup>119</sup> and as a possible replacement for CF<sub>3</sub>Br in fire extinguishing systems.<sup>120</sup>

This series of CF<sub>3</sub>X molecules have C<sub>3v</sub> symmetry, and the main effect of a change in the substituent *X* is the elongation and subsequent weakening of the C–*X* bond. The effect on the overall electronic structure of the molecule on changing *X* is not dramatic, since the orbitals of the *X* atom show little mixing with the CF<sub>3</sub> orbitals. The evidence for this property is best observed from photoelectron spectroscopy, where HeI, HeII, and threshold photoelectron (TPE) spectra have been reported for CF<sub>3</sub>Cl, CF<sub>3</sub>Br and CF<sub>3</sub>I.<sup>121–126</sup> Bands observed in the spectra from ionisation of an *X* lone pair or a C–*X* bonding electron shift to lower energy as *X* gets larger. However, bands observed from ionisation of an F lone pair or a C–F bonding electron are very similar in energy for CF<sub>3</sub>Cl, CF<sub>3</sub>Br and CF<sub>3</sub>I. Absorption data on CF<sub>3</sub>Cl have been well studied by photoabsorption spectroscopy<sup>127,128</sup> and electron energy loss spectroscopy (EELS).<sup>129,130</sup> More recent absorption<sup>131</sup> and EELS<sup>132</sup> studies compare data for all three CF<sub>3</sub>X molecules. While most of this work is restricted to energies < 15 eV, absorption data for CF<sub>3</sub>Cl is reported up to 25 eV,<sup>128,133</sup> and for CF<sub>3</sub>Br up to 30 eV.<sup>133</sup> Vacuum-UV fluorescence spectroscopy has also been studied for CF<sub>3</sub>X molecules, where *X* = F, H, Cl, and Br<sup>134</sup> and where *X* = F, H, Cl, Br, and I.<sup>133</sup>

The VUV photoion-pair formation of CF<sub>3</sub>Cl has been studied previously using a quadrupole mass analyser by Schenk *et al.*,<sup>135</sup> but this is the first report of ion-pair production following photoexcitation of CF<sub>3</sub>Br and CF<sub>3</sub>I.

### 7.B. The anions observed from $\text{CF}_3\text{Cl}$ , $\text{CF}_3\text{Br}$ and $\text{CF}_3\text{I}$

The negative ion mass spectra for the three  $\text{CF}_3\text{X}$  ( $\text{X} = \text{Cl}, \text{Br}, \text{I}$ ) molecules recorded with white light at 0 nm all show the presence of the same seven anions;  $\text{F}^-$ ,  $\text{X}^-$ ,  $\text{F}_2^-$ ,  $\text{FX}^-$ ,  $\text{CF}^-$ ,  $\text{CF}_2^-$  and  $\text{CF}_3^-$ .  $\text{F}^-$  and  $\text{X}^-$  are always the strongest signals. The remaining five anions were detected just above the sensitivity level of the apparatus, the signals being  $\leq ca. 2\%$  of that of the dominant anion ( $\text{F}^-$  or  $\text{X}^-$ ). It was observed that the  $\text{X}^-$  relative signal strengths increased with increasing mass and size of  $\text{X}$ ;  $\text{Cl}^- = 18\%$ ,  $\text{Br}^- = 37\%$ , and  $\text{I}^- = 100\%$  from  $\text{CF}_3\text{Cl}$ ,  $\text{CF}_3\text{Br}$ , and  $\text{CF}_3\text{I}$ , respectively, of the strongest anion signal ( $\text{F}^-$  from  $\text{CF}_3\text{Cl}$  and  $\text{CF}_3\text{Br}$ ,  $\text{I}^-$  from  $\text{CF}_3\text{I}$ ). Of all the anions, only  $\text{FI}^-$  was too weak to record as a function of photon energy. Negative ion yields for all other anions are presented below.

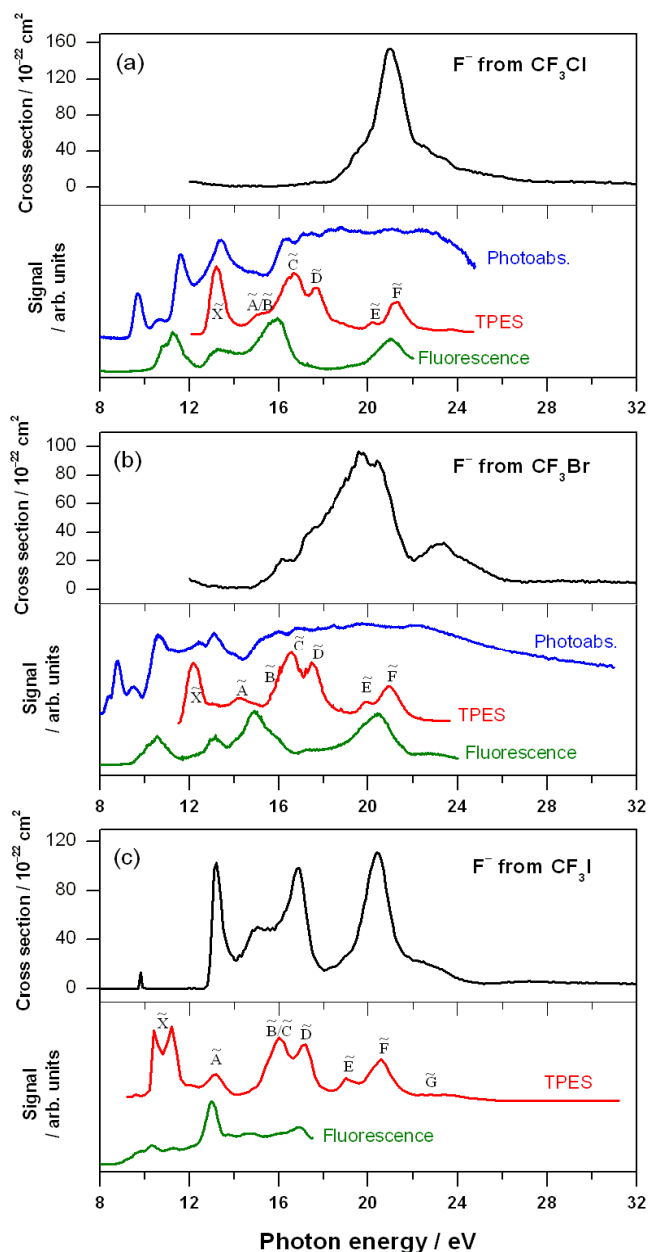
Of particular relevance to this study is the work of Schenk *et al.*,<sup>135</sup> who also investigated the valence region of  $\text{CF}_3\text{Cl}$  with VUV synchrotron radiation, and comparisons between the two sets of results are detailed in the discussion below. In summary, Schenk *et al.* were only able to detect  $\text{F}^-$ ,  $\text{Cl}^-$  and  $\text{CF}_3^-$ .  $\text{CF}_3^-$  was detected with low intensity and an ion yield was not recorded. The  $\text{F}^-$  and  $\text{Cl}^-$  ion yields are in excellent agreement with the results presented here.

### 7.C. $\text{F}^-$ from $\text{CF}_3\text{Cl}$ , $\text{CF}_3\text{Br}$ and $\text{CF}_3\text{I}$

The  $\text{F}^-$  ion yields from  $\text{CF}_3\text{Cl}$ ,  $\text{CF}_3\text{Br}$  and  $\text{CF}_3\text{I}$  are presented in Figure 7.C.(i) in the photon energy range 8-32 eV. For comparative purposes Figure 7.C.(i) also includes the total photoabsorption spectrum,<sup>133</sup> threshold photoelectron spectrum<sup>125</sup> (TPES) and total

fluorescence yield<sup>133</sup> for  $\text{CF}_3\text{Cl}$  and  $\text{CF}_3\text{Br}$ , and the TPES<sup>126</sup> and total fluorescence yield<sup>133</sup> for  $\text{CF}_3\text{I}$ . The corresponding numerical data from the  $\text{F}^-$  ion yields is presented in Table 7.C.(I).

**Figure 7.C.(i).** Cross sections for  $\text{F}^-$  production following photoexcitation of (a)  $\text{CF}_3\text{Cl}$ , and (b)  $\text{CF}_3\text{Br}$  between 12 and 32 eV. The total photoabsorption spectra,<sup>133</sup> threshold photoelectron spectra,<sup>125</sup> and total fluorescence yields<sup>133</sup> for  $\text{CF}_3\text{Cl}$  and  $\text{CF}_3\text{Br}$  are included for comparative purposes. (c) Cross section for  $\text{F}^-$  production following photoexcitation of  $\text{CF}_3\text{I}$  between 8 and 32 eV. The threshold photoelectron spectrum,<sup>126</sup> and total fluorescence yield<sup>133</sup> are included. All  $\text{F}^-$  ion yields were recorded with a step size of 0.1 eV and a wavelength resolution of 6 Å. This resolution is equivalent to 0.2 eV at 20.0 eV.



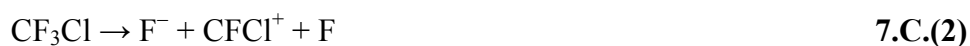
The small rise in signal at 12 eV seen in the  $\text{F}^-$  ion yields from  $\text{CF}_3\text{Cl}$  and  $\text{CF}_3\text{Br}$  is considered to result from second-order radiation, and is exaggerated by normalisation to photon flux

which is low at this energy. In all three cases the F<sup>-</sup> signal shows a linear rise with gas pressure, indicating that F<sup>-</sup> ions are formed by unimolecular ion-pair dissociation.

The F<sup>-</sup> ion yield from CF<sub>3</sub>Cl shows a gradual onset. The first indication of a rise in signal above the background is at  $16.0 \pm 0.2$  eV [Figure 7.C.(i), Table 7.C.(I)]. In the earlier work of Schenk *et al.* the F<sup>-</sup> ion yield from CF<sub>3</sub>Cl is reported with a wavelength resolution of 2 Å.<sup>135</sup> They report the onset of F<sup>-</sup> ions to be  $15.9 \pm 0.3$  eV, correlating this onset to reaction 7.C.(1) using thermochemical calculations:



Schenk *et al.* also report second ( $16.8 \pm 0.1$  eV), third ( $18.2 \pm 0.1$  eV), and fourth ( $20.0 \pm 0.1$  eV) onsets corresponding to the dissociation reactions 7.C.(2), 7.C.(3), and 7.C.(4), respectively:



The thermochemical analysis performed here, as discussed in Chapter 1, agrees with all these assignments. However, the lack of well-defined onsets and features in the F<sup>-</sup> ion yield from CF<sub>3</sub>Cl, combined with the number of different dissociation channels possible, does not allow these assignments to be made with confidence. For example, the calculated dissociation enthalpies for producing the ion pairs F<sup>-</sup>/CFCl<sup>+</sup> (+ F) [reaction 7.C.(2)] and F<sup>-</sup>/Cl<sup>+</sup> (+ CF<sub>2</sub>) are

17.0 and 17.1 eV, respectively. Not only are both these values *higher*, and not lower, in energy than the second onset, but from this analysis alone both are equally valid assignments.

The F<sup>-</sup> ion yield from CF<sub>3</sub>Br shows the first onset at  $14.7 \pm 0.2$  eV [Figure 7.C.(i), Table 7.C.(I)] which correlates best to the dissociation enthalpy of 14.9 eV calculated for reaction 7.C.(5):



For the same reasons as discussed above in the thermochemical analysis of F<sup>-</sup> from CF<sub>3</sub>Cl, even tentative assignments of other unimolecular dissociation reactions to onsets of features in the F<sup>-</sup> ion yield from CF<sub>3</sub>Br are not suggested here.

Assignments of dissociation processes to onsets in the F<sup>-</sup> ion yield from CF<sub>3</sub>I can be made more confidently; calculated thresholds for reactions 7.C.(6), 7.C.(7), 7.C.(8), and 7.C.(9) coincide with local minima, and hence with onsets to features in the ion yield [Figure 7.C.(i)].



The calculated enthalpy changes for reactions 7.C.(6) to 7.C.(9) are 14.2, 14.3, 15.7 and 18.5 eV, respectively. It is likely that features in the ion yield which occur just after these values represent the ‘turning on’ of the newly-available dissociation channel(s). In addition, the

sharp onset observed at  $12.7 \pm 0.2$  eV can be correlated to formation of the F<sup>-</sup>/I<sup>+</sup> (+ CF<sub>2</sub>) ion pair – although this assignment is made more tentatively since the calculated enthalpy is 13.2 eV, 0.5 eV *above* this onset.

The lowest energy ion-pair reaction which yields F<sup>-</sup> must be:



Lack of reliable information for  $\Delta_f H^\circ_{298}$  (CF<sub>2</sub>I<sup>+</sup>) prevented a dissociation enthalpy for CF<sub>3</sub>I in reaction 7.C.(10) to be calculated. For CF<sub>3</sub>Cl and CF<sub>3</sub>Br the calculated thresholds for this reaction are 10.2 and  $\leq 10.1$  eV, respectively. In both cases these calculated dissociation enthalpies are significantly below the experimentally-observed *AE* for F<sup>-</sup> ions; recall the *AE*s are 16.0 and 14.7 eV for F<sup>-</sup> from CF<sub>3</sub>Cl and CF<sub>3</sub>Br, respectively. There is therefore no evidence, from this thermochemical analysis, that F<sup>-</sup> ions produced from CF<sub>3</sub>Cl and CF<sub>3</sub>Br arise *via* reaction 7.C.(10). The *AE* for F<sup>-</sup> from CF<sub>3</sub>I, however, is much lower, at 9.7 eV [Figure 7.C.(i), Table 7.C.(I)]. Even though a threshold energy could not be calculated for reaction 7.C.(10) when X = I, it is the only ion-pair channel forming F<sup>-</sup> from CF<sub>3</sub>I that is likely to occur at energies below *ca.* 13 eV. The peak at 9.8 eV in the F<sup>-</sup> ion yield from CF<sub>3</sub>I, albeit very weak, must therefore arise from reaction 7.C.(10).

The photoabsorption spectra of CF<sub>3</sub>Cl and CF<sub>3</sub>Br, shown in Figure 7.C.(i),<sup>133</sup> extend over the energy range where F<sup>-</sup> ions are observed from the two molecules. Figure 7.C.(i) does not include a photoabsorption spectrum for CF<sub>3</sub>I and published data in the energy range of interest (up to 25 eV) is limited. The peak centred at 16.32 eV in the CF<sub>3</sub>Cl absorption spectrum has been assigned as a transition to a 3s Rydberg orbital converging on the fifth excited valence state of CF<sub>3</sub>Cl<sup>+</sup> ( $\tilde{E}^2 A_1$ ).<sup>133</sup> From electron energy-loss spectroscopy (EELS) of

CF<sub>3</sub>Cl, King and McConkey have assigned observed features at 16.29, 17.1 and 18.2 eV as transitions to 3*s*, 3*p* and 3*d* Rydberg orbitals, respectively, all converging to CF<sub>3</sub>Cl<sup>+</sup> ( $\tilde{E}^2A_1$ ).<sup>129</sup> These features occur in the same energy range where the gradual onset of F<sup>-</sup> ions from CF<sub>3</sub>Cl is observed. The cross section for F<sup>-</sup> ions in this energy range is relatively small ( $6 \times 10^{-22}$  cm<sup>2</sup> at 17.6 eV) and well-defined peaks are not observed. As a result, and given the tentative nature of the assignments made from the photoabsorption and EEL spectra, assigning the same transitions to the F<sup>-</sup> ion yield is speculative. The one peak that is observed at 21.0 eV has not been clearly seen in the absorption spectrum.<sup>133</sup> It may correspond to a Rydberg state of CF<sub>3</sub>Cl converging on either the  $\tilde{F}^2E$  or  $\tilde{G}^2A_1$  state of the parent ion.

The above discussion assumes the formation mechanism is predissociative, yet direct excitation to the ion-pair state should not be discounted. The gradual onset and small cross section indicate weak Franck-Condon overlap, and therefore direct ion-pair formation is plausible. If this is the case, the *AE* of F<sup>-</sup> ions may exceed the thermochemical ion-pair dissociation threshold by a greater amount than that from a predissociation mechanism where these two energies are more likely to be similar.

The feature in the CF<sub>3</sub>Br photoabsorption spectrum at 15.96 eV has been assigned as a transition to a 4*d* Rydberg orbital converging on the fourth excited valence state of CF<sub>3</sub>Br<sup>+</sup> ( $\tilde{D}^2E$ ).<sup>133</sup> It is close in energy to the first observable peak in the F<sup>-</sup> ion yield at 16.1 eV, and it is possible these two features share the same primary excitation process. The peak at 9.8 eV in the F<sup>-</sup> ion yield from CF<sub>3</sub>I is very sharp and weak, and appears anomalous by comparison to the rest of the spectrum. The abrupt nature of this feature points to a predissociative mechanism and the low cross section could indicate the extent of overlap between states is small. It has been suggested, albeit tentatively, that Rydberg states of the *ns* series converging

to the  $\tilde{X}^2E_{3/2}$  ionisation limit lie in this energy region. Indeed there is a strong absorption band between 9.4 and 9.9 eV showing detailed structure.<sup>131</sup>

It is generally accepted that the  $\tilde{X}^2E$  electronic states of the CF<sub>3</sub>X<sup>+</sup> (X = Cl, Br, I) cations result from ionisation of X lone-pair electrons, and the  $\tilde{A}^2A_1$  from ionisation of a C–X bonding electron.<sup>121-124</sup> The  $\tilde{B}$ ,  $\tilde{C}$ ,  $\tilde{D}$ ,  $\tilde{E}$  and  $\tilde{F}$  electronic states of the cations between 15 and 22 eV are most likely from fluorine lone-pair excitations. It is expected that the bonding character of the fluorine lone-pair electrons will increase with increasing ionisation energy.<sup>123</sup> Photoexcitation of these electrons leads to the production of F<sup>-</sup> anions. Only F<sup>-</sup> produced from CF<sub>3</sub>I is observed following photoexcitation of an electron associated with the X substituent. Even so, the resulting single peak at 9.8 eV appears isolated and the cross section is very small compared to the rest of the spectrum. The similarities of the photoelectron spectra for the three CF<sub>3</sub>X molecules have been highlighted by Cvitaš *et al.*,<sup>121,123</sup> and they suggest that changing substituent X affects the electronic structure of the CF<sub>3</sub> group very little. Despite this observation, the F<sup>-</sup> ion yields from these three molecules differ significantly. The extent of structure and the energy range over which F<sup>-</sup> is observed increases as X changes from Cl through to I. In addition, the *AE* of F<sup>-</sup> ions decreases. These trends appear more significant when substituting Br for I than when substituting Cl for Br. This trend possibly reflects the differing polarisabilities of the halogen atoms; the values are 2.18, 3.05 and 5.35 × 10<sup>-24</sup> cm<sup>3</sup> for neutral atomic Cl, Br and I, respectively.<sup>136</sup>



**Table 7.C.(I).** Appearance energies, cross sections and quantum yields for anions observed from photoexcitation of CF<sub>3</sub>Cl, CF<sub>3</sub>Br and CF<sub>3</sub>I.

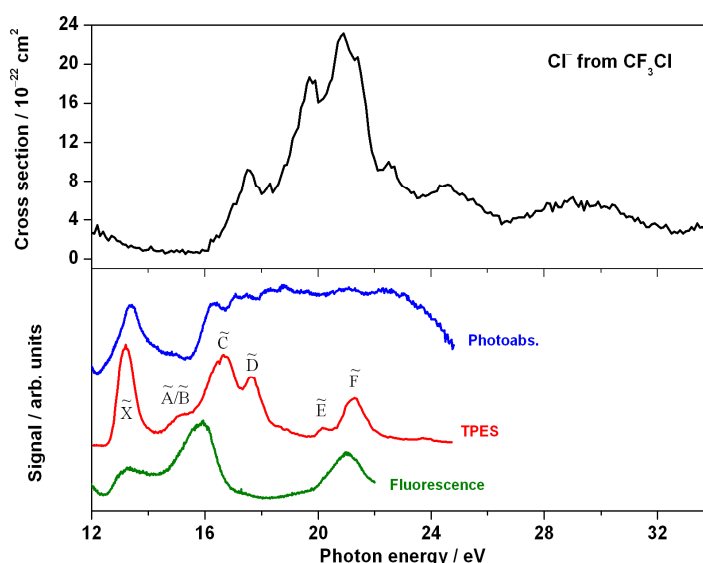
Molecule [ <i>IE</i> <sup>a</sup> / eV]	Anion	<i>AE</i> <sup>b</sup> / eV	Cross section <sup>c</sup> / cm <sup>2</sup>	Energy <sup>d</sup> / eV	Quantum Yield <sup>e</sup>
CF <sub>3</sub> Cl [12.4]	F <sup>-</sup>	16.0	$1.5 \times 10^{-20}$	21.0	$1.8 \times 10^{-4}$
	Cl <sup>-</sup>	16.1	$2.3 \times 10^{-21}$	20.9	$2.9 \times 10^{-5}$
	F <sub>2</sub> <sup>-</sup>	$\sim 21^f$	$6.8 \times 10^{-23}$	22.7	$8.5 \times 10^{-7}$
	FCI <sup>-</sup>	$\sim 18^f$	$6.5 \times 10^{-23}$	20.8	$8.0 \times 10^{-7}$
	CF <sup>-</sup>	25.5 <sup>g</sup>	$1.6 \times 10^{-22}$	27.3	- <sup>h</sup>
	CF <sub>2</sub> <sup>-</sup>	20.2	$1.5 \times 10^{-22}$	21.3	$1.8 \times 10^{-6}$
	CF <sub>3</sub> <sup>-</sup>	15.5	$2.8 \times 10^{-22}$	18.1	$3.5 \times 10^{-6}$
CF <sub>3</sub> Br [11.5]	F <sup>-</sup>	14.7	$9.7 \times 10^{-21}$	19.6	$1.2 \times 10^{-4}$
	Br <sup>-</sup>	15.1	- <sup>i</sup>	-	- <sup>i</sup>
	F <sub>2</sub> <sup>-</sup>	$\sim 19^f$	$2.8 \times 10^{-22}$	20.4	$3.4 \times 10^{-6}$
	FBr <sup>-</sup>	$\sim 18^f$	$5.5 \times 10^{-22}$	20.4	$6.6 \times 10^{-6}$
	CF <sup>-</sup>	23.6	$3.4 \times 10^{-22}$	25.6	$5.2 \times 10^{-6}$
	CF <sub>2</sub> <sup>-</sup>	18.2	$4.9 \times 10^{-22}$	19.5	$5.8 \times 10^{-6}$
	CF <sub>3</sub> <sup>-</sup>	13.6	$2.5 \times 10^{-22}$	14.8	$4.0 \times 10^{-6}$
CF <sub>3</sub> I [10.4]	F <sup>-</sup>	9.7	$1.1 \times 10^{-20}$	20.4	- <sup>j</sup>
	I <sup>-</sup>	8.8	- <sup>i</sup>	-	- <sup>i</sup>
	F <sub>2</sub> <sup>-</sup>	$\sim 17^f$	$8.5 \times 10^{-23}$	20.1	- <sup>j</sup>
	CF <sup>-</sup>	21.6	$1.1 \times 10^{-22}$	23.6	- <sup>j</sup>
	CF <sub>2</sub> <sup>-</sup>	16.0	$4.6 \times 10^{-22}$	16.8	- <sup>j</sup>
	CF <sub>3</sub> <sup>-</sup>	11.0	$5.7 \times 10^{-22}$	12.7	- <sup>j</sup>

<sup>a</sup> Adiabatic ionisation energy for CF<sub>3</sub>Cl,<sup>125</sup> CF<sub>3</sub>Br,<sup>125</sup> and CF<sub>3</sub>I.<sup>137</sup><sup>b</sup> Observed appearance energy (*AE*) from this work. The error is estimated to be  $\pm 0.2$  eV, based on the resolution and step size used when recording the ion yields.<sup>c</sup> Cross section for anion production following photoexcitation of the parent molecule.<sup>d</sup> Energy of peak maximum at which cross section and quantum yield measurements are taken.<sup>e</sup> Quantum yields for anion production, obtained by dividing cross sections for anions (column 4) by total photoabsorption cross sections. The photoabsorption cross sections are given for CF<sub>3</sub>Cl and CF<sub>3</sub>Br.<sup>133</sup><sup>f</sup> Cannot state *AE* with confidence due to poor signal/noise.<sup>g</sup> There is some ambiguity surrounding the mass of anions detected contributing to the CF<sup>-</sup> ion yield from CF<sub>3</sub>Cl. The signal observed in the range 16-25 eV is thought to arise from Cl<sup>-</sup> ions (see text), and the value of 25.5 eV represents the current interpretation of the true onset to CF<sup>-</sup> ions.<sup>h</sup> Quantum yield is not calculated because absolute photoabsorption data for CF<sub>3</sub>Cl is not available at this energy.<sup>i</sup> The Br<sup>-</sup> and I<sup>-</sup> ion yields are significantly influenced by anions arising from dissociative electron attachment and cross sections, and hence quantum yields, cannot be defined.<sup>j</sup> Quantum yields cannot be calculated at this photon energy, because the available absolute photoabsorption data for CF<sub>3</sub>I is limited to photon energies < 12 eV.

### 7.D. Cl<sup>−</sup> from CF<sub>3</sub>Cl

The Cl<sup>−</sup> ion yield from CF<sub>3</sub>Cl is shown in Figure 7.D.(i) from 12 to 34 eV. For comparative purposes it also includes the total photoabsorption spectrum,<sup>133</sup> TPES<sup>125</sup> and total fluorescence yield<sup>133</sup> for CF<sub>3</sub>Cl. The numerical information is summarised in Table 7.C.(I). The signal in the Cl<sup>−</sup> ion yield observed between 12 and 14 eV is considered to result from second-order effects, which are exaggerated when flux normalising the spectrum. The Cl<sup>−</sup> signal changes linearly with CF<sub>3</sub>Cl gas pressure, indicating that the mechanism for Cl<sup>−</sup> formation is unimolecular ion-pair dissociation.

**Figure 7.D.(i).** Cross section for Cl<sup>−</sup> production following photoexcitation of CF<sub>3</sub>Cl in the energy range 12–34 eV. The total photoabsorption spectrum,<sup>133</sup> threshold photoelectron spectrum,<sup>125</sup> and total fluorescence yield<sup>133</sup> for CF<sub>3</sub>Cl are included for comparative purposes. The F<sup>−</sup> ion yield was recorded with a step size of 0.1 eV and a wavelength resolution of 6 Å. This resolution is equivalent to 0.2 eV at 20.0 eV.



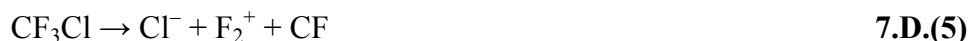
The lowest energy ion-pair fragmentation leading to Cl<sup>−</sup> production must also produce the cation CF<sub>3</sub><sup>+</sup>:



The calculated enthalpy for reaction 7.D.(1) is 9.2 eV, however, the experimentally-observed onset to Cl<sup>-</sup> production from CF<sub>3</sub>Cl is  $16.1 \pm 0.2$  eV. In the earlier work of Schenk *et al.*<sup>135</sup> a value of  $16.0 \pm 0.1$  eV is reported, in excellent agreement with this work. The observed Cl<sup>-</sup> signal at onset may be assigned to the following dissociation reaction:



The calculated enthalpy change for reaction 7.D.(2) is 15.4 eV. Other onsets to features in the Cl<sup>-</sup> ion yield, observed at 18.4, 21.3, and 23.4 eV [Figure 7.D.(i)], occur where a different fragmentation reaction becomes energetically accessible:



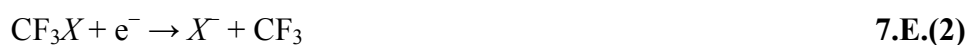
The calculated enthalpy changes for reactions 7.D.(3) to 7.D.(5) are 18.4, 21.4, and 23.3 eV, respectively.

The production of Cl<sup>-</sup> has similarities to that of F<sup>-</sup> from CF<sub>3</sub>Cl; the fragmentation reaction assumed to occur at onset [reaction 7.D.(2)] is almost identical to that assigned to F<sup>-</sup> anions from CF<sub>3</sub>Cl [reaction 7.C.(1)]. Both ion yields show a very similar *AE* [Table 7.C.(I)] and in both cases this value is much higher than the lowest-energy dissociation reaction to form the respective anion as an ion pair [reactions 7.C.(10) and 7.D.(1)]. In addition, the cross sections for F<sup>-</sup> and Cl<sup>-</sup> production peak at almost identical energies and in the range 16-18 eV the cross sections are of similar magnitude. For example, at 17.6 eV,  $\sigma_{\text{F}^-} = 5.4 \times 10^{-22}$  cm<sup>2</sup> and

$\sigma_{Cl^-} = 9.2 \times 10^{-22} \text{ cm}^2$ . Above 18 eV F<sup>-</sup> formation increases with respect to Cl<sup>-</sup> anions; at 21.0 eV,  $\sigma_{F^-} = 1.5 \times 10^{-20} \text{ cm}^2$  and  $\sigma_{Cl^-} = 2.2 \times 10^{-21} \text{ cm}^2$ .

### 7.E. Br<sup>-</sup> from CF<sub>3</sub>Br and I<sup>-</sup> from CF<sub>3</sub>I

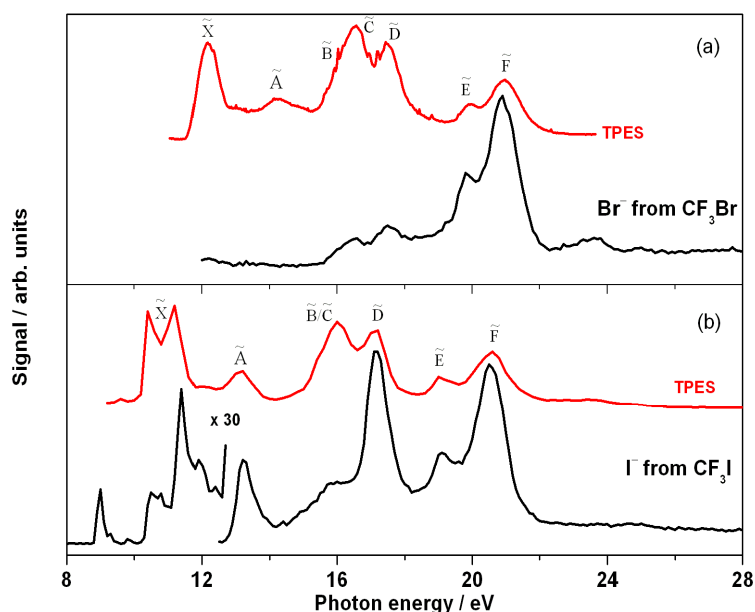
The Br<sup>-</sup> and I<sup>-</sup> ion yields from CF<sub>3</sub>Br and CF<sub>3</sub>I, respectively, are shown in Figure 7.E.(i) in the range 8-28 eV. The threshold photoelectron spectra for CF<sub>3</sub>Br<sup>125</sup> and CF<sub>3</sub>I<sup>126</sup> are superimposed above the ion yields for comparative purposes. When recorded as a function of gas pressure, both the Br<sup>-</sup> and I<sup>-</sup> signals change *non-linearly*; the rate of change in anion signal increases pseudo-exponentially with increasing pressure. When this trend has been seen before (*e.g.* SF<sub>5</sub><sup>-</sup> from SF<sub>6</sub> and SF<sub>5</sub>CF<sub>3</sub>) the anions have been shown to arise from dissociative electron attachment, following photoionisation of the parent molecule as the source of low-energy electrons<sup>86</sup> (also see Chapter 6). The same conclusion is reached in this study for the formation of Br<sup>-</sup> and I<sup>-</sup> ions from CF<sub>3</sub>X (X = Br, I). The two-step mechanism is shown below:



CF<sub>3</sub>Br<sup>138,139</sup> and CF<sub>3</sub>I<sup>119,140</sup> are both known to attach electrons rapidly: the recommended values for the thermal electron attachment rate coefficients are  $1.4 \times 10^{-8} \text{ cm}^3 \text{ s}^{-1}$  for CF<sub>3</sub>Br<sup>138</sup> and  $1.9 \times 10^{-7} \text{ cm}^3 \text{ s}^{-1}$  for CF<sub>3</sub>I.<sup>119</sup> In addition, the Br<sup>-</sup> and I<sup>-</sup> ion yields show similarities to the threshold photoelectron spectra for CF<sub>3</sub>Br and CF<sub>3</sub>I, respectively [Figure 7.E.(i)]. These similarities are much more obvious between the I<sup>-</sup> ion yield and CF<sub>3</sub>I TPES, which perhaps reflects the difference in magnitude between the attachment rate coefficients for CF<sub>3</sub>Br and

$\text{CF}_3\text{I}$ . The apparent lack of agreement between the two spectra (ion yield vs TPES) at lower photon energies in both molecules is interesting. Only background signal is observed in the  $\text{Br}^-$  ion yield over the photon energy range, 12-15 eV, where the first two bands can be seen in the  $\text{CF}_3\text{Br}$  TPES.

**Figure 7.E.(i).** (a)  $\text{Br}^-$  ion yield recorded following photoexcitation of  $\text{CF}_3\text{Br}$  between 12 and 28 eV. The threshold photoelectron spectrum<sup>125</sup> is superimposed on top of the  $\text{Br}^-$  ion yield for comparative purposes. (b)  $\text{I}^-$  ion yield recorded following photoexcitation of  $\text{CF}_3\text{I}$  between 8 and 28 eV. The 8-12 eV range of this spectrum has been blown-up by a factor of 30. The threshold photoelectron spectrum<sup>126</sup> is superimposed on top of the  $\text{I}^-$  ion yield for comparative purposes. The anion spectra are not put onto an absolute scale because the signals are shown to change non-linearly with pressure. The peak at 9.0 eV in the  $\text{I}^-$  spectrum, however, results from ion-pair formation and the cross section at this energy is  $3.8 \times 10^{-21} \text{ cm}^2$ .

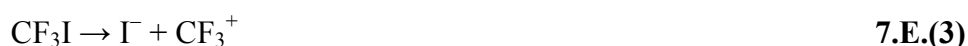


The first bands in the  $\text{CF}_3\text{I}$  TPES, representing the spin-orbit split ground state of  $\text{CF}_3\text{I}^+$ ,  $\tilde{X}^2E_{3/2}$  and  $\tilde{X}^2E_{1/2}$  are only observed very weakly in the  $\text{I}^-$  spectrum; in Figure 7.E.(i) the  $\text{I}^-$  signal over this energy region has been enlarged by a factor of 30. The ion yields of Figure 7.E.(i) are unlikely to result from dissociative electron attachment alone;  $\text{Br}^-$  or  $\text{I}^-$  anions produced by ion-pair dissociation are also detected. How much of either anion signal is due to dissociative electron attachment, and how much to ion-pair formation is unknown.

However, given the evidence above it is clear that dissociative electron attachment is the more dominant mechanism contributing to the Br<sup>-</sup> and I<sup>-</sup> ion yields.

The agreement between the TPES and the Br<sup>-</sup>/I<sup>-</sup> yield is slightly better at the higher energies scanned in Figure 7.E.(i), and the absence of the low-energy bands between 12-15 eV in the Br<sup>-</sup> channel from CF<sub>3</sub>Br, and the relative weakness of the analogous bands in the I<sup>-</sup> channel from CF<sub>3</sub>I, remain unexplained. Likewise, the reasons why the relative intensities between ion yield and TPES spectra are different, including the relative intensities of the  $\tilde{X}^2E_{3/2}$  and  $\tilde{X}^2E_{1/2}$  spin-orbit sub-bands in CF<sub>3</sub>I<sup>+</sup>, is unclear. Note that the SF<sub>6</sub><sup>-</sup> yield from SF<sub>6</sub> and the SF<sub>5</sub><sup>-</sup> yield from SF<sub>5</sub>CF<sub>3</sub> are both dominated by the two-step electron attachment mechanism over the *whole* of the valence region, and the anion yield and TPES show better agreement over a wider range of energies<sup>86</sup> (also see Chapter 6). There is limited evidence from work on other polyatomic molecules (*e.g.* *c*-C<sub>5</sub>F<sub>8</sub>) that the agreement between the two spectra is enhanced if electron attachment is *non*-dissociative.<sup>86,107</sup>

For electron attachment to occur, the parent molecule must first be ionised. Therefore, at energies below the onset to ionisation any anions produced can only arise from ion-pair dissociation. This is observed in the ion yield for I<sup>-</sup> from CF<sub>3</sub>I. The onset to ionisation in CF<sub>3</sub>I is 10.4 eV.<sup>137</sup> However, the experimentally-determined onset to I<sup>-</sup> formation is at 8.8 ± 0.2 eV and a discrete peak in the signal results at 9.0 eV [Figure 7.E.(i)]. Thermochemical calculations suggest the only possible ion-pair dissociation reaction which produces I<sup>-</sup> at this energy is:

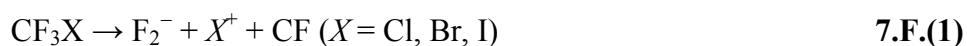


The calculated enthalpy change for reaction 7.E.(3) is 8.3 eV. The cross section for I<sup>-</sup> ion-pair formation at 9.0 eV is  $3.8 \times 10^{-21}$  cm<sup>2</sup>. Normalising this value to the total photoabsorption cross section at 9.0 eV<sup>131</sup> gives a quantum yield of *ca.*  $8 \times 10^{-5}$ . An analysis of the photoabsorption spectrum of CF<sub>3</sub>I has suggested that Rydberg states of the *ns* series converging to the  $\tilde{X}^2E_{3/2}$  ionisation limit lie in this energy region, and absorption features showing vibrational structure have been observed centred at energies 8.8 and 9.5 eV.<sup>131</sup>

### 7.F. F<sub>2</sub><sup>-</sup> and FX<sup>-</sup> (X = Cl, Br) from CF<sub>3</sub>Cl, CF<sub>3</sub>Br and CF<sub>3</sub>I

The F<sub>2</sub><sup>-</sup> ion yields from CF<sub>3</sub>X (X = Cl, Br, I) and the FX<sup>-</sup> (X = Cl, Br) yields from CF<sub>3</sub>Cl and CF<sub>3</sub>Br in the range 12-34 eV are shown in Figures 7.F.(i) and 7.F.(ii), respectively. All these anion signals show a linear increase when recorded as a function of gas pressure, indicating that F<sub>2</sub><sup>-</sup> and FX<sup>-</sup> result from unimolecular photodissociation. The Figures report absolute cross sections for these processes and further numerical information is provided in Table 7.C.(I); the cross sections for production of FCl<sup>-</sup>, FBr<sup>-</sup> and F<sub>2</sub><sup>-</sup> from CF<sub>3</sub>X are up to three orders of magnitude smaller compared to F<sup>-</sup> production.

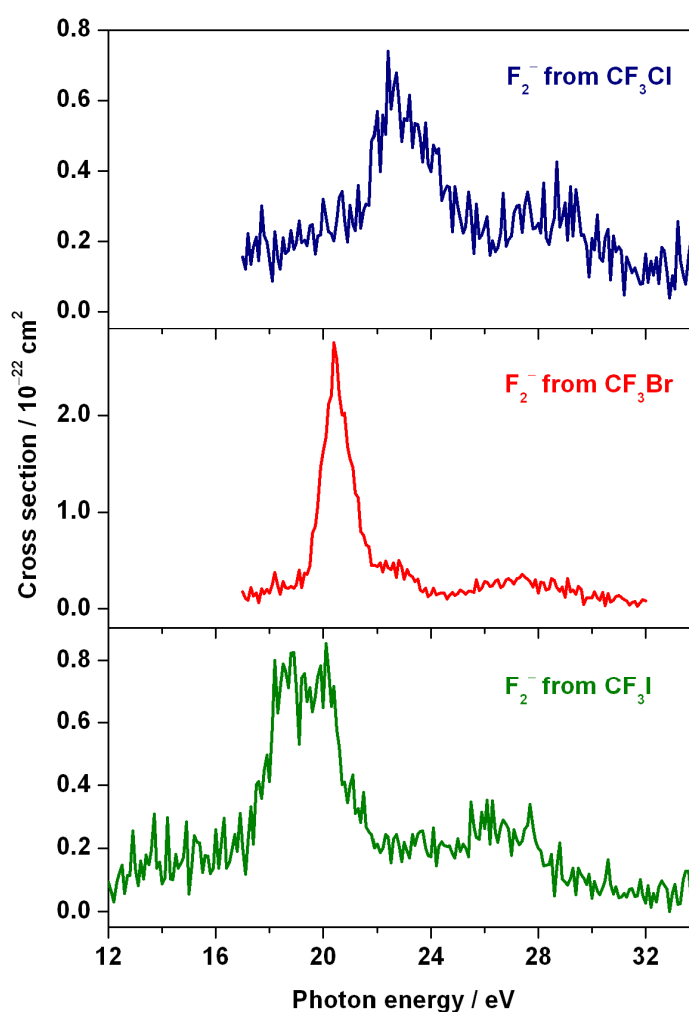
The onsets for F<sub>2</sub><sup>-</sup> production, *ca.* 21, 19 and 17 eV for X = Cl, Br, I, occur at the thermochemical thresholds for the ion-pair dissociation reaction shown below:



The calculated dissociation enthalpy changes for this reaction are 21.1, 19.2, and 17.2 eV for X = Cl, Br, and I, respectively. Two cautionary points should be made: first, the uncertainty in the values of the experimentally-determined onsets [Table 7.C.(I), Figure 7.F.(i)] is degraded by the poor signal/noise ratio in the ion yields; second, an energy barrier resulting

from forming a new F–F bond is likely – if so, the true thermochemical threshold will lie below the experimental onset, and other lower-energy dissociation reactions should be considered (*e.g.*  $\text{F}_2^-/\text{CF}^+$  ion-pair formation). A similar discussion on the dissociation reactions leading to  $\text{FCl}^-$  and  $\text{FBr}^-$  from  $\text{CF}_3\text{Cl}$  and  $\text{CF}_3\text{Br}$ , respectively, is not possible due to the lack of data on the electron affinities of  $\text{FCl}$  and  $\text{FBr}$ .

**Figure 7.F.(i).** Cross sections for  $\text{F}_2^-$  production following photoexcitation of  $\text{CF}_3\text{Cl}$ ,  $\text{CF}_3\text{Br}$  and  $\text{CF}_3\text{I}$  in the photon energy range 12–34 eV. The ion yields were recorded with a step size of 0.1 eV and a wavelength resolution of 6 Å. This resolution is equivalent to 0.2 eV at 20.0 eV.

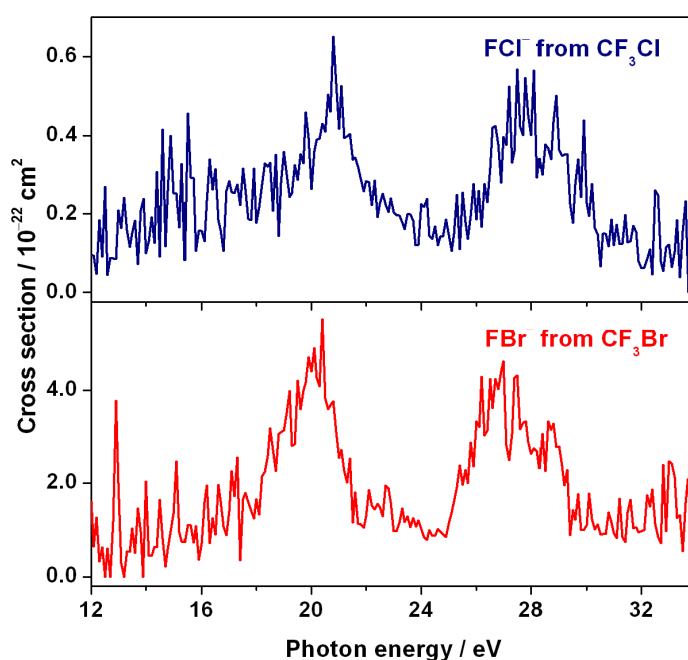


The  $\text{F}_2^-$  ion yields all show one major feature which most likely represents the presence of a Rydberg state converging to the fifth ( $\tilde{E}$ ) or sixth ( $\tilde{F}$ ) excited valence states of the  $\text{CF}_3\text{X}^+$



molecules. As discussed in Section 7.C, the origin of the excited electron is from a fluorine lone pair with significant C–F bonding character. In all three  $\text{F}_2^-$  ion yields a tentative correlation can be made between the peak energy and features in the corresponding  $\text{F}^-$  ion yields. This is unsurprising considering two F atoms must be cleaved preceding the formation of  $\text{F}_2^-$ .

**Figure 7.F.(ii).** Cross sections for  $\text{FCl}^-$  and  $\text{FBr}^-$  production following photoexcitation of  $\text{CF}_3\text{Cl}$  and  $\text{CF}_3\text{Br}$ , respectively, in the photon energy range 12–34 eV. The ion yields were recorded with a step size of 0.1 eV and a wavelength resolution of 6 Å. This resolution is equivalent to 0.2 eV at 20.0 eV.

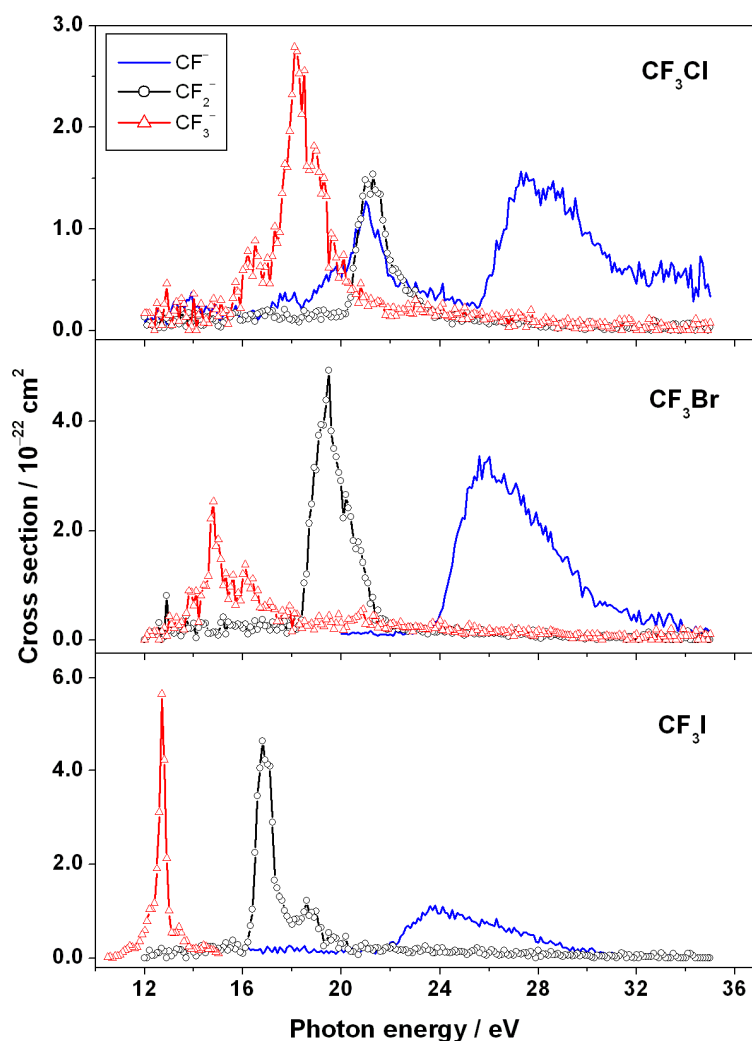


### 7.G. $\text{CF}_n^-$ ( $n = 1-3$ ) from $\text{CF}_3\text{Cl}$ , $\text{CF}_3\text{Br}$ and $\text{CF}_3\text{I}$

The  $\text{CF}^-$ ,  $\text{CF}_2^-$  and  $\text{CF}_3^-$  ion yields from  $\text{CF}_3\text{X}$  ( $\text{X} = \text{Cl}, \text{Br}, \text{I}$ ) are shown in Figure 7.G.(i). Numerical information is given in Table 7.C.(I). All these anion signals show a linear rise when recorded as a function of increasing gas pressure, indicating they result from

unimolecular photodissociation. The cross sections for  $\text{CF}_n^-$  ( $n = 1-3$ ) production are approximately two orders of magnitude smaller than those determined for  $\text{F}^-$  production.

**Figure 7.G.(i).** Cross sections for  $\text{CF}^-$ ,  $\text{CF}_2^-$  and  $\text{CF}_3^-$  production following photoexcitation of  $\text{CF}_3\text{Cl}$ ,  $\text{CF}_3\text{Br}$  and  $\text{CF}_3\text{I}$  in the photon energy range 10-35 eV. The ion yields were recorded with a step size of 0.1 eV and a wavelength resolution of 6 Å. This resolution is equivalent to 0.2 eV at 20.0 eV.



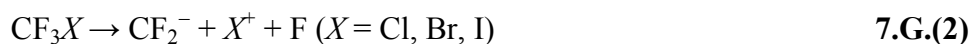
Each  $\text{CF}_n^-$  ( $n = 1-3$ ) anion from each parent  $\text{CF}_3\text{X}$  molecule shows only one feature in the ion yield, with the exception of  $\text{CF}^-$  from  $\text{CF}_3\text{Cl}$  which shows more features. It is proposed that the true onset for  $\text{CF}^-$  from  $\text{CF}_3\text{Cl}$  is 25.5 eV [Table 7.C.(I), Figure 7.G.(i)] and that the observed signal in the energy range 16-25 eV results from detecting  $\text{Cl}^-$  anions. There are

two reasons for this. First, the mass-to-charge ratios ( $m/z$ ) used when recording ion yields are close in value, 31 for CF<sup>-</sup> and 35 for Cl<sup>-</sup>. Although the Cl<sup>-</sup> signal peaks at  $m/z$  35, *weak* contributions can be detected at  $m/z$  values as low as 30. Combined with the fact that the CF<sup>-</sup> signal relative to that of Cl<sup>-</sup> is very weak, the Cl<sup>-</sup> contribution at  $m/z$  31 becomes significant. Second, the ion yield of Cl<sup>-</sup> [Figure 7.D.(i)] and that of CF<sup>-</sup> [Figure 7.G.(i)] from CF<sub>3</sub>Cl appear similar in the 16-25 eV energy range; both ion yields show an onset around 16 eV, with features at *ca.* 17.5 and 21.0 eV.

Unimolecular dissociation of CF<sub>3</sub>X ( $X = \text{Cl, Br, I}$ ) leading to CF<sub>3</sub><sup>-</sup> formation must also produce the cation  $X^+$ :



The calculated thermochemical thresholds for reaction 7.G.(1) are 14.9, 13.1, and 11.0 eV when  $X = \text{Cl, Br, and I}$ , respectively; the experimentally-determined onsets for CF<sub>3</sub><sup>-</sup> anions are 15.5, 13.6, and 11.0 eV, respectively. A similar dissociation process most likely produces the CF<sub>2</sub><sup>-</sup> anions:



The calculated thermochemical thresholds for reaction 7.G.(2) are 20.3, 18.5, and 16.4 eV when  $X = \text{Cl, Br, and I}$ , respectively; the experimentally-determined onsets for CF<sub>2</sub><sup>-</sup> anions are 20.2, 18.2, and 16.0 eV, respectively. Dissociation of CF<sub>3</sub>X ( $X = \text{Cl, Br, I}$ ) to produce the CF<sub>2</sub><sup>-</sup>/F<sup>+</sup> ion pair will only occur at excitation energies several eV *above* the experimental onset, and is therefore not a possible assignment. Dissociation to produce the CF<sub>2</sub><sup>-</sup>/FX<sup>+</sup> ion pair, however, may occur *below* the experimental onset.



The calculated thermochemical thresholds for reaction 7.G.(3) are 17.4, 15.9, and 13.6 eV when  $X = \text{Cl, Br, and I}$ , respectively. If reaction 7.G.(3) occurs, 2-3 eV excess energy must be accounted for. An experimental onset is always considered an upper limit, and small amounts of energy will undoubtedly be converted into translational energy of the fragment species. It should also be considered that an energy barrier to  $\text{FX}^+$  formation may exist, given that bonds are both broken *and* formed. Similar arguments are made in Section 7.F with respect to the anions  $\text{F}_2^-$  and  $\text{FX}^-$  ( $X = \text{Cl, Br, I}$ ). The more likely process producing  $\text{CF}_2^-$  from  $\text{CF}_3\text{X}$  is reaction 7.G.(2), rather than reaction 7.G.(3). Low excess energies favour the production of ion pairs,<sup>28</sup> and a bond-breaking-only dissociative reaction is favoured over one where bonds are additionally formed.

The considerations discussed above are also relevant in the discussion of the  $\text{CF}^-$  fragment anion. The possibilities for the associated fragment cation and neutral species are greater. Several diatomic fragments,  $\text{F}_2$ ,  $\text{F}_2^+$ ,  $\text{FX}$  or  $\text{FX}^+$ , could realistically be associated with  $\text{CF}^-$  ion-pair formation. The thermochemistry suggests all processes pairing  $\text{CF}^-$  formation with  $\text{X}^+$ ,  $\text{F}^+$  or  $\text{F}_2^+$  could be contributing to the observed  $\text{CF}^-$  signal from  $\text{CF}_3\text{X}$  photodissociation as observed in Figure 7.G.(i). This is perhaps reflected by the broad band which features in all three  $\text{CF}^-$  ion yields.

From observation of Figure 7.G.(i) it is clear that interchanging the  $X$  substituent in  $\text{CF}_3\text{X}$  with Cl, Br, or I has little effect on the structure of the ion yields of  $\text{CF}^-$ ,  $\text{CF}_2^-$ , or  $\text{CF}_3^-$ . There are consistent shifts in the  $AE$  values of  $\text{CF}_n^-$  to lower energy as  $X$  increases in size. For example, the shift in  $AE$  for each anion is almost exactly the same when substituting Cl for Br

as when substituting Br for I [Table 7.C.(I)]; the  $AE(CF^-)$  from CF<sub>3</sub>I is 2.0 eV lower in energy than  $AE(CF^-)$  from CF<sub>3</sub>Br which is 1.9 eV lower than  $AE(CF^-)$  from CF<sub>3</sub>Cl. This trend is expected because all anions are observed at their thermochemical threshold, whose values decrease as the size of  $X$  increases.

The broad nature of the features in the CF<sup>-</sup> ion yields does not allow any direct comparisons to be made with other spectra. In addition, the energy required to yield CF<sup>-</sup> from photoexciting CF<sub>3</sub>X ( $X = Cl, Br, I$ ) is comparatively large with respect to other negative ions. Intermediate excited Rydberg states at these energies probably converge on the first *inner-valence* excited state of CF<sub>3</sub>X<sup>+</sup>. Alternatively, these features may represent direct ion-pair formation with no involvement of an intermediate excited state. The energies of peak maxima in all the CF<sub>2</sub><sup>-</sup> and CF<sub>3</sub><sup>-</sup> ion yields, however, are similar to energies of features observed in other anion spectra, and likely represent common excited intermediate states and hence competing ion-pair dissociation channels.

### 7.H. Bond dissociation energies

As discussed in Chapter 1, the experimental  $AE$ s for anions determined by this work may be used to calculate upper limits to 298 K bond dissociation energies,  $D$ .<sup>28</sup> For example, using the  $AE$  of CF<sub>3</sub><sup>-</sup> can provide an upper limit to  $D(CF_3-X)$  if the ionisation energy ( $IE$ ) of  $X$  and the electron affinity ( $EA$ ) of CF<sub>3</sub> are known, where  $X = Cl, Br, I$ :

$$AE(CF_3^-) \geq D(CF_3-X) + IE(X) - EA(CF_3) \quad \mathbf{7.H.(1)}$$

Note that the  $AE(CF_3^-)$  correlates to dissociation reaction 7.G.(1). When the unimolecular dissociation involves multiple bond-breaking or the formation of a new bond, calculations

performed in this way become over-complicated and too many assumptions are made. Therefore, only *AE* values for anions resulting from *single* bond-breaking ion-pair dissociation are considered here.

**Table 7.H.(I).** Upper limits to bond dissociation energies and comparisons with literature values.

Bond	<i>D</i> <sub>298</sub> / eV	
	This work	Literature value <sup>a</sup>
CF <sub>3</sub> –F	≤ (7.4 ± 0.2) <sup>b</sup>	5.67
CF <sub>3</sub> –Cl	≤ (4.4 ± 0.2) <sup>c</sup>	3.79
CF <sub>3</sub> –Br	≤ (3.6 ± 0.2) <sup>c</sup>	3.07
CF <sub>3</sub> –I	≤ (2.4 ± 0.2) <sup>c</sup>	2.36
CF <sub>2</sub> I <sup>+</sup> –F	≤ (2.7 ± 0.2) <sup>d</sup>	- <sup>e</sup>

<sup>a</sup> Values taken from the CRC Handbook of Chemistry and Physics.<sup>141</sup>

<sup>b</sup> Calculated from the appearance energy of F<sup>−</sup> from CF<sub>4</sub><sup>86</sup> (also see Chapter 6).

<sup>c</sup> Calculated from the appearance energy of CF<sub>3</sub><sup>−</sup> from CF<sub>3</sub>Cl, CF<sub>3</sub>Br, and CF<sub>3</sub>I, respectively.

<sup>d</sup> Calculated from the appearance energy of F<sup>−</sup> from CF<sub>3</sub>I.

<sup>e</sup> Value not available in the literature.

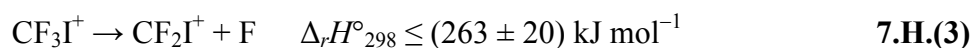
The resulting upper limits to bond dissociation energies are presented in Table 7.H.(I) and compared to literature values. In addition *D* (CF<sub>3</sub>–F) is calculated from the *AE* (F<sup>−</sup> from CF<sub>4</sub>)<sup>86</sup> (also see Chapter 6) and is also included in Table 7.H.(I). The uncertainty in the *D* upper limits calculated from these data is ± 0.2 eV which is taken directly from the estimated error in the *AE* values [Table 7.C.(I)]. The calculations for these values are explained in more detail below. Note the consistency between upper-limit values for *D* (CF<sub>3</sub>–*X*) obtained indirectly from this ion-pair work and the accepted literature values.<sup>141</sup> Furthermore, the upper-limit value for *D* tends towards the accurate value as the size of *X* increases from F through to I.

As shown in equation 7.H.(1) the  $AE$  values for  $CF_3^-$  from  $CF_3X$  [Table 7.C.(I), Figure 7.G.(i)] are used to calculate  $D(CF_3-X)$ . The  $EA$  of the  $CF_3$  radical is  $1.82 \pm 0.05$  eV,<sup>142</sup> and the ionisation energies for Cl (12.970 eV), Br (11.816 eV) and I (10.453 eV) are taken from the JANAF thermochemical tables.<sup>143</sup> The calculation is slightly different for  $D(CF_3-F)$  because  $CF_3^-$  was not observed from  $CF_4$ ,<sup>86</sup> but the  $AE(F^-)$  from  $CF_4$  can be used to yield the same information if the  $EA(F) = 3.401$  eV,<sup>144</sup> and  $IE(CF_3) = 9.04 \pm 0.04$  eV<sup>58</sup> are used instead.

The formation of  $F^-$  from  $CF_3I$  at onset arises from dissociation reaction 7.C.(10). Unfortunately, because the  $IE(CF_2I)$  is currently not known, an upper limit to  $D(CF_2I-F)$  cannot be calculated from the  $AE(F^-)$  value as described above. However, the relevant information is known in order to calculate an upper limit to  $D(CF_2I^+-F)$  if equation 7.H.(2) is considered:

$$AE(F^-) \geq IE(CF_3I) + D(CF_2I^+-F) - EA(F) \quad \mathbf{7.H.(2)}$$

The  $AE(F^-)$  is  $9.7 \pm 0.2$  eV, the  $IE(CF_3I)$  is 10.37 eV,<sup>137</sup> and the  $EA(F)$  is 3.401 eV,<sup>144</sup> giving  $D(CF_2I^+-F) \leq (2.7 \pm 0.2)$  eV or  $(263 \pm 20)$  kJ mol<sup>-1</sup>. If  $D(CF_2I^+-F)$  is simply defined as the enthalpy change for reaction 7.H.(3), then an upper limit to  $\Delta_f H^\circ_{298}(CF_2I^+)$  can be determined.



Using thermochemistry already provided (Appendix I),  $\Delta_f H^\circ_{298}(CF_2I^+)$  is calculated as  $\leq (598 \pm 22)$  kJ mol<sup>-1</sup>.

## 7.1. Conclusions

Negative ions have been detected following the photoexcitation of CF<sub>3</sub>Cl, CF<sub>3</sub>Br and CF<sub>3</sub>I in the photon energy range 8-35 eV. For the fast electron-attaching gases CF<sub>3</sub>Br and CF<sub>3</sub>I, the Br<sup>−</sup> and I<sup>−</sup> signals are heavily influenced by dissociative electron attachment. All other anions detected from these three molecules result from ion-pair formation. A collection of the numerical data from this study is compiled in Tables 7.C.(I) and 7.H.(I). It has been shown that experimental *AE* values from ion-pair formation can be used to calculate upper limits for bond dissociation energies. This same point was made by Berkowitz in 1996,<sup>28</sup> but has rarely been implemented since. New data is reported for  $D_{298}(\text{CF}_2\text{I}^+-\text{F}) \leq (2.7 \pm 0.2) \text{ eV}$  and  $\Delta_f H^\circ_{298}(\text{CF}_2\text{I}^+) \leq (598 \pm 22) \text{ kJ mol}^{-1}$ .

The most surprising observation from this work is the lack of ion-pair formation detected at lower photon energies, particularly at energies below the *IE* of the parent molecule. This anomaly is surprising because ion-pair fragmentation is energetically allowed and because significant structure is observed in the photoabsorption spectra below the *IE*. The best example of this is seen in *X*<sup>−</sup> ion pair formation from CF<sub>3</sub>X (*X* = Cl, Br, I): a comparatively large cross section for *X*<sup>−</sup> produced by reaction 7.I.(1) would be predicted, but the spectra show no contribution from Cl<sup>−</sup> or Br<sup>−</sup> anions produced in this way. I<sup>−</sup> anions, however, are observed below the *IE* of CF<sub>3</sub>I but the signal is surprisingly weak.



The total fluorescence yields and photoabsorption spectra correlate very little, and although there will be some contribution from fluorescence, it is not expected to be significant.



Therefore, the structure observed in the photoabsorption spectra for  $\text{CF}_3\text{Cl}$ ,  $\text{CF}_3\text{Br}$  and  $\text{CF}_3\text{I}$  below the  $IE$  must almost exclusively result from neutral photodissociation.

It is noted that ion-pair formation from  $\text{CF}_4$  (see Chapter 6) shows completely different properties to the  $\text{CF}_3\text{X}$  molecules studied in this paper. This should not be surprising for two reasons: first, the symmetry of the molecule changes from  $T_d$  to  $C_{3v}$ ; second, the substitution of one F by a much heavier halogen atom increases the polarisability of the molecule, and therefore enhances its propensity to attach low-energy electrons.

Finally, it is noted that the strongest anion observed,  $\text{F}^-$ , corresponds to cleavage of a strong C–F bond, whereas the anion produced by cleavage of a much weaker C–X bond,  $\text{X}^-$ , is significantly less intense. This is true for  $\text{X} = \text{Cl}, \text{Br}$  and  $\text{I}$ . It appears that the dynamics of the crossing of Rydberg states with the ion-pair continuum determines the relative intensities of the anions that are formed, and not the thermochemistry of the different dissociation channels. This point is revisited in Chapters 8 and 9.

# Chapter 8:

## *Vacuum ultraviolet negative photoion spectroscopy of SF<sub>5</sub>Cl*

The experimental data for SF<sub>5</sub>Cl was collected in May 2008 on beamline 3.1 of the Daresbury synchrotron radiation source. Many thanks go to Dr David Shaw, Professor Colin Latimer, Dr Ken Dunn and Professor Richard Tuckett for providing their experimental expertise. This work has been accepted for publication in the *Journal of Physical Chemistry A* (2010).<sup>145</sup>

### **8.A. Background information**

The anthropogenic gas sulphur chloropentafluoride (SF<sub>5</sub>Cl) is used as a reagent in chemical synthesis, but only for the infrequently required application of introducing an SF<sub>5</sub> group into other molecules.<sup>146,147</sup> Therefore gas-phase studies on this molecule are few and far between, and are generally limited to fundamental investigations where SF<sub>5</sub>Cl is compared to its better-known relation sulphur hexafluoride (SF<sub>6</sub>). More recently these studies have extended to include another related molecule, trifluoromethyl sulphur pentafluoride (SF<sub>5</sub>CF<sub>3</sub>). The negative ion spectroscopy of SF<sub>6</sub> and SF<sub>5</sub>CF<sub>3</sub> has already been reported in Chapter 6. The structure of SF<sub>5</sub>Cl, C<sub>4v</sub> symmetry in the gas phase, has been established by microwave spectroscopy<sup>148</sup> and electron diffraction.<sup>149</sup> Four equatorial S–F bonds have a slightly shorter

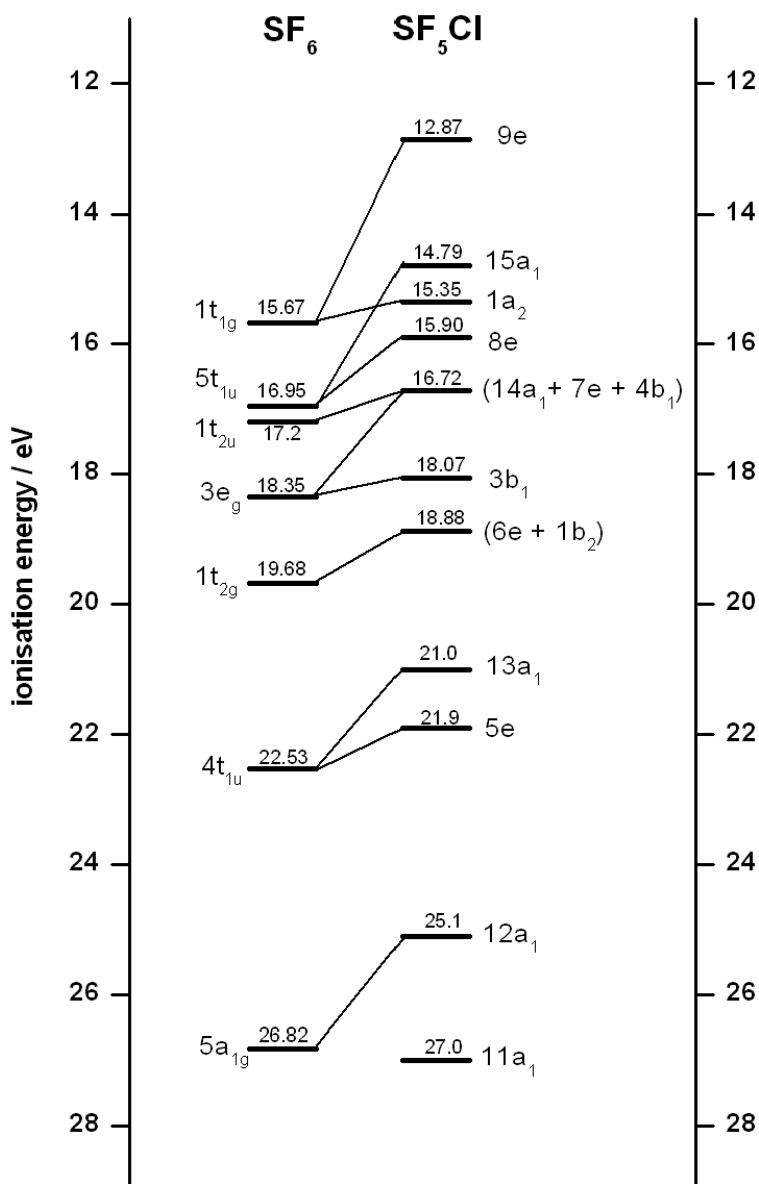
length, 0.157 nm, than the S–F axial bond, 0.159 nm, while that of S–Cl is significantly longer, 0.204 nm. Perhaps surprisingly, there are no vacuum ultraviolet photoabsorption spectra of any kind, either below or above the energy of the LiF cutoff (11.8 eV), reported in the literature.

It is the electron scavenging properties of SF<sub>6</sub> which make it such an important gas, and hence several groups have investigated electron attachment to SF<sub>5</sub>Cl.<sup>97,150-152</sup> There have been two measurements of the thermal electron attachment rate coefficient for SF<sub>5</sub>Cl are  $(4.8 \pm 1.2) \times 10^{-8} \text{ cm}^3 \text{ s}^{-1}$  by Van Doren *et al.*<sup>152</sup> and  $(2.0 \pm 0.3) \times 10^{-8} \text{ cm}^3 \text{ s}^{-1}$  by Mayhew *et al.*<sup>97</sup> In comparison, the generally accepted values for SF<sub>6</sub> and SF<sub>5</sub>CF<sub>3</sub> are  $(2.38 \pm 0.15) \times 10^{-7} \text{ cm}^3 \text{ s}^{-1}$ , and  $(8.0 \pm 0.3) \times 10^{-8} \text{ cm}^3 \text{ s}^{-1}$ , respectively.<sup>97</sup> Electron attachment to SF<sub>6</sub> is predominantly non-dissociative, whereas SF<sub>5</sub>CF<sub>3</sub> and SF<sub>5</sub>Cl attach electrons *via* dissociative processes: SF<sub>5</sub><sup>−</sup> is the major anion product in both instances.

Information on the valence electronic structure of SF<sub>5</sub>Cl is limited. Photoelectron spectra reported by DeKock *et al.*<sup>153</sup> followed up with calculations by Klyagina *et al.*<sup>154</sup> provided the first ordering for the molecular orbital (MO) configuration of SF<sub>5</sub>Cl. A more recently recorded threshold photoelectron spectrum, using synchrotron radiation, has confirmed the experimental work by DeKock in the 12 to 20 eV range.<sup>155</sup> This publication also reports results from a calculation which supports the MO assignments (to the experimentally observed bands) made by Klyagina *et al.* Figure 8.A.(i) summarises the combined findings of these three investigations and correlates the MOs for SF<sub>5</sub>Cl, of C<sub>4v</sub> symmetry, with those of SF<sub>6</sub>, of O<sub>h</sub> symmetry. While the ordering of the valence MOs in Figure 8.A.(i) for SF<sub>6</sub> is well known,<sup>106,156</sup> it is noted that the ordering and assignments given for SF<sub>5</sub>Cl is based on limited evidence.

The sample of SF<sub>5</sub>Cl used in this experiment was obtained from *Apollo Scientific* with a quoted purity of 97 %. Impurities of SF<sub>4</sub>, FCl and Cl<sub>2</sub> have been noted in previous studies using SF<sub>5</sub>Cl samples, and small amounts of SF<sub>x</sub>O<sub>y</sub> species have also been detected – identified as products from the hydrolysis of SF<sub>4</sub>.<sup>151,155</sup> There is no way of eliminating any potential contributions from these impurities to the anion spectra reported here.

**Figure 8.A.(i).** Valence electronic molecular orbitals assigned to energy maxima of features (indicated by solid lines with numeric values, in eV) observed in experimental photoelectron spectra for SF<sub>6</sub><sup>156</sup> and SF<sub>5</sub>Cl.<sup>153</sup> Following increasing ionisation energy the ordering goes from top to bottom, and where applicable, from left to right. Orbitals in parenthesis are thought to lie close in energy but have not been individually resolved in experimental spectra.

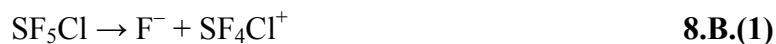


The anions F<sup>-</sup>, SF<sub>5</sub><sup>-</sup> and Cl<sup>-</sup> were detected following VUV photoexcitation of SF<sub>5</sub>Cl. The F<sup>-</sup> signal was by far the strongest of the three, whilst the other two anions were only just detected above the sensitivity limit of the apparatus.

### 8.B. F<sup>-</sup> from SF<sub>5</sub>Cl

The cross section for F<sup>-</sup> formation is shown in Figure 8.B.(i) over the range 12 to 30 eV. The F<sup>-</sup> signal was shown to increase linearly with increasing SF<sub>5</sub>Cl gas pressure, thus indicating it is formed *via* unimolecular ion-pair dissociation. The experimentally determined onset for F<sup>-</sup> production is  $12.7 \pm 0.2$  eV [Figure 8.B.(i), spectra (a) and (b)]. It is noteworthy that this value lies *above* the adiabatic ionisation energy for SF<sub>5</sub>Cl, 12.3 eV.<sup>153,155</sup> The onset is gradual and the cross section increases at a steady gradient up to about 13.6 eV. From this point the gradient appears to increase, leading to the cross section maximum of  $6.1 \times 10^{-20}$  cm<sup>2</sup> at 14.06 eV [Figure 8.B.(i), spectrum (b)].

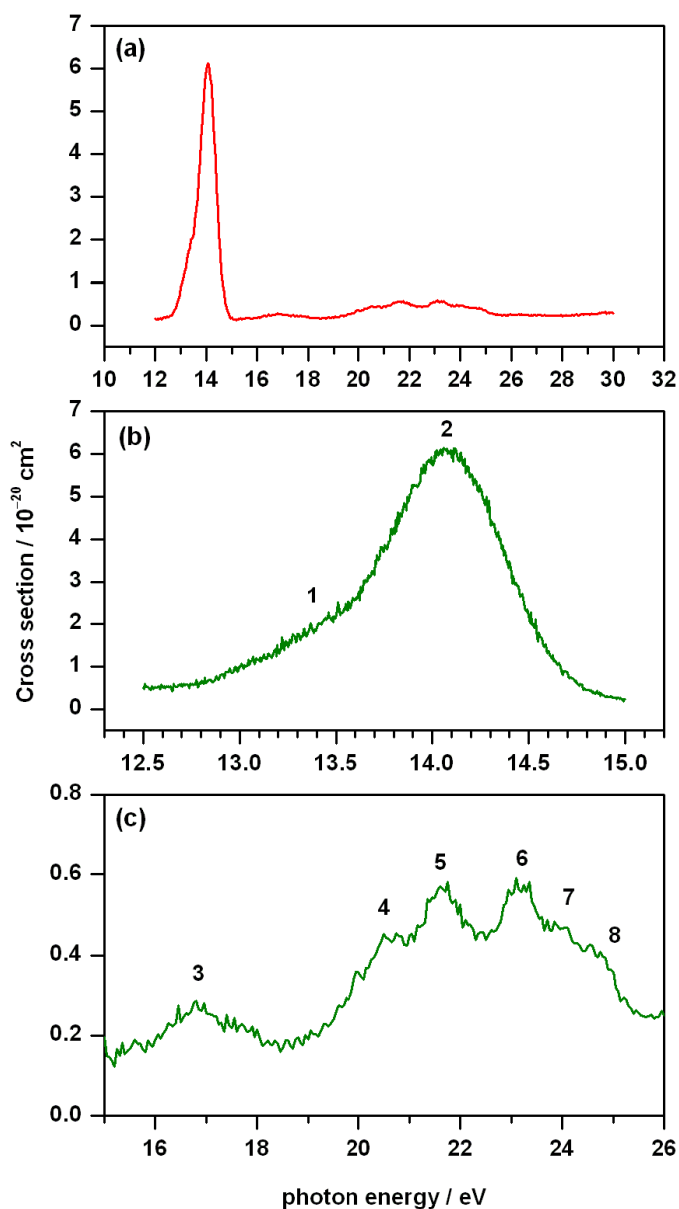
The ‘shoulder’, from onset at 12.7 eV to the point of change in gradient at 13.6 eV [labelled ‘1’ in Figure 8.B.(i), spectrum (b)] may arise from one or more of the following three ion-pair dissociation reactions:



There is uncertainty in the enthalpy of formation for SF<sub>4</sub>Cl<sup>+</sup>: the value used is +327 kJ mol<sup>-1</sup> which represents an *upper limit* determined from the appearance energy of SF<sub>4</sub>Cl<sup>+</sup> ions

following the dissociative photoionisation of SF<sub>5</sub>Cl.<sup>155</sup> The corresponding upper limit for the enthalpy change of reaction 8.B.(1) is  $\leq 11.6$  eV, whilst the enthalpy change for reaction 8.B.(2) is 11.4 eV.

**Figure 8.B.(i).** Cross section for F<sup>-</sup> formation from SF<sub>5</sub>Cl; (a) from 12 to 30 eV recorded with a step size of 0.05 eV and a wavelength resolution of 6 Å, (b) from 12.5 to 15.0 eV recorded with a step size of 0.005 eV and a wavelength resolution of 1.2 Å, and (c) a blow-up of spectrum (a) between 15 and 26 eV. All of the observable features in the F<sup>-</sup> cross section are labelled 1-8 in spectra (b) and (c) and are referred to in the text.



The enthalpy change for reaction 8.B.(3) is also expected to be less than the appearance energy of F<sup>-</sup> ions of 12.7 eV, but the value for  $\Delta_f H^\circ_{298}$  (SF<sub>3</sub>Cl<sup>+</sup>) is not known. It is worth

noting that the SF<sub>3</sub>Cl<sup>+</sup> species has *not* been observed in photon excitation or electron impact excitation experiments,<sup>155</sup> casting doubt over the production of F<sup>-</sup> ions from reaction 8.B.(3).

The feature in the F<sup>-</sup> ion yield between 13.6 and 14.8 eV is labelled '2' in Figure 8.B.(i), spectrum (b). The increase in gradient of the cross section at 13.6 eV, giving rise to feature 2, correlates to the thermochemical onset of 13.5 eV for the dissociation reaction shown in 8.B.(4).



This evidence suggests that the most significant contribution to the F<sup>-</sup> cross section at 14.06 eV is from the F<sup>-</sup>/SF<sub>4</sub><sup>+</sup> ion-pair process in which the S-Cl bond is also broken, and not from dissociation reactions 8.B.(1) to 8.B.(3).

It is difficult to assign features in ion-pair spectra to specific dissociation reactions with any confidence. This is particularly true at higher photon energies because the number of accessible ion-pair reaction products increases. Some examples of the many reactions which may be occurring at photon energies > 14 eV [giving rise to features 3-8 shown in Figure 8.B.(i), spectrum (c)] are listed below:





Feature 1 in the F<sup>-</sup> ion yield exhibits characteristics often associated with *direct* ion-pair formation; the onset is gradual and the resulting feature is broad and structureless. However, it is not possible to rule out an *indirect* process, identifying feature 1 as a Rydberg state. There is no identifiable maximum to feature 1 – it appears in the cross section as a shoulder – and therefore no attempt is made to assign it using the Rydberg formula. Features 2-8 in Figure 8.B.(i) have been assigned and the results are shown in Table 8.B.(I). In producing this table it is assumed, in most cases, that the given Rydberg state converges towards the excited state of SF<sub>5</sub>Cl<sup>+</sup> closest in energy to that of the feature. For example, it is assumed that feature 2 at 14.06 eV converges to SF<sub>5</sub>Cl<sup>+</sup> ( $\tilde{A} \ ^2A_1$ ) at 14.79 eV and not to SF<sub>5</sub>Cl<sup>+</sup> ( $\tilde{B} \ ^2A_2$ ) at 15.35 eV. However, this assumption is not made for feature 4 and two potential assignments have been given.

The cross section for F<sup>-</sup> formation at its maximum point, at feature 2, is  $6.1 \times 10^{-20} \text{ cm}^2$ . Features 3 to 8 are much weaker in comparison and the cross section is approximately an order of magnitude smaller; the cross section at 23.2 eV, corresponding to feature 6, is  $5.9 \times 10^{-21} \text{ cm}^2$ . This may be due to the nature of the Rydberg state assigned to feature 2. Gaussian 03 calculations have shown the first excited state of SF<sub>5</sub>Cl<sup>+</sup> involves the removal of an



electron from the 15a<sub>1</sub> molecular orbital which has both S–F<sub>eq</sub> and S–Cl bonding character.<sup>155,157</sup> The Rydberg state represented by feature 2 is thought to converge on the first excited state of SF<sub>5</sub>Cl<sup>+</sup> and is identified to come from the dissociation reaction shown in 8.B.(4) where a fluorine anion and a chlorine atom are both cleaved from the molecule.

**Table 8.B.(I).** Rydberg assignments to features observed in the F<sup>-</sup> ion yield recorded following the photoexcitation of SF<sub>5</sub>Cl.

Feature <sup>a</sup>	E / eV <sup>b</sup>	IE <sup>c</sup>	δ <sup>d</sup>	assignment <sup>e</sup>
2	14.06	14.79 ( $\tilde{A}^2A_1$ )	1.68	6p <sup>1</sup> A <sub>1</sub>
3	16.80	18.07 ( $\tilde{G}^2A_1$ )	1.73	5p <sup>1</sup> A <sub>1</sub>
4	20.65	21.0 ( $\tilde{J}^2A_1$ ) 21.9 ( $\tilde{K}^2E$ )	1.80 1.70	8p <sup>1</sup> A <sub>1</sub> 5p <sup>1</sup> E
5	21.65	21.9 ( $\tilde{K}^2E$ )	1.62	9p <sup>1</sup> E
6	23.20	25.1 ( $\tilde{L}^2A_1$ )	1.33	4p <sup>1</sup> A <sub>1</sub>
7	23.95	25.1 ( $\tilde{L}^2A_1$ )	1.56	5p <sup>1</sup> A <sub>1</sub>
8	24.60	25.1 ( $\tilde{L}^2A_1$ )	1.78	7p <sup>1</sup> A <sub>1</sub>

<sup>a</sup> The feature in the F<sup>-</sup> ion yield as labelled in Figure 8.B.(i).

<sup>b</sup> The photon energy of the feature identified from the spectra in Figure 8.B.(i). The uncertainty in these values is estimated to be ± 0.01 eV for feature 2 and ± 0.1 eV for features 3-8.

<sup>c</sup> The electronic state of SF<sub>5</sub>Cl<sup>+</sup> to which the assigned Rydberg state converges. Vertical ionisation energy values are taken from the work by DeKock *et al.*<sup>153</sup>

<sup>d</sup> Value of the quantum defect calculated from the Rydberg formula.

<sup>e</sup> Rydberg orbital assignment.

### 8.C. Cl<sup>-</sup> from SF<sub>5</sub>Cl

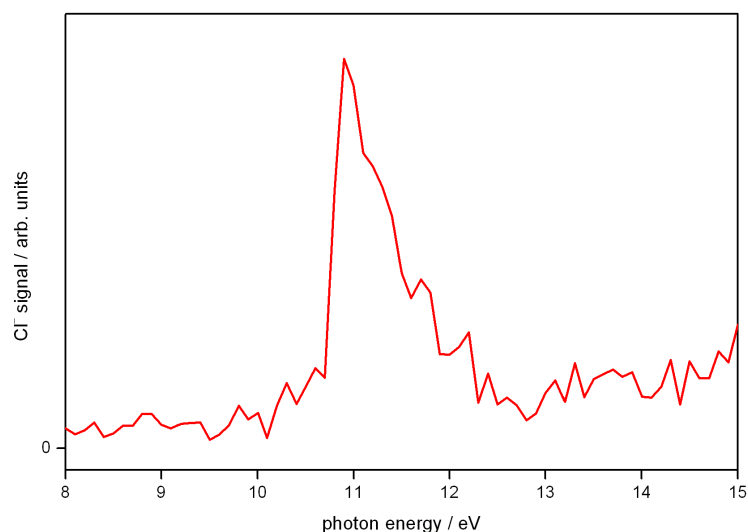
Cl<sup>-</sup> anions were observed following the VUV photoexcitation of SF<sub>5</sub>Cl, but the signal was very weak. Only one peak was detected in the range 8-35 eV, shown in Figure 8.C.(i). This feature was reproducible when scanning over the same energy region with a LiF window in place and so it is not an artefact arising from higher-order radiation. The appearance energy for Cl<sup>-</sup> anions is 10.6 ± 0.2 eV and the maximum of the resulting single peak is 10.9 eV.

Now, these energies lie *below* the adiabatic ionisation energy of SF<sub>5</sub>Cl, 12.3 eV;<sup>153,155</sup> therefore, Cl<sup>-</sup> can only form from an ion-pair dissociation. The only energetically accessible ion-pair dissociation reaction at this energy is:



The experimental onset therefore occurs 1.9 eV above the thermochemical threshold. This feature may be assigned as the initial transition from the highest occupied molecular orbital to an excited Rydberg state,  $9e \rightarrow 4p$ , converging on SF<sub>5</sub>Cl<sup>+</sup> ( $\tilde{X}^2E$ ) which then predissociates into the Cl<sup>-</sup>/SF<sub>5</sub><sup>+</sup> ion-pair state. The spectrum in Figure 8.C.(i) has not been put onto an absolute scale because the signal detected was so weak.

**Figure 8.C.(i).** The observation of Cl<sup>-</sup> anions following the photoexcitation of SF<sub>5</sub>Cl in the range 8 to 15 eV. The spectrum was recorded with a step size of 0.1 eV and a wavelength resolution of 6 Å.



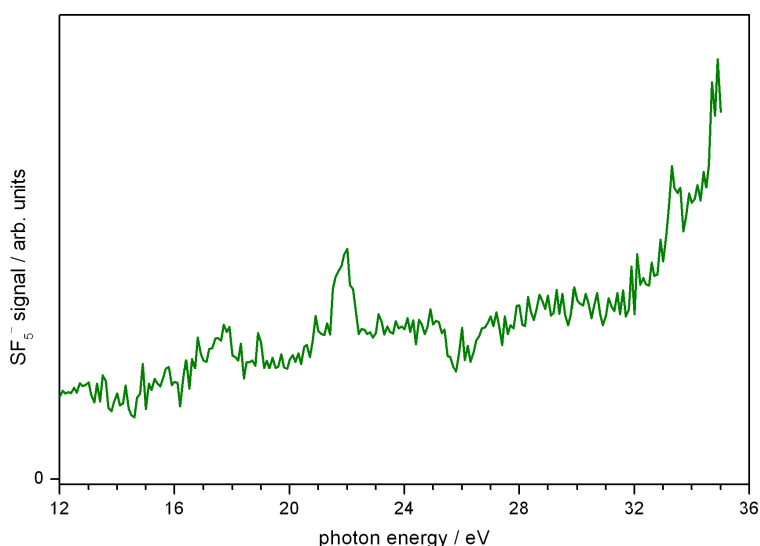
### 8.D. SF<sub>5</sub><sup>−</sup> from SF<sub>5</sub>Cl

SF<sub>5</sub><sup>−</sup> anions were also detected from SF<sub>5</sub>Cl. A spectrum was recorded in the range 12 to 35 eV which is presented in Figure 8.D.(i). The SF<sub>5</sub><sup>−</sup> signal was very weak and the spectrum is noisy as a result. There is only one distinct feature in the spectrum, at 22.0 eV, and when the excitation source was fixed at this energy the SF<sub>5</sub><sup>−</sup> signal was shown to increase *non-linearly* with increasing SF<sub>5</sub>Cl gas pressure. It is concluded, therefore, that the SF<sub>5</sub><sup>−</sup> anions are produced by the dissociative electron attachment process outlined below, where photoionisation provides the source of low-energy electrons:



It is noted that this anion is the dominant species from studies of thermal electron attachment to SF<sub>5</sub>Cl.<sup>97</sup>

**Figure 8.D.(i).** SF<sub>5</sub><sup>−</sup> ion yield recorded following the photoexcitation of SF<sub>5</sub>Cl in the range 12 to 35 eV. The spectrum was recorded with a step size of 0.1 eV and a wavelength resolution of 6 Å



As discussed in Section 8.A the thermal electron attachment rate coefficient for SF<sub>5</sub>Cl is in the region of  $(2\text{--}5) \times 10^{-8} \text{ cm}^3 \text{ s}^{-1}$ . This value is of a similar magnitude to that of other

molecules such as SF<sub>5</sub>CF<sub>3</sub> ( $k_a = 8.0 \times 10^{-8} \text{ cm}^3 \text{ s}^{-1}$ , see Chapter 6) and CF<sub>3</sub>Br ( $k_a = 1.4 \times 10^{-8} \text{ cm}^3 \text{ s}^{-1}$ , see Chapter 7). In the photon experiments reported in this thesis, the anions SF<sub>5</sub><sup>−</sup> and Br<sup>−</sup> from SF<sub>5</sub>CF<sub>3</sub> and CF<sub>3</sub>Br, respectively, are observed and identified as products from electron attachment reactions rather than from ion-pair dissociation. Thus, SF<sub>5</sub>Cl is following the same pattern. It is predicted that an anion spectrum resulting from an electron attachment process will mimic, at least to some extent, a threshold photoelectron spectrum. The feature in Figure 8.D.(i) at 22.0 eV matches the vertical ionisation energy for the band observed from photoelectron spectroscopy at 21.9 eV [see Figure 8.A.(i)]. This is, however, the *only* such similarity between the two different types of spectra and the reasons for this is not known.

### 8.E. Conclusions

The anions F<sup>−</sup>, Cl<sup>−</sup>, and SF<sub>5</sub><sup>−</sup> have been observed following the VUV photoexcitation of SF<sub>5</sub>Cl. The F<sup>−</sup> and Cl<sup>−</sup> anions arise from ion-pair dissociation but SF<sub>5</sub><sup>−</sup> is produced from dissociative electron attachment. Only the production of F<sup>−</sup> can be put onto an absolute cross section scale, but the quantum yield for its production cannot be determined since photoabsorption cross section data are not available. Indeed, the analysis of the results is limited by the lack of other complimentary spectroscopic investigations, *e.g.* fluorescence excitation as well as photoabsorption spectra.

It is an apparent coincidence that the *AE* for F<sup>−</sup> from both SF<sub>5</sub>Cl and SF<sub>6</sub> takes the same value,  $12.7 \pm 0.2 \text{ eV}$  [Table 8.E.(I)]: there is no reasonable explanation for their equality. It is the relative position of the *AE* to the adiabatic *IE* of the parent molecule which is more interesting. The most significant features in the F<sup>−</sup> spectrum from SF<sub>6</sub> appear below the *IE* [Figure 6.B.(i)], yet for SF<sub>5</sub>Cl the *AE* (F<sup>−</sup>) exceeds the *IE*. In fact, the same comment is made

when comparing F<sup>-</sup> from CF<sub>4</sub> [Figure 6.C.(i)] with F<sup>-</sup> from CF<sub>3</sub>Cl [Figure 7.C.(i)]: for CF<sub>4</sub> the  $AE(F^-) < IE$ , for CF<sub>3</sub>Cl the  $AE(F^-) > IE$  [Table 8.E.(I)].

**Table 8.E.(I).** Comparisons of data obtained for the ion-pair formation of F<sup>-</sup> from SF<sub>5</sub>Cl, SF<sub>6</sub> and SF<sub>5</sub>CF<sub>3</sub>. The separate comparison of CF<sub>3</sub>Cl vs CF<sub>4</sub> is also included. The complete data for SF<sub>6</sub>, SF<sub>5</sub>CF<sub>3</sub>, and CF<sub>4</sub> are presented and discussed in Chapter 6, and those for CF<sub>3</sub>Cl in Chapter 7.

Molecule	$IE^a$ / eV	$AE(F^-)^b$ / eV	Reaction at $AE^c$	$E(\sigma_{max})^d$ / eV	Reaction at $\sigma_{max}^c$
SF <sub>5</sub> Cl	12.3	$12.7 \pm 0.2$	not known	14.06	SF <sub>5</sub> Cl → F <sup>-</sup> + SF <sub>4</sub> <sup>+</sup> + Cl
SF <sub>6</sub>	15.1	$12.7 \pm 0.2$	SF <sub>6</sub> → F <sup>-</sup> + SF <sub>5</sub> <sup>+</sup>	14.2	SF <sub>6</sub> → F <sup>-</sup> + SF <sub>5</sub> <sup>+</sup>
SF <sub>5</sub> CF <sub>3</sub>	12.9	$11.05 \pm 0.05$	SF <sub>5</sub> CF <sub>3</sub> → F <sup>-</sup> + CF <sub>3</sub> <sup>+</sup> + SF <sub>4</sub>	16.9	not known
CF <sub>3</sub> Cl	12.4	$16.0 \pm 0.2$	CF <sub>3</sub> Cl → F <sup>-</sup> + CF <sub>2</sub> <sup>+</sup> + Cl	21.0	not known
CF <sub>4</sub>	15.4	$13.0 \pm 0.2$	CF <sub>4</sub> → F <sup>-</sup> + CF <sub>3</sub> <sup>+</sup>	14.0	CF <sub>4</sub> → F <sup>-</sup> + CF <sub>3</sub> <sup>+</sup>

<sup>a</sup> Adiabatic ionisation energy for SF<sub>5</sub>Cl,<sup>153</sup> SF<sub>6</sub>,<sup>106</sup> SF<sub>5</sub>CF<sub>3</sub>,<sup>99</sup> CF<sub>3</sub>Cl,<sup>125</sup> and CF<sub>4</sub>.<sup>104</sup>  
<sup>b</sup> Experimentally observed appearance energy for F<sup>-</sup> anions.  
<sup>c</sup> The ion-pair dissociation reactions are assigned by comparing calculated reaction enthalpies with onsets to features observed in the anion spectra.  
<sup>d</sup> The energy position of the maximum point in the cross section.

SF<sub>6</sub> and CF<sub>4</sub> follow the ‘expected’ trend that the probability for an excited electronic state to predissociate into ion pairs is greater in the absence of a competing autoionisation process. It is possible, therefore, that the change in symmetry on substituting a F for a Cl atom (*e.g.* SF<sub>6</sub> → SF<sub>5</sub>Cl) suppresses the formation of ion pairs below the ionisation energy – or rather *increases* the probability of a competing process, such as neutral dissociation (*e.g.* SF<sub>5</sub>Cl → SF<sub>5</sub> + Cl). With respect to SF<sub>5</sub>Cl this idea is only speculative because data from other VUV experiments, such as fluorescence excitation spectra let alone photoabsorption spectra, are not available. However, when comparing the data for ion-pair formation from CF<sub>3</sub>Cl with total photoabsorption and fluorescence excitation spectra, the evidence suggested that photoexcitation below the  $IE$  must almost exclusively result from neutral photodissociation<sup>116</sup> (also see Section 7.I).

The lack of ion-pair formation processes from SF<sub>5</sub>Cl producing Cl<sup>−</sup> anions cannot be explained. Indeed, perhaps the most interesting aspect of this work is the observation that the F<sup>−</sup> cross sections are orders of magnitude greater than the Cl<sup>−</sup> cross sections, yet the S–Cl bond is significantly weaker than the S–F bond; the bond dissociation energies are 2.5 and 3.7 eV, respectively (calculated from  $\Delta_f H^\circ_{298}$  values provided in Appendix I). These and other generic issues on ion-pair dissociation reactions are addressed in Chapter 9.

# Chapter 9:

## *Vacuum ultraviolet negative photoion spectroscopy of small polyatomic molecules*

### **9.A. Summary of results**

A total of 24 small polyatomic molecules have been studied by the Chemical Physics groups in Birmingham and Belfast from 2005-2008 using VUV negative photoion spectroscopy: the data for SF<sub>5</sub>CF<sub>3</sub>, SF<sub>6</sub> and CF<sub>4</sub> were published in 2008 in the *Journal of Chemical Physics*,<sup>86</sup> and updated here in Chapter 6; the data for CF<sub>3</sub>Cl, CF<sub>3</sub>Br and CF<sub>3</sub>I were published in 2009 in the *Journal of Chemical Physics*,<sup>116</sup> and are also presented here in Chapter 7; the data for SF<sub>5</sub>Cl were published in 2010 in the *Journal of Physical Chemistry A*,<sup>145</sup> and are also presented here in Chapter 8; the data for CH<sub>4</sub>, CH<sub>3</sub>F, CH<sub>3</sub>Cl and CH<sub>3</sub>Br were published in 2010 by Rogers *et al.*,<sup>45,46</sup> the data recorded for the remaining 13 molecules (C<sub>2</sub>H<sub>4</sub>, C<sub>2</sub>H<sub>6</sub>, C<sub>3</sub>H<sub>8</sub>, C<sub>2</sub>F<sub>4</sub>, C<sub>2</sub>F<sub>6</sub>, C<sub>3</sub>F<sub>8</sub>, CH<sub>2</sub>F<sub>2</sub>, CHF<sub>3</sub>, CH<sub>2</sub>Cl<sub>2</sub>, CHCl<sub>3</sub>, CCl<sub>4</sub>, CF<sub>2</sub>Cl<sub>2</sub>, CFCl<sub>3</sub>) are presented here in Appendix IV. Specific data for *all* of these molecules [such as anions observed, appearance energies (*AEs*), cross sections ( $\sigma$ ) and quantum yields ( $\Phi$ )] are compiled in Table 9.A.(I). This forms the most comprehensive collection of information about ion-pair formation from polyatomic molecules since the 1996 Berkowitz review.<sup>28</sup>

**Table 9.A.(I).** A summary of data collected for anion production following the VUV photoexcitation of twenty four gas-phase polyatomic molecules.

Molecule	$IE^a / \text{eV}$	Anion	$AE_{298}^b / \text{eV}$	Reaction at $AE^c$	$\Delta_e H_{298}^\circ / \text{eV}^d$	$\sigma_{\text{max}}^e / \text{cm}^2$	$E(\sigma_{\text{max}})^f / \text{eV}$	$\Phi(\sigma_{\text{max}})^g$
1	2	3	4	5	6	7	8	9
$\text{CH}_4^h$	12.61	$\text{H}^-$	$13.30 \pm 0.10$	$\text{CH}_4 \rightarrow \text{H}^- + \text{CH}_3^+$	13.7	$1.4 \times 10^{-22}$	20.6	$4.4 \times 10^{-6}$
$\text{C}_2\text{H}_4^i$	10.51	$\text{H}^-$	$13.06 \pm 0.10$	$\text{C}_2\text{H}_4 \rightarrow \text{H}^- + \text{C}_2\text{H}_3^+$	12.5	$8.3 \times 10^{-22}$	18.0	$1.4 \times 10^{-5}$
$\text{C}_2\text{H}_6^i$	11.52	$\text{H}^-$	$12.00 \pm 0.10$	$\text{C}_2\text{H}_6 \rightarrow \text{H}^- + \text{C}_2\text{H}_5^+$	11.9	$1.7 \times 10^{-21}$	19.3	$2.7 \times 10^{-5}$
$\text{C}_3\text{H}_8^i$	10.9	$\text{H}^-$	$13.2 \pm 0.2$	$\text{C}_3\text{H}_8 \rightarrow \text{H}^- + \text{C}_3\text{H}_7^+$	11.7	$3.3 \times 10^{-21}$	18.6	$3.3 \times 10^{-5}$
$\text{CF}_4^j$	15.4	$\text{F}^-$	$13.0 \pm 0.2$	$\text{CF}_4 \rightarrow \text{F}^- + \text{CF}_3^+$	11.3	$1.4 \times 10^{-21}$	14.0	$2.8 \times 10^{-5}$
		$\text{F}_2^-$	$20.1 \pm 0.2$	$\text{CF}_4 \rightarrow \text{F}_2^- + \text{CF}^+ + \text{F}$	19.3	$4.0 \times 10^{-23}$	21.6	$5.6 \times 10^{-7}$
$\text{C}_2\text{F}_4^i$	10.12	$\text{F}^-$	$13.17 \pm 0.05$	$\text{C}_2\text{F}_4 \rightarrow \text{F}^- + \text{C}_2\text{F}_3^+$	12.4	$1.7 \times 10^{-20}$	16.5	$_{-}^m$
		$\text{CF}^-$	$22.4 \pm 0.5$	$\text{C}_2\text{F}_4 \rightarrow \text{CF}^- + \text{CF}^+ + 2\text{F}$	19.7	$2.4 \times 10^{-22}$	27.5	$_{-}^m$
$\text{C}_2\text{F}_6^i$	13.4	$\text{F}^-$	$13.62 \pm 0.10$	$\text{C}_2\text{F}_6 \rightarrow \text{F}^- + \text{C}_2\text{F}_5^+$	11.5	$7.4 \times 10^{-21}$	14.7	$_{-}^n$
$\text{C}_3\text{F}_8^i$	13.0	$\text{F}^-$	$13.1 \pm 0.2$	$\text{C}_3\text{F}_8 \rightarrow \text{F}^- + \text{C}_3\text{F}_7^+$	12.2	$4.7 \times 10^{-21}$	23.4	$_{-}^m$
		$\text{CF}_2^-$	$20.4 \pm 0.2$	$_{-}^k$	-	$4.9 \times 10^{-22}$	21.8	$_{-}^m$
$\text{CH}_3\text{F}^L$	12.53	$\text{H}^-^p$	-	-	-	-	-	-
		$\text{F}^-$	$12.28 \pm 0.02$	$\text{CH}_3\text{F} \rightarrow \text{F}^- + \text{CH}_3^+$	11.2	$1.2 \times 10^{-19}$	13.4	$2.3 \times 10^{-3}$
		$\text{CF}^-$	$24.4 \pm 0.2$	$\text{CH}_3\text{F} \rightarrow \text{CF}^- + \text{H}^+ + 2\text{H}$	22.1	$4.2 \times 10^{-23}$	27.2	$1.5 \times 10^{-6}$
		$\text{CHF}^-$	$21.5 \pm 0.2$	$\text{CH}_3\text{F} \rightarrow \text{CHF}^- + \text{H}^+ + \text{H}$	21.7	$8.8 \times 10^{-23}$	22.4	$2.2 \times 10^{-6}$
$\text{CH}_2\text{F}_2^i$	12.729	$\text{CH}_2\text{F}^-$	$18.2 \pm 0.2$	$\text{CH}_3\text{F} \rightarrow \text{CH}_2\text{F}^- + \text{H}^+$	17.7	$4.1 \times 10^{-23}$	19.7	$8.9 \times 10^{-7}$
		$\text{H}^-^q$	$12.08 \pm 0.05^r$	$\text{CH}_2\text{F}_2 \rightarrow \text{H}^- + \text{CHF}_2^+$	$12.5^r$	-	-	-
		$\text{F}^-$	$11.86 \pm 0.05$	$\text{CH}_2\text{F}_2 \rightarrow \text{F}^- + \text{CH}_2\text{F}^+$	10.7	$6.6 \times 10^{-21}$	18.8	$1.4 \times 10^{-4}$
		$\text{F}_2^-$	$17.20 \pm 0.05$	$\text{CH}_2\text{F}_2 \rightarrow \text{F}_2^- + \text{CH}_2^+$	15.9	$3.3 \times 10^{-22}$	18.5	$6.9 \times 10^{-6}$
$\text{CHF}_3^i$	13.8	$\text{H}^-^q$	$12.82 \pm 0.05^r$	$\text{CHF}_3 \rightarrow \text{H}^- + \text{CF}_3^+$	$12.9^r$	-	-	-
		$\text{F}^-$	$\leq 12.4^s$	$\text{CHF}_3 \rightarrow \text{F}^- + \text{CHF}_2^+$	11.0	$4.5 \times 10^{-21}$	23.1	$8.2 \times 10^{-5}$
		$\text{CF}_3^-$	$16.6 \pm 0.2$	$\text{CHF}_3 \rightarrow \text{CF}_3^- + \text{H}^+$	16.5	$2.7 \times 10^{-20}$	18.0	$4.4 \times 10^{-4}$
$\text{CH}_3\text{Cl}^L$	11.29	$\text{H}^-^p$	-	-	-	-	-	-
		$\text{Cl}^-$	$10.04 \pm 0.02$	$\text{CH}_3\text{Cl} \rightarrow \text{Cl}^- + \text{CH}_3^+$	9.9	$1.2 \times 10^{-19}$	11.3	$2.3 \times 10^{-3}$
		$\text{CH}_2\text{Cl}^-$	$17.2 \pm 0.2$	$\text{CH}_3\text{Cl} \rightarrow \text{CH}_2\text{Cl}^- + \text{H}^+$	17.2	$7.6 \times 10^{-21}$	18.2	$1.0 \times 10^{-4}$
$\text{CH}_2\text{Cl}_2^i$	11.326	$\text{H}^-^q$	$11.5 \pm 0.2^r$	$\text{CH}_2\text{Cl}_2 \rightarrow \text{H}^- + \text{CHCl}_2^+$	$11.7^r$	-	-	-
		$\text{Cl}^-$	$9.31 \pm 0.05$	$\text{CH}_2\text{Cl}_2 \rightarrow \text{Cl}^- + \text{CH}_2\text{Cl}^+$	8.6	$6.6 \times 10^{-20}$	10.1	$1.0 \times 10^{-3}$
		$\text{Cl}_2^-$	$13.74 \pm 0.10$	$\text{CH}_2\text{Cl}_2 \rightarrow \text{Cl}_2^- + \text{CH}_2^+$	13.0	$1.4 \times 10^{-21}$	16.0	$1.5 \times 10^{-5}$
$\text{CHCl}_3^i$	11.30	$\text{H}^-^q$	$11.2 \pm 0.2$	$\text{CHCl}_3 \rightarrow \text{H}^- + \text{CCl}_3^+$	11.2	-	-	-
		$\text{Cl}^-$	$9.26 \pm 0.05$	$\text{CHCl}_3 \rightarrow \text{Cl}^- + \text{CHCl}_2^+$	7.9	$7.0 \times 10^{-21}$	20.3	$5.4 \times 10^{-5}$
		$\text{CH}^-$	$22.7 \pm 0.2$	$\text{CHCl}_3 \rightarrow \text{CH}^- + \text{Cl}^+ + 2\text{Cl}$	22.8	$3.7 \times 10^{-22}$	24.8	$5.7 \times 10^{-6}$
		$\text{CCl}^-$	$19.3 \pm 0.5$	$_{-}^T$	-	$5.7 \times 10^{-22}$	20.3	$4.4 \times 10^{-6}$
$\text{CCl}_4^i$	11.30	$\text{Cl}^-^u$	$11.35 \pm 0.05$	$[\text{CCl}_4 + \text{e}^- \rightarrow \text{CCl}_3 + \text{Cl}^-]$	-	-	-	-
		$\text{CCl}^-$	$21.2 \pm 0.2$	$_{-}^T$	-	$1.6 \times 10^{-21}$	23.8	$1.7 \times 10^{-5}$



Molecule	$IE^a / \text{eV}$	Anion	$AE_{298}^b / \text{eV}$	Reaction at $AE^c$	$\Delta_r H_{298}^\circ{}^d / \text{eV}$	$\sigma_{\text{max}}^e / \text{cm}^2$	$E(\sigma_{\text{max}})^f / \text{eV}$	$\Phi(\sigma_{\text{max}})^g$
1	2	3	4	5	6	7	8	9
$\text{CF}_3\text{Cl}^w$	12.4	$\text{F}^-$	$16.0 \pm 0.2$	$\text{CF}_3\text{Cl} \rightarrow \text{F}^- + \text{CF}_2^+ + \text{Cl}$	15.6	$1.5 \times 10^{-20}$	21.0	$1.8 \times 10^{-4}$
		$\text{Cl}^-$	$16.1 \pm 0.2$	$\text{CF}_3\text{Cl} \rightarrow \text{Cl}^- + \text{CF}_2^+ + \text{F}$	15.4	$2.3 \times 10^{-21}$	20.9	$2.9 \times 10^{-5}$
		$\text{F}_2^-$	$21 \pm 2$	$\text{CF}_3\text{Cl} \rightarrow \text{F}_2^- + \text{Cl}^+ + \text{CF}$	21.1	$6.8 \times 10^{-23}$	22.7	$8.5 \times 10^{-7}$
		$\text{FCI}^-$	$18 \pm 2$	${}_T$	-	$6.5 \times 10^{-23}$	20.8	$8.0 \times 10^{-7}$
		$\text{CF}^-$	$25.5 \pm 0.2$	${}_k$	-	$1.6 \times 10^{-22}$	27.3	${}_m$
		$\text{CF}_2^-$	$20.2 \pm 0.2$	$\text{CF}_3\text{Cl} \rightarrow \text{CF}_2^- + \text{Cl}^+ + \text{F}$	20.3	$1.5 \times 10^{-22}$	21.3	$1.8 \times 10^{-6}$
		$\text{CF}_3^-$	$15.5 \pm 0.2$	$\text{CF}_3\text{Cl} \rightarrow \text{CF}_3^- + \text{Cl}^+$	14.9	$2.8 \times 10^{-22}$	18.1	$3.5 \times 10^{-6}$
$\text{CF}_2\text{Cl}_2^i$	11.734	$\text{F}^-$	$12.2 \pm 0.1$	$\text{CF}_2\text{Cl}_2 \rightarrow \text{F}^- + \text{CFCl}_2^+$	9.8	$1.1 \times 10^{-20}$	19.1	$1.0 \times 10^{-4}$
		$\text{Cl}^-$	$10.35 \pm 0.1$	$\text{CF}_2\text{Cl}_2 \rightarrow \text{Cl}^- + \text{CF}_2\text{Cl}^+$	8.2	$1.3 \times 10^{-20}$	20.0	$1.2 \times 10^{-4}$
		$\text{CF}^-$	$23.5 \pm 0.5$	${}_k$	-	$2.2 \times 10^{-22}$	25.6	${}_m$
$\text{CFCl}_3^i$	11.53	$\text{F}^-$	$14.4 \pm 0.2$	$\text{CFCl}_3 \rightarrow \text{F}^- + \text{CCl}_2^+ + \text{Cl}$	13.7	$1.2 \times 10^{-21}$	18.3	$1.0 \times 10^{-5}$
		$\text{Cl}^-$	$11.54 \pm 0.10$	$[\text{CFCl}_3 + \text{e}^- \rightarrow \text{CFCl}_2 + \text{Cl}^-]$	-	-	-	-
$\text{CH}_3\text{Br}^L$	10.54	$\text{H}^-$	$12.1 \pm 0.2$	$\text{CH}_3\text{Br} \rightarrow \text{H}^- + \text{CH}_2\text{Br}^+$	11.6	-	-	-
		$\text{Br}^-$	$9.46 \pm 0.02$	$\text{CH}_3\text{Br} \rightarrow \text{Br}^- + \text{CH}_3^+$	9.5	$2.5 \times 10^{-20}$	10.0	$4.1 \times 10^{-4}$
		$\text{CHBr}^-$	$20 \pm 2$	$\text{CH}_3\text{Br} \rightarrow \text{CHBr}^- + \text{H}^+ + \text{H}$	20.9	$1.3 \times 10^{-22}$	22.4	$3.3 \times 10^{-6}$
		$\text{CH}_2\text{Br}^-$	$17.1 \pm 0.2$	$\text{CH}_3\text{Br} \rightarrow \text{CH}_2\text{Br}^- + \text{H}^+$	17.0	$5.6 \times 10^{-22}$	17.8	$8.1 \times 10^{-6}$
$\text{CF}_3\text{Br}^w$	11.5	$\text{F}^-$	$14.7 \pm 0.2$	$\text{CF}_3\text{Br} \rightarrow \text{F}^- + \text{CF}_2^+ + \text{Br}$	14.9	$9.7 \times 10^{-21}$	19.6	$1.2 \times 10^{-4}$
		$\text{Br}^-$	$15.1 \pm 0.2$	$[\text{CF}_3\text{Br} + \text{e}^- \rightarrow \text{CF}_3 + \text{Br}^-]$	-	-	-	-
		$\text{F}_2^-$	$19 \pm 0.2$	$\text{CF}_3\text{Br} \rightarrow \text{F}_2^- + \text{Br}^+ + \text{CF}$	19.2	$2.8 \times 10^{-22}$	20.4	$3.4 \times 10^{-6}$
		$\text{FBr}^-$	$18 \pm 2$	${}_T$	-	$5.5 \times 10^{-22}$	20.4	$6.6 \times 10^{-6}$
		$\text{CF}^-$	$23.6 \pm 0.2$	${}_k$	-	$3.4 \times 10^{-22}$	25.6	$5.2 \times 10^{-6}$
		$\text{CF}_2^-$	$18.2 \pm 0.2$	$\text{CF}_3\text{Br} \rightarrow \text{CF}_2^- + \text{Br}^+ + \text{F}$	18.5	$4.9 \times 10^{-22}$	19.5	$5.8 \times 10^{-6}$
		$\text{CF}_3^-$	$13.6 \pm 0.2$	$\text{CF}_3\text{Br} \rightarrow \text{CF}_3^- + \text{Br}^+$	13.1	$2.5 \times 10^{-22}$	14.8	$4.0 \times 10^{-6}$
$\text{CF}_3\text{I}^w$	10.37	$\text{F}^-$	$9.7 \pm 0.2$	$\text{CF}_3\text{I} \rightarrow \text{F}^- + \text{CF}_2\text{I}^+$	${}_T$	$1.1 \times 10^{-20}$	20.4	${}_m$
		$\text{I}^-$	$8.8 \pm 0.2$	$\text{CF}_3\text{I} \rightarrow \text{I}^- + \text{CF}_3^+$	8.3	-	-	${}_x$
		$\text{F}_2^-$	$17 \pm 2$	$\text{CF}_3\text{I} \rightarrow \text{F}_2^- + \text{I}^+ + \text{CF}$	17.2	$8.5 \times 10^{-23}$	20.1	${}_m$
		$\text{CF}^-$	$21.6 \pm 0.2$	${}_k$	-	$1.1 \times 10^{-22}$	23.6	${}_m$
		$\text{CF}_2^-$	$16.0 \pm 0.2$	$\text{CF}_3\text{I} \rightarrow \text{CF}_2^- + \text{I}^+ + \text{F}$	16.4	$4.6 \times 10^{-22}$	16.8	${}_m$
		$\text{CF}_3^-$	$11.0 \pm 0.2$	$\text{CF}_3\text{I} \rightarrow \text{CF}_3^- + \text{I}^+$	11.0	$5.7 \times 10^{-22}$	12.7	${}_m$
$\text{SF}_6^j$	15.116	$\text{F}^-$	$12.7 \pm 0.2$	$\text{SF}_6 \rightarrow \text{F}^- + \text{SF}_5^+$	10.4	$7.1 \times 10^{-21}$	14.2	$2.4 \times 10^{-4}$
		$\text{F}_2^-$	$16.3 \pm 0.2$	$\text{SF}_6 \rightarrow \text{F}_2^- + \text{SF}_3^+ + \text{F}$	14.1	$1.4 \times 10^{-22}$	18.3	$1.9 \times 10^{-6}$
		$\text{SF}_5^-$	$15.1 \pm 0.2$	$[\text{SF}_6 + \text{e}^- \rightarrow \text{F} + \text{SF}_5^-]$	-	-	-	-
		$\text{SF}_6^-$	$15.1 \pm 0.2$	$[\text{SF}_6 + \text{e}^- \rightarrow \text{SF}_6^-]$	-	-	-	-
$\text{SF}_5\text{Cl}^y$	12.3	$\text{F}^-$	$12.7 \pm 0.2$	${}_k$	-	$6.1 \times 10^{-20}$	14.1	${}_m$
		$\text{Cl}^-$	$10.6 \pm 0.2$	$\text{SF}_5\text{Cl} \rightarrow \text{Cl}^- + \text{SF}_5^+$	8.7	-	10.9	-
		$\text{SF}_5^-$	-	$[\text{SF}_5\text{Cl} + \text{e}^- \rightarrow \text{Cl} + \text{SF}_5^-]$	-	-	-	-
$\text{SF}_5\text{CF}_3^j$	12.9	$\text{F}^-$	$11.05 \pm 0.2$	$\text{SF}_5\text{CF}_3 \rightarrow \text{F}^- + \text{CF}_3^+ + \text{SF}_4$	11.5	$3.4 \times 10^{-20}$	16.9	$3.4 \times 10^{-4}$
		$\text{F}_2^-$	$16.1 \pm 0.2$	$\text{SF}_5\text{CF}_3 \rightarrow \text{F}_2^- + \text{CF}_3^+ + \text{SF}_3$	14.3	$1.2 \times 10^{-21}$	17.9	$1.1 \times 10^{-5}$
		$\text{SF}^-$	$24.0 \pm 0.2$	$\text{SF}_5\text{CF}_3 \rightarrow \text{SF}^- + \text{CF}_3^+ + 4\text{F}$	23.0	$2.8 \times 10^{-22}$	28.8	$2.4 \times 10^{-6}$
		$\text{SF}_2^-$	$20.2 \pm 0.2$	$\text{SF}_5\text{CF}_3 \rightarrow \text{SF}_2^- + \text{CF}_3^+ + 3\text{F}$	20.0	$3.9 \times 10^{-22}$	24.2	$2.5 \times 10^{-6}$
		$\text{SF}_3^-$	$15.4 \pm 0.2$	$\text{SF}_5\text{CF}_3 \rightarrow \text{SF}_3^- + \text{CF}_3^+ + 2\text{F}$	16.0	$1.0 \times 10^{-20}$	17.6	$1.0 \times 10^{-4}$
		$\text{SF}_4^-$	$13.0 \pm 0.2$	$\text{SF}_5\text{CF}_3 \rightarrow \text{SF}_4^- + \text{CF}_3^+ + \text{F}$	13.4	$1.3 \times 10^{-20}$	14.1	$1.7 \times 10^{-4}$
		$\text{SF}_5^-$	$13.0 \pm 0.2$	$[\text{SF}_5\text{CF}_3 + \text{e}^- \rightarrow \text{CF}_3 + \text{SF}_5^-]$	-	-	-	-

- <sup>a</sup> Adiabatic ionisation energy (*IE*) values are taken from the following sources: CH<sub>4</sub>,<sup>158,159</sup> C<sub>2</sub>H<sub>4</sub>,<sup>54</sup> C<sub>2</sub>H<sub>6</sub>,<sup>160</sup> C<sub>3</sub>H<sub>8</sub>,<sup>161</sup> CF<sub>4</sub>,<sup>104</sup> C<sub>2</sub>F<sub>4</sub>,<sup>59</sup> C<sub>2</sub>F<sub>6</sub>,<sup>162</sup> C<sub>3</sub>F<sub>8</sub>,<sup>162</sup> CH<sub>3</sub>F,<sup>163</sup> CH<sub>2</sub>F<sub>2</sub>,<sup>164</sup> CHF<sub>3</sub>,<sup>165</sup> CH<sub>3</sub>Cl,<sup>163</sup> CH<sub>2</sub>Cl<sub>2</sub>,<sup>166</sup> CHCl<sub>3</sub>,<sup>167</sup> CCl<sub>4</sub>,<sup>168</sup> CF<sub>3</sub>Cl,<sup>125</sup> CF<sub>2</sub>Cl<sub>2</sub>,<sup>164</sup> CFCl<sub>3</sub>,<sup>167</sup> CH<sub>3</sub>Br,<sup>169</sup> CF<sub>3</sub>Br,<sup>125</sup> CF<sub>3</sub>I,<sup>137</sup> SF<sub>6</sub>,<sup>106</sup> SF<sub>5</sub>Cl,<sup>153,155</sup> SF<sub>5</sub>CF<sub>3</sub>.<sup>99</sup>
- <sup>b</sup> Experimentally determined appearance energy (*AE*).
- <sup>c</sup> Reaction occurring at onset.
- <sup>d</sup> The enthalpy change at 298 K for the reaction in column 5, calculated from enthalpies of formation (listed in Appendix I).
- <sup>e</sup> Absolute value for the ion-pair formation cross section ( $\sigma$ ) at its maximum point.
- <sup>f</sup> Energy (*E*) at which the ion-pair formation cross section reaches its maximum point.
- <sup>g</sup> Quantum yield ( $\Phi$ ) for ion-pair formation at *E* ( $\sigma_{\max}$ ). The ion-pair cross section is divided by the total photoabsorption cross section ( $\sigma_{\text{abs}}$ ), from the following sources (for molecules not listed here see references in column 1): C<sub>2</sub>H<sub>4</sub>,<sup>170</sup> C<sub>2</sub>H<sub>6</sub>,<sup>171</sup> C<sub>3</sub>H<sub>8</sub>,<sup>171</sup> CH<sub>2</sub>F<sub>2</sub>,<sup>172</sup> CHF<sub>3</sub>,<sup>133</sup> CH<sub>2</sub>Cl<sub>2</sub>,<sup>173</sup> CHCl<sub>3</sub>,<sup>174</sup> CCl<sub>4</sub>,<sup>133</sup> CF<sub>2</sub>Cl<sub>2</sub>,<sup>172</sup> CFCl<sub>3</sub>,<sup>174</sup>
- <sup>h</sup> Data in columns 3-9 taken, with permission, from the work of Rogers *et al.*<sup>46</sup>
- <sup>i</sup> Preliminary results for this molecule are presented in Appendix IV, from which the anion data (columns 3, 4, 7 and 8) are taken.
- <sup>j</sup> Data in columns 3-9 for CF<sub>4</sub>, SF<sub>6</sub> and SF<sub>5</sub>CF<sub>3</sub> are taken from Chapter 6.
- <sup>k</sup> The reaction occurring at the *AE* for this anion is not known due to the many different thermochemically available dissociation channels.
- <sup>l</sup> Data in columns 3-9 taken, with permission, from the work of Rogers *et al.*<sup>45</sup>
- <sup>m</sup> Total photoabsorption cross section is absent in the literature *or* not available over the required energy range, thus the ion-pair quantum yield cannot be calculated.
- <sup>n</sup> Total photoabsorption cross section for C<sub>2</sub>F<sub>6</sub> is reported from 16-62 eV and so  $\Phi(\sigma_{\max})$ , at 14.7 eV, cannot be calculated. However,  $\Phi_{17.7 \text{ eV}}$  for F<sup>-</sup> formation from C<sub>2</sub>F<sub>6</sub> is  $4.8 \times 10^{-5}$  [ $\sigma_{\text{abs}}(\text{C}_2\text{F}_6, 17.7 \text{ eV}) = 7.3 \times 10^{-17} \text{ cm}^2$ ].<sup>112</sup>
- <sup>p</sup> H<sup>-</sup> detected at *m/z* 1, but signal was significantly weaker than the dominant anion. The H<sup>-</sup> ion yield matches that of the dominant anion, presumably because of the *zero blast* effect<sup>44</sup> in the quadrupole mass spectrometer, and therefore cannot be trusted.
- <sup>q</sup> H<sup>-</sup> detected at *m/z* 1, and the signal was of similar intensity to that of other anions. The H<sup>-</sup> ion yield is unique, but may contain contributions from other anions due to the *zero blast* effect.<sup>44</sup> As a result, only limited information is presented here. For example, absolute cross sections cannot be determined for H<sup>-</sup> ion-pair formation unless it is the only detected anion.<sup>45</sup>
- <sup>r</sup> The fact that  $\Delta_r H^\circ_{298}$  exceeds the *AE*<sub>298</sub> may result from other anions being detected due to the *zero blast* effect (see notes <sup>p</sup> and <sup>q</sup>), giving an *AE* lower than it should be. Alternatively, thermal effects (*i.e.* hotbands) could cause the *AE*<sub>298</sub> to precede  $\Delta_r H^\circ_{298}$ ; the *AE*<sub>298</sub> for H<sup>-</sup> from CH<sub>4</sub>, where the *zero blast* effect from other anions does not affect the spectrum, precedes the calculated  $\Delta_r H^\circ_{298}$  value by 0.4 eV.<sup>46</sup>
- <sup>s</sup> Uncertainty in the *AE*<sub>298</sub> arises from contributions to the cross section from absorptions of second order radiation over the energy range of interest (see Appendix IV).
- <sup>t</sup>  $\Delta_r H^\circ_{298}$  is not known for CCl<sub>3</sub><sup>-</sup>, FCl<sub>2</sub><sup>-</sup>, FBr<sup>-</sup> and CF<sub>2</sub>I<sup>-</sup>.
- <sup>u</sup> Anion signal was shown to increase non-linearly with increasing parent gas pressure and electron attachment to the parent molecule is well documented; anion production is dominated by a two-step electron attachment process where photoionisation provides the source of electrons. The thermal electron attachment rate coefficients, *k<sub>a</sub>*, in units of cm<sup>3</sup> s<sup>-1</sup> are: CCl<sub>4</sub> [ $3.6 \times 10^{-7}$ ],<sup>175</sup> CFCl<sub>3</sub> [ $2.4 \times 10^{-7}$ ],<sup>175,176</sup> CF<sub>3</sub>Br [ $1.4 \times 10^{-8}$ ],<sup>138</sup> CF<sub>3</sub>I [ $1.9 \times 10^{-7}$ ],<sup>119</sup> SF<sub>6</sub> [ $2.4 \times 10^{-7}$ ],<sup>97</sup> SF<sub>5</sub>Cl [(2-5)  $\times 10^{-8}$ ],<sup>97,132</sup> SF<sub>5</sub>CF<sub>3</sub> [ $8.0 \times 10^{-8}$ ].<sup>97</sup>
- <sup>w</sup> Data in columns 3-9 for CF<sub>3</sub>X molecules (X = Cl, Br, I) are taken from Chapter 7.
- <sup>x</sup> The I<sup>-</sup> ion yield at *E* ≥ 10.4 eV is dominated by dissociative electron attachment to CF<sub>3</sub>I (see note <sup>u</sup>). However, below 10.4 eV the observed I<sup>-</sup> signal must arise by unimolecular ion-pair dissociation; the cross section for I<sup>-</sup> formation at 9.0 eV is  $3.8 \times 10^{-21} \text{ cm}^2$  with a corresponding quantum yield of  $8 \times 10^{-5}$  (photoabsorption cross section reported by Eden *et al.*).<sup>131</sup>
- <sup>y</sup> Data in columns 3-9 for SF<sub>5</sub>Cl are taken from Chapter 8.

Of these 24 molecules, several have been studied previously, by other research groups, using VUV anion spectroscopy. These data are available in the literature for CF<sub>4</sub>,<sup>41</sup> SF<sub>6</sub>,<sup>40,103</sup> CH<sub>4</sub>,<sup>177</sup> CH<sub>3</sub>X (X = F, Cl, Br),<sup>178</sup> C<sub>2</sub>H<sub>4</sub>,<sup>179</sup> C<sub>2</sub>H<sub>6</sub>,<sup>180,181</sup> C<sub>3</sub>H<sub>8</sub>,<sup>180</sup> and the chlorofluoromethanes (CFCl<sub>3</sub>, CF<sub>2</sub>Cl<sub>2</sub>, CF<sub>3</sub>Cl).<sup>135</sup> The present work is in excellent agreement with these earlier studies and in most cases the quality and quantity of data obtained have improved. For

example, anion spectra have been recorded over a larger photon energy range (typically from onset up to 35 eV) and new anions have been observed. Indeed the apparatus used to collect these data provides excellent sensitivity which is crucial when detecting negative ions. New results are presented here for  $\text{SF}_5\text{CF}_3$ ,  $\text{SF}_5\text{Cl}$ ,  $\text{CF}_3\text{X}$ , the perfluorocarbons, the fluoromethanes and the chloromethanes.

### 9.B. *Ion-pair appearance energies and thermochemical thresholds*

Consider the comparison between the experimental appearance energy ( $AE$ ) for ion-pair formation and the thermochemically determined threshold [Table 9.A.(I), columns 4 and 6, respectively]. The former quantity must be greater than or equal to the latter. This is true for the majority of results shown in Table 9.A.(I). For the few instances where this inequality is disobeyed (*e.g.*  $\text{H}^-$  from  $\text{CH}_4$ ), thermal effects and/or uncertainty in the calculated  $\Delta_r H^\circ_{298}$  values are expected to be responsible. In most cases, when only one dissociation process is thermodynamically accessible, the reaction occurring at the  $AE$  can be unambiguously identified. These are *single* bond-breaking ion-pair dissociation reactions. *Multiple* bond-breaking ion-pair dissociation reactions are assigned more tentatively, assuming the process yielding the least amount of excess energy prevails (*e.g.*  $\text{CF}_3\text{Cl} \rightarrow \text{Cl}^- + \text{CF}_2^+ + \text{F}$  rather than  $\text{CF}_3\text{Cl} \rightarrow \text{Cl}^- + \text{CF}_3^+$ ). This assumption is justified by experimental observations: it is common for the appearance of a feature in an ion-pair spectrum to correlate with a possible dissociation threshold.

The difference between  $AE_{298}$  and  $\Delta_r H^\circ_{298}$  is plotted in Figure 9.B.(i) [graph (a)] for all anions listed in Table 9.A.(I) that result from *single* bond-breaking ion-pair dissociation. The apparently random distribution of points in this plot is expected. However, if the points for

$H^-$  and  $F^-$  ions are plotted separately (Figure 9.B.(i), graphs (b) and (c), respectively), the distributions show an interesting trend: the points for  $H^-$  ions are clustered around  $AE - \Delta_r H^\circ = 0$ , whilst those for  $F^-$  take larger values. This indicates the dynamics for  $H^-$  ion-pair formation allow for a tendency for this anion to ‘turn on’ at the thermochemical threshold, favouring dissociation with low excess energy.

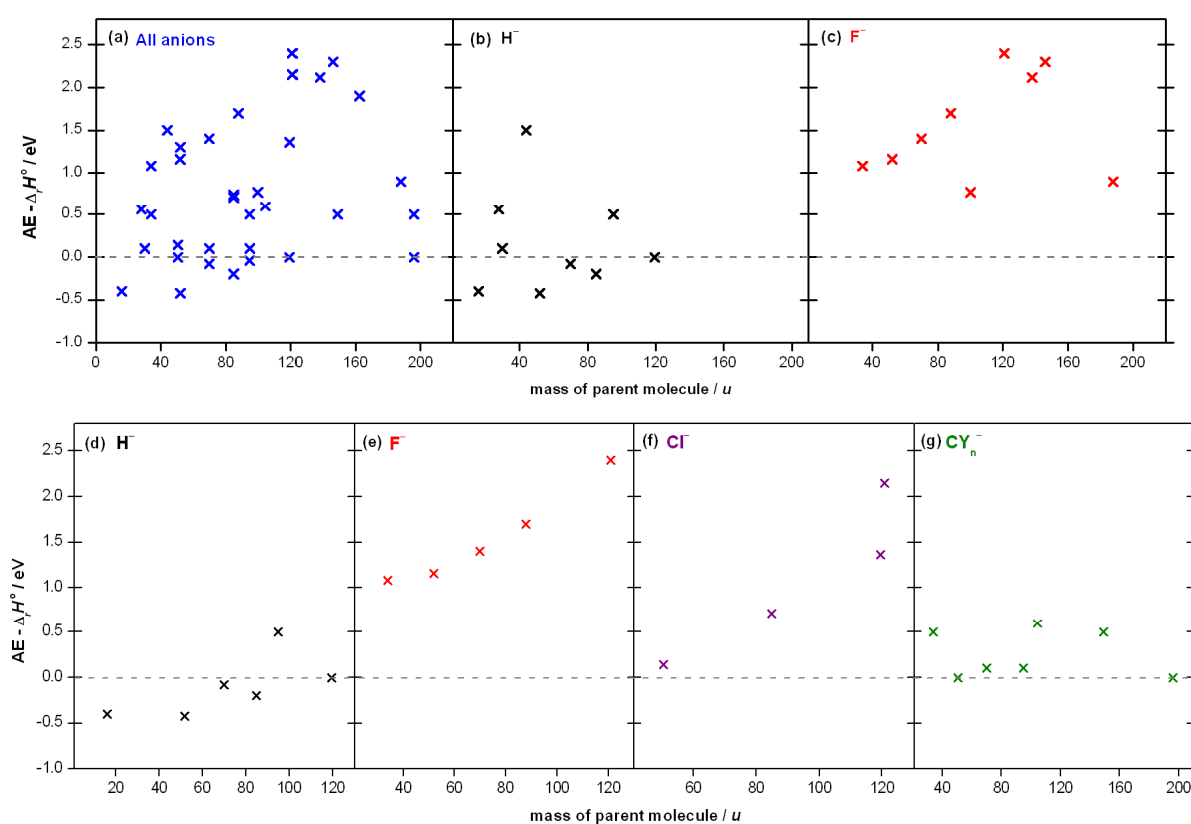


**Figure 9.B.(i).** (a)-(c) The distribution of  $AE_{298} - \Delta_r H^\circ_{298}$  for anions produced from a single bond-breaking ion-pair dissociation reaction [see Table 9.A.(I)]. (d)-(g) Data extracted from graph (a) for methane and the halo-substituted methanes only.  $CY_n^-$  includes data for  $CF_3^-$ ,  $CH_2F^-$ ,  $CH_2Cl^-$  and  $CH_2Br^-$  ions.

It is also interesting that the anion is  $H^-$  for four out of five instances in Figure 9.B.(i) [graph (a)] where  $AE - \Delta_r H^\circ < 0$  (the other is for  $Br^-$  with a value of  $-0.04$  eV). In contrast,  $F^-$  ion

pairs are formed with relatively larger excess energies. These trends become even clearer when the dataset is limited to methane and the halo-substituted methanes [Figure 9.B.(i), graphs (d)-(g)]. Now, the data for  $\text{Cl}^-$  and  $\text{CY}_3^-$  (*i.e.*  $\text{CF}_3^-$ ,  $\text{CH}_2\text{F}^-$ ,  $\text{CH}_2\text{Cl}^-$  and  $\text{CH}_2\text{Br}^-$ ) anions are also isolated and plotted. Low excess energies are also observed for  $\text{CY}_3^-$  anion formation; all points in graph (g) have values for  $AE - \Delta_r H^\circ$  between 0 and 0.6 eV. In graphs (e) and (f) of Figure 9.B.(i), for  $\text{F}^-$  and  $\text{Cl}^-$  ions from halo-substituted methanes, a positive correlation between  $(AE - \Delta_r H^\circ)$  and mass of the parent molecule is observed. This is surprising given that the data were plotted against mass for no particular reason, the primary aim always being to observe the scattering about the *y* axis. Indeed, the same correlation is observed if the *x* axis represents the total number of electrons in the molecule, or the molecular polarisability. There is no explanation for this observation and ideally more data points are required if this trend is to be confirmed.

### 9.C. Ion-pair formation below the ionisation energy

From an experimental point of view it is advantageous to look for ion pairs below the ionisation energy (*IE*); there will be zero background signal, and anions or cations can be detected with the confidence that they must originate from ion-pair formation.

It is energetically possible for ion-pair formation to occur below the *IE* of the parent molecule if, for the generic reaction  $\text{AB} \rightarrow \text{A}^- + \text{B}^+$ , the electron affinity (*EA*) of A exceeds the bond dissociation energy (*D*) of  $\text{A}-\text{B}^+$  (discussed in Chapter 1). This condition is most likely satisfied when A is a halogen atom and its *EA* is large. Indeed, *theoretically*, this is true for every halogen-containing molecule in Table 9.A.(I), with one exception:  $\text{F}^-$  from  $\text{C}_2\text{F}_4$ . Thus,  $D(\text{F}-\text{C}_2\text{F}_3^+) > EA(\text{F})$ , where  $EA(\text{F})$  is 3.401 eV.<sup>14</sup> Tetrafluoroethene is an unsaturated

perfluorinated molecule and is a classic example of the ‘perfluoro effect’; the C–F bonds in C<sub>2</sub>F<sub>4</sub> are strengthened by the combined inductive effect of the fluorine atoms at the expense of a significantly weakened C=C bond (also see Figure 4.B.(i) and the corresponding discussion in Chapter 4). Bond dissociation energies for ionised and neutral molecules of interest can be found in Appendix V.

The observation of ion-pair formation below the *IE* is not always restricted to instances where A is a halogen. Despite the small *EA* of the hydrogen atom, 0.754 eV,<sup>14</sup> H<sup>−</sup> ions may be observed below the *IE* from three out of the eleven hydrogen-containing molecules listed in Table 9.A.(I): CH<sub>2</sub>F<sub>2</sub>, CHF<sub>3</sub> and CHCl<sub>3</sub>. For these three molecules  $D(\text{H}-\text{CY}_3^+) < 0.754 \text{ eV}$  (see Appendix V).

From all of the data in Table 9.A.(I), there are only four instances where the cross section maximum,  $\sigma_{\text{max}}$ , was observed below the *IE* of the parent molecule: F<sup>−</sup> from CF<sub>4</sub>, Cl<sup>−</sup> from CH<sub>2</sub>Cl<sub>2</sub>, Br<sup>−</sup> from CH<sub>3</sub>Br and F<sup>−</sup> from SF<sub>6</sub>. In all other cases,  $\sigma_{\text{max}}$  was recorded at photon energies above the *IE*. It is also worth noting that, for the majority of molecules,  $\sigma_{\text{max}}$  for producing *atomic* anions occurs between 16 and 22 eV – enough energy to access multiple bond-breaking ion-pair dissociation channels. Exceptions to this are for CF<sub>4</sub>, C<sub>2</sub>F<sub>6</sub>, SF<sub>6</sub>, SF<sub>5</sub>Cl, CH<sub>3</sub>F, CH<sub>3</sub>Cl, CH<sub>2</sub>Cl<sub>2</sub> and CH<sub>3</sub>Br, where the lowest-energy ion-pair dissociation reaction occurs at the cross section maximum.

### 9.D. Quantum yields

The quantum yield values,  $\Phi$ , in Table 9.A.(I) are probabilities for the formation of a given anion (*via* an ion-pair reaction) following the absorption of a photon by the parent

molecule. The quantum yield is calculated by dividing the anion cross section by the total photoabsorption cross section. A quantum yield value is always quoted at a given energy. Each quantum yield listed in column 9 of Table 9.A.(I) represents the maximum value calculated within the energy range studied. The largest quantum yield value is  $2.3 \times 10^{-3}$ , or 0.23 % (for both  $F^-$  from  $CH_3F$  and  $Cl^-$  from  $CH_3Cl$ ). The smallest value is  $5.6 \times 10^{-7}$ , or 0.000056 % (for  $F_2^-$  from  $CF_4$ ). The majority of quantum yields, however, lie between  $5 \times 10^{-4}$  and  $1 \times 10^{-6}$  (*i.e.* 0.05-0.0001 %).

Some interesting observations are made based on the quantum yield data in column 9 in Table 9.A.(I). By comparing these data between all of the listed molecules the following general statements are made:

1. Quantum yields for the production of an *atomic* anion are greater than quantum yields for the production of a *molecular* anion. There are some exceptions to this statement (*e.g.*  $CF_3^-$  formation from  $CHF_3$ ).
2. Quantum yields for the production of an atomic halogen anion are greater than quantum yields for the production of  $H^-$  anions. Note that for instances where the  $H^-$  cross section (and hence quantum yield) was not determined [footnotes *p* and *q* in Table 9.A.(i)], its intensity was always similar to, or weaker than that for the halogen anion.
3. The quantum yield at  $E$  ( $\sigma_{max}$ ) for  $F^-$  formation from the fluoromethanes increases as the number of fluorine atoms decreases:  $\Phi(F^- \text{ from } CH_3F) > \Phi(F^- \text{ from } CH_2F_2) > \Phi(F^- \text{ from } CHF_3) > \Phi(F^- \text{ from } CF_4)$ . The opposite trend is observed for  $F^-$  anions produced from the chlorofluoromethanes:  $\Phi(F^- \text{ from } CF_3Cl) > \Phi(F^- \text{ from } CF_2Cl_2) > \Phi(F^- \text{ from } CFCl_3)$ .

4. The quantum yield at  $E(\sigma_{\max})$  for  $\text{Cl}^-$  formation from the chloromethanes increases as the number of chlorine atoms decreases:  $\Phi(\text{Cl}^- \text{ from } \text{CH}_3\text{Cl}) > \Phi(\text{Cl}^- \text{ from } \text{CH}_2\text{Cl}_2) > \Phi(\text{Cl}^- \text{ from } \text{CHCl}_3)$ . The opposite trend is observed for  $\text{Cl}^-$  anions produced from the chlorofluoromethanes:  $\Phi(\text{Cl}^- \text{ from } \text{CF}_2\text{Cl}_2) > \Phi(\text{Cl}^- \text{ from } \text{CF}_3\text{Cl})$ . Note that  $\text{Cl}^-$  spectra recorded for  $\text{CFCl}_3$  and  $\text{CCl}_4$  were dominated by dissociative electron attachment; the contribution from  $\text{Cl}^-$  anions produced by ion-pair formation is not known.
5. The quantum yield at  $E(\sigma_{\max})$  for  $\text{H}^-$  formation from the hydrocarbons increases as the number of hydrogen atoms increases:  $\Phi(\text{H}^- \text{ from } \text{C}_3\text{H}_8) > \Phi(\text{H}^- \text{ from } \text{C}_2\text{H}_6) > \Phi(\text{H}^- \text{ from } \text{C}_2\text{H}_4) > \Phi(\text{H}^- \text{ from } \text{CH}_4)$ .

These statements may be understood better if one considers the *electronegativity* of the individual atoms, and therefore the overall polarisation of the electron density across the molecule. Pauling electronegativities for relevant atoms are: F (3.98), Cl (3.16), Br (2.96), I (2.66), S (2.58), C (2.55) and H (2.20).<sup>182</sup> For example, the bond polarisation in  $\text{CH}_4$  can be represented by  $\text{C}^{\delta-}-\text{H}^{\delta+}$ , and in  $\text{CF}_4$  by  $\text{C}^{\delta+}-\text{F}^{\delta-}$ . The effects of fluorine substitution in methane have been studied in great detail by Brundle *et al.*,<sup>165</sup> and the following extract from their publication is particularly relevant:

*“As expected, the protons in  $\text{CH}_4$  are positively charged, while the carbon atom assumes a rather large negative charge. Upon the substitution of fluorine for hydrogen, the charges on the remaining protons are calculated to be very much what they are in  $\text{CH}_4$ , whereas the fluorines drain charge from the carbon and very quickly make it electropositive. In going from  $\text{CH}_4$  to  $\text{CF}_4$ , the carbon atom surrenders over 1.6 electrons to the fluorines, mostly through the polarisation of the C–X bonds.”*

Qualitatively, one can therefore appreciate how  $\text{F}^-$  formation from  $\text{CF}_4$  is more probable than  $\text{H}^-$  from  $\text{CH}_4$ . Also consider statement 3 for the fluoromethanes. Although the carbon atom



gives up more charge as more H atoms are substituted for F atoms, the electron density on any *one* given F atom will be reduced when the total number of F atoms within the molecule increases. The same logic is followed for the chloromethanes and statement 4. For any chlorofluoromethane, however, the central carbon is always bonded to four highly electronegative species – the difference between electronegativities for F and Cl is relatively small. Now perhaps a statistical factor plays a part, whereby the number of F or Cl atoms determines which anion is formed in preference to the other; indeed the quantum yields at  $E$  ( $\sigma_{\max}$ ) for  $F^-$  and  $Cl^-$  from  $CF_2Cl_2$  are almost identical [Table 9.A.(I)].

It is incorrect to attempt to understand any of the above statements by considering absolute energetic quantities such as electron affinities or bond dissociation energies; these values simply determine the asymptotic dissociation energy for the ion-pair state. Assuming indirect formation of ion pairs *via* an excited neutral state, it is the dynamics of the crossing between states which is important, and indeed the probability for the excited state to decay by a different process. Therefore, the position of the ion-pair state along the reaction coordinate (*i.e.* the value for  $r_e$ ) and its shape are significant.

### 9.E. Competing ion-pair reactions

It is observed from many ion-pair studies that different anions from the same molecule display peaks in their spectrum at the same energy. These peaks most likely identify the same excited intermediate state, and this is further evidence that ion pairs are commonly formed by the indirect mechanism. Specific examples for  $CH_2F_2$  and  $CF_3Cl$  are discussed below.

The spectra for anions produced from  $CH_2F_2$  are presented in Appendix IV. The first band in the  $H^-$  spectrum shows vibrational structure consistent with that observed by

photoelectron spectroscopy for the ground state of  $\text{CH}_2\text{F}_2^+$ ,  $\tilde{X}^2B_2$ .<sup>164</sup> The peaks in this band are assigned using the Rydberg formula to overlapping members of the  $np^1B_2$  Rydberg series ( $n = 5-7$ ). The first peak in the  $\text{F}^-$  spectrum, however, is assigned to the  $5p^1B_2$  Rydberg member only. It is clear that two different ion-pair dissociation channels are competing following excitation to the  $5p$  Rydberg state ( $\text{CH}_2\text{F}_2^* \rightarrow \text{F}^- + \text{CH}_2\text{F}^+$  and  $\text{CH}_2\text{F}_2^* \rightarrow \text{H}^- + \text{CHF}_2^+$ ). However, the  $\text{F}^-$  channel no longer competes following excitation to higher- $n$  Rydberg members; the first peak in the  $\text{F}^-$  spectrum spans between 11.8 and 13.1 eV only. These high-lying  $np$  Rydberg states overlap with the ground state of  $\text{CH}_2\text{F}_2^+$ ,  $\tilde{X}^2B_2$ ; the adiabatic  $IE$  is 12.73 eV and the vertical  $IE$  is 13.28 eV.<sup>164</sup> At 13.08 eV,  $\text{CH}_2\text{F}_2^+$  becomes unstable with respect to  $\text{H} + \text{CHF}_2^+$ .<sup>183</sup> Certainly, this dissociation is complementary to the  $\text{CH}_2\text{F}_2^* \rightarrow \text{H}^- + \text{CHF}_2^+$  ion-pair dissociation, and *not* to the  $\text{CH}_2\text{F}_2^* \rightarrow \text{F}^- + \text{CH}_2\text{F}^+$  reaction. This may explain why the  $\text{F}^-$  dissociation channel diminishes at 13.1 eV, while that for  $\text{H}^-$  continues. Although a cross section for  $\text{H}^-$  formation was not determined, its signal strength at *ca.* 12.6 eV was comparable to, if not weaker than the  $\text{F}^-$  signal.

Ion-pair formation from  $\text{CF}_3\text{Cl}$  has been discussed in detail in Chapter 7. The  $\text{F}^-$  and  $\text{Cl}^-$  spectra [Figures 7.C.(i) and 7.D.(i), respectively] share some common features. For the benefit of the discussion below, these two spectra are compared directly and plotted on the same axis in Figure 9.E.(i).  $\text{F}^-$  and  $\text{Cl}^-$  anions were both detected at 17.6 eV, but only the  $\text{Cl}^-$  ion yield displays a true peak at this energy. Clearly shown in Figure 9.E.(i), this is the only region across the two spectra where the  $\text{Cl}^-$  cross section is larger than that for  $\text{F}^-$ . The two spectra cross at 18.4 eV and 28.2 eV and between these energies the  $\text{F}^-$  cross section is significantly larger than that for  $\text{Cl}^-$ . The fact that features are observed in both spectra at similar energies suggests these do indeed represent competing decay channels from the same

Rydberg states. Vertical ionisation energies for  $\text{CF}_3\text{Cl}^+ \tilde{D}^2E$ ,  $\tilde{E}^2A_1$ ,  $\tilde{F}^2E$  and  $\tilde{G}^2A_1$  are 17.71, 20.20, 21.20 and 23.80 eV, respectively.<sup>121</sup> The features in the spectra at 17.6, 19.7 and 20.9 eV are assigned to high-lying Rydberg states ( $n > 5$ ) converging on the  $\tilde{D}$ ,  $\tilde{E}$  and  $\tilde{F}$  ionisation limits, respectively. The feature at 22.5 eV is assigned as either the  $3p^1A_1$  or  $4s^1A_1$  Rydberg state.

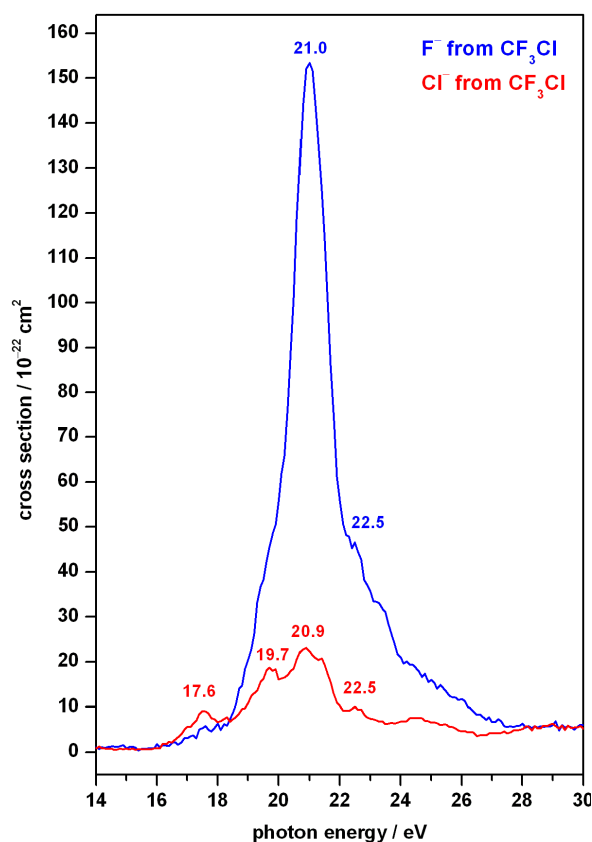


**Figure 9.E.(i).**  $\text{F}^-$  and  $\text{Cl}^-$  cross sections recorded following the VUV photoexcitation of  $\text{CF}_3\text{Cl}$ . Only the 14 to 30 eV range is shown here. The complete spectra are presented and discussed in Chapter 7.

Section 9.D addressed *general* trends in quantum yield and cross section values, only comparing those in Table 9.A.(I) quoted at  $E_{\text{max}}$ . The data for  $\text{F}^-$  and  $\text{Cl}^-$  from  $\text{CF}_3\text{Cl}$ ,

however, is one example showing that cross section and quantum yield values should be compared at the same energy. This point is perhaps obvious, but it serves to highlight the challenges in understanding why one particular anion has a higher probability for formation than another.

### 9.F. *Electron attachment*

For a molecule under study by negative photoion spectroscopy, below the *IE* any anion produced must result from an ion-pair reaction. Above the *IE*, however, photoelectrons are produced and negative ions resulting from electron attachment processes can be detected. Examples where this has been observed include:  $\text{SF}_5^-$  and  $\text{SF}_6^-$  from  $\text{SF}_6$ ,  $\text{SF}_5^-$  from  $\text{SF}_5\text{CF}_3$  (Chapter 6);  $\text{Br}^-$  from  $\text{CF}_3\text{Br}$  and  $\text{I}^-$  from  $\text{CF}_3\text{I}$  (Chapter 7);  $\text{SF}_5^-$  from  $\text{SF}_5\text{Cl}$  (Chapter 8);  $\text{Cl}^-$  from  $\text{CFC}_3$  and  $\text{Cl}^-$  from  $\text{CCl}_4$  (Appendix IV). The electron attachment process observed may be generically described by the following two reactions:



Four points are made when identifying such electron attachment processes:

1. A plot of the anion signal as a function of gas pressure will be linear for ion-pair formation, but non-linear (with the rate of change in signal increasing with increasing pressure) if electron attachment is detected. Figure 6.B.(ii) shows examples for  $\text{F}^-$  and  $\text{SF}_5^-$  from  $\text{SF}_6$ . Following reactions 9.F.(1) and 9.F.(2),  $[\text{A}^-]$  is proportional to  $[\text{AB}]^2$ , and

these two quantities may be indirectly measured in the experiment as the  $A^-$  signal and pressure of AB, respectively.

2. It is evident that the molecule must have an electron attachment rate coefficient,  $k_a$ , of sufficient magnitude in order for this process to be observed. The molecules listed above have thermal  $k_a$  values between  $1 \times 10^{-8}$  and  $4 \times 10^{-7} \text{ cm}^3 \text{ molecule}^{-1} \text{ s}^{-1}$  [refer to footnote *u* in Table 9.A.(I)]. Molecules with slightly lower  $k_a$  values were also studied [*e.g.*  $\text{CHCl}_3$  and  $\text{CF}_2\text{Cl}_2$  ( $k_a = 4.7 \times 10^{-9}$  and  $1.9 \times 10^{-9} \text{ cm}^3 \text{ molecule}^{-1} \text{ s}^{-1}$ , respectively)<sup>175</sup>], but the anion signals were all attributed to ion-pair formation.
3. There is usually only one anion produced by electron attachment from any given molecule which is detected by negative photoion spectroscopy (the exception being  $\text{SF}_6^-$  and  $\text{SF}_5^-$  from  $\text{SF}_6$ ). This anion always matches the dominant species identified from independent thermal electron attachment experiments.
4. The spectrum of an anion produced by electron attachment matches, to varying extent depending on the molecule and signal strength, the threshold photoelectron spectrum (TPES) for that molecule. In most cases peak positions are the same, but relative intensities of peaks can vary significantly.

The most interesting of these points is number 4. The similarities/differences between anion spectrum and TPES have already been discussed for the molecules  $\text{SF}_6$ ,  $\text{SF}_5\text{CF}_3$ ,  $\text{CF}_3\text{Br}$ ,  $\text{CF}_3\text{I}$  and  $\text{SF}_5\text{Cl}$  in Chapters 6-8. There is no general trend and the reasons for any differences cannot be explained. New data for  $\text{Cl}^-$  from  $\text{CFCl}_3$  and  $\text{CCl}_4$  are shown in Appendix IV. Both spectra show a remarkable tendency for the relative anion signal to increase with increasing photon energy, especially above *ca.* 22 eV. It is even possible that some of the

features observed above 22 eV identify ionisation potentials which are very weak or absent in the TPES. Furthermore, signal vs pressure plots recorded at these peak energies show a non-linear dependence as discussed in point 1. For the  $\text{Cl}^-$  from  $\text{CCl}_4$  example, a close examination of the TPES does reveal weak and partially resolved features between 22 and 27 eV.

### 9.G. Concluding remarks

The formation of ion pairs from polyatomic molecules is a weak process. Quantum yield values are less than or equal to *ca.* 0.2 %. The detection of ion-pair formation therefore requires a sensitive experimental apparatus, and most spectra could only be recorded at a modest resolution.

Ion-pair formation is most commonly formed by the indirect mechanism *via* an initially excited Rydberg state. Many peaks in ion-pair spectra occur between adiabatic and vertical ionisation energy values. Indeed many of the strongest anion signals result following the predissociation of high-lying Rydberg states ( $n > 5$ ). It can be difficult to resolve these overlapping excited states, let alone assign them, especially when the resolution of the experiment is limited.

One of the most interesting questions raised is: why is one anion produced preferentially to another? This question can be asked when comparing the same anion from different molecules (*e.g.*  $\text{Cl}^-$  from  $\text{CF}_3\text{Cl}$  and  $\text{CF}_2\text{Cl}_2$ ), different anions from different molecules (*e.g.*  $\text{H}^-$  from  $\text{CH}_4$  and  $\text{F}^-$  from  $\text{CF}_4$ ), and different anions from the same molecule (*e.g.*  $\text{F}^-$  and  $\text{Cl}^-$  from  $\text{CF}_3\text{Cl}$ ). Some trends are apparent when comparing a series of similar molecules [*e.g.* the methyl halides,<sup>45</sup> the fluoromethanes or the chloromethanes (Section 9.D)], but there is no

common explanation. Another unanswered question is: why are some anions not observed at all? Examples include the absence of  $\text{Cl}^-$  anions from  $\text{CF}_3\text{Cl}$  below 16 eV (Chapter 7), and the absence of  $\text{Cl}^-$  anions from  $\text{SF}_5\text{Cl}$  above 12 eV (Chapter 8).

Thermochemistry is a useful tool to identify the cation and neutral dissociation fragments accompanying the detected anion. However, conclusive assignments are only made at the onset for ion-pair formation when only one dissociation reaction is energetically allowed. The ideal experiment would detect anion and cation fragments above the ionisation energy in coincidence, and perhaps this is where the future of ion-pair spectroscopy lies. Such coincidence experiments would identify both the anion *and* cation fragments, allowing for a more detailed analysis of ion-pair dissociation dynamics.

Little information is known about ion-pair potential energy surfaces in polyatomic molecules and I am convinced that the vast collection of experimental data collected in this thesis would provide interest and direction for a theoretical study. For example, one can use equation 1.B.(4) to model the potential energy function of an ion-pair state if constants  $A$  and  $\alpha$  can be derived using experimental results [for example,  $r$  can be estimated at known values for  $V(r)$ ].

Finally, it is noted that much of the data collected during my time at Birmingham has not been fully analysed. The spectra recorded from these experiments are presented in Appendix IV.

# Notes



# Notes

# References

1. C. A. Mayhew, *Journal of Physics B* **25**, 1865 (1992).
2. D. Smith, P. Spanel, and C. A. Mayhew, *International Journal of Mass Spectrometry and Ion Processes* **117**, 457 (1992).
3. G. K. Jarvis, C. A. Mayhew, and R. P. Tuckett, *Journal of Physical Chemistry* **100**, 17166 (1996).
4. G. K. Jarvis, R. A. Kennedy, C. A. Mayhew, and R. P. Tuckett, *International Journal of Mass Spectrometry* **202**, 323 (2000).
5. C. Atterbury, R. A. Kennedy, C. A. Mayhew, and R. P. Tuckett, *Physical Chemistry and Chemical Physics* **3**, 1949 (2001).
6. C. Atterbury, A. Critchley, R. A. Kennedy, C. A. Mayhew, and R. P. Tuckett, *Physical Chemistry and Chemical Physics* **4**, 2206 (2002).
7. C. A. Mayhew, R. Thomas, and P. Watts, *International Journal of Mass Spectrometry* **223**, 91 (2003).
8. A. Critchley, C. R. Howle, C. A. Mayhew, and R. P. Tuckett, *Chemical Physics* **303**, 235 (2004).
9. C. R. Howle, C. A. Mayhew, and R. P. Tuckett, *Journal of Physical Chemistry A* **109**, 3626 (2005).
10. M. A. Parkes, R. Y. L. Chim, C. A. Mayhew, V. Mikhailov, and R. P. Tuckett, *Molecular Physics* **104**, 263 (2006).
11. M. A. Parkes, S. Ali, R. P. Tuckett, V. Mikhailov, and C. A. Mayhew, *Physical Chemistry and Chemical Physics* **8**, 3643 (2006).
12. V. Mikhailov, M. A. Parkes, M. J. Simpson, R. P. Tuckett, and C. A. Mayhew, *Journal of Physical Chemistry A* **112**, 9012 (2008).
13. R. A. Kennedy and C. A. Mayhew, *Physical Chemistry and Chemical Physics* **3**, 5511 (2001).
14. J. C. Rienstra-Kiracofe, G. S. Tschumper, H. F. Schaefer, S. Nandi, and B. Ellison, *Chemical Reviews* **102**, 231 (2002).
15. R. A. Kennedy, C. A. Mayhew, R. Peverall, and P. Watts, *Physical Chemistry and Chemical Physics* **2**, 3145 (2000).
16. E. P. F. Lee, J. M. Dyke, and C. A. Mayhew, *Journal of Physical Chemistry A* **102**, 8349 (1998).
17. S. T. Arnold, T. M. Miller, A. A. Viggiano, and C. A. Mayhew, *International Journal of Mass Spectrometry* **223**, 403 (2003).
18. W. J. Chesnavich, T. Su, and M. T. Bowers, *Journal of Chemical Physics* **72**, 2641 (1980).
19. T. Su and W. J. Chesnavich, *Journal of Chemical Physics* **76**, 5183 (1982).
20. T. Su, *Journal of Chemical Physics* **88**, 4102 (1988).

21. T. Su, *Journal of Chemical Physics* **89**, 5355 (1988).
22. P. M. Langevin, *Annales de Chimie et de Physique* **5**, 245 (1905).
23. G. Gioumousis and D. P. Stevenson, *Journal of Chemical Physics* **29**, 294 (1958).
24. K. J. Miller, *Journal of the American Chemical Society* **112**, 8533 (1990).
25. D. R. Lide, *Handbook of Chemistry and Physics*, 89th ed. (Taylor & Francis, London, 2008), Sections 9 and 10.
26. K. P. Lawley and R. J. Donovan, *Journal of the Chemical Society, Faraday Transactions* **89**, 1885 (1993).
27. A. G. Suits and J. W. Hepburn, *Annual Review of Physical Chemistry* **57**, 431 (2006).
28. J. Berkowitz, in *VUV and Soft X-Ray Photoionization*, Ed. U. Becker and D. A. Shirley. (Plenum Press, New York, 1996) p263.
29. J. Berkowitz, *Photoabsorption, Photoionization, and Photoelectron Spectroscopy* (Academic Press, London, 1979), p14.
30. J. K. G. Watson, in *The Role of Rydberg States in Spectroscopy and Photochemistry*, Ed. C. Sandorfy. (Kluwer Academic Publishers, London, 1999) p293.
31. C. Sandorfy, in *The Role of Rydberg States in Spectroscopy and Photochemistry*, Ed. C. Sandorfy. (Kluwer Academic Publishers, London, 1999) p1.
32. C. E. Theodosiou, M. Inokuti, and S. Manson, *Atomic Data and Nuclear Data Tables* **35**, 473 (1986).
33. J. C. Traeger and R. G. McLoughlin, *Journal of the American Chemical Society* **103**, 3647 (1981).
34. D. Smith and N. Adams, *Advances in Atomic and Molecular Physics* **24**, 1 (1988).
35. S. T. Graul and R. R. Squires, *Mass Spectrometry Reviews* **7**, 263 (1988).
36. D. K. Bohme, *International Journal of Mass Spectrometry* **200**, 97 (2000).
37. S. L. Hulbert and G. P. Williams, in *Vacuum Ultraviolet Spectroscopy*, Ed. J. A. Samson and D. L. Ederer. (Academic Press, London, 2000) p1.
38. C. R. Howle, S. Ali, R. P. Tuckett, D. A. Shaw, and J. B. West, *Nuclear Instruments and Methods in Physics Research Section B* **237**, 656 (2005).
39. K. F. Dunn and C. J. Latimer, private communication (September 2005).
40. K. Mitsuke, S. Suzuki, T. Imamura, and I. Koyano, *Journal of Chemical Physics* **93**, 8717 (1990).
41. K. Mitsuke, S. Suzuki, T. Imamura, and I. Koyano, *Journal of Chemical Physics* **95**, 2398 (1991).
42. P. M. Dehmer and W. A. Chupka, *Journal of Chemical Physics* **62**, 4525 (1975).
43. National Institute of Standards and Technology website (<http://webbook.nist.gov/chemistry/>).
44. P. H. Dawson, *Quadrupole Mass Spectrometry and its Applications* (American Institute of Physics, New York, 1995).

45. N. J. Rogers, M. J. Simpson, R. P. Tuckett, K. F. Dunn, and C. J. Latimer, '*Vacuum-UV negative photoion spectroscopy of CH<sub>3</sub>F, CH<sub>3</sub>Cl and CH<sub>3</sub>Br*' in *Physical Chemistry Chemical Physics*, **in press** (2010).
46. N. J. Rogers, M. J. Simpson, R. P. Tuckett, K. F. Dunn, and C. J. Latimer, *Molecular Physics* **108**, 895 (2010).
47. V. Mikhailov, M. A. Parkes, R. P. Tuckett, and C. A. Mayhew, *Journal of Physical Chemistry A* **110**, 5760 (2006).
48. G. A. W. Derwish, A. Galli, A. Giardini-Guidoni, and G. G. Volpi, *Journal of the American Chemical Society* **86**, 4563 (1964).
49. V. G. Anicich, M. T. Bowers, R. M. O'Malley, and K. R. Jennings, *International Journal of Mass Spectrometry and Ion Physics* **11**, 99 (1973).
50. R. A. Morris, A. A. Viggiano, and J. F. Paulson, *Journal of Physical Chemistry* **97**, 6208 (1993).
51. R. A. Morris, E. R. Brown, A. A. Viggiano, J. M. Van Doren, J. F. Paulson, and V. Motevalli, *International Journal of Mass Spectrometry and Ion Processes* **121**, 95 (1992).
52. M. Tsuji, M. Aizawa, and Y. Nishimura, *Journal of Physical Chemistry* **99**, 3195 (1995).
53. R. M. O'Malley, K. R. Jennings, M. T. Bowers, and V. G. Anicich, *International Journal of Mass Spectrometry and Ion Physics* **11**, 89 (1973).
54. B. A. Williams and T. A. Cool, *Journal of Chemical Physics* **94**, 6358 (1991).
55. G. Bieri, W. Von Niessen, L. Åsbrink, and A. Svensson, *Chemical Physics* **60**, 61 (1981).
56. J. M. Dyke, A. E. Lewis, and A. Morris, *Journal of Chemical Physics* **80**, 1382 (1984).
57. National Institute of Standards and Technology website (<http://webbook.nist.gov/chemistry/>), on 1 June 2009.
58. G. A. Garcia, P. M. Guyon, and I. Powis, *Journal of Physical Chemistry A* **105**, 8296 (2001).
59. S. Eden, P. Limao-Vieira, P. A. Kendall, N. J. Mason, J. Delwiche, M. J. Hubin-Franskin, T. Tanaka, M. Kitajima, H. Tanaka, H. Cho, and S. V. Hoffmann, *Chemical Physics* **297**, 257 (2004).
60. A. J. Ferrer-Correia and K. R. Jennings, *International Journal of Mass Spectrometry and Ion Physics* **11**, 111 (1973).
61. V. G. Anicich and M. T. Bowers, *International Journal of Mass Spectrometry and Ion Physics* **13**, 351 (1974).
62. V. G. Anicich and M. T. Bowers, *International Journal of Mass Spectrometry and Ion Physics* **13**, 359 (1974).
63. T. Su and L. Kevan, *International Journal of Mass Spectrometry and Ion Physics* **11**, 57 (1973).
64. S. A. Sullivan and J. L. Beauchamp, *Journal of the American Chemical Society* **98**, 1160 (1976).
65. S. A. Sullivan and J. L. Beauchamp, *Journal of the American Chemical Society* **99**, 5017 (1977).
66. D. A. Parkes, *Journal of the Chemical Society, Faraday Transactions* **68**, 613 (1972).
67. W. Lindinger, D. L. Albritton, F. C. Fehsenfeld, and E. E. Ferguson, *Journal of Chemical Physics* **63**, 3238 (1975).

68. A. A. Viggiano and J. F. Paulson, *Journal of Chemical Physics* **79**, 2241 (1983).
69. J. Dawson and K. R. Jennings, *Journal of the Chemical Society, Faraday Transactions* **72**, 700 (1976).
70. D. K. Bohme and L. Brewster Young, *Journal of the American Chemical Society* **92**, 3301 (1970).
71. R. A. Morris, *Journal of Chemical Physics* **97**, 2372 (1992).
72. T. Su, A. Su, A. A. Viggiano, and J. F. Paulson, *Journal of Physical Chemistry* **91**, 3683 (1987).
73. A. C. Simmonett, S. E. Wheeler, and H. F. Schaefer, *Journal of Physical Chemistry* **108**, 1608 (2004).
74. S. G. Lias, J. E. Bartmess, J. F. Liebman, J. L. Holmes, R. D. Levin, and W. G. Mallard, *Journal of Physics and Chemical Reference Data* **17**, 1 (1988).
75. S. Spyrou, I. Sauers, and L. G. Christophorou, *Journal of Chemical Physics* **78**, 7200 (1983).
76. P. W. Harland and J. C. J. Thynne, *International Journal of Mass Spectrometry and Ion Physics* **18**, 73 (1975).
77. C. Lifshitz and R. Grajower, *International Journal of Mass Spectrometry and Ion Physics* **10**, 25 (1972).
78. C. W. Bauschlicher and A. Ricca, *Journal of Physical Chemistry A* **104**, 4581 (2000).
79. P. V. R. Schleyer and A. Kos, *Tetrahedron* **39**, 1141 (1983).
80. R. D. Bach and C. Evans, *Journal of the American Chemical Society* **108**, 1374 (1986).
81. M. Roy and T. B. McMahon, *Canadian Journal of Chemistry* **63**, 708 (1985).
82. J. J. Rabasco and S. R. Kass, *Journal of the American Society for Mass Spectrometry* **3**, 91 (1992).
83. R. Knorr, *Chemical Reviews* **104**, 3795 (2004).
84. L. R. Cox, private communication (2005).
85. R. N. McDonald and A. Kasem Chowdhury, *Journal of the American Chemical Society* **107**, 4123 (1985).
86. M. J. Simpson, R. P. Tuckett, K. F. Dunn, C. A. Hunniford, C. J. Latimer, and S. W. J. Scully, *Journal of Chemical Physics* **128**, 124315 (2008).
87. W. T. Sturges, T. J. Wallington, M. D. Hurley, K. P. Shine, K. Sihra, A. Engel, D. E. Oram, S. A. Penkett, R. Mulvaney, and C. A. M. Brenninkmeijer, *Science* **289**, 611 (2000).
88. R. Y. L. Chim, R. A. Kennedy, and R. P. Tuckett, *Chemical Physics Letters* **367**, 697 (2003).
89. P. A. Kendall, N. J. Mason, G. A. Buchanan, G. Marston, P. Tegeder, A. Dawes, S. Eden, P. Limao-Vieira, and D. A. Newnham, *Chemical Physics* **287**, 137 (2003).
90. P. A. Kendall and N. J. Mason, *Journal of Electron Spectroscopy and Related Phenomena* **120**, 27 (2001).
91. O. J. Nielsen, F. M. Nicolaisen, C. Bacher, M. D. Hurley, T. J. Wallington, and K. P. Shine, *Atmospheric Environment* **36**, 1237 (2002).
92. P. Limao-Vieira, S. Eden, P. A. Kendall, N. J. Mason, A. Giuliani, J. Heinesch, M. J. Hubin-Franskin, J. Delwiche, and S. V. Hoffmann, *International Journal of Mass Spectrometry* **233**, 335 (2004).

93. L. Huang, L. Zhu, X. Pan, J. Zhang, B. Ouyang, and H. Hou, *Atmospheric Environment* **39**, 1641 (2005).
94. R. A. Kennedy and C. A. Mayhew, *International Journal of Mass Spectrometry* **206**, AR1 (2001).
95. W. Sailer, H. Drexel, A. Pelc, V. Grill, N. J. Mason, E. Illenberger, J. D. Skalny, T. Mikoviny, P. Scheier, and T. D. Märk, *Chemical Physics Letters* **351**, 71 (2002).
96. T. M. Miller, S. T. Arnold, A. A. Viggiano, and W. B. Knighton, *Journal of Chemical Physics* **116**, 6021 (2002).
97. C. A. Mayhew, A. Critchley, D. C. Howse, V. Mikhailov, and M. A. Parkes, *European Physical Journal D* **35**, 307 (2005).
98. H. Hotop, private communication (2007).
99. R. Y. L. Chim, R. A. Kennedy, R. P. Tuckett, W. Zhou, G. K. Jarvis, D. J. Collins, and P. A. Hatherly, *Journal of Physical Chemistry A* **105**, 8403 (2001).
100. R. Y. L. Chim, R. A. Kennedy, R. P. Tuckett, W. Zhou, G. K. Jarvis, C. A. Mayhew, D. J. Collins, and P. A. Hatherly, *Surface Review and Letters* **9**, 129 (2002).
101. R. P. Tuckett, *Advances in Fluorine Science* **1**, 89 (2006).
102. D. M. P. Holland, D. A. Shaw, I. C. Walker, I. J. McEwen, E. Apra, and M. F. Guest, *Journal of Physics B* **38**, 2047 (2005).
103. S. W. J. Scully, R. A. Mackie, R. Browning, K. F. Dunn, and C. J. Latimer, *Journal of Physics B* **35**, 2703 (2002).
104. J. C. Creasey, H. M. Jones, D. M. Smith, R. P. Tuckett, P. A. Hatherly, K. Codling, and I. Powis, *Chemical Physics* **174**, 441 (1993).
105. L. G. Christophorou and J. K. Olthoff, *Journal of Physics and Chemical Reference Data* **29**, 267 (2000).
106. A. J. Yench, D. B. Thompson, A. J. Cormack, D. R. Cooper, M. Zubek, P. Bolognesi, and G. C. King, *Chemical Physics* **216**, 227 (1997).
107. M. A. Parkes, Ph.D. thesis, University of Birmingham, 2007.
108. D. M. P. Holland, D. A. Shaw, A. Hopkirk, M. A. MacDonald, and S. M. McSweeney, *Journal of Physics B* **25**, 4823 (1992).
109. S. W. J. Scully, Ph.D. thesis, Queen's University Belfast, 2004.
110. A. J. Yench, A. Hopkirk, A. Hiraya, G. Dujardin, A. Kvaran, L. Hellner, M. J. Besnard-Ramage, R. J. Donovan, J. G. Goode, R. R. J. Maier, G. C. King, and S. Spyrou, *Journal of Electron Spectroscopy and Related Phenomena* **70**, 29 (1994).
111. D. M. P. Holland, A. W. Potts, A. B. Trofimov, J. Breidbach, J. Schirmer, R. Feifel, T. Richter, K. Godehusen, M. Martins, A. Tutay, M. Yalcinkaya, M. Al-Hada, S. Eriksson, and L. Karlsson, *Chemical Physics* **308**, 43 (2005).
112. L. C. Lee, E. Phillips, and D. L. Judge, *Journal of Chemical Physics* **67**, 1237 (1977).
113. W. Xu, C. Xiao, Q. Li, Y. Xie, and H. F. Schaefer, *Molecular Physics* **102**, 1415 (2004).
114. J. A. Ruiz, A. Kivimäki, M. Stankiewicz, E. M. Garcia, M. Coreno, S. Ali, J. Koperski, E. Rachlew, G. Serrano, V. Feyer, and R. P. Tuckett, *Physical Chemistry and Chemical Physics* **8**, 5199 (2006).

115. D. A. Shaw, D. M. P. Holland, and I. C. Walker, *Journal of Physics B* **39**, 3549 (2006).
116. M. J. Simpson, R. P. Tuckett, K. F. Dunn, C. A. Hunniford, and C. J. Latimer, *Journal of Chemical Physics* **130**, 194302 (2009).
117. United Nations Environment Programme website (<http://ozone.unep.org/>), on 3 October 2008.
118. S. Solomon, J. B. Burkholder, A. R. Ravishankara, and R. R. Garcia, *Journal of Geophysical Research D* **99**, 20929 (1994).
119. L. G. Christophorou and J. K. Olthoff, *Journal of Physics and Chemical Reference Data* **29**, 553 (2000).
120. Y. Li, K. O. Patten, D. Youn, and D. J. Wuebbles, *Atmospheric Chemistry and Physics* **6**, 4559 (2006).
121. T. Cvitaš, H. Güsten, and L. Klasinc, *Journal of Chemical Physics* **67**, 2687 (1977).
122. R. Jadrny, L. Karlsson, L. Mattsson, and K. Siegbahn, *Physica Scripta* **16**, 235 (1977).
123. T. Cvitaš, H. Güsten, L. Klasinc, I. Novadj, and H. Vančik, *Zeitschrift für Naturforschung* **33A**, 1528 (1978).
124. J. Doucet, P. Sauvageau, and C. Sandorfy, *Journal of Chemical Physics* **58**, 3708 (1972).
125. J. C. Creasey, D. M. Smith, R. P. Tuckett, K. R. Yoxall, K. Codling, and P. A. Hatherly, *Journal of Physical Chemistry* **100**, 4350 (1996).
126. I. Powis, O. Dutult, M. Richard-Viard, and P. M. Guyon, *Journal of Chemical Physics* **92**, 1643 (1990).
127. R. Gilbert, P. Sauvageau, and C. Sandorfy, *Journal of Chemical Physics* **60**, 4820 (1974).
128. H. W. Jochims, W. Lohr, and H. Baumgärtel, *Berichte Bunsenges-Gesellschaft für Physikalische Chemie* **80**, 130 (1976).
129. G. C. King and McConkey, *Journal of Physics B* **11**, 1861 (1978).
130. J. W. Au, G. R. Burton, and C. E. Brion, *Chemical Physics* **221**, 151 (1997).
131. S. Eden, P. Limão-Vieira, S. V. Hoffmann, and N. J. Mason, *Chemical Physics* **323**, 313 (2006).
132. M. Hoshino, K. Sunohara, C. Makocheke, L. Pichl, H. Cho, and H. Tanaka, *Journal of Chemical Physics* **126**, 024303 (2007).
133. S. Ali, Ph.D. thesis, University of Birmingham, 2007.
134. H. Biehl, K. J. Boyle, R. P. Tuckett, H. Baumgärtel, and H. W. Jochims, *Chemical Physics* **214**, 367 (1997).
135. H. Schenk, H. Oertel, and H. Baumgärtel, *Berichte Bunsenges-Gesellschaft für Physikalische Chemie* **83**, 683 (1979).
136. D. R. Lide, *Handbook of Chemistry and Physics*, 88th ed. (Taylor & Francis, London, 2007), Section 10 page 194.
137. N. A. Macleod, S. Wang, J. Hennessy, T. Ridley, K. P. Lawley, and R. J. Donovan, *Journal of the Chemical Society, Faraday Transactions* **94**, 2689 (1998).
138. L. G. Christophorou, *Zeitschrift für Physikalische Chemie* **195**, 195 (1996).

139. S. Marienfield, T. Sunagawa, I. I. Fabrikant, M. Braun, M.-W. Ruf, and H. Hotop, *Journal of Chemical Physics* **124**, 154316 (2006).
140. S. Marienfield, I. I. Fabrikant, M. Braun, M.-W. Ruf, and H. Hotop, *Journal of Physics B* **39**, 105 (2006).
141. D. R. Lide, *Handbook of Chemistry and Physics*, 88th ed. (Taylor & Francis, London, 2007), Section 9 page 63.
142. H. J. Deyerl, L. S. Alconcel, and R. E. Continetti, *Journal of Physical Chemistry A* **105**, 552 (2001).
143. M. W. Chase, *Journal of Physics and Chemical Reference Data, Monograph no. 9* (1998).
144. C. Blondel, C. Delsart, and F. Goldfarb, *Journal of Physics B* **34**, L281 (2001).
145. M. J. Simpson and R. P. Tuckett, *Journal of Physical Chemistry A* **114**, 8043 (2010).
146. C. W. Tullock, D. D. Coffman, and E. L. Muetterties, *Journal of the American Chemical Society* **86**, 357 (1964).
147. U. Jonethal, R. Kuschel, and K. Seppelt, *Journal of Fluorine Chemistry* **88**, 3 (1998).
148. J. Bellet, R. Jurek, and J. Chanussot, *Journal of Molecular Spectroscopy* **78**, 16 (1979).
149. C. J. Marsden and L. S. Bartell, *Inorganic Chemistry* **15**, 3004 (1976).
150. C. A. Mayhew, A. Critchley, and G. K. Jarvis, *International Journal of Mass Spectrometry* **233**, 259 (2004).
151. M. Braun, M.-W. Ruf, H. Hotop, C. Cicman, P. Scheier, T. D. Märk, E. Illenberger, R. P. Tuckett, and C. A. Mayhew, *International Journal of Mass Spectrometry* **252**, 234 (2006).
152. J. M. Van Doren, T. M. Miller, A. A. Viggiano, P. Spanel, D. Smith, C. Bopp, and J. Troe, *Journal of Chemical Physics* **128**, 094309 (2008).
153. R. L. DeKock, B. R. Higginson, and D. R. Lloyd, *Faraday Discussions* **54**, 84 (1972).
154. A. P. Klyagina, A. A. Levin, and G. L. Gutzev, *Chemical Physics Letters* **77**, 365 (1981).
155. R. Y. L. Chim, C. Cicman, T. D. Märk, C. A. Mayhew, P. Scheier, and R. P. Tuckett, *International Journal of Mass Spectrometry* **261**, 208 (2007).
156. D. M. P. Holland, M. A. MacDonald, P. Baltzer, L. Karlsson, M. Lundqvist, B. Wannberg, and W. Von Niessen, *Chemical Physics* **192**, 333 (1995).
157. R. P. Tuckett and M. A. Parkes, private communication (February 2010).
158. J. W. Rabalais, T. Bergmark, L. O. Werme, L. Karlsson, and K. Siegbahn, *Physica Scripta* **3**, 13 (1971).
159. A. W. Potts and W. C. Price, *Proceedings of the Royal Society A* **326**, 165 (1972).
160. J. Berkowitz, *Atomic and Molecular Photoabsorption: Absolute Total Cross Sections* (Academic Press, London, 2002), p 268.
161. G. Bieri and L. Åsbrink, *Journal of Electron Spectroscopy and Related Phenomena* **20**, 149 (1980).
162. G. K. Jarvis, K. J. Boyle, C. A. Mayhew, and R. P. Tuckett, *Journal of Physical Chemistry A* **102**, 3219 (1998).



163. L. Karlsson, R. Jadrny, L. Mattsson, F. T. Chau, and K. Siegbahn, *Physica Scripta* **16**, 225 (1977).
164. T. Pradeep and D. A. Shirley, *Journal of Electron Spectroscopy and Related Phenomena* **66**, 125 (1993).
165. C. R. Brundle, M. B. Robin, and H. Basch, *Journal of Chemical Physics* **53**, 2196 (1970).
166. A. F. Lago, J. P. Kercher, A. Bödi, B. Sztáray, B. Miller, D. Wurzelmann, and T. Baer, *Journal of Physical Chemistry A* **109**, 1802 (2005).
167. D. P. Secombe, R. Y. L. Chim, G. K. Jarvis, and R. P. Tuckett, *Physical Chemistry and Chemical Physics* **2**, 769 (2000).
168. J. Harvey, N. J. Rogers, R. P. Tuckett, *TPES of CCl<sub>4</sub> recorded at the SLS, PSI Villigen*, **unpublished data** (2009).
169. R. Locht, B. Leyh, D. Dehareng, K. Hottmann, H. W. Jochims, and H. Baumgärtel, *Chemical Physics* **323**, 458 (2006).
170. J. Berkowitz, *Atomic and Molecular Photoabsorption: Absolute Total Cross Sections* (Academic Press, London, 2002), p263.
171. K. Kameta, S. Machida, M. Kitajima, M. Ukai, N. Kouchi, Y. Hatano, and K. Ito, *Journal of Electron Spectroscopy and Related Phenomena* **79**, 391 (1996).
172. D. P. Secombe, R. Y. L. Chim, R. P. Tuckett, H. W. Jochims, and H. Baumgärtel, *Journal of Chemical Physics* **114**, 4058 (2001).
173. R. Y. L. Chim, Ph.D. thesis, University of Birmingham, 2003.
174. N. Secombe and R. P. Tuckett, *Absorption cross section for CHCl<sub>3</sub> and CFCl<sub>3</sub>*, **unpublished data** (1998).
175. S. J. Burns, J. M. Matthews, and D. L. McFadden, *Journal of Physical Chemistry* **100**, 19436 (1996).
176. D. Klar, M.-W. Ruf, I. I. Fabrikant, and H. Hotop, *Journal of Physics B* **34**, 3855 (2001).
177. K. Mitsuke, S. Suzuki, T. Imamura, and I. Koyano, *Journal of Chemical Physics* **94**, 6003 (1991).
178. S. Suzuki, K. Mitsuke, T. Imamura, and I. Koyano, *Journal of Chemical Physics* **96**, 7500 (1992).
179. R. A. Mackie, S. W. J. Scully, A. M. Sands, R. Browning, K. F. Dunn, and C. J. Latimer, *International Journal of Mass Spectrometry* **223-224**, 67 (2003).
180. K. Mitsuke, H. Hattori, and H. Yoshida, *Journal of Chemical Physics* **99**, 6642 (1993).
181. R. A. Mackie, A. M. Sands, S. W. J. Scully, D. M. P. Holland, D. A. Shaw, K. F. Dunn, and C. J. Latimer, *Journal of Physics B* **35**, 1061 (2002).
182. D. F. Shriver and P. W. Atkins, *Inorganic Chemistry Third Edition* (Oxford University Press, Oxford, 1999), p31.
183. D. P. Secombe, R. P. Tuckett, and B. O. Fisher, *Journal of Chemical Physics* **114**, 4074 (2001).

# Appendix I:

## *Enthalpies of formation*

a.m.u	Species	$\Delta_f H^\circ_{298} / \text{kJ mol}^{-1}$	Source(s)
<i>Neutrals</i>			
1	H	$+217.99 \pm 0.006$	Ref. <i>a</i>
13	CH	$+594.1 \pm 17.5$	Ref. <i>a</i>
14	CH <sub>2</sub>	$+386.4 \pm 4.2$	Ref. <i>a</i>
16	CH <sub>4</sub>	$-74.87 \pm 0.34$	Ref. <i>a</i>
16	O	$+249.17 \pm 0.10$	Ref. <i>a</i>
17	OH	$+38.99 \pm 1.21$	Ref. <i>a</i>
18	H <sub>2</sub> O	$-241.83 \pm 0.04$	Ref. <i>a</i>
19	F	$+79.4 \pm 0.3$	Ref. <i>a</i>
20	HF	$-272.5 \pm 0.8$	Ref. <i>a</i>
26	C <sub>2</sub> H <sub>2</sub>	$+228 \pm 1$	Ref. <i>b</i>
28	CO	$-110.5 \pm 0.2$	Ref. <i>a</i>
28	C <sub>2</sub> H <sub>4</sub>	$+52.47 \pm 0.29$	Ref. <i>a</i>
30	C <sub>2</sub> H <sub>6</sub>	$-84.0 \pm 0.2$	Ref. <i>b</i>
30	CH <sub>2</sub> O	$-115.90 \pm 6.3$	Ref. <i>a</i>
31	CF	$+255.2 \pm 8$	Ref. <i>a</i>
32	CHF	$+125.5 \pm 29$	Ref. <i>a</i>
33	HO <sub>2</sub>	$+2.09 \pm 8.4$	Ref. <i>a</i>
34	CH <sub>3</sub> F	$-247$	Ref. <i>b</i>
35	OF	$+109.9$	Ref. <i>k</i>
35.5	Cl	$+121.30 \pm 0.01$	Ref. <i>a</i>
44	C <sub>3</sub> H <sub>8</sub>	$-104.5 \pm 0.3$	Ref. <i>b</i>
44	CO <sub>2</sub>	$-393.52 \pm 0.05$	Ref. <i>a</i>
44	C <sub>2</sub> HF	$+107$	Ref. <i>b</i>
44	C <sub>2</sub> H <sub>4</sub> O		
44	CH <sub>2</sub> =CHOH	$-125$	Ref. <i>b</i>
44	CH <sub>3</sub> CHO	$-165.8 \pm 0.4$	Ref. <i>b</i>
44	<i>c</i> -CH <sub>2</sub> (O)CH <sub>2</sub>	$-52.6 \pm 0.6$	Ref. <i>b</i>
45	HC(O)O	$-132.98$	Ref. <i>k</i>
46	C <sub>2</sub> H <sub>3</sub> F	$-138.8 \pm 1.7$	Ref. <i>b</i>

a.m.u	Species	$\Delta_f H^\circ_{298} / \text{kJ mol}^{-1}$	Source(s)
47	FCO	$-171.5 \pm 63$	Ref. <i>a</i>
47.5	CCl	$+502.1 \pm 20$	Ref. <i>a</i>
48	HFCO	$-376.56$	Ref. <i>a</i>
50	CF <sub>2</sub>	$-182 \pm 6.3$	Ref. <i>a</i>
50.5	CH <sub>3</sub> Cl	$-83.68$	Ref. <i>a</i>
51	CHF <sub>2</sub>	$-237 \pm 5$	Ref. <i>b</i>
51	SF	$+3.0$	Ref. <i>p</i>
52	CH <sub>2</sub> F <sub>2</sub>	$-450.66 \pm 1.7$	Ref. <i>a</i>
54.5	FCl	$-50.292 \pm 0.42$	Ref. <i>a</i>
62	C <sub>2</sub> F <sub>2</sub>	$+20.9 \pm 21$	Ref. <i>a</i>
64	C <sub>2</sub> H <sub>2</sub> F <sub>2</sub> (1,1)	$-345 \pm 10$	Ref. <i>b</i>
64	C <sub>2</sub> H <sub>2</sub> F <sub>2</sub> (Z -1,2)	$-297$	Ref. <i>b</i>
64	C <sub>2</sub> H <sub>2</sub> F <sub>2</sub> (E-1,2)	$-293$	Ref. <i>b</i>
66	CF <sub>2</sub> O	$-638.9 \pm 1.7$	Ref. <i>a</i>
69	CF <sub>3</sub>	$-465.7 \pm 2.1$	Ref. <i>e</i>
70	CHF <sub>3</sub>	$-697.1 \pm 3.3$	Ref. <i>a</i>
70	SF <sub>2</sub>	$-295.2$	Ref. <i>p</i>
78	CF <sub>2</sub> CO	$-290.3 \pm 13.2$	Ref. <i>n</i>
80	Br	$+111.86 \pm 0.06$	Ref. <i>a</i>
82	C <sub>2</sub> HF <sub>3</sub>	$-491 \pm 8$	Ref. <i>b</i>
83	CCl <sub>2</sub>	$+238.5 \pm 21$	Ref. <i>a</i>
85	CH <sub>2</sub> Cl <sub>2</sub>	$-95.52$	Ref. <i>a</i>
85	CF <sub>3</sub> O	$-630.56$	Ref. <i>k</i>
88	CF <sub>4</sub>	$-933.2 \pm 1.3$	Ref. <i>a</i>
89	SF <sub>3</sub>	$-441.6$	Ref. <i>p</i>
94	FCOCOF	$-728$	Ref. <i>b</i>
95	CH <sub>3</sub> Br	$-34.3 \pm 0.8$	Ref. <i>h</i>
97	CF <sub>3</sub> CO	$-608.68$	Ref. <i>k</i>
98	CF <sub>3</sub> CHO	$-778.47$	Ref. <i>k</i>
99	FBr	$-58.463 \pm 1.7$	Ref. <i>a</i>
100	C <sub>2</sub> F <sub>4</sub>	$-658.6 \pm 2.9$	Ref. <i>a</i>
101	CF <sub>3</sub> OO	$-635.02$	Ref. <i>k</i>
104	CF <sub>3</sub> OF	$-785$	Ref. <i>b</i>
104.5	CF <sub>3</sub> Cl	$-709.2 \pm 3$	Ref. <i>e</i>
108	SF <sub>4</sub>	$-768.4$	Ref. <i>p</i>
119.5	CHCl <sub>3</sub>	$-103.18 \pm 1.3$	Ref. <i>a</i>
121	CF <sub>2</sub> Cl <sub>2</sub>	$-491.6 \pm 8$	Ref. <i>a</i>
127	SF <sub>5</sub>	$-908$	Ref. <i>a</i>
127	I	$+106.76 \pm 0.04$	Ref. <i>a</i>

a.m.u	Species	$\Delta_f H^\circ_{298} / \text{kJ mol}^{-1}$	Source(s)
137.5	CFCl <sub>3</sub>	$-288.7 \pm 6.3$	Ref. <i>a</i>
138	C <sub>2</sub> F <sub>6</sub>	-1343	Ref. <i>b</i>
143.5	SF <sub>4</sub> Cl	-761	Ref. <i>y</i>
146	SF <sub>6</sub>	$-1220.47 \pm 0.8$	Ref. <i>a</i>
146	FI	-94.76	Ref. <i>s</i>
149	CF <sub>3</sub> Br	$-649.8 \pm 2$	Ref. <i>e</i>
150	C <sub>3</sub> F <sub>6</sub>	-1125	Ref. <i>b</i>
154	CCl <sub>4</sub>	$-95.98 \pm 2.1$	Ref. <i>a</i>
162.5	SF <sub>5</sub> Cl	$-1038.9 \pm 10.5$	Ref. <i>a</i>
188	C <sub>3</sub> F <sub>8</sub>	$-1783 \pm 7$	Ref. <i>b</i>
196	SF <sub>5</sub> CF <sub>3</sub>	$-1717.1 \pm 63$	Ref. <i>a</i>
196	CF <sub>3</sub> I	$-586.2 \pm 2$	Ref. <i>e</i>
<i>Cations</i>			
1	H <sup>+</sup>	+1536.25	Ref. <i>a</i>
13	CH <sup>+</sup>	+1622	Ref. <i>b</i>
14	CH <sub>2</sub> <sup>+</sup>	+1386	Ref. <i>b</i>
15	CH <sub>3</sub> <sup>+</sup>	+1098	Ref. <i>b</i>
19	F <sup>+</sup>	+1760.6	Ref. <i>a</i>
27	C <sub>2</sub> H <sub>3</sub> <sup>+</sup>	+1112	Ref. <i>b</i>
28	C <sub>2</sub> H <sub>4</sub> <sup>+</sup>	+1066	Ref. <i>b</i>
29	C <sub>2</sub> H <sub>5</sub> <sup>+</sup>	$+914 \pm 4$	Ref. <i>b</i>
31	CF <sup>+</sup>	$+1149.4 \pm 5$	Ref. <i>a</i>
33	CH <sub>2</sub> F <sup>+</sup>	+833	Ref. <i>b</i>
35.5	Cl <sup>+</sup>	+1372.6	Ref. <i>a</i>
38	F <sub>2</sub> <sup>+</sup>	+1514	Ref. <i>s</i> <sup>s</sup>
39	C <sub>3</sub> H <sub>3</sub> <sup>+</sup>	+1179	Ref. <i>b</i>
43	<i>n</i> -C <sub>3</sub> H <sub>7</sub> <sup>+</sup>	+881	Ref. <i>b</i>
45	C <sub>2</sub> H <sub>2</sub> F <sup>+</sup>	+951	Ref. <i>b</i>
46	C <sub>2</sub> H <sub>3</sub> F <sup>+</sup>	+861.1	Ref. <i>b</i>
47.5	CCl <sup>+</sup>	+1311	Ref. <i>r</i>
49.5	CH <sub>2</sub> Cl <sup>+</sup>	+959	Ref. <i>b</i>
50	CF <sub>2</sub> <sup>+</sup>	$+941.8 \pm 12.6$	Ref. <i>a</i>
51	CHF <sub>2</sub> <sup>+</sup>	+611	Ref. <i>b</i>
51	SF <sup>+</sup>	+998.3	Ref. <i>p</i>
54.5	FCI <sup>+</sup>	$+1171 \pm 2$	Ref. <i>a</i> and <i>s</i> <sup>Ω</sup>
64	C <sub>2</sub> H <sub>2</sub> F <sub>2</sub> <sup>+</sup> (1,1)	+648	Ref. <i>b</i>
64	C <sub>2</sub> H <sub>2</sub> F <sub>2</sub> <sup>+</sup> (Z -1,2)	+690	Ref. <i>b</i>
64	C <sub>2</sub> H <sub>2</sub> F <sub>2</sub> <sup>+</sup> (E-1,2)	+692	Ref. <i>b</i>
66.5	CFCl <sup>+</sup>	+1101	Ref. <i>r</i>

a.m.u	Species	$\Delta_f H^\circ_{298} / \text{kJ mol}^{-1}$	Source(s)
69	$\text{CF}_3^+$	+406	Ref. <i>c</i>
70	$\text{SF}_2^+$	+693.4	Ref. <i>p</i>
80	$\text{Br}^+$	+1250.9	Ref. <i>a</i>
81	$\text{C}_2\text{F}_3^+$	+791	Ref. <i>b</i>
82	$\text{C}_2\text{HF}_3^+$	+487	Ref. <i>b</i>
83	$\text{CCl}_2^+$	+1163	Ref. <i>b</i>
84	$\text{CHCl}_2^+$	+887	Ref. <i>b</i>
85.5	$\text{CF}_2\text{Cl}^+$	+526	Ref. <i>w</i>
89	$\text{SF}_3^+$	+361.1	Ref. <i>p</i>
94	$\text{CH}_2\text{Br}^+$	+937	Ref. <i>b</i>
99	$\text{FBr}^+$	+1086 $\pm$ 2	Ref. <i>a</i> and <i>s</i> <sup><i>c</i></sup>
100	$\text{C}_2\text{F}_4^+$	+316	Ref. <i>b</i>
102	$\text{CFCl}_2^+$	+703	Ref. <i>b</i>
108	$\text{SF}_4^+$	+389.3	Ref. <i>p</i>
118.5	$\text{CCl}_3^+$	+831	Ref. <i>b</i>
119	$\text{C}_2\text{F}_5^+$	15.0	Ref. <i>l</i>
127	$\text{SF}_5^+$	+29	Ref. <i>q</i>
127	$\text{I}^+$	+1115.2	Ref. <i>a</i>
130	$\text{CF}_2\text{Br}^+$	$\leq$ +570	Ref. <i>x</i>
138	$\text{C}_2\text{F}_6^+$	-99.9	Ref. <i>l</i>
146	$\text{FI}^+$	+922.1	Ref. <i>s</i> <sup><i>!</i></sup>
143.5	$\text{SF}_4\text{Cl}^+$	$\leq$ +327	Ref. <i>q</i>
169	$\text{C}_3\text{F}_7^+$	-358.1	Ref. <i>l</i>
177	$\text{CF}_2\text{I}^+$	$\leq$ +598 $\pm$ 22	Ref. <i>t</i> <sup><i>£</i></sup>
196	$\text{CF}_3\text{I}^+$	+414.5 $\pm$ 2	Refs. <i>e</i> and <i>u</i> <sup><i>#</i></sup>
<i>Anions</i>			
1	$\text{H}^-$	+145	Ref. <i>b</i>
13	$\text{CH}^-$	+477 $\pm$ 27	Ref. <i>b</i>
16	$\text{O}^-$	+101.85	Ref. <i>a</i>
17	$\text{OH}^-$	-143.6 $\pm$ 3.8	Ref. <i>a</i>
19	$\text{F}^-$	-248.7 $\pm$ 0.3	Refs. <i>a</i> and <i>d</i> <sup><i>†</i></sup>
26	$\text{H}_2\text{C}=\text{C}^-$	+385 $\pm$ 15	Ref. <i>h</i>
27	$\text{C}_2\text{H}_3^-$	+221 $\pm$ 9	Ref. <i>b</i>
31	$\text{CF}^-$	-63 $\pm$ 106	Ref. <i>a</i> and <i>v</i> <sup><i>‡</i></sup>
32	$\text{O}_2^-$	-48.59	Ref. <i>a</i>
35.5	$\text{Cl}^-$	-227.27 $\pm$ 0.01	Ref. <i>a</i> and <i>m</i> <sup><i>%</i></sup>
37	$\text{F}^-\cdots\text{H}_2\text{O}$	-605.8	Ref. <i>g</i>
38	$\text{F}_2^-$	-301 $\pm$ 7	Ref. <i>j</i> <sup><i>§</i></sup>
39	$\text{HF}_2^-$	-683 $\pm$ 11	Ref. <i>b</i>

a.m.u	Species	$\Delta_f H^\circ_{298} / \text{kJ mol}^{-1}$	Source(s)
43	$\text{CH}_2=\text{CHO}^-$	$-165 \pm 13$	Ref. <i>b</i>
43	$\text{CH}_3\text{CO}^-$	$-60 \pm 11$	Ref. <i>b</i>
44	$\text{HFC}=\text{C}^-$	$+92 \pm 21$	Ref. <i>i</i>
47	$\text{FCO}^-$	$-435$	Ref. <i>b</i>
50	$\text{CF}_2^-$	$-199 \pm 6$	Ref. <i>a</i> and <i>m</i> <sup>Ⓟ</sup>
51	$\text{SF}^-$	$-224.4$	Ref. <i>p</i>
62	$\text{F}_2\text{C}=\text{C}^-$	$-75 \pm 50$	Ref. <i>i</i>
69	$\text{CF}_3^-$	$-641.3 \pm 5.2$	Refs. <i>e</i> and <i>f</i> <sup>*</sup>
70	$\text{Cl}_2^-$	$-229.6 \pm 9.7$	Ref. <i>m</i> <sup>^</sup>
70	$\text{SF}_2^-$	$-431.7$	Ref. <i>p</i>
80	$\text{Br}^-$	$-212.68 \pm 0.06$	Ref. <i>a</i> and <i>m</i> <sup>π</sup>
81	$\text{C}_2\text{F}_3^-$	$-504$	Ref. <i>l</i> and <i>m</i> <sup>‡</sup>
89	$\text{SF}_3^-$	$-742.7$	Ref. <i>p</i>
108	$\text{SF}_4^-$	$-907.2$	Ref. <i>p</i>
119	$\text{C}_2\text{F}_5^-$	$-1067 \pm 23$	Ref. <i>b</i>
127	$\text{I}^-$	$-188.39 \pm 0.04$	Ref. <i>a</i> and <i>m</i> <sup>Ⓜ</sup>

## Footnotes:

\* The value of  $-641.3 \pm 5.2 \text{ kJ mol}^{-1}$  uses the  $\Delta_f H^\circ_{298}(\text{CF}_3) = -465.7 \pm 2.1 \text{ kJ mol}^{-1}$  from Ref. *e* and the electron affinity of  $\text{CF}_3 = +1.82 \pm 0.05 \text{ eV}$  ( $+175.6 \pm 4.8 \text{ kJ mol}^{-1}$ ) from Ref. *f*.

† The value of  $-248.7 \pm 0.3 \text{ kJ mol}^{-1}$  uses the  $\Delta_f H^\circ_{298}(\text{F}) = +79.4 \pm 0.3 \text{ kJ mol}^{-1}$  from Ref. *a* and the electron affinity of  $\text{F} = +3.401 \text{ eV}$  ( $+328.1 \text{ kJ mol}^{-1}$ ) from Ref. *d*.

§ The value of  $-301 \text{ kJ mol}^{-1}$  is taken directly from the value for the electron affinity of  $\text{F}_2$ ,  $3.12 \pm 0.07 \text{ eV}$ , reported in Ref. *j*.

‡ This value uses  $\Delta_f H^\circ(\text{C}_2\text{F}_3) = -224 \text{ kJ mol}^{-1}$  from Ref. *l* and the electron affinity of  $\text{C}_2\text{F}_3 = 2.90 \text{ eV}$  ( $+280 \text{ kJ mol}^{-1}$ ) from Ref. *m*. Both values were chosen from a range of available data based on experimental results from proton abstraction reaction with  $\text{C}_2\text{HF}_3$  (see Chapter 5).

! This value uses the  $\Delta_f H^\circ_{298}(\text{FI}) = -94.76$  from Ref. *s*, and the ionisation energy of  $\text{FI} = 10.54 \text{ eV}$  ( $+1017 \text{ kJ mol}^{-1}$ ) from Ref. *s*.

§ This value is taken directly as the ionisation energy for  $\text{F}_2$ ,  $15.697 \pm 0.003 \text{ eV}$  (Ref. *s*).

£ This value is derived from the experimental appearance energy of  $\text{F}^-$  anions following the photoexcitation of  $\text{CF}_3\text{I}$ . In addition to the reference provided, the derivation of this value can be found in Chapter 7 of this thesis.

# This value combines the  $\Delta_f H^\circ_{298}(\text{CF}_3\text{I}) = -586.2 \pm 2 \text{ kJ mol}^{-1}$  from Ref. *e*, and the ionisation energy of  $\text{CF}_3\text{I} = 83652 \pm 2 \text{ cm}^{-1}$  ( $10.37 \text{ eV}$  or  $1000.7 \text{ kJ mol}^{-1}$ ) from Ref. *u*.

£ This value combines the  $\Delta_f H^\circ_{298}(\text{FBr}) = -58.463 \pm 1.7 \text{ kJ mol}^{-1}$  from Ref. *a*, and the ionisation energy of  $\text{FBr} = 11.86 \text{ eV}$  ( $1144.3 \text{ kJ mol}^{-1}$ ) from Ref. *s*.

Ω This value combines the  $\Delta_f H^\circ_{298}(\text{FCl}) = -50.292 \pm 0.42 \text{ kJ mol}^{-1}$  from Ref. *a*, and the ionisation energy of  $\text{FCl} = 12.66 \pm 0.01 \text{ eV}$  ( $1221.5 \text{ kJ mol}^{-1}$ ) from Ref. *s*.

Ⓟ The value of  $-199 \pm 6 \text{ kJ mol}^{-1}$  uses the  $\Delta_f H^\circ_{298}(\text{CF}_2) = -182 \pm 6.3 \text{ kJ mol}^{-1}$  from Ref. *a* and the electron affinity of  $\text{CF}_2 = +0.179 \pm 0.005 \text{ eV}$  ( $+17.3 \text{ kJ mol}^{-1}$ ) from Ref. *m*.

τ This value uses the  $\Delta_f H^\circ_{298}(\text{CF}) = +255.2 \pm 8 \text{ kJ mol}^{-1}$  from Ref. *a* and the electron affinity of  $\text{CF} = +3.3 \pm 1.1 \text{ eV}$  ( $+318 \pm 106 \text{ kJ mol}^{-1}$ ) from Ref. *v*.

% This value uses the  $\Delta_f H^\circ_{298}(\text{Cl}) = +121.3 \pm 0.01 \text{ kJ mol}^{-1}$  from Ref. *a* and the electron affinity of  $\text{Cl} = +3.612724 \pm 0.00003 \text{ eV}$  ( $+348.57 \pm 0.005 \text{ kJ mol}^{-1}$ ) from Ref. *m*.

π This value uses the  $\Delta_f H^\circ_{298}(\text{Br}) = +111.86 \pm 0.06 \text{ kJ mol}^{-1}$  from Ref. *a* and the electron affinity of  $\text{Br} = +3.363588 \pm 0.000006 \text{ eV}$  ( $+324.54 \pm 0.0006 \text{ kJ mol}^{-1}$ ) from Ref. *m*.

Ⓜ This value uses the  $\Delta_f H^\circ_{298}(\text{I}) = +106.76 \pm 0.04 \text{ kJ mol}^{-1}$  from Ref. *a* and the electron affinity of  $\text{I} = +3.059038 \pm 0.00001 \text{ eV}$  ( $+295.15 \pm 0.001 \text{ kJ mol}^{-1}$ ) from Ref. *m*.

---

---

<sup>A</sup> Taken directly from the value for the electron affinity of Cl<sub>2</sub>,  $2.38 \pm 0.10$  eV, reported in Ref. *m*.

*References:*

- <sup>a</sup> M. W. Chase, *J. Phys. Chem. Ref. Data Monograph* 9, 1 (1998).
- <sup>b</sup> S. G. Lias, J. E. Bartmess, J. F. Liebman, J. L. Holmes, R. D. Levin, and W. G. Mallard, *J. Phys. Chem. Ref. Data* **17**, 1 (1988).
- <sup>c</sup> G.A. Garcia, P. M. Guyon, and I. Powis, *J. Phys. Chem. A* **105**, 8296 (2001).
- <sup>d</sup> C. Blondel, C. Delsart, and F. Goldfarb, *J. Phys. B: At. Mol. Opt. Phys.* **34**, L281 (2001).
- <sup>e</sup> B. Ruscic, J. Michael, P. Redfern, L. Curtiss, and K. Raghavachari, *J. Phys. Chem. A* **102**, 10889 (1998).
- <sup>f</sup> H.-J. Deyerl, L. Alconcel, and R. Continetti, *J. Phys. Chem. A* **105**, 552 (2001).
- <sup>g</sup> NIST Chemistry Webbook, <http://webbook.nist.gov/chemistry/>, on 26.08.09.
- <sup>h</sup> NIST Chemistry Webbook, <http://webbook.nist.gov/chemistry/>, on 30.09.09.
- <sup>i</sup> NIST Chemistry Webbook, <http://webbook.nist.gov/chemistry/>, on 30.09.09, from the work of Heni and Illenberger, *J. Elec. Spec. Rel. Phen.* **41**, 453 (1986).
- <sup>j</sup> A. Artau, K. E. Nizzi, B. T. Hill, L. S. Sunderlin, and P. G. Wenthold, *J. Am. Chem. Soc.* **122**, 10667 (2000).
- <sup>k</sup> R. Janoschek and M. Rossi, *Int. J. Chemical Kinetics* **36**, 661 (2004).
- <sup>l</sup> C. W. Bauschlicher and A. Ricca, *J. Phys. Chem. A* **104**, 4581 (2000).
- <sup>m</sup> J. C. Rienstra-Kiracofe, G. S. Tschumper, H. F. Schaefer, S. Nandi and B. Ellison, *Chemical Reviews* **102**, 231 (2002).
- <sup>n</sup> D. F. Dawson and J. L. Holmes, *J. Phys. Chem. A* **103**, 5217 (1999).
- <sup>p</sup> C. W. Bauschlicher and A. Ricca, *J. Phys. Chem. A* **102**, 4722 (1998).
- <sup>q</sup> R. Y. L. Chim, P. Cicman, T. D. Märk, C. A. Mayhew, P. Scheier, and R. P. Tuckett, *Int. J. Mass Spectrom.* **261**, 208 (2007).
- <sup>r</sup> H. Schenk, H. Oertel, and H. Baumgärtel, *Ber. Bunsenges. Phys. Chem.* **83**, 683 (1979).
- <sup>s</sup> NIST Chemistry Webbook, <http://webbook.nist.gov/chemistry/>, on 16.12.09.
- <sup>t</sup> M.J. Simpson, R. P. Tuckett, K. F. Dunn, C. A. Hunniford, and C. J. Latimer, *J. Chem. Phys.* **130**, 194302 (2009).
- <sup>u</sup> N. A. Macleod, S. Wang, J. Hennessy, T. Ridley, K. P. Lawley, and R. J. Donovan, *J. Chem. Soc., Faraday Trans.* **94**, 2689 (1998).
- <sup>v</sup> J. C. J. Thynne and K. A. G. MacNeil, *Int. J. Mass Spectrom. Ion Phys.* **5**, 329 (1970).
- <sup>w</sup> J. C. Creasey, D. M. Smith, R. P. Tuckett, and K. R. Yoxall, *J. Phys. Chem.* **100**, 4350 (1996).
- <sup>x</sup> D. P. Secombe, R. P. Tuckett, and B. O. Fisher, *J. Chem. Phys.* **114**, 4074 (2001).
- <sup>y</sup> M. Braun *et al.*, *Int. J. Mass Spectrom.* **252**, 234 (2006).
- 
-

## Appendix II:

### *Measuring the neutral reactant concentration in a Selected Ion Flow Tube experiment*

The neutral reactant gas,  $B$ , is passed through a capillary prior to it entering the flow tube. The flow of  $B$  through the capillary is viscous, and the corresponding flow rate of  $B$  can therefore be determined by applying Poiseuille's law:

$$Q_B = \frac{\pi a^4}{8\eta_{He}L} p_c \Delta p \quad \text{A.II.(1)}$$

where  $Q_B$  is the flow rate of reactant gas  $B$  in units of  $\text{Pa m}^3 \text{s}^{-1}$ ,  $a$  and  $L$  are the radius and length of the capillary in m, respectively,  $\eta_{He}$  is the viscosity of helium in  $\text{Pa s}$ ,  $p_c$  is the pressure in Pa at the centre of the capillary, and  $\Delta p$  is the pressure drop across the capillary, in Pa. The pressure into the capillary,  $p_{in}$ , and  $\Delta p$  are measured directly by transducers, and so  $p_c$  can be calculated as follows:

$$p_c = p_{in} - \frac{\Delta p}{2} \quad \text{A.II.(2)}$$

Different gases have different viscosities, which is taken into account by dividing the flow rate,  $Q_B$ , by the ratio of the viscosity of  $B$  with that of helium. This viscosity ratio is defined as  $\eta_r$ . After passing through the capillary the reactant  $B$  enters the flow tube and will be diluted, so the fraction of the bulk gas in the flow tube which reactant  $B$  contributes must be calculated.  $Q_B$  is therefore divided by the helium carrier gas flow rate,  $Q_{He}$ , as measured



by a flowmeter. Thus, the amount of  $B$  as a fraction of the total bulk gas in the flow tube is given by:

$$\frac{Q_B}{\eta_r Q_{He}} \cdot \frac{293.2}{T_B} \quad \text{A.II.(3)}$$

where  $T_B$  is the absolute temperature of reactant gas  $B$ , and 293.2 is the absolute temperature at which the flowmeter measuring  $Q_{He}$  is calibrated. Essentially,  $Q_B$  is divided by  $T_B$  and  $Q_{He}$  is divided by 293.2, allowing for temperature normalisation.

Using the ideal gas law, 1 Pa of gas pressure at 273.2 K is shown to be equivalent to  $2.651 \times 10^{14}$  molecules  $\text{cm}^{-3}$ . Knowing the pressure in the flow tube,  $p_{tube}$ , and adding an additional temperature normalisation term, the absolute concentration in molecules  $\text{cm}^{-3}$ ,  $[B]$ , can be calculated:

$$[B] = \frac{Q_B}{\eta_r Q_{He}} \cdot \frac{293.2}{T_B} \cdot 2.651 \times 10^{14} \cdot p_{tube} \cdot \frac{273.2}{T_{tube}} \quad \text{A.II.(4)}$$

## Appendix III:

*Results obtained from the reactions of some cations with the fluorinated ethenes using a Selected Ion Flow Tube*

Cation <sup>a</sup>	C <sub>2</sub> H <sub>3</sub> F <sup>b</sup>	CH <sub>2</sub> CF <sub>2</sub> <sup>b</sup>	C <sub>2</sub> HF <sub>3</sub> <sup>b</sup>
<b>Ne<sup>+</sup></b> (21.56)	$k_{\text{exp}} = 2.2 \times 10^{-9}$ $k_{\text{c}} = 2.3 \times 10^{-9}$	$k_{\text{exp}} = 2.0 \times 10^{-9}$ $k_{\text{c}} = 2.2 \times 10^{-9}$	$k_{\text{exp}} = 2.0 \times 10^{-9}$ $k_{\text{c}} = 2.0 \times 10^{-9}$
	C <sub>2</sub> H <sub>2</sub> <sup>+</sup> (60 %)	CF <sup>+</sup> (34 %)	CF <sup>+</sup> (60 %)
	C <sub>2</sub> HF <sup>+</sup> (13 %)	C <sub>2</sub> HF <sup>+</sup> (25 %)	C <sub>2</sub> HF <sub>2</sub> <sup>+</sup> (13 %)
	C <sub>2</sub> H <sub>3</sub> <sup>+</sup> (11 %)	C <sub>2</sub> H <sub>2</sub> <sup>+</sup> (18 %)	CF <sub>2</sub> <sup>+</sup> (11 %)
	CF <sup>+</sup> (4 %)	CH <sub>2</sub> <sup>+</sup> (13 %)	C <sub>2</sub> HF <sup>+</sup> (7 %)
	CHF <sup>+</sup> (4 %)	C <sub>2</sub> H <sub>2</sub> F <sup>+</sup> (8 %)	CHF <sup>+</sup> (7 %)
	C <sub>2</sub> H <sub>2</sub> F <sup>+</sup> (3 %)	CF <sub>2</sub> <sup>+</sup> (2 %)	CHF <sub>2</sub> <sup>+</sup> (1 %)
	C <sub>2</sub> H <sub>3</sub> F <sup>+</sup> (2 %)		C <sub>2</sub> F <sup>+</sup> (1 %)
	C <sub>2</sub> H <sup>+</sup> (2 %)		
	CH <sub>2</sub> F <sup>+</sup> (1 %)		
<b>F<sup>+</sup></b> (17.42)	No data collected	$k_{\text{exp}} = 2.4 \times 10^{-9}$ $k_{\text{c}} = 2.3 \times 10^{-9}$	$k_{\text{exp}} = 2.5 \times 10^{-9}$ $k_{\text{c}} = 2.1 \times 10^{-9}$
		C <sub>2</sub> H <sub>2</sub> F <sup>+</sup> (45 %)	Products not identified
		CH <sub>2</sub> F <sup>+</sup> (28 %)	
		CF <sup>+</sup> (18 %)	
		C <sub>2</sub> HF <sub>2</sub> <sup>+</sup> (5 %)	
		C <sub>2</sub> H <sub>2</sub> F <sub>2</sub> <sup>+</sup> (4 %)	
<b>Ar<sup>+</sup></b> (15.76)	$k_{\text{exp}} = 1.8 \times 10^{-9}$ $k_{\text{c}} = 1.9 \times 10^{-9}$	$k_{\text{exp}} = 1.8 \times 10^{-9}$ $k_{\text{c}} = 1.8 \times 10^{-9}$	$k_{\text{exp}} = 1.6 \times 10^{-9}$ $k_{\text{c}} = 1.6 \times 10^{-9}$
	C <sub>2</sub> H <sub>3</sub> <sup>+</sup> (57 %)	C <sub>2</sub> H <sub>2</sub> F <sup>+</sup> (44 %)	CHF <sub>2</sub> <sup>+</sup> (51 %)
	C <sub>2</sub> H <sub>2</sub> F <sup>+</sup> (18 %)	CH <sub>2</sub> F <sup>+</sup> (22 %)	CHF <sup>+</sup> (20 %)
	C <sub>2</sub> H <sub>2</sub> <sup>+</sup> (12 %)	C <sub>2</sub> HF <sup>+</sup> (19 %)	C <sub>2</sub> HF <sub>2</sub> <sup>+</sup> (13 %)
	C <sub>2</sub> HF <sup>+</sup> (7 %)	CF <sup>+</sup> (12 %)	CF <sup>+</sup> (8 %)
	CF <sup>+</sup> (5 %)	C <sub>2</sub> H <sub>2</sub> F <sub>2</sub> <sup>+</sup> (3 %)	C <sub>2</sub> HF <sub>3</sub> <sup>+</sup> (4 %)
	C <sub>2</sub> H <sub>3</sub> F <sup>+</sup> (1 %)		C <sub>2</sub> F <sub>2</sub> <sup>+</sup> (4 %)

Cation <sup>a</sup>	C <sub>2</sub> H <sub>3</sub> F <sup>b</sup>	CH <sub>2</sub> CF <sub>2</sub> <sup>b</sup>	C <sub>2</sub> HF <sub>3</sub> <sup>b</sup>
<b>N<sub>2</sub><sup>+</sup></b> <b>(15.58)</b>	$k_{\text{exp}} = 1.7 \times 10^{-9}$ $k_{\text{c}} = 2.1 \times 10^{-9}$ C <sub>2</sub> H <sub>3</sub> <sup>+</sup> (40 %) C <sub>2</sub> H <sub>2</sub> F <sup>+</sup> (29 %) C <sub>2</sub> H <sub>2</sub> <sup>+</sup> (15 %) C <sub>2</sub> HF <sup>+</sup> (12 %) C <sub>2</sub> H <sub>3</sub> F <sup>+</sup> (4 %)	$k_{\text{exp}} = 2.0 \times 10^{-9}$ $k_{\text{c}} = 2.0 \times 10^{-9}$ C <sub>2</sub> H <sub>2</sub> F <sup>+</sup> (33 %) CH <sub>2</sub> F <sup>+</sup> (28 %) C <sub>2</sub> HF <sup>+</sup> (20 %) CF <sup>+</sup> (11 %) C <sub>2</sub> H <sub>2</sub> F <sub>2</sub> <sup>+</sup> (8 %)	$k_{\text{exp}} = 1.8 \times 10^{-9}$ $k_{\text{c}} = 1.8 \times 10^{-9}$ CHF <sub>2</sub> <sup>+</sup> (66 %) CF <sup>+</sup> (16 %) CHF <sup>+</sup> (12 %) C <sub>2</sub> HF <sub>3</sub> <sup>+</sup> (6 %)
<b>N<sup>+</sup></b> <b>(14.53)</b>	$k_{\text{exp}} = 1.8 \times 10^{-9}$ $k_{\text{c}} = 1.9 \times 10^{-9}$ C <sub>2</sub> H <sub>3</sub> F <sup>+</sup> (52 %) C <sub>2</sub> H <sub>2</sub> F <sup>+</sup> (21 %) C <sub>2</sub> H <sub>3</sub> <sup>+</sup> (20 %) C <sub>2</sub> HF <sup>+</sup> (6 %) C <sub>2</sub> H <sub>2</sub> <sup>+</sup> (1 %)	$k_{\text{exp}} = 2.4 \times 10^{-9}$ $k_{\text{c}} = 2.6 \times 10^{-9}$ C <sub>2</sub> H <sub>2</sub> F <sub>2</sub> <sup>+</sup> (82 %) C <sub>2</sub> H <sub>2</sub> F <sup>+</sup> (16 %) C <sub>2</sub> HF <sup>+</sup> (2 %)	$k_{\text{exp}} = 2.3 \times 10^{-9}$ $k_{\text{c}} = 2.3 \times 10^{-9}$ C <sub>2</sub> HF <sub>3</sub> <sup>+</sup> (100 %)
<b>CO<sup>+</sup></b> <b>(14.01)</b>	$k_{\text{exp}} = 2.2 \times 10^{-9}$ $k_{\text{c}} = 2.1 \times 10^{-9}$ C <sub>2</sub> H <sub>3</sub> F <sup>+</sup> (39 %) C <sub>2</sub> H <sub>2</sub> <sup>+</sup> (27 %) C <sub>2</sub> H <sub>2</sub> F <sup>+</sup> (16 %) C <sub>2</sub> H <sub>3</sub> <sup>+</sup> (16 %) C <sub>2</sub> HF <sup>+</sup> (2 %)	$k_{\text{exp}} = 2.2 \times 10^{-9}$ $k_{\text{c}} = 2.0 \times 10^{-9}$ C <sub>2</sub> H <sub>2</sub> F <sub>2</sub> <sup>+</sup> (84 %) C <sub>2</sub> H <sub>2</sub> F <sup>+</sup> (16 %)	$k_{\text{exp}} = 1.8 \times 10^{-9}$ $k_{\text{c}} = 1.8 \times 10^{-9}$ CHF <sub>2</sub> <sup>+</sup> (50 %) C <sub>2</sub> HF <sub>3</sub> <sup>+</sup> (41 %) CF <sup>+</sup> (9 %)
<b>Kr<sup>+</sup></b> <b>(14.00)</b>	$k_{\text{exp}} = 1.6 \times 10^{-9}$ $k_{\text{c}} = 1.6 \times 10^{-9}$ C <sub>2</sub> H <sub>3</sub> F <sup>+</sup> (39 %) C <sub>2</sub> H <sub>2</sub> <sup>+</sup> (25 %) C <sub>2</sub> H <sub>2</sub> F <sup>+</sup> (23 %) C <sub>2</sub> HF <sup>+</sup> (7 %) C <sub>2</sub> H <sub>3</sub> <sup>+</sup> (6 %)	$k_{\text{exp}} = 1.2 \times 10^{-9}$ $k_{\text{c}} = 1.4 \times 10^{-9}$ Products not identified	$k_{\text{exp}} = 1.2 \times 10^{-9}$ $k_{\text{c}} = 1.3 \times 10^{-9}$ C <sub>2</sub> HF <sub>3</sub> <sup>+</sup> (86 %) CHF <sub>2</sub> <sup>+</sup> (14 %)
<b>CO<sub>2</sub><sup>+</sup></b> <b>(13.76)</b>	$k_{\text{exp}} = 1.9 \times 10^{-9}$ $k_{\text{c}} = 1.8 \times 10^{-9}$ C <sub>2</sub> H <sub>3</sub> F <sup>+</sup> (90 %) C <sub>2</sub> H <sub>2</sub> <sup>+</sup> (9 %) C <sub>2</sub> H <sub>3</sub> <sup>+</sup> (1 %)	$k_{\text{exp}} = 1.4 \times 10^{-9}$ $k_{\text{c}} = 1.7 \times 10^{-9}$ C <sub>2</sub> H <sub>2</sub> F <sub>2</sub> <sup>+</sup> (100 %)	$k_{\text{exp}} = 1.2 \times 10^{-9}$ $k_{\text{c}} = 1.5 \times 10^{-9}$ C <sub>2</sub> HF <sub>3</sub> <sup>+</sup> (100 %)
<b>O<sup>+</sup></b> <b>(13.62)</b>	$k_{\text{exp}} = 2.5 \times 10^{-9}$ $k_{\text{c}} = 2.5 \times 10^{-9}$ C <sub>2</sub> H <sub>3</sub> F <sup>+</sup> (100 %)	$k_{\text{exp}} = 2.0 \times 10^{-9}$ $k_{\text{c}} = 2.4 \times 10^{-9}$ Products not identified	$k_{\text{exp}}$ not measured $k_{\text{c}} = 2.2 \times 10^{-9}$ C <sub>2</sub> HF <sub>3</sub> <sup>+</sup> (100 %)
<b>OH<sup>+</sup></b> <b>(13.25)</b>	$k_{\text{exp}} = 2.4 \times 10^{-9}$ $k_{\text{c}} = 2.5 \times 10^{-9}$ Products not identified	No data collected	$k_{\text{exp}} = 2.2 \times 10^{-9}$ $k_{\text{c}} = 2.2 \times 10^{-9}$ Products not identified

Cation <sup>a</sup>	C <sub>2</sub> H <sub>3</sub> F <sup>b</sup>	CH <sub>2</sub> CF <sub>2</sub> <sup>b</sup>	C <sub>2</sub> HF <sub>3</sub> <sup>b</sup>
<b>N<sub>2</sub>O<sup>+</sup></b> <b>(12.89)</b>	$k_{\text{exp}} = 1.5 \times 10^{-9}$ $k_{\text{c}} = 1.8 \times 10^{-9}$ C <sub>2</sub> H <sub>3</sub> F <sup>+</sup> (100 %)	$k_{\text{exp}} = 1.4 \times 10^{-9}$ $k_{\text{c}} = 1.7 \times 10^{-9}$ C <sub>2</sub> H <sub>2</sub> F <sub>2</sub> <sup>+</sup> (100 %)	$k_{\text{exp}} = 1.1 \times 10^{-9}$ $k_{\text{c}} = 1.5 \times 10^{-9}$ C <sub>2</sub> HF <sub>3</sub> <sup>+</sup> (100 %)
<b>H<sub>2</sub>O<sup>+</sup></b> <b>(12.62)</b>	$k_{\text{exp}} = 2.4 \times 10^{-9}$ $k_{\text{c}} = 2.4 \times 10^{-9}$ Products not identified	No data collected	$k_{\text{exp}} = 2.0 \times 10^{-9}$ $k_{\text{c}} = 2.1 \times 10^{-9}$ Products not identified
<b>Xe<sup>+</sup></b> <b>(12.13)</b>	$k_{\text{exp}} = 1.4 \times 10^{-9}$ $k_{\text{c}} = 1.5 \times 10^{-9}$ C <sub>2</sub> H <sub>3</sub> F <sup>+</sup> (100 %)	$k_{\text{exp}} = 8.0 \times 10^{-10}$ $k_{\text{c}} = 1.3 \times 10^{-9}$ C <sub>2</sub> H <sub>2</sub> F <sub>2</sub> <sup>+</sup> (100 %)	$k_{\text{exp}} = 8.0 \times 10^{-10}$ $k_{\text{c}} = 1.1 \times 10^{-9}$ C <sub>2</sub> HF <sub>3</sub> <sup>+</sup> (100 %)
<b>O<sub>2</sub><sup>+</sup></b> <b>(12.07)</b>	$k_{\text{exp}} = 2.1 \times 10^{-9}$ $k_{\text{c}} = 2.0 \times 10^{-9}$ C <sub>2</sub> H <sub>3</sub> F <sup>+</sup> (100 %)	$k_{\text{exp}} = 1.8 \times 10^{-9}$ $k_{\text{c}} = 1.9 \times 10^{-9}$ C <sub>2</sub> H <sub>2</sub> F <sub>2</sub> <sup>+</sup> (100 %)	$k_{\text{exp}} = 1.9 \times 10^{-9}$ $k_{\text{c}} = 1.7 \times 10^{-9}$ C <sub>2</sub> HF <sub>3</sub> <sup>+</sup> (100 %)
<b>SF<sub>4</sub><sup>+</sup></b> <b>(11.99)</b>	$k_{\text{exp}} = 1.1 \times 10^{-9}$ $k_{\text{c}} = 1.5 \times 10^{-9}$ Products not identified	$k_{\text{exp}} = 1.5 \times 10^{-9}$ $k_{\text{c}} = 1.4 \times 10^{-9}$ C <sub>2</sub> H <sub>2</sub> F <sub>2</sub> <sup>+</sup> (100 %) or CHSF <sup>+</sup>	$k_{\text{exp}} = 1.2 \times 10^{-9}$ $k_{\text{c}} = 1.2 \times 10^{-9}$ C <sub>2</sub> HF <sub>3</sub> <sup>+</sup> (100 %)
<b>SF<sup>+</sup></b> <b>(10.31)</b>	$k_{\text{exp}} = 1.6 \times 10^{-9}$ $k_{\text{c}} = 1.8 \times 10^{-9}$ Products not identified	$k_{\text{exp}} = 1.4 \times 10^{-9}$ $k_{\text{c}} = 1.6 \times 10^{-9}$ CH <sub>2</sub> SF <sup>+</sup> (80 %) <sup>c</sup> or 2° C <sub>2</sub> H <sub>3</sub> F <sub>2</sub> <sup>+</sup> C <sub>2</sub> H <sub>2</sub> F <sub>2</sub> <sup>+</sup> (20 %) or CHSF <sup>+</sup>	$k_{\text{exp}} = 1.4 \times 10^{-9}$ $k_{\text{c}} = 1.4 \times 10^{-9}$ C <sub>2</sub> HF <sub>3</sub> <sup>+</sup> (100 %)
<b>SF<sub>2</sub><sup>+</sup></b> <b>(10.24)</b>	No reaction	No reaction	No reaction
<b>SF<sub>5</sub><sup>+</sup></b> <b>(9.78)</b>	$k_{\text{exp}} = 6.4 \times 10^{-10}$ $k_{\text{c}} = 1.5 \times 10^{-9}$ Products not identified	$k_{\text{exp}} = 1.0 \times 10^{-10}$ $k_{\text{c}} = 1.3 \times 10^{-9}$ SF <sub>3</sub> <sup>+</sup> (53 %) C <sub>2</sub> H <sub>2</sub> F <sub>3</sub> <sup>+</sup> (32 %) or CHSF <sub>2</sub> <sup>+</sup> C <sub>2</sub> H <sub>2</sub> F <sub>2</sub> <sup>+</sup> (15 %) or CHSF <sup>+</sup>	No reaction
<b>NO<sup>+</sup></b> <b>(9.26)</b>	No reaction	No reaction	No reaction
<b>SF<sub>3</sub><sup>+</sup></b> <b>(8.32)</b>	No reaction	No reaction	No reaction

Cation <sup>a</sup>	C <sub>2</sub> H <sub>3</sub> F <sup>b</sup>	CH <sub>2</sub> CF <sub>2</sub> <sup>b</sup>	C <sub>2</sub> HF <sub>3</sub> <sup>b</sup>
H <sub>3</sub> O <sup>+</sup> (6.27)	$k_{\text{exp}} = 2.3 \times 10^{-9}$ $k_{\text{c}} = 2.4 \times 10^{-9}$ [C <sub>2</sub> H <sub>3</sub> F + H] <sup>+</sup> (100 %)	$k_{\text{exp}} = 2.3 \times 10^{-9}$ $k_{\text{c}} = 2.3 \times 10^{-9}$ [C <sub>2</sub> H <sub>2</sub> F <sub>2</sub> + H] <sup>+</sup> (100 %)	No data collected

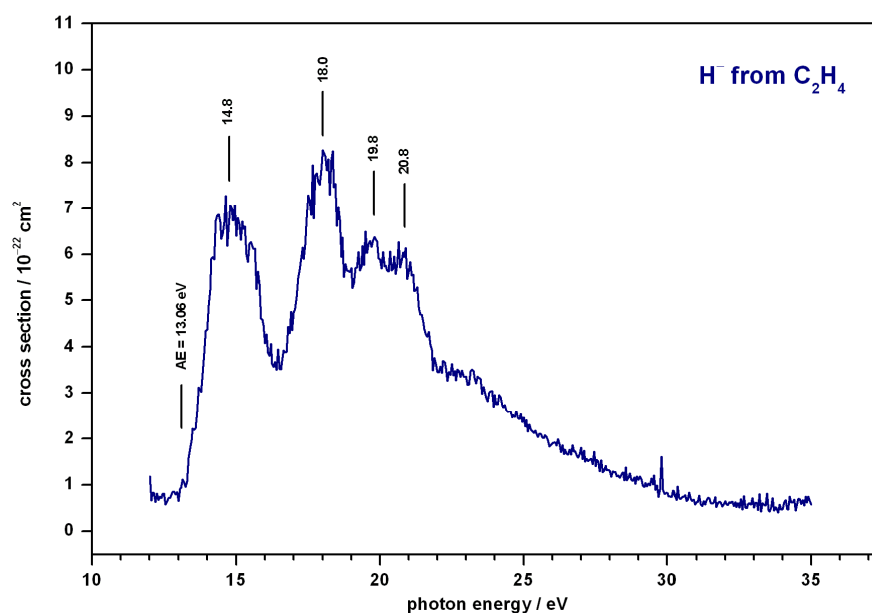
<sup>a</sup> Reactant cation and the value, in eV, of its recombination energy (*RE*). For example, the *RE* of A<sup>+</sup> is defined as the ionisation energy of neutral A. All values are taken in October 2009 from the NIST Chemistry Database; [webbook.nist.gov/chemistry/](http://webbook.nist.gov/chemistry/).

<sup>b</sup> The results include the product cation species, their branching ratios in %, and the experimental reaction rate coefficient,  $k_{\text{exp}}$ . In addition, values for the calculated collisional rate coefficient,  $k_{\text{c}}$ , are also included. All values for  $k$  are in cm<sup>3</sup> molecule<sup>-1</sup> s<sup>-1</sup>.

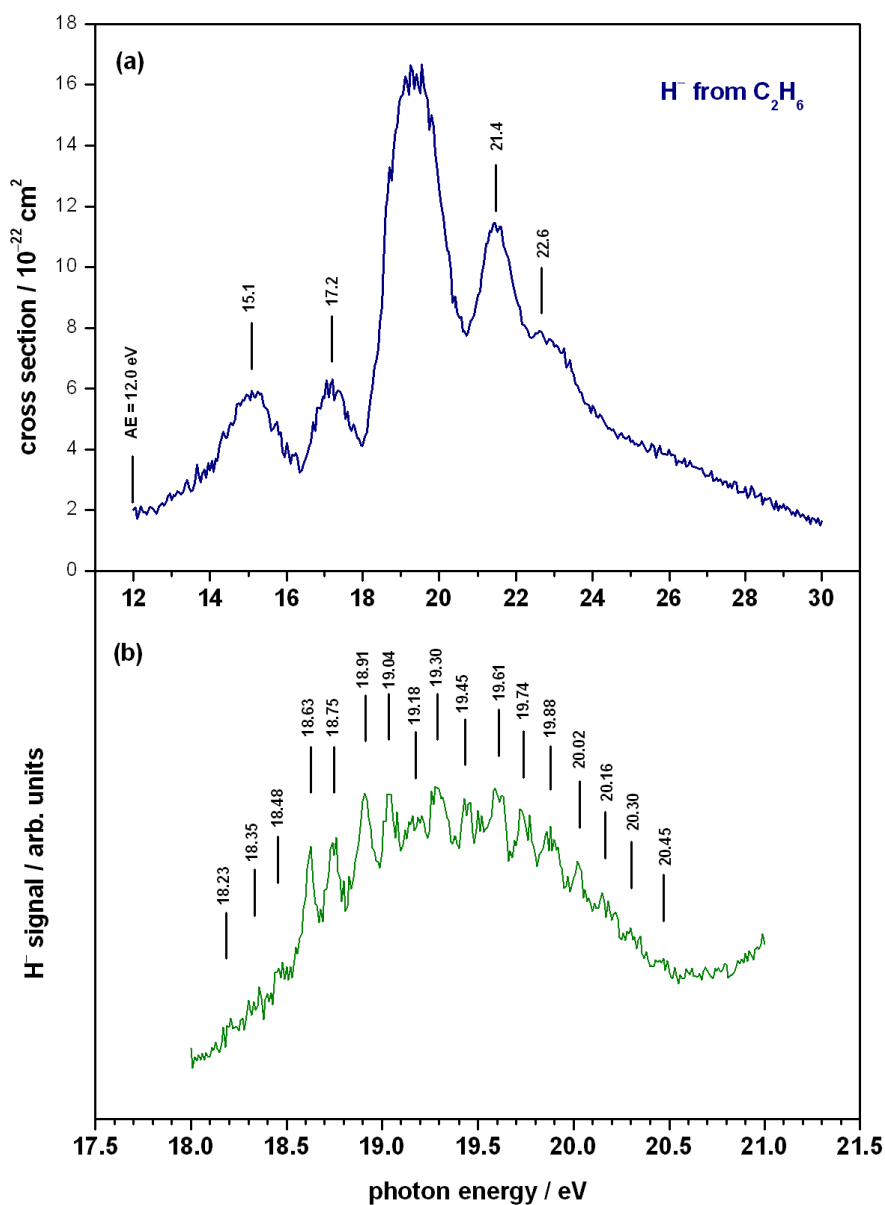
<sup>c</sup>  $m/z$  65 detected which could be a primary product CH<sub>2</sub>SF<sup>+</sup>, or a secondary product C<sub>2</sub>H<sub>3</sub>F<sup>+</sup>. If  $m/z$  65 is actually a secondary product then the branching ratio for  $m/z$  64 (C<sub>2</sub>H<sub>2</sub>F<sub>2</sub><sup>+</sup> or CHSF<sup>+</sup>) will be 100 %.

## Appendix IV:

### *Cross sections for anion production following the vacuum ultraviolet photoexcitation of some gas-phase molecules*

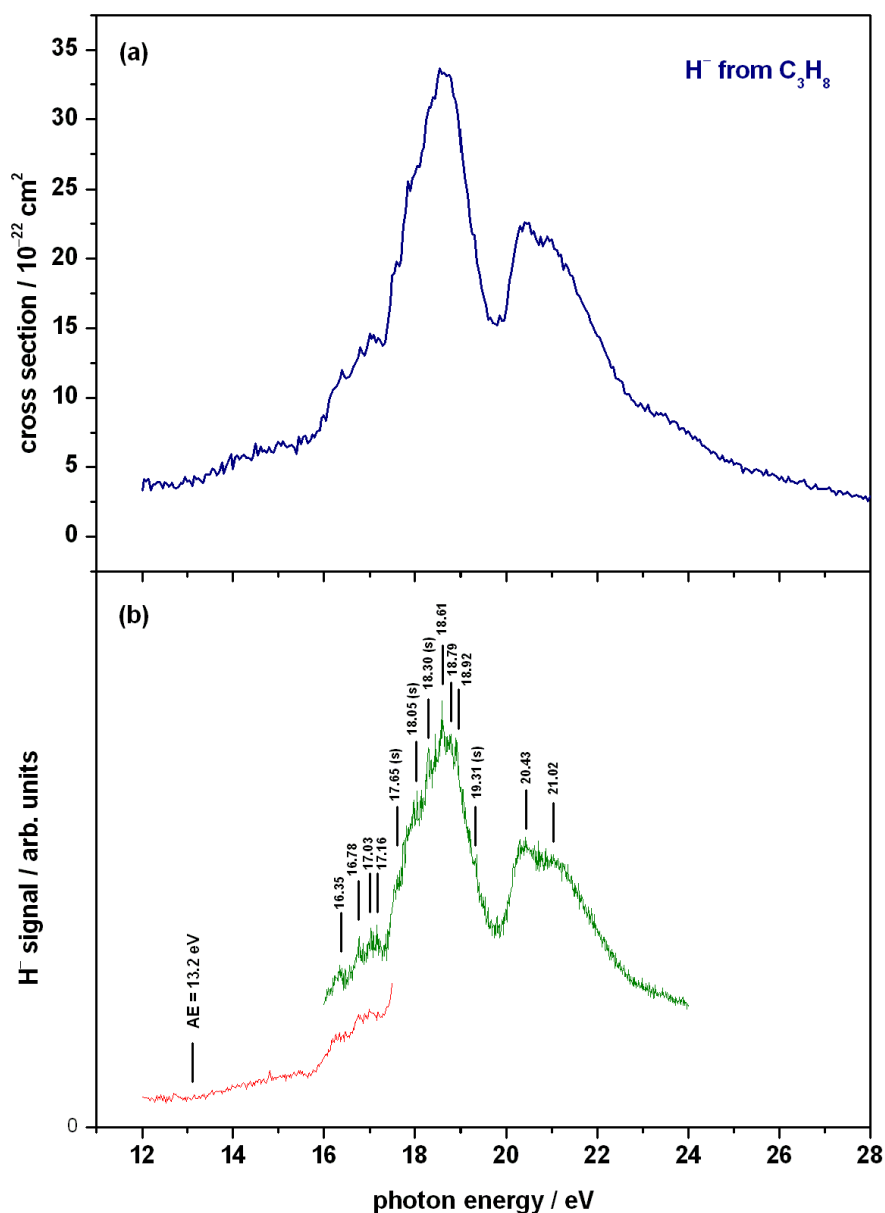


**A.IV.(1).**  $\text{H}^-$  detected following the unimolecular photodissociation of  $\text{C}_2\text{H}_4$ . The scan was recorded on beamline 3.1 at the Daresbury SRS in April 2008, with a wavelength resolution of 6 Å and a step size of 0.05 eV. The appearance energy (AE) was determined from a different scan, recording the onset region with better statistics: a wavelength resolution of 2 Å and a step size of 0.02 eV. The solid lines and corresponding numbers show energy positions of features in the spectrum.



**A.IV.(2).** Data recorded on beamline 3.1 at the Daresbury SRS in June 2008 for  $\text{H}^-$  detected following the unimolecular photodissociation of  $\text{C}_2\text{H}_6$ : **(a)** in the photon energy range 12–30 eV with a step size of 0.05 eV and a wavelength resolution of 6 Å; **(b)** in the range 18–21 eV with a step size of 0.01 eV and a wavelength resolution of 1.2 Å.

The appearance energy (AE) was determined from a different scan, not shown here, recording the onset region with a wavelength resolution of 3 Å and a step size of 0.02 eV. The solid lines and corresponding numbers show energy positions of features in the spectra.



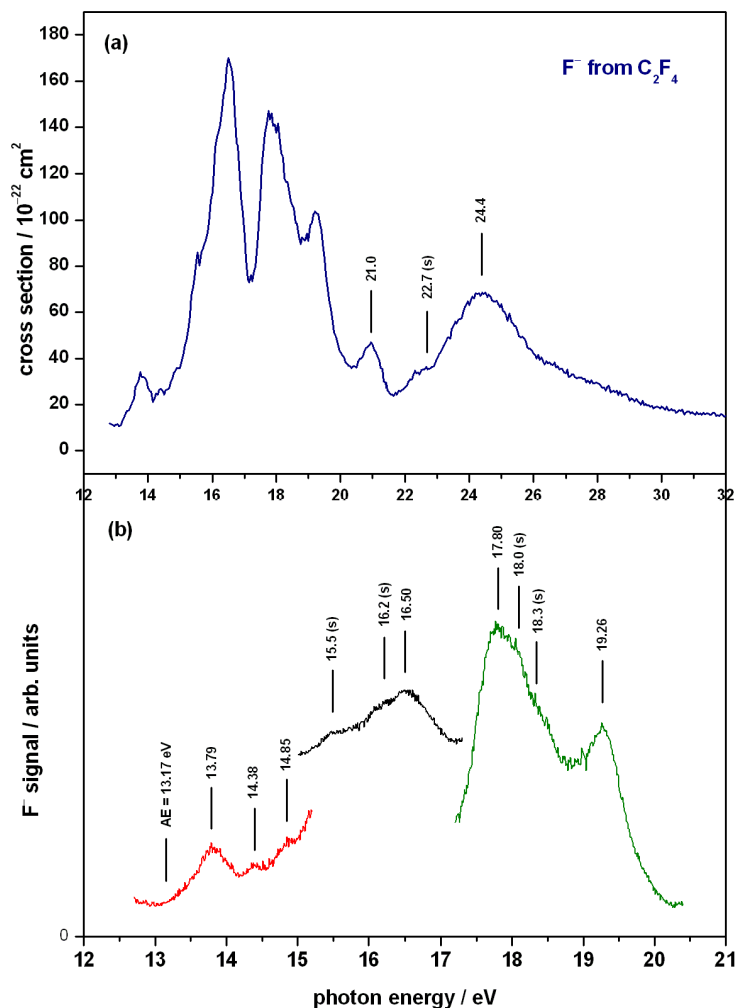
**A.IV.(3).**  $\text{H}^-$  detected following the unimolecular photodissociation of  $\text{C}_3\text{H}_8$ : **(a)** in the photon energy range 12-28 eV with a step size of 0.05 eV and a wavelength resolution of 6 Å; **(b)** two separate scans covering the 12-24 eV range with better statistics, from 12-17.5 eV recorded with a step size of 0.02 eV and a wavelength resolution of 2 Å, and from 16-24 eV recorded with a step size of 0.01 eV and a wavelength resolution of 1.2 Å.

The data were recorded on beamline 3.1 at the Daresbury SRS in May 2008. The appearance energy ( $\text{AE}$ ) is indicated and solid lines (with corresponding numbers) show energy positions of features in the spectra, where ‘(s)’ indicates a shoulder feature.

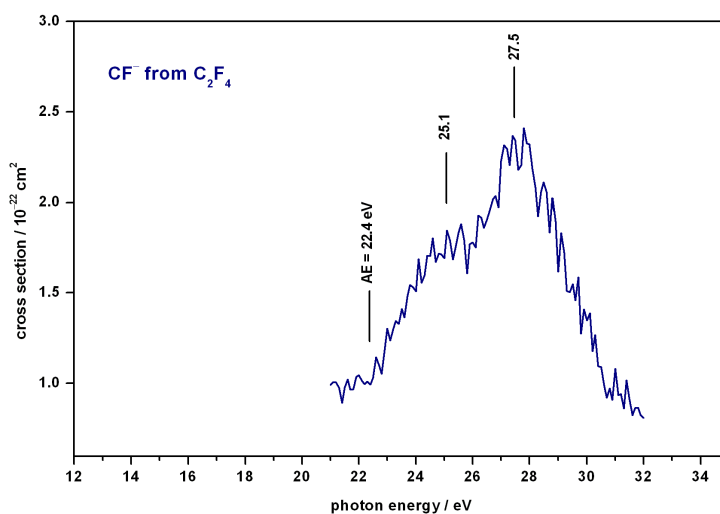


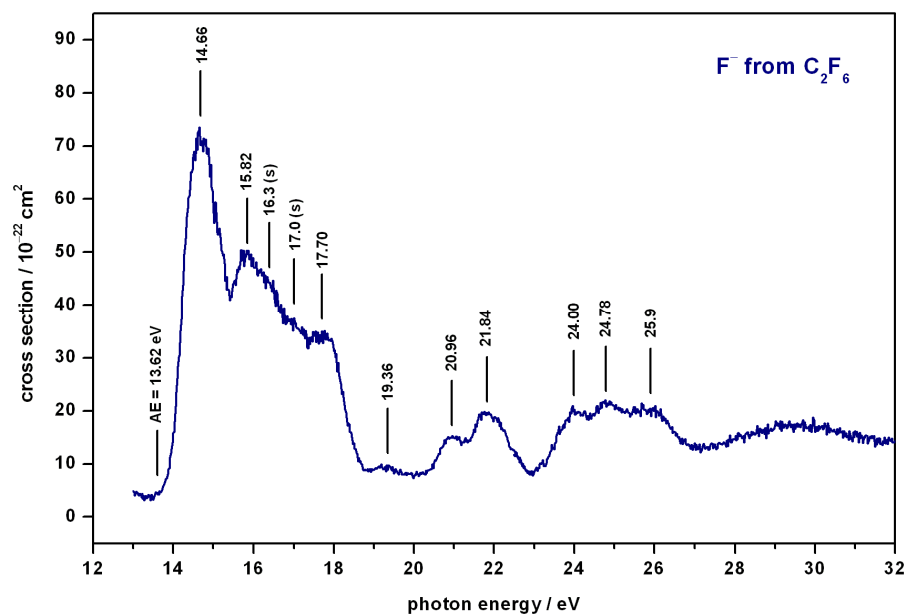
**A.IV.(4).**  $F^-$  detected following the unimolecular photodissociation of  $C_2F_4$ : **(a)** in the photon energy range 13-32 eV with a step size of 0.05 eV and a wavelength resolution of 6 Å; **(b)** three separate scans covering the 12.7-20.4 eV range with better statistics, all with a step size of 0.01 eV and a wavelength resolution of 2 Å.

The data for  $C_2F_4$  were recorded on beamline 3.1 at the Daresbury SRS in May 2008. The appearance energy ( $AE$ ) is indicated and solid lines (with corresponding numbers) show energy positions of features in the spectra, where '(s)' indicates a shoulder feature.



**A.IV.(5).**  $CF^-$  detected following the unimolecular photodissociation of  $C_2F_4$  in the photon energy range 21-32 eV with a step size of 0.1 eV and a wavelength resolution of 6 Å. Only background signal was observed from 12-21 eV, and only the 21-32 eV range was scanned to minimise data acquisition time due to the weak  $CF^-$  signal.



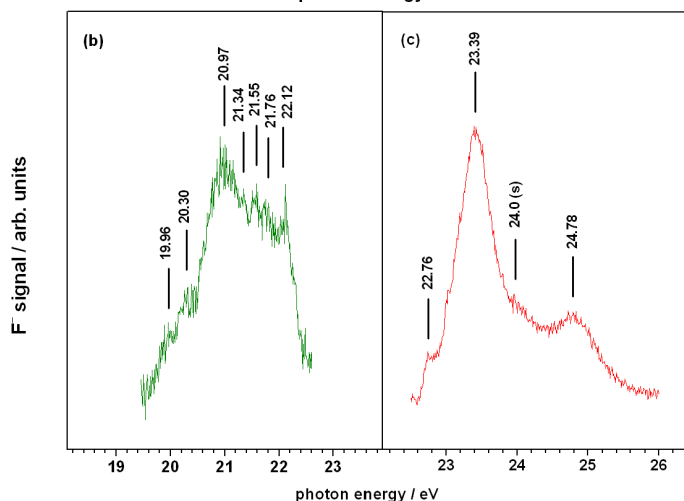
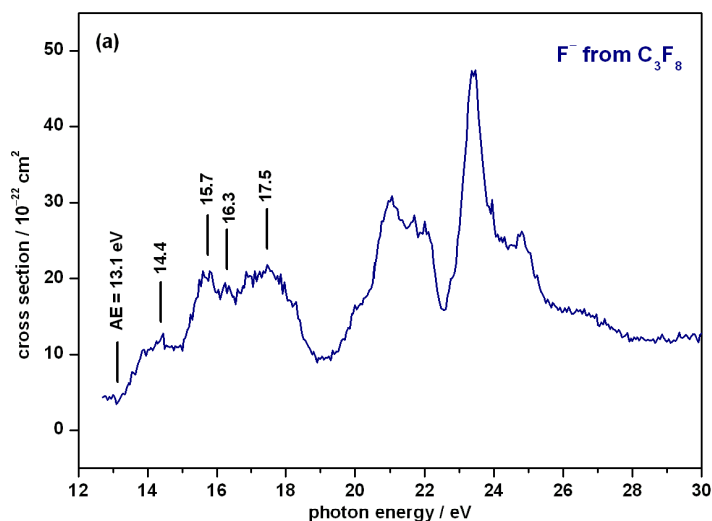


**A.IV.(6).**  $\text{F}^-$  detected following the unimolecular photodissociation of  $\text{C}_2\text{F}_6$  in the photon energy range 13-32 eV with a step size of 0.02 eV and a wavelength resolution of 2 Å.

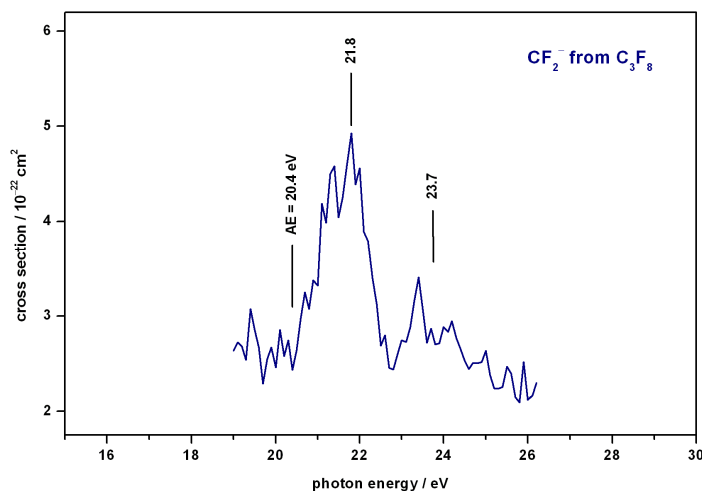
This scan was recorded on beamline 3.1 at the Daresbury SRS in May 2008. The appearance energy (AE) is indicated and solid lines (with corresponding numbers) show energy positions of features in the spectrum, where '(s)' indicates a shoulder feature.

**A.IV.(7).**  $F^-$  detected following the unimolecular photodissociation of  $C_3F_8$ : **(a)** in the photon energy range 12.7-30 eV with a step size of 0.05 eV and a wavelength resolution of 6 Å; **(b)** covering the 19.5-22.5 eV range with better statistics, using a step size of 0.01 eV and a wavelength resolution of 1.2 Å; **(c)** covering the 22.5-26 eV range with better statistics, using a step size of 0.01 eV and a wavelength resolution of 1.2 Å.

The data for  $C_3F_8$  were recorded on beamline 3.1 at the Daresbury SRS in May 2008. The appearance energy ( $AE$ ) is indicated and solid lines (with corresponding numbers) show energy positions of features in the spectra, where '(s)' indicates a shoulder feature.



**A.IV.(8).**  $CF_2^-$  detected following the unimolecular photodissociation of  $C_3F_8$  in the photon energy range 19-26 eV with a step size of 0.1 eV and a wavelength resolution of 6 Å. Only background signal was observed from 12-19, and from 26-35 eV, and only the 19-26 eV range was scanned to minimise data acquisition time due to the weak signal.



**A.IV.(9).** Ion yields for anions observed following the photoexcitation of  $\text{CH}_2\text{F}_2$ . All scans were recorded on beamline 3.2 at the Daresbury SRS in July 2007.

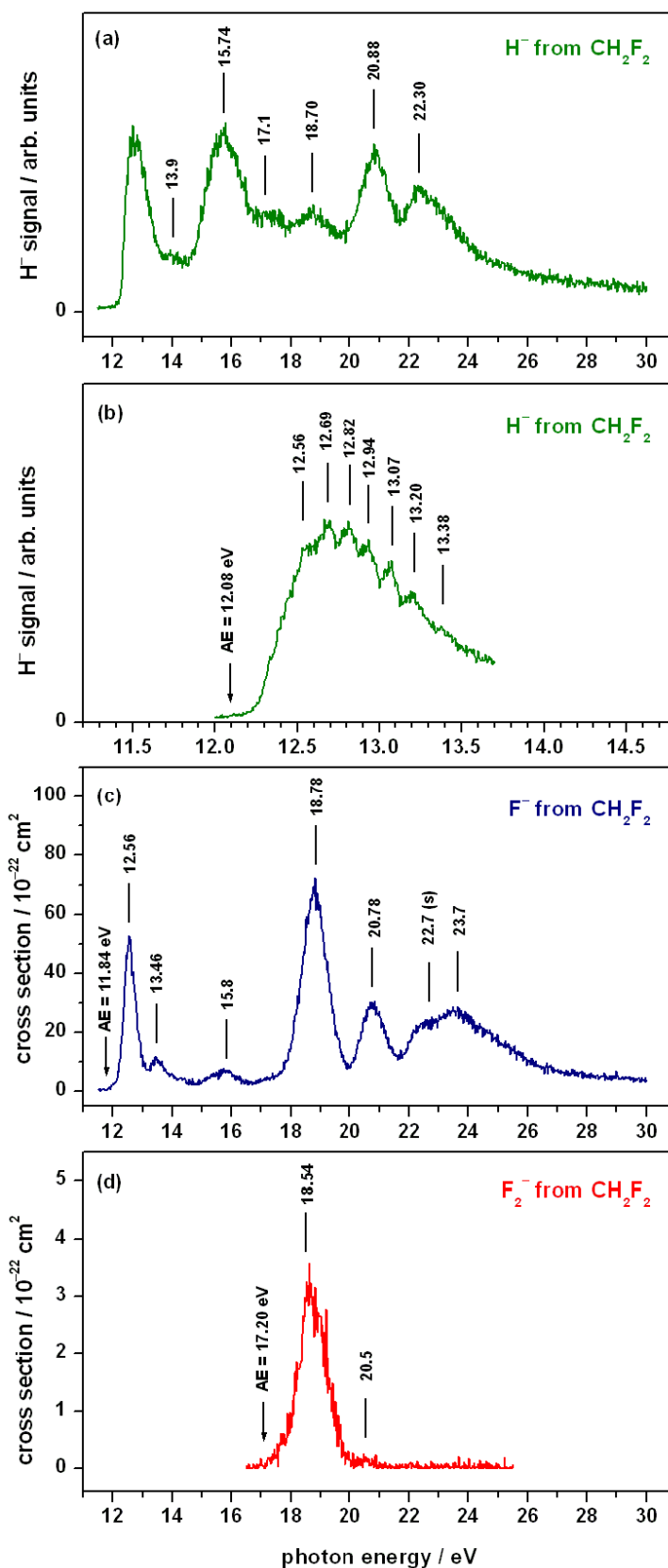
(a)  $\text{H}^-$  ion yield in the photon energy range 11.5-30.0 eV recorded with a step size of 0.02 eV and a wavelength resolution of 2 Å. Due to the *zero blast* effect in the quadrupole mass spectrometer, the ion signal detected at  $m/z$  1 (*i.e.*  $\text{H}^-$ ) may also contain contributions from other ions present (*i.e.*  $\text{F}^-$  and  $\text{F}_2^-$ ). Thus, an absolute cross section cannot be determined for the  $\text{H}^-$  spectra and it is possible that the observed features do not result exclusively from  $\text{H}^-$  anions.

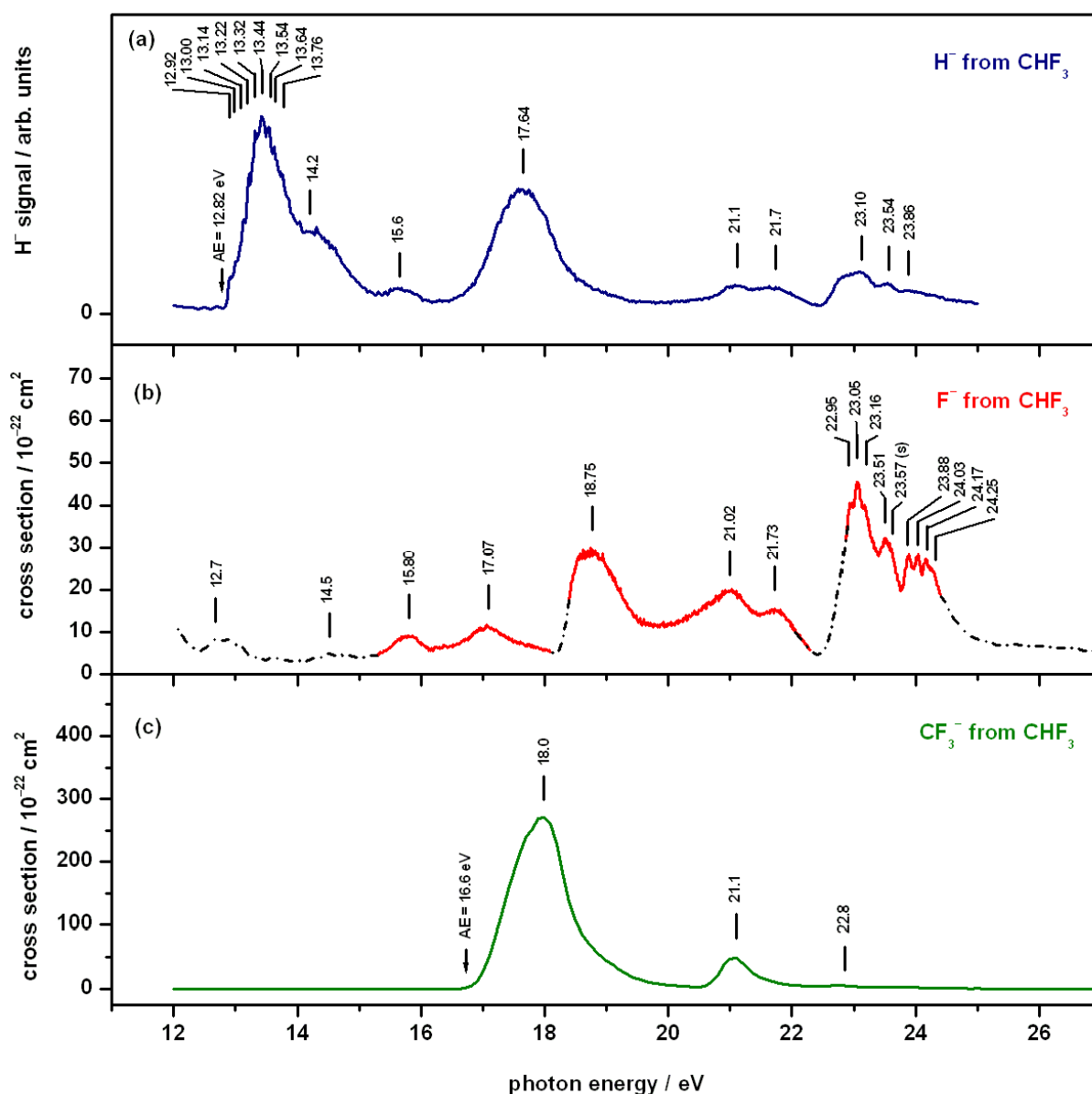
(b) A separate  $\text{H}^-$  scan covering the 12.0-13.7 eV region with better statistics: a step size of 0.005 eV and a wavelength resolution of 1 Å. It should be noted that a similar scan of the feature at 12.56 eV in the  $\text{F}^-$  spectrum was structureless and did *not* reproduce that in (b) for  $\text{H}^-$ .

(c)  $\text{F}^-$  cross section in the photon energy range 11.5-30.0 eV recorded with a step size of 0.02 eV and a wavelength resolution of 2 Å.

(d)  $\text{F}_2^-$  cross section in the photon energy range 16.5-25.5 eV recorded with a step size of 0.02 eV and a wavelength resolution of 2 Å.

The appearance energies (*AE*) are indicated and solid lines (with corresponding numbers) show energy positions of features in the spectra, where '(s)' indicates a shoulder feature.





**A.IV.(10).** Ion yields for anions observed following the photoexcitation of  $\text{CHF}_3$ . All scans were recorded on beamline 3.1 at the Daresbury SRS in April 2007. The appearance energies (*AE*) are indicated (where possible) and solid lines (with corresponding numbers) show energy positions of features in the spectra, where ‘(s)’ indicates a shoulder feature. **(a)**  $\text{H}^-$  ion yield in the photon energy range 12–25 eV recorded with a step size of 0.02 eV and a wavelength resolution of 3 Å. Due to the *zero blast* effect in the quadrupole mass spectrometer, the ion signal detected at  $m/z$  1 (*i.e.*  $\text{H}^-$ ) may also contain contributions from other ions present (*i.e.*  $\text{F}^-$  and  $\text{F}_2^-$ ). Thus, an absolute cross section cannot be determined for the  $\text{H}^-$  spectra and it is possible that the observed features do not result exclusively from  $\text{H}^-$  anions. **(b)**  $\text{F}^-$  cross section in the photon energy range 12–25 eV constructed by merging four different scans: the dotted line is from a scan recorded with a step size of 0.1 eV and a wavelength resolution of 6 Å; the solid line from 15.3–18.1 eV was recorded with a step size of 0.01 eV and a wavelength resolution of 2 Å; the solid line from 18.4–22.3 eV was recorded with a step size of 0.01 eV and a wavelength resolution of 1.6 Å; the solid line from 22.86–24.40 eV was recorded with a step size of 0.005 eV and a wavelength resolution of 1.2 Å. The rise in signal at  $h\nu < 12.4$  eV is suspected to arise from second order radiation, and a separate scan from 8–11.8 eV, using a LiF window, showed only background signal. **(c)**  $\text{CF}_3^-$  cross section in the photon energy range 12–27 eV recorded with a step size of 0.1 eV and a wavelength resolution of 6 Å.

**A.IV.(11).** Ion yields for anions observed following the photoexcitation of  $\text{CH}_2\text{Cl}_2$ . All scans were recorded on beamline 3.2 at the Daresbury SRS in July 2007.

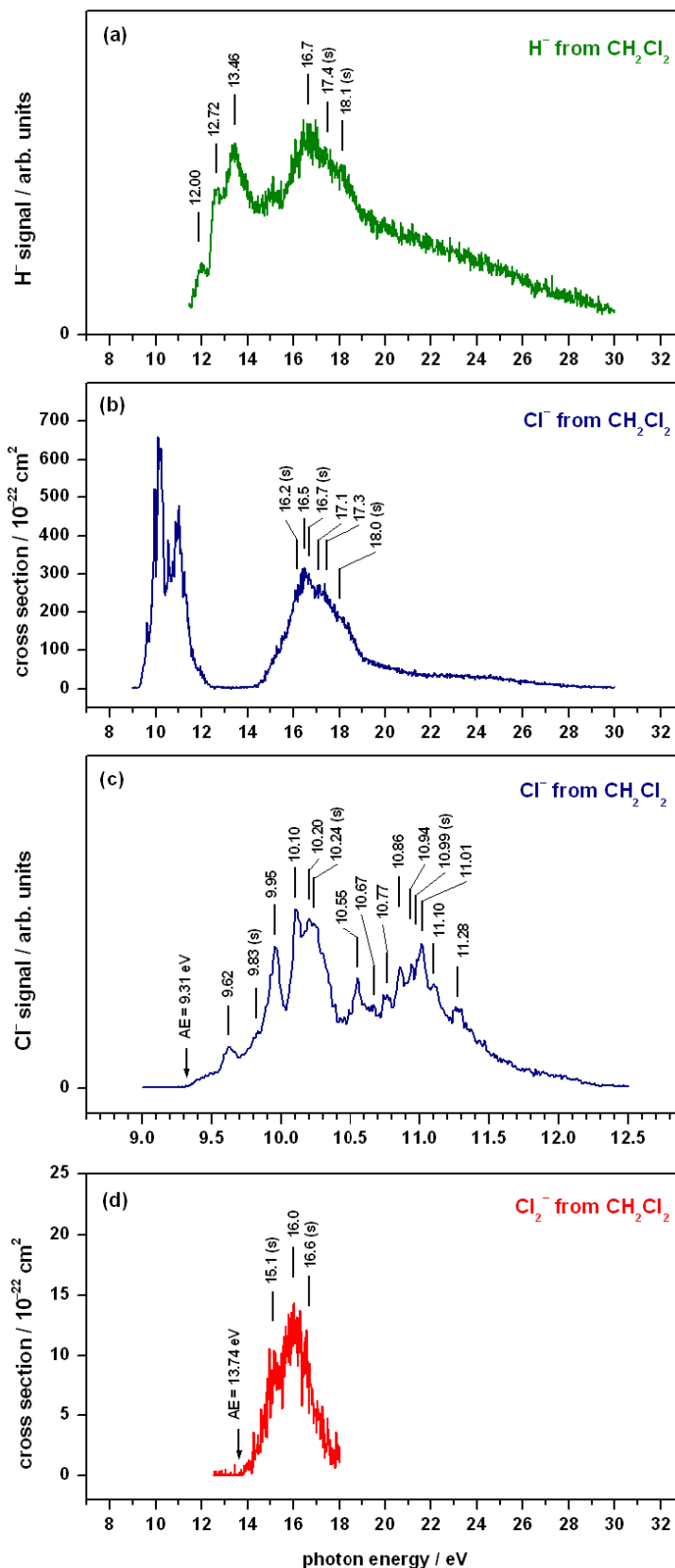
(a)  $\text{H}^-$  ion yield in the photon energy range 11.5-30.0 eV recorded with a step size of 0.02 eV and a wavelength resolution of 2 Å. Due to the *zero blast* effect in the quadrupole mass spectrometer, the ion signal detected at  $m/z$  1 (*i.e.*  $\text{H}^-$ ) may also contain contributions from other ions present (*i.e.*  $\text{Cl}^-$  and  $\text{Cl}_2^-$ ). Thus, an absolute cross section cannot be determined for the  $\text{H}^-$  spectrum and it is possible that the observed features do not result exclusively from  $\text{H}^-$  anions.

(b)  $\text{Cl}^-$  cross section from 9-30 eV recorded with a step size of 0.02 eV and a wavelength resolution of 2 Å.

(c) A separate  $\text{Cl}^-$  scan, covering the 9.0-12.5 eV region with better statistics: a step size of 0.01 eV and a wavelength resolution of 2 Å.

(d)  $\text{Cl}_2^-$  cross section in the photon energy range 12.5-18.0 eV recorded with a step size of 0.02 eV and a wavelength resolution of 2 Å. A separate scan from 18-30 eV showed only background signal, and is not included here.

The appearance energies (*AE*) are indicated and solid lines (with corresponding numbers) show energy positions of features in the spectra, where '(s)' indicates a shoulder feature.



**A.IV.(12).** Ion yields for anions observed following the photoexcitation of  $\text{CHCl}_3$ . All scans were recorded on beamline 3.1 at the Daresbury SRS in April 2008.

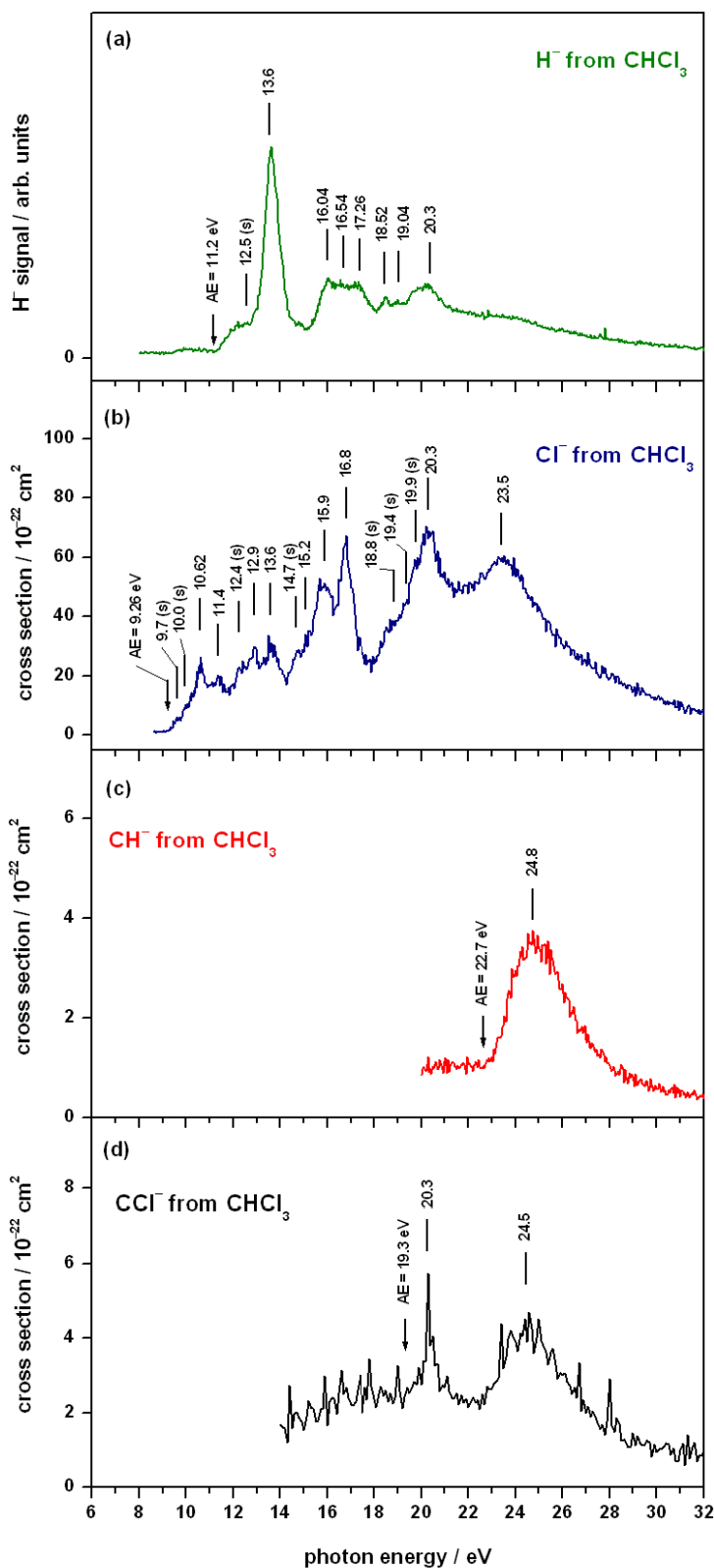
(a) Three separate scans have been merged to generate the  $\text{H}^-$  ion yield: from 8-15 eV with a step size of 0.05 eV and a wavelength resolution of 6 Å; 15-19.5 eV with a step size of 0.02 eV and a wavelength resolution of 2 Å; 19.5-32 eV with a step size of 0.05 eV and a wavelength resolution of 6 Å. Due to the *zero blast* effect in the quadrupole mass spectrometer, the ion signal detected at  $m/z$  1 (*i.e.*  $\text{H}^-$ ) may also contain contributions from other ions present (*e.g.*  $\text{Cl}^-$ ). Thus, an absolute cross section cannot be determined for the  $\text{H}^-$  spectrum and it is possible that the observed features do not result exclusively from  $\text{H}^-$  anions.

(b)  $\text{Cl}^-$  cross section from 8-32 eV generated by merging three separate scans: from 8.60-10.64 eV with a step size of 0.02 eV and a wavelength resolution of 4 Å; 10.65-16.80 eV with a step size of 0.05 eV and a wavelength resolution of 6 Å; 16.85-32.00 eV with a step size of 0.05 eV and a wavelength resolution of 6 Å.

(c)  $\text{CH}^-$  cross section in the photon energy range 20-32 eV recorded with a step size of 0.05 eV and a wavelength resolution of 6 Å.

(d)  $\text{CCl}^-$  cross section in the photon energy range 14-32 eV recorded with a step size of 0.1 eV and a wavelength resolution of 6 Å.

The appearance energies (*AE*) are indicated and solid lines (with corresponding numbers) show energy positions of features in the spectra, where '(s)' indicates a shoulder feature.



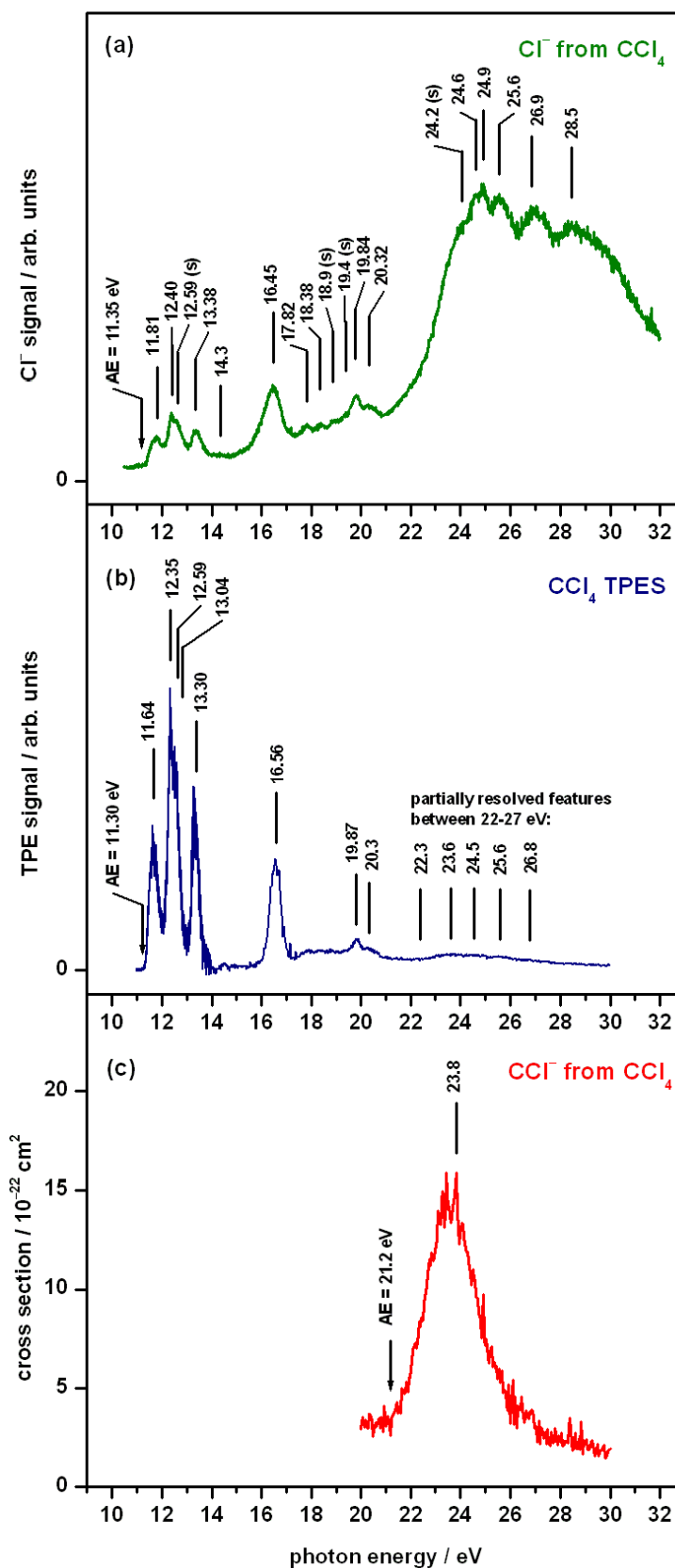
**A.IV.(13).** Ion yields for anions observed following the photoexcitation of  $\text{CCl}_4$ .

(a) Three separate scans have been merged to generate the  $\text{Cl}^-$  ion yield: from 10.5–17.2 eV with a step size of 0.01 eV and a wavelength resolution of 2 Å; 17.2–22.0 eV with a step size of 0.02 eV and a wavelength resolution of 2 Å; 22–32 eV with a step size of 0.02 eV and a wavelength resolution of 2 Å. The  $\text{Cl}^-$  signal at 16.45 and 24.9 eV was shown to increase non-linearly with increasing gas pressure and an absolute cross section cannot be determined; the formation of  $\text{Cl}^-$  is dominated by the dissociative electron attachment to  $\text{CCl}_4$ .

(b)  $\text{CCl}_4$  threshold photoelectron spectrum (TPES) included to compare with the  $\text{Cl}^-$  ion yield [taken with permission from J. Harvey, R. P. Tuckett, N. J. Rogers, unpublished data recorded in 2009 at the Swiss Light Source (SLS)].

(c)  $\text{CCl}^-$  ion-pair formation cross section in the photon energy range 20–32 eV recorded with a step size of 0.05 eV and a wavelength resolution of 6 Å.

The appearance energies ( $AE$ ) are indicated and solid lines (with corresponding numbers) show energy positions of features in the spectra, where '(s)' indicates a shoulder feature.





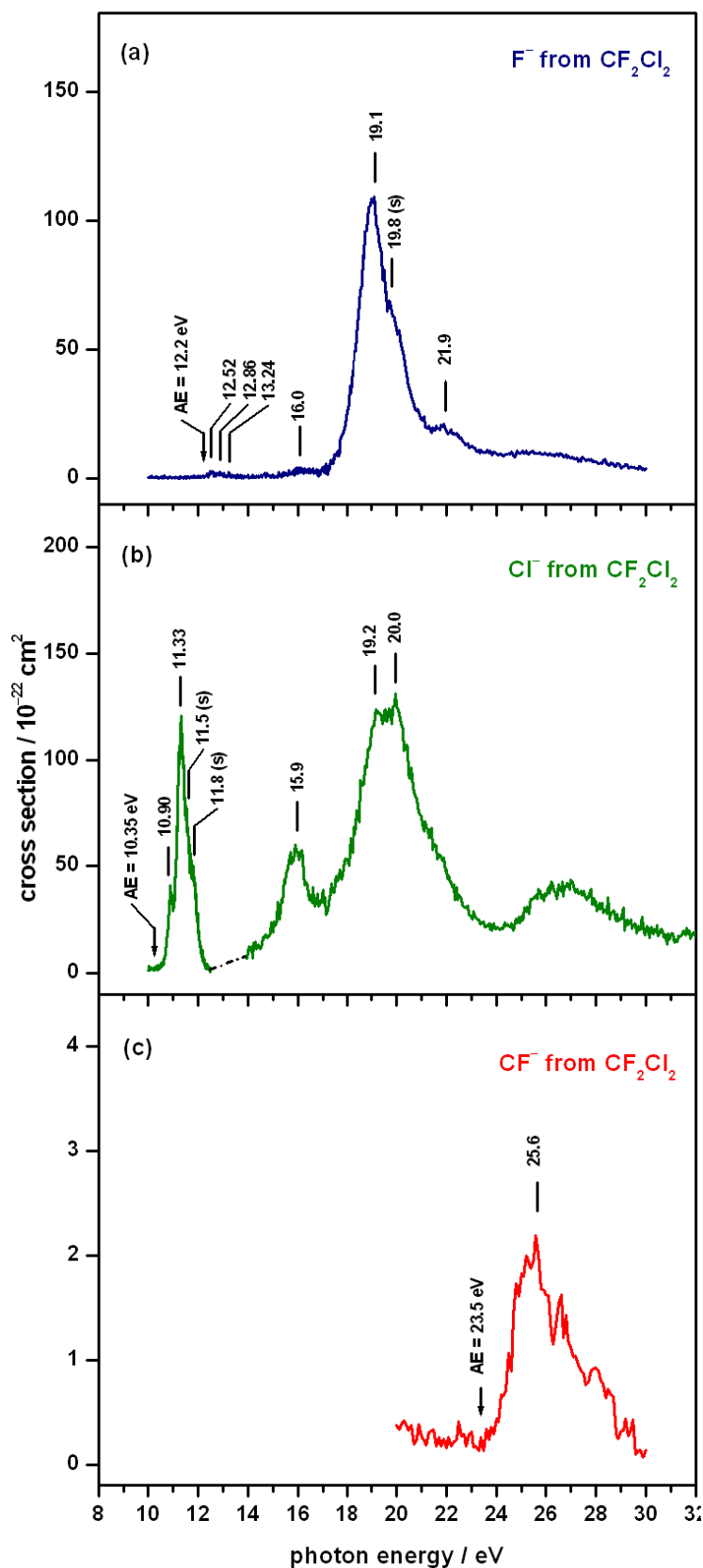
**A.IV.(14).** Ion yields for anions observed following the photoexcitation of  $\text{CF}_2\text{Cl}_2$ .

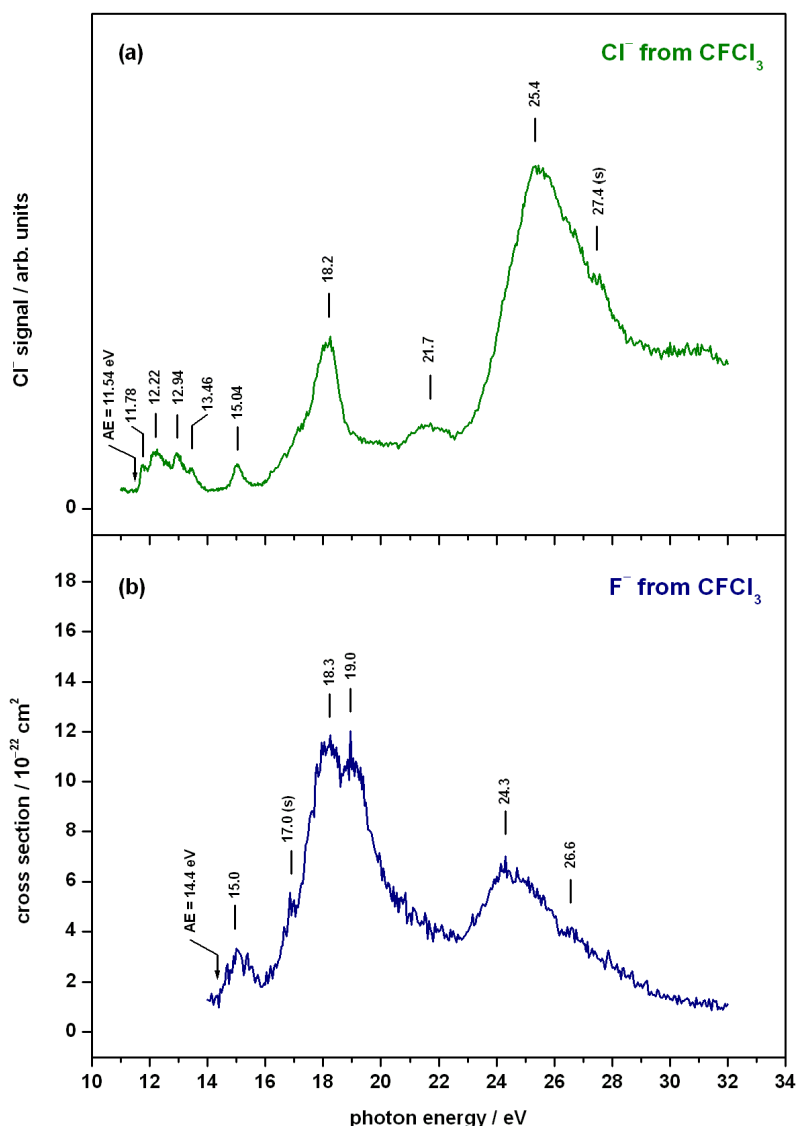
(a) Two scans are merged to generate the  $\text{F}^-$  ion-pair cross section: from 10.0-17.7 eV recorded with a step size of 0.02 eV and a wavelength resolution of 2 Å; from 17.7-30.0 eV recorded with a step size of 0.05 eV and a wavelength resolution of 6 Å

(b) Two separate scans, put on the same absolute scale, forming the  $\text{Cl}^-$  cross section: from 10.0-12.5 eV recorded with a step size of 0.01 eV and a wavelength resolution of 2 Å; from 13.9-32.0 eV recorded with a step size of 0.05 eV and a wavelength resolution of 6 Å.

(c)  $\text{CF}^-$  ion-pair formation cross section in the photon energy range 20-30 eV recorded with a step size of 0.1 eV and a wavelength resolution of 6 Å.

The appearance energies ( $AE$ ) are indicated and solid lines (with corresponding numbers) show energy positions of features in the spectra, where '(s)' indicates a shoulder feature.





**A.IV.(15).** Ion yields for anions observed following the photoexcitation of  $\text{CFCI}_3$ . **(a)** Two scans are merged to generate the  $\text{Cl}^-$  ion yield 11-16 eV recorded with a step size of 0.02 eV and a wavelength resolution of 3 Å, and from 16-32 eV recorded with a step size of 0.05 eV and a wavelength resolution of 6 Å. The  $\text{Cl}^-$  signal at 12.2, 18.2, 21.7 and 25.4 eV was shown to increase non-linearly with increasing gas pressure and an absolute cross section cannot be determined; electron attachment processes are significant in the formation of  $\text{Cl}^-$  from  $\text{CFCI}_3$ . **(b)**  $\text{F}^-$  ion-pair cross section from 14-32 eV recorded with a step size of 0.05 eV and a wavelength resolution of 6 Å.

# Appendix V:

## *Bond dissociation energies*

		$D_{therm.}^+ / \text{eV}$	$D_{expt.}^+ / \text{eV}$		$D_{lit.}^+ / \text{eV}$
1		2	3	4	5
1	$\text{H-C}_2\text{H}_3^+$	$2.7 \pm 0.3$	$\leq (3.3 \pm 0.2)$	$\text{H-C}_2\text{H}_3$	$4.81 \pm 0.03$
2	$\text{H-C}_3\text{H}_7^+$	$1.6 \pm 0.4$	$\leq (3.1 \pm 0.3)$	$\text{H-C}_3\text{H}_7$	$4.38 \pm 0.02$
3	$\text{H-C}_2\text{H}_5^+$	$1.1 \pm 0.1$	$\leq (1.2 \pm 0.2)$	$\text{H-C}_2\text{H}_5$	$4.36 \pm 0.01$
4	$\text{H-CH}_3^+$	$1.8 \pm 0.3$	$\leq (1.4 \pm 0.2)$	$\text{H-CH}_3$	$4.55 \pm 0.01$
5	$\text{H-CH}_2\text{Br}^+$	$1.8 \pm 0.4$	$\leq (2.3 \pm 0.2)$	$\text{H-CH}_2\text{Br}$	$4.43 \pm 0.02$
6	$\text{H-CH}_2\text{Cl}^+$	$1.8 \pm 0.4$	-	$\text{H-CH}_2\text{Cl}$	$4.34 \pm 0.02$
7	$\text{H-CHCl}_2^+$	$1.1 \pm 0.4$	$\leq (0.9 \pm 0.2)$	$\text{H-CHCl}_2$	$4.15 \pm 0.02$
8	$\text{H-CH}_2\text{F}^+$	$0.9 \pm 0.4$	-	$\text{H-CH}_2\text{F}$	$4.39 \pm 0.04$
9	$\text{H-CCl}_3^+$	$0.7 \pm 0.3$	$\leq (0.7 \pm 0.3)$	$\text{H-CCl}_3$	$4.07 \pm 0.03$
10	$\text{H-CHF}_2^+$	$0.5 \pm 0.3$	$\leq (0.1 \pm 0.1)$	$\text{H-CHF}_2$	$4.48 \pm 0.04$
11	$\text{H-CF}_3^+$	$-0.1 \pm 0.4$	$\leq (-0.2 \pm 0.2)$	$\text{H-CF}_3$	$4.61 \pm 0.03$
12	$\text{F-C}_2\text{F}_3^+$	$5.7 \pm 0.2$	$\leq (6.5 \pm 0.1)$	$\text{F-C}_2\text{F}_3$	$5.66 \pm 0.13$
13	$\text{F-C}_3\text{F}_7^+$	$2.6 \pm 0.3$	$\leq (3.5 \pm 0.3)$	$\text{F-C}_3\text{F}_7$	-
14	$\text{F-C}_2\text{F}_5^+$	$1.5 \pm 0.3$	$\leq (3.6 \pm 0.2)$	$\text{F-C}_2\text{F}_5$	$5.52 \pm 0.07$
15	$\text{F-CH}_3^+$	$2.1 \pm 0.3$	$\leq (3.2 \pm 0.1)$	$\text{F-CH}_3$	$4.77 \pm 0.09$
16	$\text{F-CFCl}_2^+$	$1.5 \pm 0.2$	$\leq (3.9 \pm 0.1)$	$\text{F-CFCl}_2$	$5.00 \pm 0.11$
17	$\text{F-CH}_2\text{F}^+$	$1.4 \pm 0.2$	$\leq (2.5 \pm 0.1)$	$\text{F-CH}_2\text{F}$	$5.14 \pm 0.09$
18	$\text{F-CF}_2\text{Cl}^+$	$1.2 \pm 0.3$	-	$\text{F-CF}_2\text{Cl}$	5.30
19	$\text{F-CCl}_3^+$	$0.9 \pm 0.2$	-	$\text{F-CCl}_3$	$4.55 \pm 0.04$
20	$\text{F-CHF}_2^+$	$0.6 \pm 0.3$	$\leq (2.0 \pm 0.4)$	$\text{F-CHF}_2$	$5.53 \pm 0.06$
21	$\text{F-CF}_3^+$	$-0.7 \pm 0.3$	$\leq (1.0 \pm 0.3)$	$\text{F-CF}_3$	$5.67 \pm 0.02$
22	$\text{Cl-CH}_3^+$	$2.2 \pm 0.2$	$\leq (2.4 \pm 0.1)$	$\text{Cl-CH}_3$	$3.63 \pm 0.02$
23	$\text{Cl-CH}_2\text{Cl}^+$	$0.9 \pm 0.2$	$\leq (1.6 \pm 0.1)$	$\text{Cl-CH}_2\text{Cl}$	$3.50 \pm 0.03$
24	$\text{Cl-CF}_3^+$	$0.4 \pm 0.3$	-	$\text{Cl-CF}_3$	$3.79 \pm 0.04$
25	$\text{Cl-CHCl}_2^+$	$0.2 \pm 0.2$	$\leq (1.6 \pm 0.1)$	$\text{Cl-CHCl}_2$	$3.22 \pm 0.02$

		$D_{therm.}^+ / \text{eV}$	$D_{expt.}^+ / \text{eV}$		$D_{lit.}^+ / \text{eV}$
	1	2	3	4	5
26	Cl-CF <sub>2</sub> Cl <sup>+</sup>	0.1 ± 0.2	≤ (2.2 ± 0.1)	Cl-CF <sub>2</sub> Cl	3.46 ± 0.11
27	Cl-CFCl <sub>2</sub> <sup>+</sup>	0.0 ± 0.2	-	Cl-CFCl <sub>2</sub>	3.33 ± 0.09
28	Cl-CCl <sub>3</sub> <sup>+</sup>	-0.4 ± 0.2	-	Cl-CCl <sub>3</sub>	3.07
29	Cl-SF <sub>5</sub> <sup>+</sup>	0.0 ± 0.2	≤ (1.9 ± 0.3)	Cl-SF <sub>5</sub>	< 2.82

<sup>a</sup> Thermochemical ionic bond dissociation energy at 298 K ( $D_{therm}^+$ ) for the bond shown in column 1. This value is calculated from the equation  $D_{therm}^+ = E - IE(AB) + EA(A)$ , if  $E$  is the enthalpy change for the reaction  $AB \rightarrow A^- + B^+$ ,  $IE$  is an ionisation energy and  $EA$  an electron affinity.  $E$  and  $IE$  values are included in Table 9.A.(I). The  $EA$  values for H, F and Cl are 0.754, 3.401 and 3.613 eV, respectively [J. C. Rienstra-Kiracofe, G. S. Tschumper, H. F. Schaefer, S. Nandi and B. Ellison, *Chemical Reviews* **102**, 231 (2002)].

<sup>b</sup> Experimental ionic bond dissociation energy at 298 K ( $D_{expt}^+$ ) for the bond shown in column 1. This value is calculated from the equation  $D_{expt}^+ \leq AE - IE(AB) + EA(A)$ , if  $AE$  is the appearance energy for the anion detected from the reaction  $AB \rightarrow A^- + B^+$ ,  $IE$  is an ionisation energy and  $EA$  an electron affinity.  $AE$  and  $IE$  values are included in Table 9.A.(I). The  $EA$  values for H, F and Cl are 0.754, 3.401 and 3.613 eV, respectively [J. C. Rienstra-Kiracofe, G. S. Tschumper, H. F. Schaefer, S. Nandi and B. Ellison, *Chemical Reviews* **102**, 231 (2002)].

<sup>c</sup> Neutral bond dissociation energy at 298 K for the bond shown in column 4 [D. R. Lide, *Handbook of Chemistry and Physics*, 88th ed. (Taylor & Francis, London, 2007), Section 9 pages 61-67].